BIODEGRADATION OF POLYCYCLIC AROMATIC HYDROCARBONS IN CONTAMINATED WASTEWATER AND BIODIESEL PRODUCTION USING THE OLEAGINOUS BACTERIUM *RHODOCOCCUS OPACUS*

A Thesis

Submitted in partial fulfillment of the requirement for the degree of

DOCTOR OF PHILOSOPHY

by

Lalit Goswami

Centre for the Environment

Indian Institute of Technology Guwahati

Guwahati 781039, Assam, India.

February 2019

Dedicated to My Parents and

My Grand Parents

Indian Institute of Technology Guwahati

Centre for the Environment

Statement

I, hereby declare that the content embodied in this thesis entitled "Biodegradation of polycyclic aromatic hydrocarbons in contaminated wastewater and biodiesel production using the oleaginous bacterium *Rhodococcus opacus*" is the result of investigations carried out by me at the Centre for the Environment, Indian Institute of Technology Guwahati, Guwahati, India, under the supervision of **Professor Kannan Pakshirajan Sir (Supervisor) and Professor G. Pugazhenthi Sir (Supervisor)**.

In keeping with the general practice of reporting scientific observations, due acknowledgements have been made wherever the work described is based on the findings of other investigators.

Date: 26 February, 2019 Lalit Goswami

Indian Institute of Technology Guwahati

Centre for the Environment

Certificate

It is certified that the work described in this thesis entitled "Biodegradation of polycyclic aromatic hydrocarbons in contaminated wastewater and biodiesel production using the oleaginous bacterium *Rhodococcus opacus*" by Lalit Goswami for the award of degree of Doctor of Philosophy is an authentic record of the results obtained from the research work carried out under our supervision at the Centre for the Environment, Indian Institute of Technology Guwahati, Guwahati, India, and this work has not been submitted elsewhere for any degree.

Dr. Kannan Pakshirajan
Professor
(Thesis Supervisor)
Department of Biosciences
and Bioengineering
IIT Guwahati, Guwahati – 781039
Assam, India

Dr. G. Pugazhenthi
Professor
(Thesis Supervisor)
Department of Chemical
Engineering
IIT Guwahati, Guwahati – 781039
Assam, India

Acknowledgements

First of all, there are no words to express The Gratitude, but it's a duty, that I cannot even think, imagine and feel the pain, hard work and sacrifices made by my Parents, my Grandparents (Late but always with me), my strong sister, my strong brother, Pushpanjali Mishra and The Lord.

I would like to express my sincere gratitude to my research supervisors, **Professor Kannan Pakshirajan Sir (**Department of Biosciences and Bioengineering, IIT Guwahati) **and Professor G. Pugazhenthi Sir** (Department of Chemical Engineering, IIT Guwahati) for their continuous care, support and encouragement throughout my research work. I must acknowledge the unconditional freedom to think, plan, execute and express, that I was given in every step of my research work, while keeping faith and confidence on my capabilities. They have always motivated me to prove my mettle. I feel I should be always at their foot service.

I would also like to extend my heartfelt gratitude to my Doctoral committee members. Dr. Senthilkumar Sivaprakasam Sir (Chairman, Doctoral committee), Dr. Shankar Prasad Kanaujia Sir and Dr. Vairakannu Prabu Sir. Their constant support and constructive criticism that has helped and improved the work pertaining to the PhD thesis. I would also thank present Head of Department Prof. Mihir Kumar Purkait Sir and past HoD's Prof. Gopal Das Sir and Prof. Vikash Kumar Dubey Sir, under whose able administration I was able to carry out my research work in a collegial environment.

I owe my sincere thanks to the Centre for the Environment, Department of Biosciences and Bioengineering, Department of Chemical engineering, Department of Physics, Centre for Civil Engineering, and Central Instrumental Facility, IIT Guwahati for providing the necessary facilities to fulfill the PhD thesis objectives.

I am grateful to each and every member of the interview panel for selecting me during PhD interview (2013) and Professor Gopal Das Sir, Partha Protim Bakal Sir, and Rupendir Sir for permitting me to attend the interview without having original certificates at the time of interview (in 2013). I would like to acknowledge all the staff members (Mr. Rajiv Kumar Gogoi bhaiya and Mr. Kaustubh Rakshit) of Centre for the Environment for their healthy support in this endeavor.

I would also like to acknowledge my earlier supervisors Dr. Alok Milton Lal Sir (SHUATS, Prayagraj) and Dr. Lalit Kumar Singh Sir (HBTU, Kanpur) for their regular motivation and encouragement. I would express thank to my seniors and my friends Mr. Siddharth Mohan Bhasney Sir, Mr. Narendra Naik Deshavath Sir, Mr. Sachin Tomar Sir, Dr. Mothe Gopi Kiran Sir, Dr. R. Vinoth Kumar, Mr. Somnath Chanda Sir, Dr. Manish Kamal Sir, Mr. Rajneesh Kumar, Ms. Deepa Sachan, Mr. Chandrabhanu Gupt, Dr. Siddharth Narayan Borah Sir, Ms. Pallavi Mukherjee, Dr. Kartikeya Tiwari (Indiana University) and Mr. Vivek Kumar Yadav for their valuable suggestions and time (anytime).

Also big heartfelt thanks goes to the past and present lab members Dr. Madhavi Singh Madam, Mr. Sanjay Kumar, Dr. Arindham Sinharoy, Mr. Arun Sakthivel, and Mr. Manoj Kumar. Also, to my research fraternity outside the IIT Guwahati, Dr. Sumit Kumar Sonker (MNIT Jaipur), Dr. Balendu Giri (IIT-BHU), Dr. Anamika Kushwaha (MNNIT Allahabad), Mr. Rahul Kumar (University of Auckland, New Zealand), Dr. Pankaj Kumar Gupta (University of Waterloo, Canada), Dr. Amit Kumar Sonker (Sejong University, South Korea), Dr. Joyabrata Mal (University of Berkley, USA), and Mr. Rajesh Kumar Patel (IIT Roorkee) also to all my summer and winter trainees and fellow researchers (Mr. Tondosama Koromory, Mr. Addis Kokeb and Dr. Ben Dolman (University of Manchester)).

In order to avoid missing any name, would like to pay gratitude to each and every one who supported me (knowingly or unknowingly) in completing this work and from whom I have learned and gained many things.

I acknowledge MHRD and our institute for providing fellowship throughout the PhD program. Special thanks to the academic people, library facilities, computer center, centre staff and Core I-IV people for their necessary support in every aspect. I would like to thank each and every website from where we have acquired beneficial information. Also, like to acknowledge all the staff members, security bhaiya and didi, cleaners, electricity, plumbing, hospital, workers, gardeners, AC, mess, general stores and bus services for their friendly and kind support throughout my stay in the campus.

I am grateful to The Lord Maa Kamakhya for blessing me and lastly, a big thank to Guwahati Medical College and Indian Air Force.

Date: 26 February, 2019 Lalit Goswami

Abstract

Polycyclic aromatic hydrocarbons (PAHs) represent a unique class of ubiquitous semi-volatile organic contaminants. They are well-known for their persistent, bio-accumulative, toxic, carcinogenic, teratogenic and mutagenic nature. Wastewater from industries, such as coal combustion, biomass gasification, power generation, incineration and petroleum refineries contains a complex mixture of PAHs. Owing to their molecular complexity, high melting point, low water solubility and low volatility, PAHs in aquatic systems tend to accumulate in sediments, thereby posing detrimental effect onto the organisms. Due to these reasons, the permissible concentration of PAHs in contaminated environment is kept very low at 10 μg L^{-1}. In comparison with the conventional treatment methods, including adsorption, volatilization, flocculation, reverse osmosis, photolysis, advanced oxidation processes and chemical degradation, biological methods are proving to be cost-effective, efficient and eco-friendly for treating of PAH contaminated wastewater.

In the present study, a hydrocarbonoclastic oleaginous bacterium *Rhodococcus opacus*, which is well-known to biodegrade recalcitrant organics, was investigated for its potential to simultaneous degrade naphthalene (2-ring), anthracene (3-ring), phenanthrene (3 ring) and fluoranthene (4-ring) as model PAHs, in single, multi-component and co-contaminated heavy metal system. In single-component system containing minimal salt medium with the 2-, 3- or 4- ring PAH compound as the sole source of carbon and energy and at an initial concentration in the range 50-500 mg L^{-1}, *R. opcaus* was capable of degrading 69.5% - 83.8% naphthalene, 67.8 - 81.4% anthracene, 64.7% - 76.9% phenenthrene and 58% - 73.2% fluoranthene, within 7 days. The amount of lipids accumulated by the bacteria was in the range 72.4% (w/w, CDW) for naphthalene, 70.6%

(w/w, CDW) for anthracene, 68.7% (w/w, CDW) for phenanthrene, and 63% (w/w, CDW) for fluoranthene.

For the biodegradation of PAHs in a multi-component system, a 2^3 full factorial design of experiments was employed with the three PAHs at two different levels by varying their initial concentration in the range 50 - 200 mg L^{-1} each. A maximum removal of 91.6%, 82.3% and 80.7% was achieved for naphthalene, phenanthrene and fluoranthene, respectively. The individual effect of PAH concentration was found to be more significant than 2-way and 3-way interaction effects on their biodegradation. PAH biodegradation efficiency in the mixture was mainly affected by initial concentration and aromatic complexity of the PAHs. Identification of the PAH degradation metabolites was carried out using liquid chromatography-mass spectrometry analysis, which clearly revealed that the PAHs were degraded primarily via the ortho/para pathway. In the study involving PAH (anthracene) contaminated system with six different heavy metals, viz. Fe (III), Cu (II), Zn (II), Cd (II), Ni (II), and Pb (II) present individually at 10 mg L^{-1} initial concentration, a decline in the biomass growth, PAH biodegradation and lipid accumulation was observed. The effect of heavy metals on these results followed the order: Cd > Ni > Pb > Cu > Zn > Fe.

In order to enhance PAH bioavailability by *R. opacus*, biochar derived cheaply from biomass gasification waste was evaluated. In the biochar aided PAH biodegradation experiments conducted in batch system with synthetic media containing 2-, 3- or 4- ring PAH compounds, at an initial concentration in the range 50 - 200 mg L^{-1}. An enhancement in PAH biodegradation from 79.6% to 92.3%, 76.1 to 90.5%, 74.1% to 88.2% and 71.6% to 82.3% for naphthalene, anthracene, phenanthrene and fluoranthene, respectively, were

achieved along with a corresponding high lipid accumulation of 68.1%, 74.2%, 72.4%, and 63% (w/w) of cell dry weight (CDW).

Valorization of biomass gasification wastewater (BGWW) for lipids accumulation by *Rhodococcus opacus* was further examined. Using the raw wastewater (untreated), the bacterium accumulated 54.3% (w/w) lipid with a wastewater chemical oxygen demand (COD) removal efficiency of 64%. However, these values were further enhanced to 62.8% (w/w) and 74%, respectively, following supplementation of the wastewater with MSM in the ratio 4:1. To further evaluate the potential of the *R. opcaus* to treat BGWW, an up-flow packed bed bioreactor (UFPBBR) with nano-biochar loaded polyurethane foam as the packing material was used. The novel packing material was utilized to improve the efficiency of the strain to treat BGWW at different influent COD concentrations and hydraulic retention time (HRT). Initially, the bioreactor was operated utilizing PUF as the support material, and a maximum of 81.65% COD removal was achieved at 1820 mg L^{-1} of influent COD concentration and 24 h of HRT. Using nano-biochar loaded PUF as the support material, more than 92% of COD removal was achieved for an influent COD concentration of 1820 mg L^{-1} and 24 h of HRT. Furthermore, 96.2% of toxicity associated with the BGWW was achieved demonstrating that the treated wastewater could be safely discharged into the waste stream.

A novel integrated biodegradation - microfiltration system for sustainable wastewater treatment and energy recovery was utilized. Initially, wastewater treatment by *R. opacus* was first carried out employing a stirred tank bioreactor. Subsequently, a microfiltration system was applied to recover the lipid-rich bacterial biomass as well as for residual COD removal from the effluent. The combined process showed excellent results in terms of COD removal from BGWW with 68.9% of COD removal by biodegradation. This value was further improved to 88.2%; following the microfiltration

step performed by employing a low-cost ceramic membrane. For upscaling this integrated approached, a stirred tank bioreactor was utilized in addition with the tubular ceramic membrane for the tangential microfiltration treatment. The biodegradation process showed a COD removal of 72.3% in the continuous stirred tank bioreactor along with a further enhancement to 95.12%; following the tangential microfiltration system. ^{1}H and ^{13}C nuclear magnetic resonance spectroscopy analyses of the bacterial lipids revealed the presence of more saturated fatty acids than unsaturated fatty acids. Thermogravimetric analysis of the accumulated lipids showed four thermal decomposition regions each with a good stability. Transesterification of the bacterial lipids to biodiesel and its properties revealed a very good potential of the strain for the production of biodiesel from PAH containing wastewater.

Abstract…… i

Contents…… v

List of Tables…… xii

List of Figures……... xvi

Abbreviations……. xxii

INTRODUCTION

1.1. Polycyclic aromatic hydrocarbons……. 1

1.2. Biomass gasification wastewater…… 2

1.3. Treatment methods for PAH containing wastewater…… 2

1.4. Biodegradation of PAHs…… 3

LITERATURE REVIEW

2.1. Polycyclic Aromatic Hydrocarbons and the environment…… 7

2.1.1. Properties and environmental regulations of PAHs…… 7

2.2. Sources and distribution of PAHs in the environment…… 7

2.3 Natural Sources of PAHs……. 9

2.4. Anthropogenic sources of PAHs in the aquatic environment…… 10

2.4.1. Fossil fuel extraction, refining, and burning…… 11

2.4.2. Industrial sources…….. 11

2.4.3. Municipal sources…….. 12

2.4.4. Agriculture sources…… 12

2.4.5. Contaminated sites…….. 13

2.4.6 Extra-terrestrial Sources…… 13

2.5. Toxicity of PAHs……. 13

2.6. Fate of PAHs in aquatic environment…… 14

2.6.1. Main Processes Affecting PAH Fate in the Aquatic Environment…… 14

2.6.2. Environmental regulations for drinking water and discharges into surface water..... 15

2.6.3. Analysis of PAH in environmental samples…… 16

2.7. Remediation of PAHs contaminated environment…… 18

2.7.1. Physical methods…… 18

2.7.1.1. Liquid-liquid extraction…… 18

2.7.1.2. Liquid-phase microextraction (LPME)…… 19

2.7.1.3. Filtration method……. 20

2.7.1.3.1. Reverse osmosis (RO)…… 20

2.7.1.3.2. Ultrafiltration…… 20

2.7.1.3.3. Nanofiltration…… 21

2.7.1.3.4. Forward osmosis (FO)…… 21

2.7.1.4. Adsorption…… 22

2.7.1.4.1. Alkyl bonded silica sorbent……. 22

2.7.1.4.2. Copolymer sorbents…… 23

2.7.1.4.3. Magnetic sorbents…….. 23

2.7.2. Chemical methods……..…….. 24

2.7.2.1. Supercritical fluid extraction (SFE)…… 24

2.7.2.2. Extraction with surfactants…… 24

2.7.2.2.1. Synthetic surfactants……. 25

2.7.2.2.2. Biosurfactants…….…….. 25

2.7.2.2.3. Gemini surfactants…… 25

2.7.2.3. Chemical oxidation…… 26

2.7.2.3.1. Ozonation ……. 26

2.7.2.3.2. Fenton method…… 26

2.7.2.3.3. Other oxidants…… 27

2.7.3. Biological methods…… 27

2.7.3.1. Plant assisted PAH biodegradation…… 27

2.7.3.2. Algae assisted PAH biodegradation…… 28

2.7.3.3. Biodegradation of PAHs mixture…… 29

2.7.3.4. Fungal biodegradation of PAHs…… 30

2.8. Biodegradation of PAHs mixture…… 32

2.9. Biomass gasification wastewater…… 33

2.10. Different bioreactor systems for PAH contaminated wastewater……. 34

2.10.1. Stirred tank bioreactor…… 34

2.10.2. Rotating biological contractor bioreactor…… 35

2.10.3. Membrane bioreactor system……. 35

2.10.4. Different integrated MBR systems and hybrid processes for PAHs removal…… 37

2.11. Statistical Design of Experiments…… 39

2.12. Aim and Objectives……. 40

2.13. Presentation and Layout of the Thesis…… 41

MATERIALS AND METHODS

3. Materials and methods……..….. 43

3.1. Microorganism and culture conditions…… 43

3.2. Chemicals and reagents…… 43

3.3. Batch biodegradation of PAHs and lipid accumulation by *R. opacus*…… 44

3.3.1 Single component system…… 44

3.3.1.1. PAHs biodegradation and lipid accumulation by *R. opacus*…… 44

3.3.1.2. Total lipids analysis, characterization and transesterification…… 46

3.3.1.3. Biodiesel characterization and its properties…… 47

3.3.1.4. Microscopy analysis of *R. opacus* biomass and lipids…… 48

3.3.2. Biodegradation of PAHs in a multi-component system …… 49

3.3.2.1. PAH biodegradation and lipid accumulation by *R. opacus*…… 49

3.3.2.2. Toxicity test …… 51

3.3.3. Effect of heavy metals on PAH biodegradation……. 52

3.3.3.1. Characterization of the bacterial biomass……... 54

3.3.3.1.1. FESEM and TEM analyses…… 54

3.3.3.1.2. FTIR and FESEM-EDX analyses…… 54

3.4. Biochar aided PAH biodegradation by *R. opacus* …… 55

3.4.1. Biochar preparation from biomass gasification effluent …….. 55

3.4.2. Biochar characterization……. 58

3.4.2.1. Physical properties……. 58

3.4.2.2. Chemical properties…… 58

3.4.2.3. Thermal and magnetic properties ……. 59

3.4.3. Effect of biochar on simultaneous PAH biodegradation and lipid accumulation …… 59

3.4.4. Determination of bacterial growth, PAH biodegradation and total lipid content……..…… 60

3.4.5. Morphology of *R. opacus* and contact angle measurement…..…… 61

3.5. BGWW treatment by oleaginous *R. opacus* and biodiesel production… 61

3.5.1. Source and characterization of BGWW……. 61

3.5.2. Batch shake flask experiments …… 62

3.5.2.1. Analysis of *R. opacus* biomass, total lipid and COD removal…… 63

3.5.2.2. Lipid characterization and transesterification…… 64

3.6. Integrated biodegradation- microfiltration approach…… 64

3.7. UFPBBR with biochar immobilized PUF as the packing material…… 66

3.7.1. Bioreactor setup and BGWW treatment…… 66

3.7.2. Characterization of the bio-supporting materials (PUF and biochar)… 69

3.7.3. Abiotic degradation of biomass gasification wastewater in UFPBBR .. 69

3.8. Analysis of R. opacus biomass, lipid content and COD removal (%)…… 71

3.8.1. Bioreactor set-up and operation for BGWW treatment……... 71

3.8.2. Analysis of *R. opacus* biomass, lipid content and COD removal (%)…….. 73

RESULTS AND DISCUSSION

4.1. Batch PAHs biodegradation and lipid accumulation by *R. opacus* …… 71

4.1.1. Batch shake flask study…….. 71

4.1.1.1. Biomass growth, PAH biodegradation and lipid accumulation…… 71

4.1.1.2. Kinetics of *R. opacus* biomass growth on PAHs ……... 78

4.1.1.3. Characterization and properties of FAMEs for biodiesel application…… 85

4.1.2. Biodegradation of PAHs in a multi-component system…… 88

4.1.2.1. Biomass growth, PAH biodegradation and lipid accumulation……. 88

4.1.2.2. Analysis of variance of PAH degradation……. 94

4.1.2.3. Identification of intermediate biodegradation metabolites……. 99

4.1.2.3.1. Identification of naphthalene metabolites ……... 99

4.1.2.3.2. Identification of phenanthrene metabolites……..... 102

4.1.2.3.2. Identification of phenanthrene metabolites…… 105

4.1.3. Effect of heavy metals on PAH biodegradation…… 111

4.1.3.1. *R. opacus* growth and PAH biodegradation in the presence of heavy metals…. 111

4.1.3.2. Characterization of the bacterial biomass…… 114

4.1.3.2.1. FTIR spectroscopy analysis…… 114

4.1.3.2.2. FESEM, EDX and TEM analyses…… 115

4.2. Biochar aided PAH biodegradation by *R. opacus*…… 118

4.2.1. Biochar characterization…… 118

4.2.1.1. Physical properties…… 118

4.2.1.2. Chemical properties…… 119

4.2.1.3. Thermal degradation analysis…… 122

4.2.1.4. Magnetic properties…….. 123

4.2.2. Cost analysis of the waste derived biochar…….. 123

4.2.3. Effect of biochar on PAH biodegradation…… 125

4.2.4. Effect of biochar on *R. opacus* biomass growth and lipid accumulation 129

4.3. BGWW using *R. opacus* and biodiesel production…… 132

4.3.1. Biomass growth, lipid production and COD removal by *R. opacus*... 132

4.3.2. TGA profiles of the accumulated lipids…… 136

4.3.3. Composition of FAMEs and assessment of biodiesel…… 137

4.4. Integrated biodegradation-microfiltration system for BGWW treatment and energy recovery…… 141

4.4.1. Biomass growth, COD removal and lipid accumulation by *R. opacus*... 141

4.4.2. Microfiltration system……... 144

4.4.3. Toxicity removal from BGWW after integrated process treatment…. 147

4.5. UFPBBR with biochar immobilized PUF as the packing material…… 148

4.5.1. Characterization of the bio-support material……. 148

4.5.1.1. TEM and XPS analyses of the biochar…… 148

4.5.1.2. FESEM, EDX and TEM analyses of the bio-support material…… 151

4.5.2. Abiotic losses/degradation of BGWW…… 151

4.5.3. Optimization of DO concentration……. 153

4.5.4. BGWW treatment……. 153

4.5.4.1. Performance using PUF as the bio-support material…… 153

4.5.4.2. Performance using PUF-biochar as the bio-support material……. 157

4.5.5. Toxicity removal…… 160

4.6. A hybrid continuous system using STR and microfiltration for simultaneous BGWW treatment and bioenergy recovery..... 161

4.6.1. COD removal and lipid accumulation by *R. opacus*…… 161

4.6.2. Tangential microfiltration system and COD removal…… 162

SUMMARY AND CONCLUSIONS

5. Summary and conclusions……. 165

Scope for Future Work…… 171

BIBLIOGRAPHY

Bibliography…….. 173

APPENDIX…….. 195

LIST OF PUBLICATIONS…….. 201

Lists of Tables

S. No.	Description	Page No.
Table 2.1:	Physicochemical properties of 16 PAHs enlisted by USEPA	8
Table 2.2:	PAH permissible limits for drinking water……	16
Table 2.3:	Risk limits for individual PAHs in the aquatic environment…	17
Table 2.4:	Different advantages and limitations of MBR system for wastewater treatment……	38
Table 3.1:	Bio-kinetic models tested in this study……	45
Table 3.2:	2^3 Full Factorial experimental design matrix showing different combination levels in the mixed PAHs biodegradation study along with the initial concentrations……	50
Table 3.3:	Composition of the raw BGWW used in this study……	62
Table 3.4:	Operational schedule with UFPBBR for BGWW treatment	70
Table 3.5:	Operational schedule with CSTR for BGWW treatment	74
Table 3.6:	Properties of tubular ceramic membrane sintered at 950°C	75
Table 4.1:	Estimated bio-kinetic model parameters for *R. opacus* grown using PAHs as the sole carbon source…….....	84
Table 4.2:	Composition of the FAMEs produced by transesterification of the accumulated lipids …….....	87
Table 4.3:	Estimated property values of the biodiesel obtained by lipid transesterification and comparison with those of the international standards……..…….	88

Table 4.4: 2^3 Full Factorial experimental design matrix showing different combination levels of PAHs in the ternary system along with their biodegradation efficiency values…… 90

Table 4.5: ANOVA of batch biodegradation of PAHs by *R. opacus* in the ternary system for Naphthalene; Phenanthrene and Fluoranthene 95

Table 4.6: Student 't' test for estimating the significance of individual and interaction effects of PAHs on each other degradation by *R. opacus* in the ternary system …….. 96

Table 4.7: Literature on biodegradation of PAH in a multicomponent pollutant system using different microorganisms…… 98

Table 4.8: Mass spectra of phenanthrene metabolites formed during PAHs biodegradation in the ternary system…… 105

Table 4.9: Mass spectra of fluoranthene metabolites formed during PAHs biodegradation in the ternary system…… 109

Table 4.10: Elemental composition, surface and magnetic properties of the biochar…… 124

Table 4.11: Cost estimation for biochar preparation…… 124

Table 4.12: Estimated property values of the biodiesel obtained by lipid transesterification and comparison with those of the international standards…….. 139

Table 4.13: BGWW toxicity removal using the UFPBBR with two different support material and at different HRT…… 161

Lists of Figures

S. No.	Description	Page No.
Fig. 2.1: Parent structures of the USEPA enlisted PAHs (a) low-molecular weight and (b) high-molecular weight PAHs……		9
Fig. 2.2: Scheme of the conventional wastewater treatment process, Side stream MBR and submerged MBR……..		36
Fig. 2.3: An overview of MBR and integrated MBR systems……		38
Fig. 2.4: Schematic diagram of some hybrid MBR systems ……		39
Fig. 3.1: Biochar preparation steps followed in the present study……		57
Fig. 3.2: Schematic showing the microfiltration set up in the integrated biodegradation-microfiltration approach for BGWW treatment……		65
Fig. 3.3: Schematic showing experimental set up of the UFPBBR with support material PUF, (b) PUF-biochar and (c) inset of PBBR……		68
Fig. 3.4: Schematic CSTR tank……		72
Fig. 3.5: (a) Steps followed for fabricating the tubular ceramic membrane and (b) Schematic of the MF setup……		76
Fig. 4.1: Time profile of PAHs biodegradation at different initial concentration and 10% inoculum size: (a) naphthalene, (b) anthracene, (c) phenanthrene and (d) fluoranthene……...		79
Fig. 4.2: Time profile of *R. opacus* biomass grown on naphthalene, (b) anthracene, (c) phenanthrene and (d) fluoranthene at different initial concentrations……..		80
Fig. 4.3: Time profile of lipid accumulation by *R. opacus* grown using (a) naphthalene, (b) anthracene, (c) phenanthrene and (d) fluoranthene at		81

different initial concentrations……

Fig. 4.4: Experimental and model predicted specific growth rate of *R. opacus* grown using different initial PAHs concentration…… 82

Fig. 4.5: ^{1}H-NMR and ^{13}C-NMR spectra of the *R. opacus* accumulated lipids…… 85

Fig. 4.6: Maximum biomass growth of *R. opacus* in multi-component PAHs system…… 91

Fig. 4.7: PAH biodegradation in multi-component PAHs system …… 91

Fig. 4.8: Total lipid accumulation by *R. opacus* in the multi-component PAH system…….. 93

Fig. 4.9: Pareto chart showing the effect of different PAHs on each other biodegradation by *R. opacus* ……. 97

Fig. 4.10: Mass spectra of intermediate metabolites formed during biodegradation of PAHs in ternary system ……. 100

Fig. 4.11: (a) Proposed pathway for naphthalene biodegradation in ternary PAH system by *R. opacus*…… 101

Fig. 4.11: (b) Proposed pathway for phenanthrene biodegradation in ternary PAH system by *R. opacus*…… 103

Fig. 4.11: (c) Proposed pathway for fluoranthene biodegradation in ternary PAH system by *R. opacus*…… 107

Fig. 4.12: Time profile of (a) anthracene biodegradation; (b) biomass grown and (c) total lipid accumulation by *R. opacus* in presence of different heavy metals …….. 113

Fig. 4.13: Estimated specific anthracene uptake rate and specific lipid accumulation rate by *R. opacus* in presence of different heavy metals… 114

Fig. 4.14: FTIR spectra of control biomass and metal loaded biomass…… 115

Fig. 4.15: FESEM micrographs of the bacteria (a) control biomass and (b) heavy metal loaded biomass…… 116

Fig. 4.16: TEM micrographs showing lipid globules accumulated inside *R. opacus*: (a) control biomass and (b) heavy metal loaded biomass……. 116

Fig. 4.17: EDX spectrum of (a) control biomass and biomass loaded with (b) Pb (II); (c) Fe (III); (d) Cd (II); (e) Cu (II); (f) Zn (II)…… 117

Fig. 4.18: FESEM micrographs of biochar prepared in this study (a) 1 µm and (b) 10 µm and (c) FESEM-EDX spectrum of the biochar ……. 119

Fig. 4.19: (a) Fourier transform infrared spectroscopy; (b) X-ray diffraction; (c) Raman spectra; (d) Thermogravimetric analysis (TGA) curve; and (b) Vibrating sample magnetometer analyses of the biochar…….. 120

Fig. 4.20: Effect of biochar on (a) naphthalene; (b) anthracene; (c) phenantrene and (d) fluoranthene biodegradation by *R. opcaus* …… 126

Fig. 4.21: Effect of biochar on *R. opacus* biomass growth by utilizing naphthalene, anthracene, phenanthrene and fluoranthene as the substrate… 127

Fig. 4.22: Effect of biochar on lipid accumulation by *R. opacus* utilizing (a) naphthalene; (b) anthracene (c) phenanthrene and (d) fluoranthene 128

Fig. 4.23: Contact angle of (a) biochar along with PAH and (b) *R. opcaus* biomass along with PAH and biochar…… 131

Fig. 4.24: FESEM images of *R. opacus*: (a) without biochar and (b) with biochar …… 132

Fig. 4.25: *R. opacus* biomass growth on BGWW based media (a) 5% inoculum size and (b) 10% inoculum size……..…… 133

Fig. 4.26: Lipid production by *R. opacus* using BGWW based media and COD removal efficiency…… 134

Fig. 4.27: TGA and DTG curves of the lipids produced by *R. opacus* using BGWW as the substrate…….. 137

Fig. 4.28: Percentage FAMEs composition in the biodiesel product…… 138

Fig. 4.29: Fourier transform infrared (FTIR) spectra of the biodiesel…… 139

Fig. 4.30: Time profile of *R. opacus* biomass growth with BGWW …… 143

Fig. 4.31: Lipid production and COD remaining by *R. opacus* with BGWW (during biodegradation)…….. 143

Fig. 4.32: *R. opacus* cells stained with Nile red (The cells were grown using BGWW as the substrate)…… …… 145

Fig. 4.33: Influence of applied pressure on permeate flux and residual COD removal (following the biodegradation process by microfiltration 145

Fig. 4.34: Overall COD removal (%) using BGWW……. 146

Fig. 4.35: TEM micrographs of biochar…….. 149

Fig. 4.36: XPS scanning of biochar (a) full scan and its short scan: (b) C_{1s} (c) O_{1s} (d) N_{1s} and (d) Fe_{2p}……. 150

Fig. 4.37: (a) FESEM micrographs of PUF and biochar loaded PUF as the support material, (b) FESEM-EDX of the support material (c) mapping of biofilm formation onto the support material……. 152

Fig. 4.38: Time profile of COD and DO in the UFPBBR treating BGWW (a) PUF as the bio-support material and (b) biochar-loaded PUF as the support material…….. 154

Fig. 4.39: Plausible mechanism for the removal of organic contaminants in wastewater by adsorption onto biochar……... 160

Fig. 4.40: Time profile of influent and effluent COD concentration, COD removal and pH in stirred tank bioreactor for treating BGWW from *R. opacus* grown with different PAHs as the sole carbon source…… 163

Abbreviations

AAS: Atomic absorption spectroscopy

ANOVA: Analysis of variance

ANTH: Anthracene

APHA: American Public Health Association

ASTM: American Society for Testing and Materials

BET: Brunauer-Emmett-Teller

BGWW: Biomass gasification wastewater

CA: Contact angle

CDW: Cell dry weight

CFU: Colony forming unit

CN: Cetane number

COD: chemical oxygen demand

CP: Cloud point

CSTR: Continuous stirred tank reactor

DCM: Dichloromethane

DO: Dissolved oxygen

DU: Degree of saturation

EDX: Energy dispersive spectroscopy

FAME: Fatty acid methyl ester

FESEM: Field emission scanning electron microscopy

FLOR: Fluoranthene

FTIR: Fourier transform infrared spectrometry

GC: Gas chromatography

HPLC: High-pressure liquid chromatography

HRT: Hydraulic retention time

IV: Iodine value

LB: Luria Bertani

LCMS: Liquid chromatography mass spectrometry

MLSS: Mixed liquor suspended solids

MLVSS: Mixed liquor volatile suspended solids

MSM: Minimal salt medium

MTCC: Microbial Type Cell Culture

NAPH: Naphthalene

NMR: Nuclear magnetic resonance

NTU: Nephelometric Turbidity Unit

PAH: Polycyclic aromatic hydrocarbon

PBS: Phosphate buffer solution

PHEN: Phenanthrene

PP: Pour point

PUF: Polyurethane foam

RO: Reverse osmosis

SV: saponification value

TEM: Transmission electron microscopy

TGA: Thermogravimetric analysis

UFPBBR: Up-flow packed bed reactor

VSM: Vibrating sample magnetometer

XRD: X-ray diffractometer

ZP: Zeta potential

CHAPTER 1

INTRODUCTION

1. Introduction

With the rapid increase in industrialization, release of different pollutants into the environment has increased noticeably, and as a consequence of which environmental quality has diminished to the frightening levels (Roy et al., 2015). Environmental pollutants are also well-known to affect both the living and non-living assets of the biosphere via numerous routes (Ye et al., 2013). Among the different environmental pollutants, polycyclic aromatic hydrocarbons (PAHs) are the most important because of their persistence, recalcitrance, abundance and toxicity in the environment (Titaley et al., 2016; Samanta et al., 2002). PAHs are ubiquitously found at wood preservation plants, industrial sites associated with petroleum and coal tar manufacturing, gas plants, runoff from asphalt pavement and combustion processes (Hadibarata et al., 2012; Yap et al., 2011; Mahanty et al., 2008). They are well-studied to act as a human skin photosensitizer, mild allergen, whereas some are reported to cause haemolytic anaemia and nephrotoxicity (Bucker et al., 1979). Hence, removal of PAHs from wastewater prior to its discharge into the environment is becoming inevitable.

1.1. Polycyclic aromatic hydrocarbons

Polycyclic aromatic hydrocarbons (PAHs), a prevalent class of organic pollutants that are abundant in the environmental domain, are of prime concern to human health and natural ecosystems (Parinos et al., 2016; Rodrigues et al., 2013). PAHs are considered among the priority pollutants, owing to their recalcitrance to microbial degradation and potential toxicity to higher microorganisms (Sherafatmand et al., 2015; Zhang and Tao, 2008). Their wide distribution in the environment is directly related to their utilization in various industrial and domestic products. They are found ubiquitously in the wastewater from wood preservation plants, industries associated with petroleum,

coal tar, creosote manufacturing, gas plants, biomass gasification and other combustion processes (Cheng et al., 2016). Furthermore, these PAHs are considered hazardous due to its toxic, carcinogenic, teratogenic and mutagenic properties (Zhou and Zhao, 2012). Their environmental persistence and recalcitrant nature is mainly due to their low aqueous solubility, which causes deleterious effects on both flora and fauna (Biswas et al., 2015). Hence, removal of PAHs from wastewater prior to its discharge into the environment is highly essential.

1.2. Biomass gasification wastewater

Biomass gasification wastewater (BGWW) is generated during the wet scrubbing of synthesis gas, which primarily contains phenols, heterocyclic compounds, mono- and poly-cyclic aromatic hydrocarbons (Tian et al., 2006). There is a huge variation in BGWW chemical oxygen demand, which is generally in the range 920-1,60,000 mg L^{-1} and it is attributed mainly to the presence of diverse organic compounds present in the wastewater (Jeswani et al., 2013). Moreover, the generated wastewater is toxic, mutagenic and carcinogenic to both flora and fauna due to the presence of these organics (Samanta et al., 2002). Hence, there is a continuous search for economical, effective and eco-friendly processes for the removal of PAHs for ensuring their presence in the environment below the permissible limits.

1.3. Treatment methods for polycyclic aromatic hydrocarbon containing wastewater

The treatment of PAHs contaminated wastewater can be carried out through physical, chemical and biological processes (Tian et al., 2012). Physical processes viz. volatilization and adsorption, greatly reduce the PAHs concentration but, these processes are insufficient due to their inability to degrade PAHs to less toxic form. In addition, the

chemical methods (direct photolysis, oxidation through ozonation and chlorination) are relatively much costlier than the other two treatment processes, and in many cases only transfer of the pollutant from one phase to another is effected without any major treatment (Haritash and Kaushik, 2009). Compared with these methods, microbial biodegradation and biotransformation is proving to be more successful as complete mineralization of these complex and toxic compounds into simple and non-toxic ones is possible. Moreover, biological processes seem to be more attractive, economic, effective and efficient than the conventional techniques for treating PAHs contaminated wastewater (Pires et al., 2011).

1.4. Biodegradation of PAHs

In the recent years, biological methods are proving to be efficient for the treatment of PAHs contaminated wastewater. Many bacterial species, including *Bacillus, Burkholderia, Mycobacterium, Pseudomonas, Rhodococcus* and *Sphingomonas* have been identified for their capability to degrade or transform PAHs (Walter, 1991). These microorganisms are able to bio-transform and/or mineralize the PAHs into fewer non-toxic simple metabolites. Recent studies have also reported the capability of some microbes to exploit PAHs as the sole source of carbon and energy. Among these microorganisms, *Rhodococcus* species, belonging to the family *Nocardiaceae* is effective for PAHs biodegradation. Moreover, the genus is capable of accumulating a very high fatty acid content of its cell dry weight (CDW) (Kumar et al., 2015), which is further attractive for converting the accumulated lipids to bioenergy rich compounds.

Wastewater generated from industries such as petroleum, biomass gasification and coke-oven contains a complex mixture of PAHs; hence, for increased industrial relevance it is important to understand PAH degradation in a mixed pollutant system.

Interaction between different substrates on microorganism growth and PAH biodegradation rate may play a major role in such a mixed pollutant system. However, in literature, most of the studies are restricted to the metabolic evaluation of PAH biodegradation in a single pollutant system and there is very limited information available on biodegradation of a mixture of PAHs (Zhong et al., 2011). In addition to PAHs, various other inorganic pollutants are also present in real wastewater. Amongst the different environmental pollutants, heavy metals (HMs) are the most important because of their persistence, recalcitrance, abundance and toxicity in the environment (Manikandan et al., 2016). Therefore, industrial effluent containing these contaminants when released from the main stream affects biodeterioration and biotransformation by microorganisms. For instance, heavy metals, including cadmium (Cd), lead (Pb) and nickel (Ni) are shown to adversely affect biodegradation of organic contaminants in the environment (Atagana et al., 2006; Riis et al., 2002).

Therefore, it is very important from the standpoint of designing biological processes for treating a variety of pollutants in mixture, i.e. evaluate biological treatment of wastewater containing a mixture of PAHs and bioremediation of wastewater contaminated with PAH and heavy metal removal.

Biodegradation of PAHs is generally limited due to their poor aqueous solubility. Various surface-active compounds (SACs) (e.g. surfactants) have been studied to enhance the bioavailability of PAHs, thereby to overcoming the diffusion-related mass transfer limitations (Bezza and Chirwa, 2016). But supplementation of SACs leads to additional cost of the process making it more expensive. Therefore, use of cheap and abundantly available biomaterials are very much needed to keep the process cost low.

A better alternative to SACs seems to be biochar as it is economically viable and inert to microbial degradation. Biochar is an aromatized, amorphous and carbonaceous solid by-product formed during partial thermochemical conversion of biomass in an oxygen-limited environment (Cui et al., 2016) with highly desirable properties, including large specific surface area, pore volume and hydrophobicity. It is being seen as an efficient biomaterial in the recent years for different applications (She et al., 2016).

Biodegradation of PAHs using different microorganisms has been well studied, but bioreactor systems for treating PAH contaminated wastewater is very scanty. Among the suspended bioreactor systems available to treat wastewater, membrane bioreactor (MBR) and stirred tank bioreactor have shown promising results, in the case of attached growth bioreactors, up-flow packed bed bioreactor is well-known for treating various types of effluents (Sahoo et al. 2011; Haritash and Kaushik, 2009). Furthermore, the application of low-cost ceramic membranes for the separation of biomass during the continuous operation of stirred tank bioreactor as well as for the residual COD removal seems to be attractive and technically feasible for large-scale applications (Kumar et al., 2016).

Hence, this study was aimed at biodegradation of PAHs in contaminated wastewater by the oleaginous bacterium *R. opacus* in batch and continuous treatment system and its potential for biofuel production.

CHAPTER 2

LITERATURE REVIEW

2. Literature Review

2.1. Properties and environmental regulations of PAHs

In general, PAHs are neutral, hydrophobic, non-polar compounds composed of two or more fused aromatic rings in linear, angular or clustered arrangements containing only carbon and hydrogen (Sims and Overcash, 1983). They are well-known as persistent organic pollutant due to their high hydrophobicity or low water solubility (Cerniglia, 1992). Owing to their molecular complexity, high melting point, low water solubility and low volatility, PAHs in aquatic systems tend to accumulate in sediments, thereby affecting the benthic organisms (Ge at al. 2016). These are also probably considered as the starting compounds for the abiological synthesis of the earliest materials for life (Hayakawa, 2018). PAHs are very commonly present in oil, tar and coal, and are produced through the incomplete combustion of organic matter (e.g. coal combustions, biomass gasification, automobile engines, incinerators, biomass burning in forest and slash-and-burn agriculture, smoking and cooking, etc.) (Hayakawa, 2018). PAHs are classified into two different groups: (1) low molecular weight PAHs (LMW-PAHs), containing three or more aromatic rings and (2) high molecular weight PAHs (HMW-PAHs), containing four or more aromatic rings. Among the different PAHs compounds, sixteen parent PAHs are designated by the US Environmental Protection Agency (USEPA) and the European Union (EU) as priority pollutants. Table 2.1 presents various physicochemical properties of PAHs and Fig. 2.1 depicts the structure of these PAHs.

2.1.2. Sources and distribution of PAHs in the environment

PAHs originate from both natural and anthropogenic sources. Natural sources of PAHs include forest-fires, natural petroleum seeps and post-depositional transformation of

biogenic precursors (Young and Cerniglia, 1995). Anthropogenic source of PAHs include combustion of

Table 2.1: Physicochemical properties of 16 PAHs enlisted by the USEPA

Compound	Molecular Weight	Log K_{ow}	Water solubility at 25°C (mg L^{-1})	Melting Point (°C)	Vapour Pressure at 25°C (mPa)
Naphthalene	128	3.5	31.7	80.5	11960
Acenaphthalene	154	4.33	3.42	95	594
Fluorene	166	4.18	1.98	116.5	94.7
Phenanthrene	178	4.5	1.29	101	90.7
Anthracene	178	4.5	0.045	216	25
Pyrene	202	4.9	0.135	156	91.3×10^{-6}
Fluoranthene	202	5.1	0.26	111	328
Chrysene	228	5.3	0.088	158	82.2×10^{-6}
Benz[a]anthracene	228	5.6	0.0057	162	14.7×10^{-3}
Benzo[a]pyrene	252	6.0	0.0038	179	0.37×10^{-6}
Benzo[b]fluoranthene	252	6.06	0.014	168	0.13×10^{-5}
Benzo[f] fluoranthene	252	6.0	0.008	166	0.18×10^{-5}
Benzo[k] fluoranthene	252	6.06	0.0043	217	2.8×10^{-9}
Indeno[1,2,3-c,d] pyrene	276	6.4	0.00053	164	1.3×10^{-5}
Benzo[g,h,i]perylene	276	5.8	0.003	152	3.5×10^{-5}
Dibenzo[a,h]anthracene	278	5.2	0.0008	176	1.1×10^{-5}

fossil fuels (coal and petroleum) or wood (pyrolytic) and crude/refined petroleum through accidental oil spills, discharge from routine tanker operations (petrogenic) (Zakaria et al., 2002; Kannan et al., 2005). However, among these various natural and anthropogenic sources, emission from the latter is considered as the major source of these highly recalcitrant compounds in the environment.

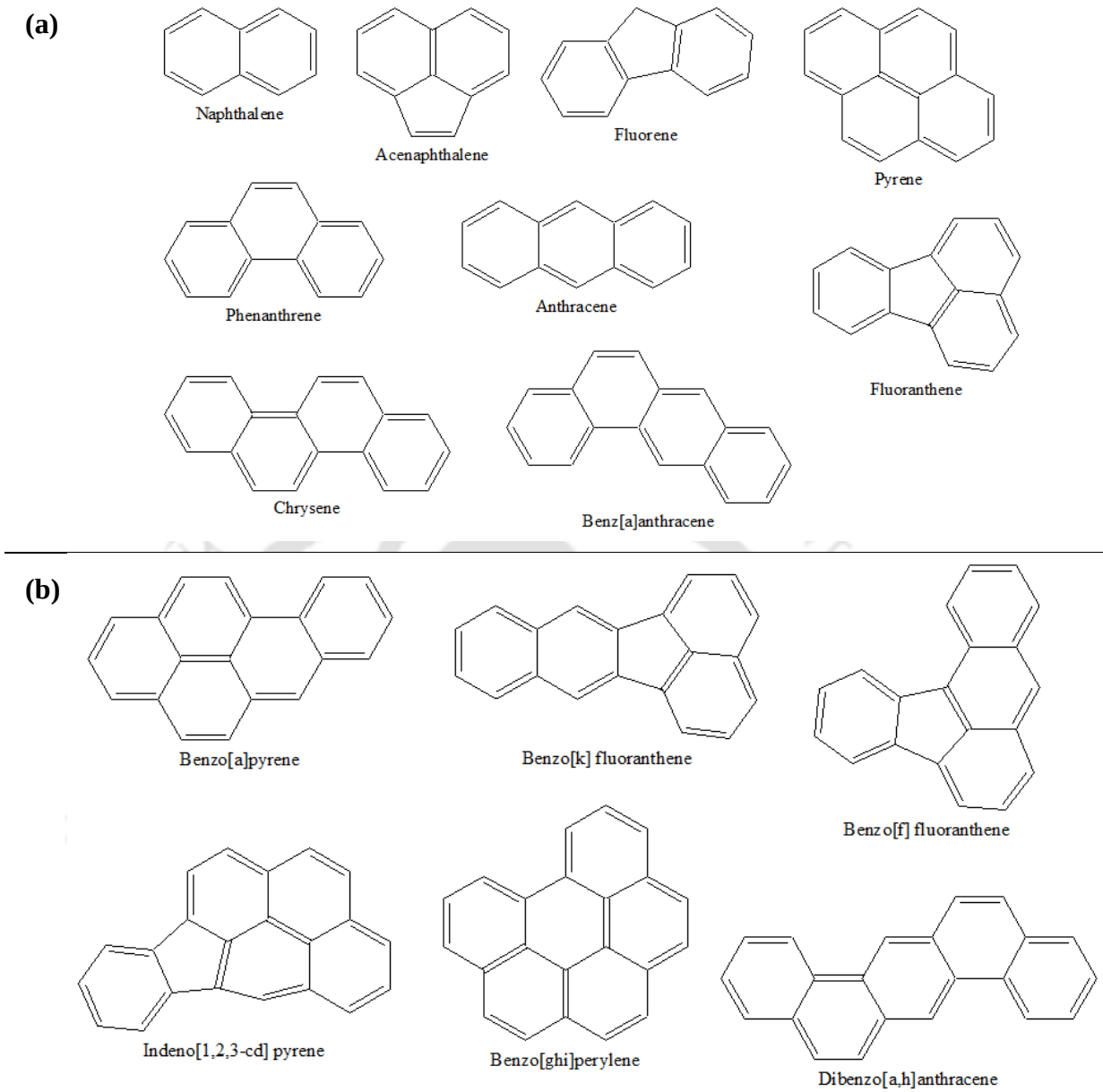

Fig. 2.1: Parent structures of the USEPA enlisted PAHs (a) low-molecular weight and (b) high-molecular weight PAHs

2.3 Natural Sources of PAHs

Forest fires, prairie fires and agricultural burning contribute the most of PAHs from natural sources to the atmosphere. The total amount of PAHs emitted from these sources depends upon the amount of organic matter burnt, nature of the blaze (wild vs. prescribed, flaming vs. smoldering), type (heading fire vs. backing fire) and intensity of fire. PAHs

generated from fires have a tendency to sorb to suspended particulates and ultimately reach the terrestrial and aquatic environments as atmospheric fallout (Eisler 1987). Furthermore, these PAHs may undergo photolytic and chemical transformations. Also, PAHs occur naturally in bituminous fossil fuels, viz., coal and petroleum oil (NRC 1983). The petroleum tar is capable of adding PAHs to both atmospheric and aquatic environments (Timoney and Lee 2011).

It has recently been found that naphthalene, phenanthrene, and perylene are produced biologically. The biological production of naphthalene has been concluded from its presence in Magnolia flowers (Azuma et al. 1996) or flower scents of different *Annonaceae* species from the Amazon rain forest (Jürgens et al. 2000). *Muscodor vitigenus*, an endophytic fungus growing in the Peruvian Amazon region, has shown production of naphthalene (Daisy et al. 2002). Also, a high naphthalene concentration in *Coptotermes formosanus* termite nests of subtropical North America and nests of various termite genera from tropical Brazil suggest naphthalene synthesis by termites or associated microorganisms (Wilcke et al. 2004; Chen et al. 1998) whereas Perylene is known to be produced biologically in anaerobic environments in soils and sediments (Wilcke et al. 2002).

2.4. Anthropogenic sources of PAHs in the aquatic environment

In general, anthropogenic sources of PAHs in the aquatic environment can be divided into two categories: sources that discharge directly into the water body and sources that discharge into the atmosphere. Atmospheric deposition is considered the main source of PAHs in the aquatic environment; therefore, atmospheric emission sources are related to PAH water pollution. Discharges from petroleum terminals, shipyards, aluminum smelting, manufactured gas production plants, tar distillation plants, rail yards, loading/unloading

facilities, and spilled or seeped petroleum or coal- or oil-derived tars and associated distillation products are some of the common sources of PAHs discharges into the waste stream (Battelle 2003).

2.4.1. Fossil fuel extraction, refining, and burning

PAHs are generally found in coal at a concentration varying from 0.4 to 36 mg kg^{-1} (Ogala and Iwegbue 2011; Bojakowska and Sokołowska 2001; Zhao et al. 2000). These compounds may leach out from the coal during storage and transportation. Also, huge amount of PAHs are generated during coal burning (Liu et al. 2008a). In 2004, around 530,000 tons of the 16 PAHs enlisted by USEPA were emitted into the environment globally, including China, India and United States which produced 1,14,000, 90,000 and 32,000 tons, respectively (Zhang and Tao 2009). The oil and gas offshore extraction generates huge volumes of wastewater known as produced water containing mono- and polycyclic hydrocarbons. Hence, there is growing concern regarding ill-effects of PAHs to the aquatic ecosystem. In addition, ship-related operational discharges of petroleum oil contains discharge of bilge water generated from machinery and oily ballast water from fuel tanks that is flushed out in the marine environment.

2.4.2. Industrial sources

Emissions generated from industries, such as aluminum and coke, petrochemical, rubber, tire, cement manufacturing, bitumen and asphalt, biomass gasification, wood preservative, commercial heat and power generation, and waste incineration contribute to major PAHs in the aquatic environment. Around 0.13 - 0.4 mg g^{-1} and 0.5 - 9.0 mg g^{-1} PAHs emission were reported by the thermal degradation of cellulose and tire (Chen et al. 2007; Fabbri and Vassura 2006). The overall emission of PAHs reported in the literature is approximately 0.08 - 3.97 mg kg^{-1} feedstock (Yang et al. 1998). Furthermore, 6.19% were

in the form of high molecular weight carcinogenic hydrocarbons of the total PAH emissions (Shen et al. 2013). According to the European Environmental Agency (EEA) (2012) that in 2010, the total PAH emission from EU countries was 1447 Mg which mainly includes the emissions from commercial institutions and households (59%), Agriculture (16%), Industrial processes (9%) and energy uses in industry (5%).

2.4.3. Municipal sources

In urban areas, mobile sources are the prime causes of PAH emissions. They are basically emitted from exhaust fumes of vehicles, including automobiles, railways, ships, and aircrafts and are associated with use of diesel, coal, gasoline, oils, and lubricant oil (Baek et al. 1991). It is reported that coal tar-based pavement sealcoat is a source of PAH contamination of water in the United States (Mahler et al. 2014, 2012; Van Metre and Mahler 2010). Also, the PAH profiles in the various compartments showed the fate of PAHs in the air-water system: the proportion of carcinogenic PAHs was more important in runoff waters (35%) than in air (6%) (Motelay-Massei et al. 2006).

2.4.4. Agriculture sources

The burning of lignocellulosic agricultural residues viz. brushwood, straw, moorland heather and stubble is the chief cause of PAHs generation. Such activities include the burning of organic matters under suboptimum combustion conditions. PAHs emission from wood combustion ranged from 16.4 - 1282 mg kg^{-1} wood (Schauer et al. 2001) whereas 9.29 - 23.6 µg g^{-1} for rice and 3.13 - 49.9 µg g^{-1} for bean straw (Lu et al. 2009). PAH concentrations released from wood combustion depend on wood type, kiln type and combustion temperature. Although 80 - 90% of the PAHs emitted from biomass combustion generates low-molecular weight PAHs that includes naphthalene, phenanthrene, anthracene, pyrene, and fluoranthene.

2.4.5. Contaminated sites

Since the industrial revolution because of the unrestricted industrial activity and lack of stringent environmental regulations till the middle of the 20th century, numerous areas are contaminated due to discharge of industrial wastewater containing PAHs. One of the main such contamination sources is former manufactured gas plants (MGPs). From a long time, MGP sites have been identified to be the source of groundwater contamination (Mackay and Gschwend 2001). About 5000, 2300, and 1200 MGP sites have been identified in the United States, United Kingdom and Germany, respectively (Wehrer et al. 2011).

2.4.6 Extraterrestrial Sources

Over a decade, ground based and space-based observations have shown infrared emission features characteristic of very large (more than 100 carbon atoms) PAH molecules present at various areas of the universe (Ricca et al. 2012). These reports suggest that PAHs are most abundant in universe also, comprising 10 to 20% of all total carbon (Allamandola et al. 1989). The analysis of meteorites also depicts the presence of PAHs (Plows et al. 2003). Therefore, it could be expected that some PAHs, possibly in trace amount, on Earth have come from outer space/universe.

2.5. Toxicity of PAHs

In 1880s, people working in coal tar industry and paraffin refinery and later, in 1920s, working with the organic extracts of soot were found to be affected by skin cancer. In 1933, benzo[a]pyrene was reported as the “coal tar carcinogen” by the British Chemist E. Kenneway (Waller 1994). Many PAHs have known to be toxic, mutagenic and carcinogenic in nature. Various literature reported about acute toxicity of LMW-PAHs, whereas HMW

PAHs are considered to be genotoxic (Goswami et al. 2018). Additionally, the structure-complexity of a PAH becomes more complex following substitution of the molecular structure; for instance, benz[a]anthracene is a fairly weak carcinogen, whereas 7,12-dimethylbenz[a]anthracene is a very potent carcinogen. Also, PAH intermediates produced by incomplete degradation (Kazunga and Aitken 2000) or photo-oxidized PAHs (McConkey et al. 1997) or nitrated PAHs (Bandowe and Meusel, 2017) or oxygenated PAHs (Walgraeve et al. 2010) are more toxic than the parent PAHs. In 2013, the World Health Organization (WHO) ranked $PM_{2.5}$ as Group 1 contaminants because of their carcinogenicity (IARC 2017).

A mixture of PAHs in the aquatic ecosystem can increase the genotoxic and carcinogenic potential of individual components (Delistraty 1997). PAHs are readily absorbed onto the gastrointestinal tract of mammals and are rapidly distributed in a wide variety of tissues, but accumulate primarily in adipose tissues of the body. Toxic effects of PAH exposure have been reported by the U.S. Agency for Toxic Substances and Diseases Registry (ATSDR 2009). Various studies performed on laboratory animals confirmed that PAH exerts toxicity by targeting the skin, blood and the lymph system (Wieczorek et al. 2015). Short-time exposure to high doses of PAHs is harmful to skin, which further leads to burning and itching and accumulation of fluid in tissues. Thus, PAHs presence in the environment is of serious health concern chiefly due to its bioaccumulation potential across the food chains (Das and Mukherjee, 2007).

2.6. Fate of PAHs in aquatic environment

2.6.1. Main Processes Affecting PAH Fate in the Aquatic Environment

Owing to their low solubility and high affinity, PAHs in the aquatic ecosystem are chiefly found adsorbed to particles that have either settled to bottom or suspended in the

water column. It is reported that approximately 67% of PAHs in the aquatic systems are associated with particles and 33% are present in dissolved form (Eisler 1987). PAHs present in sediments are predominantly bound to natural organic matter that considerably affects its distribution (Zhao et al. 2014). Usually, PAH-laden sediment deposits below the photolytic zone, and hence photodecomposition and oxidation are not promising. Thus, the main factor affecting the persistence of deposited PAH is microbial degradation (Cerniglia and Heitkamp 1989). Also, PAHs sorbed by sediments are available to organisms only after desorption into the dissolved phase. Therefore, a continuous dynamic exchange between PAHs in the solid and dissolved phases occurs; it has been reported that the most rapid biodegradation of PAHs occurs by such dynamic interface only (Latimer and Zheng 2003). But, PAH biodegradation rates in both natural sediment and water are inversely related to the number of fused benzene rings in the aromatic nucleus, aromatic complexity and the number of alkyl groups present at the rings. Therefore, it is expected that LMW-PAHs will biodegrade fast in comparison to the HMW-PAHs over time (Cerniglia and Heitkamp 1989). Such phenomenon can be utilized for the bioremediation of PAH-laden areas which are exposed to the incessant pollution. In general, volatilization and adsorption are the primary removal processes for HMW-PAHs, whereas volatilization and biodegradation are the major removal processes for LMW-PAHs.

2.6.2. Environmental regulations for drinking water and discharges into the surface waters

The criteria for all the sixteen enlisted parent PAHs designated by USEPA and EU as the priority pollutants have been studied and discussed for many decades. But the limits for PAH concentrations in drinking water have been defined only for few. The maximum contaminant levels (MCLs) for PAHs in drinking water as defined by USEPA are as

follows: benz [a] anthracene, 0.0001; benzo [b] fluoranthene 0.0002; benzo [k] fluoranthene 0.0002; dibenzo [a,h]anthracene 0.0003; indeno [1,2,3-c,d] pyrene 0.0004; (Table 2.2).

Table 2.2: PAH permissible limits for drinking water

Agency	Level (mg L^{-1})	Maximum contaminant levels
USEPA	0.0001	benz[a]anthracene
	0.0002	benzo[a]pyrene, benzo[b]fluoranthene, benzo[k]fluoranthene, chrysene
	0.0003	dibenzo[a,h]anthracene
	0.0004	indeno[1,2,3-c,d]pyrene
WHO	0.0007	benzo[a]pyrene
	0.00001	benzo[a]pyrene
	0.0001	benzo[b]fluoranthene, benzo[k]fluoranthene, benzo[g,h,i]perylene, indeno[1,2,3-c,d]pyrene

Recently, the National Institute for Public Health and the Environment (RIVM) in the Netherlands published a report (RIVM 2012) with specific ecological risk criteria for 16 EPA-enlisted PAHs. The reported limits for the individual PAH in water and sediment on the basis of studies conducted in various countries over 25 years are summarized in Table 2.3.

2.6.3. Analysis of PAH in environmental samples

Approximately 33 various types of PAHs including those enlisted by USEPA have been analyzed in environmental samples (Ma et al., 2013). Techniques such as gas chromatography (GC) and high-performance liquid chromatography (HPLC) and HPLC-fluorescence detection (HPLC-FL) are typically utilized for determining the environmental samples containing PAHs and their metabolites (Zhang et al. 2010).

Table 2.3: Risk limits for individual PAHs in the aquatic environment

Compound	$MAC_{eco,water}$ (μg L^{-1})	$MPC_{eco,water}$ (μg L^{-1})	$SRC_{eco,water}$ (μg L^{-1})
Naphthalene	130	2.0	518
Acenaphthalene	33	1.3	72
Fluorene	34	1.5	117
Phenanthrene	6.7	1.1	43
Anthracene	0.1	0.1	4.2
Pyrene	0.023	0.023	4.2
Fluoranthene	0.12	0.12	12
Chrysene	0.07	0.07	1.6
Benz[a]anthracene	0.1	0.012	3.1
Benzo[a]pyrene	0.01	0.01	0.87
Benzo[b]fluoranthene	-	0.017	1.3
Benzo[k] fluoranthene	-	0.017	0.93
Indeno[1,2,3-c,d] pyrene	-	0.0027	0.64
Benzo[g,h,i]perylene	0.0082	0.0082	0.16
Dibenzo[a,h]anthracene	0.014	0.0014	0.14

$MAC_{eco,water}$: maximum acceptable concentration for aquatic ecosystem;

$MPC_{eco,water}$: maximum permissible concentration for ecosystem;

$SRC_{eco,water}$: serious risk concentration for ecosystem

Fifteen kinds of US-EPA priority 16 PAHs were easily and sensitively examined, except for acenaphthylene because it is a non-fluorescent substance. On the other hand, other minor methods include GC-electron capture detection, LC-GC-MS, HPLC-ultraviolet (HPLC-UV), HPLC-photodiode array and HPLC-FL/UV detection methods are also used to identify PAHs in the environmental samples.

2.7. Remediation of PAHs Contaminated Environment

PAHs have an inherent hydrophobic property and affinity to get adsorbed onto the solid particulates (Kohl *et al.*, 2005). The most prompting parameters affecting PAHs sorption are their solubility of the aqueous medium whereas temperature, salinity and the presence of other dissolved organic matter also plays an important role for their removal (Huang *et al.*, 2003). In relation with the adsorption process for the remediation, adsorbed hydrophobic compounds show a declining availability from the aqueous medium. The toxicity values of sequestered hydrophobic compounds are quite different from the dissolved substances or weakly adsorbed compounds (Brion and Pelletier, 2005). Various physical, chemical and biological methods have been proposed for the remediation of PAHs contaminated wastewater (Venkata-Mohan *et al.*, 2006).

2.7.1. Physical methods

Of the various physical methods, liquid-liquid extractions (LLE), Liquid-phase micro-extraction (LPME), membrane filtration, usage of different adsorbents is well studied and applied techniques for wastewater remediation (Lagadec *et al.*, 2000). Although each of these techniques has some advantages, there are serious concerns regarding their usage either from the consideration of the environment or economics or both.

2.7.1.1. Liquid-liquid extraction

This remediation technique works on the principle of differential solubility performance of the target analytes (PAHs) in two immiscible solvents, typically water and an organic solvent. It includes the movement of analytes present in the aqueous solution into another immiscible solvent (organic solvent) that has more affinity for PAH binding (Pin and Rodriguez, 2014). LLE or solvent extraction is usually applied to the temperature-

sensitive target analytes where distillation fails and is among the oldest and most widely considered methods. This method has been considered for the removal and quantification of PAHs in contaminated water by environmental protection agency (EPA) having EPA number of 6440B (American Public Health Association et al., 2005). Generally, for the extraction or removal of PAHs from aqueous medium methylene chloride or a combination of methylene chloride and hexane is utilized. If the quantification of PAHs is needed, the extract is further concentrated and analyzed on gas chromatographic coupled with mass spectroscopy (MS) detector (American Public Health Association et al., 2005). However, there are still much concern regarding the usage of LLE for PAHs removal as it usually contains a high volume of toxic, flammable, volatile and sometimes chlorinated organic solvent.

2.7.1.2. Liquid-phase microextraction (LPME)

The rising emphasis on the clean environmentally remediation processes has subjected LLE to incessant denunciation owing to the high utilization of hazardous, combustible, volatile organic solvents and cost-ineffectiveness (Robles-Molina et al., 2013) which has led to the miniaturization of the LLE process to the liquid-phase microextraction process (LPME) (Ratola et al., 2008). whereby only a few µL of solvent is required to remove the analytes from aqueous solution rather than traditional LLE method that utilizes several mL of the solvents (Sarafraz-Yazdi and Amiri, 2010). They have further categorized into three broad types: single-drop microextraction (SDME) (Wu et al., 2008) hollow-fiber microextraction (HF-LPME) and dispersive liquid-liquid microextraction (DLLME) (Sarafraz-Yazdi and Amiri, 2010; Shi and Lee, 2010).

2.7.1.3. Filtration method

Filtration method is a process that removes solutes from fluids through a medium (filter) by permitting the fluid to pass and retains the solutes. It could either be mechanical, physical or biological. Membrane separation is the common technique used by the filtration process for PAHs removal. Considering the low size of the filtrate (PAHs), microfiltration has not really been considered for PAHs removal as the pore size of microfiltration membranes (MF) are much larger than the particle size of PAHs (Smol and Włodarczyk-Makuła, 2016). Thus, reverse osmosis (RO), forward osmosis (FO), nanofiltration (NF) and ultrafiltration (UF) are the most common processes used for PAHs removal.

2.7.1.3.1. Reverse osmosis (RO)

Reverse osmosis (RO) is a process that is power-driven by an external hydrostatic pressure that push the solution in against direction of natural osmosis through the membrane. There are various reports on the utilization of different membranes for PAHs removal from contaminated water. In the municipal wastewater, PAHs concentration was reported a removal efficiency of 81–86% using the commercially available SEPA CF-NP membrane. Also, for PAHs removal from the contaminated leachates, nylon membrane (ADF) was used as RO membrane. Nevertheless, many of the highly efficient membranes cannot be used for the RO process due to its high-pressure demand (2 MPa) leading to high energy demand (Smol et al., 2014).

2.7.1.3.2. Ultrafiltration

Ultrafiltration (UF) technique utilizes an external hydrostatic pressure that thrusts the sample through a semipermeable membrane that removes PAHs from the solution. It is commonly used to remove the particles with sizes > 10-20 nm that led to the disinfection of contaminated water by removing pollen, algae, fungi, bacteria, viruses, and organic solutes.

It also requires lesser pressure (0.1-0.2 MPa) to operate in comparison to RO. For PAHs and phthalates, retention coefficients ranged between 50.0–99.9% (Dudziak et al., 2004) whereas in the presence of humic acid, around 97% of anthracene was removal was achieved (Smol and WłodarczykMakuła, 2016; Yoon et al., 2004).

2.7.1.3.3. Nanofiltration

Nanofiltration (NF) is an another pressure-driven membrane filtration processes that retains some of the useful minerals in the water and uses smaller energy (Shon et al., 2013). NF are capable for selective removal of target solutes (small uncharged solutes) from the complex samples because its pore size is very small (~ 1 nm) (Shon et al., 2013). NF can be used for PAHs and pesticide removal from contaminated drinking water due to the strong hydrophobic interactions between these compounds and NF membrane (Sanches et al., 2011). However, the membrane fouling along with the pressure driven processes that require more energy and special apparatus requirements are the major issues related with RO, NF and UF (Mohammad et al., 2015).

2.7.1.3.4. Forward osmosis (FO)

For addressing the fouling and energy extensive nature of RO, NF, and UF, forward osmosis is recently explored as a potential filtration process that is relatively more advantages to the other pressure-driven methods with less energy demand and less prone to fouling along with a high water reclamation (Akinpelu et al., 2019). FO involves the natural osmotic pressure gradient to propel aqueous sample (low osmotic pressure) across the semipermeable membrane to the draw solution (high osmotic pressure) side (Zhao et al., 2012). Li et al., (2017) reported the removal of PAHs from landfill leachate by using FO technique. However, FO method is not commercially and practically viable as the process is extremely slow to match up with the present industrial need. This has led the researchers to

look for better membranes such as carbon nano-tubes (CNTs) or CNT-based materials (Das et al., 2014). In general, CNTs as nanofilters can be functionalized to improve its performance and making it more selective (Ong et al., 2010). Taking these into consideration, the application of CNTs in the filtration process could be useful for PAHs removal from contaminated wastewater with some better improvisations.

2.7.1.4. Adsorption

Adsorption is an another physical phenomenon in which the adhesion of the particles (pollutants) takes place onto surfaces or interfaces of the solid adsorbent through the interaction with contaminated water (Ali et al., 2012; Saleh 2018). It has commonly been used for PAHs removal of PAHs because it is very fast, simple to use and high recovery (Ma et al., 2010). Materials such as porous organoclay composite, matrix-immobilized organoclay, polyvinylidene fluoride, biochar and bamboo charcoal are considered to be the potential adsorbents for PAHs (Ma et al., 2010). However, for recovering high molecular weight (HMW)-PAHs is still a challenge thereby creating a need for further advancement (Ma et al., 2010).

2.7.1.4.1. Alkyl bonded silica sorbent

Bonding of alkyl chain (C1 - C30) to silica gel base material leads to the formation of alkyl-bonded silica adsorbent e.g., octadecyl (C18) (Spivakov et al., 2006). This alkyl bonded silica creates a hydrophobic phase leading to a stronger affinity for the hydrophobic compounds. Limam and Driss, (2013) reported the HMW-PAHs from the aqueous solution using a C18 cartridge in addition with 10% organic modifier. Li et al., (2007) examined the effect of alkyl chain length on PAH removal and have reported that with the increase in the number of carbon atoms, increases the distribution coefficients of PAHs in the porous layer of polymeric C18 (Ma et al., 2010).

2.7.1.4.2. Copolymer sorbents

Copolymer sorbents (CS) comprise of two monomers module in balanced proportion for instance, hydrophilic-lipophilic balanced polymers (HLB) e.g., lipophilic divinyl benzene vinyl pyrrolidone and hydrophilic N-vinyl pyrrolidone. Simultaneously, the hydrophilic component of CS helps in high mass flow of solution and lipophilic part deals with the reverse phase adsorption of PAHs in the flowing solution (Song et al., 2012). He et al., (2014) utilized the magnetic nanoparticles for organochlorine pesticides and triazine herbicides removal from contaminated water samples.

2.7.1.4.3. Magnetic sorbents

Recently, the magnetic solid-phase based sorbents is a new technique for the removal and concentration of target compound from a large volume of the sample (Gao and Chen, 2013). The magnetic or magnetizable adsorbents adsorb target analytes in the crude sample matrix and then the adsorbent with the adsorbate on it is further recovered from the solution by apt magnetic separator for its quantification analysis (Andrade-Eiroa et al., 2016; Zhang et al., 2011). Hayatsu, (1992) prepared cotton containing covalently linked copper phthalocyanine trisulphonate as magnetic SPE to remove PAHs from the complex sample matrix. Wang et al, (2013) demonstrated that microsphere-confined graphene adsorbent successfully extracted five PAHs from contaminated wastewater. However, the magnetic adsorbents are thermally thermally unstable during desorption procedures at high temperatures highly sensitive to pH (pH < 4.0) driving Fe (III) to form chelates with the target analytes such as sulfonamides (Andrade-Eiroa et al., 2016).

2.7.2. Chemical methods

Chemical oxidation method usually involves oxidants like ozone, hydrogen peroxide, permanganate and persulfate for the PAHs contaminated wastewater remediation. The oxidation processes of the chemical reactants generate highly reactive radicals that are capable of mineralizing PAHs, involving activated persulfate and perozone as the commonly utilized oxidants. Fenton's reagent is typically used in wastewater treatment for oxidation of PAHs (Bissey et al., 2006; Rivas, 2006; Bogan and Trbovic, 2003). Further, to examine the PAHs fractions, a series of extraction techniques are utilized including mild solvent extraction, cyclodextrin extraction, cosolvents addition, the addition of surfactants, supercritical fluid extraction, thermal desorption and persulphate oxidation (Maletić et al., 2019).

2.7.2.1. Supercritical fluid extraction (SFE)

SFE are well known to degrade the organic pollutants present in industrial wastewater that utilizes carbon dioxide (CO_2) alone or along with supercritical fluids to extract PAHs (Cui et al., 2013). Since the polarity of CO_2 is to the biological lipids and PAHs solubility in aqueous and supercritical CO_2 are similar (Hawthorne et al., 2007; Librando et al., 2004). It is used to evaluate sorption/desorption processes and to examine PAHs bioavailability in the sample.

2.7.2.2. Extraction with surfactants

To enhance extraction of PAHs from contaminated wastewater many studies have utilized surfactants (bio-based and artificial). Based on the type of source, the surfactants can be categorized as non-ionic, anionic or zwitter-ionic based on to the ionic charge of the hydrophilic group present (Paria, 2008). Those within two or more hydrophilic or hydrophobic groups are called gemini surfactants.

2.7.2.2.1. Synthetic surfactants

Ionic and nonionic synthetic surfactants have been broadly utilized for the PAHs remediation from the aqueous media (Mulligan et al., 2001). The solubilisation order of surfactants was found to be nonionic > cationic > anionic with logarithmic scale values of the micelle-water partition coefficient (K_m). Few example are: nonionic (Brij30 and Brij56), cationic (dodecyl ethyl dimethyl ammonium bromide, cetyl trimethyl ammonium bromide (CTAB) and anionic (sodium dodecyl sulfate) are very commonly used. Amongst all, nonionic synthetic surfactant (Tween80) is more biodegradable and less toxic than anionic and cationic surfactants and had also been mostly utilized.

2.7.2.2.2. Biosurfactants

Biosurfactants are well-reported to increase the apparent solubility of PAHs, which further facilitates their mobility and biodegradability (Tecon and van der Meer, 2010). Generally, there are two different types of biosurfactants: (a) microbial-based surfactants such as glycolipids (rhamnolipids, trehalolipids and sorphorolipids), lipopeptides, surfactins, lichenysin and phospholipids (Gudina et al., 2016; Vijayakumar and Saravanan, 2015) and (b) plant-based surfactants such as saponin, sapindus saponin and sapindus mukurossi (Blyth et al., 2015; Iglesias et al., 2014). They offer various potential advantages such as their economic production, biodegradability, low toxicity and a wide range of environmental resilience) compared to synthetic surfactants.

2.7.2.2.3. Gemini surfactants

They comprise of more than one hydrophobic and hydrophilic groups (anionic, cationic, nonionic, zwitterionic), that are joined by an alkyl spacer (Esumi et al., 1996) (for example: sodiumbis(2-ethylhexyl) sulfosuccinate (AOT), Brij56). The hydrophilic portions of gemini surfactants can be anionic sulfates, carboxylates, phosphates, cationic quaternary

ammoniums, nonionic polyethers, polysaccharides and complicated hydrophilic oligomers, while the hydrophobic portions are hydrocarbon chains (Wang et al., 2013).

2.7.2.3. Chemical oxidation

2.7.2.3.1. Ozonation

Ozone (O_3) is a highly reactive and powerful oxidizing agent that initiates the oxidation reactions by decomposing into $^{\bullet}OH$ radicals for the treatment of drinking water (Rositono *et al.*, 2001). In ozone oxidation process, PAHs undergo degradation either through the direct reaction or through the radical reaction as shown by the following expressions below, respectively (Miller *et al*., 2014):

PAH + O_3 = products

PAH + $^{\bullet}OH$ = products

Masten and Davies, (1997) reported that with the increase in structural complexity of PAHs leads to rise in hydrophobic nature there is decline in the removal efficiency by the ozonation method. Low molecular weight (LMW)-PAHs can be more effectively degraded by using ozone as the oxidizing agent (Jonsson et al., 2006).

2.7.2.3.2. Fenton method

Hydrogen peroxide (H_2O_2), a very well-known strong non-selective liquid oxidizing agents that has extensively been utilized for the environmental applications. The hydroxyl radicals ($^{\bullet}OH$) generated from hydrogen peroxide is able to react with PAHs at a very slow reaction rate. As a result, H_2O_2, is dosed together with a solution of a transition metal (ferrous ions) for increasing the peroxide oxidative strength by enhancing the radical formation (Flotron *et al.*, 2005; Watts and Teel, 2005). Further, in the modified Fenton's

system, the radical formation is enhanced by the addition of chelating agents along with high peroxide concentrations generating huge amount of hydroxyl radicals, viz. hydroperoxide radicals, superoxide anions and hydroperoxide anions (Watts and Teel, 2005). In comparison to ozone degradation efficiency (10-70%), Fenton's reagent is more efficient for PAHs degradation (40-86%).

2.7.2.3.3. Other oxidants

Alderman et al. (2007) reported the utilization of peroxy-acid along with hydrogen peroxide to oxidise PAHs by releasing a hydroxyl radical. Also, the feasibility of potassium permanganate ($KMnO_4$) as oxidant for PAH removal was evaluated and have shown good results (Brown et al., 2003). Various oxidants were also performed such as H_2O_2, modified Fenton's reagent, activated sodium persulphate, $KMnO_4$, and the combination of $KMnO_4$ and H_2O_2 for the PAHs contaminated wastewater remediation (Ferrarese et al. 2008).

2.7.3. Biological methods

Biological method of remediation refers to the application of biological systems or their products for degradation, mineralization or detoxification of target pollutants in a given environment. Biological treatment of PAHs has largely been reviewed by many researchers and reported that a catabolically diverse microbial community, consisting of bacteria, fungi and algae, along with some plants can metabolizes PAHs in the wastewater.

2.7.3.1. Plant assisted PAH biodegradation

Phytoremediation is an advanced bioremediation approach, which is highly ecofriendly technique for the remediation of PAHs contaminated soils. Plant roots accumulate these contaminants significantly in rhizospheric soil (Cunningham et al. 1996). Liste and Alexander (2000) reported the degradation of pyrene in soil assisted by plant.

They observed 74% removal of pyrene from vegetative soil which was planted while in unplanted soil only 40% remediation was observed in 8 weeks. Under greenhouse conditions, Lee et al. (2008) reported 74-94% removal of pyrene from soil planted with four korean native plant species, viz.., *Panicum bisulcatum*, *Echinogalus crusgalli*, *Astragalus membranaceus* and *Aeschynomene indica*, as compared to control (69%) in 80 days. Similarly, Cheema et al. (article in press) studied the degradation of PAH contaminated soil using *Festuca arundinacea*, reported a maximum removal of phenanthrene (91.7-97.8%) followed by of pyrene (70.8-90.0%) in planted soils as compared to unplanted soil. Authors depicted that enhanced removal of phenanthrene and pyrene in planted soil is due to the activity of increase in the activity of rhizospheric microorganisms.

However, at higher concentrations of phenanthrene and pyrene plant growth was greatly affected. It is quite evident from the previous research that phytoremediation is an eco-friendly and viable technique for remediation of soil contaminated with PAH, but it is a long term process and less efficient which makes this technique very less suitable. Gerhardt et al. (2009) also reported the inadequacy of PAH detection in PAH contaminated soil by analytical techniques making this technique less efficient.

2.7.3.2. Algae assisted PAH biodegradation

PAHs biodegradation needs a consortium of different hydrocarbonoclastic microorganisms in which algae is not an exception. Several literatures have reported about the prokaryotic and eukaryotic photoautotrophic marine algae (i.e. cyanobacteria, green algae, and diatoms) are capable of naphthalene mineralization (Narro et al., 1992; Cerniglia et al., 1980). There are several reports that naphthalene cishydroxylation by cyanobacteria, *Oscillatoria* and *Agmenellum* spp. follow similar pathways followed by fungus (Narro et al., 1992). Also, marine algae are known to biotransform benzo[a]pyrenec (BaP) to diols and

quinones in 5-6 days (Haritash and Kaushik, 2009). *Selenastrum capricornutum*, a freshwater green alga mineralizes BaP to cis-dihydrodiols using the dioxygenase enzyme (Warshawsky et al. 1995). Warshawsky et al., (1995, 1988) reported that PAHs is completely biodegraded by green algae only while yellow algae and blue green algae are not capable of PAHs mineralization. In 2003, it was firstly reported that algal-bacterial (*Pseudomonas migulae* and *Sphingomonas yanoikuyae*) microcosms are capable of biodegrading fluoranthene and pyrene in a single-stage treatment (Lei et al., 2007; Borde et al., 2003).

Another green alga *Chlorella sorokiniana*, cultivated different PAHs shows an inhibitory effect in the order: salicylate < phenol < phenanthrene. In a binary PAHs contaminated system (fluoranthene and pyrene) by *Chlorella vulgaris*, *Scenedesmus platydiscus*, *Scenedesmus quadricauda*, and *Selenastrum capricornutum* reported that the removal efficiency is dependent on the species-specific and toxicant-dependent. *Prototheca zopfii*, a heterotrophic green microalga was immobilized in polyurethane foam is capable of accumulating PAHs mixture in the matrix (Ueno et al., 2008). *S. costatum* and *Nitzschia* sp. algae enriched from mangrove ecosystem were capable of phenanthrene and fluoranthene biodegradation (Hong et al., 2008). Henceforth, the literature clearly depicted that algae are well-capable of PAH biodegradation and also can co-metabolically mineralize PAHs with bacteria.

2.7.3.3. Bacterial biodegradation of PAHs

In recent decades, degradation of low molecular weight PAHs (phenanthrene and naphthalene) and high molecular weight PAHs by bacteria has been investigated. The HMW PAHs (pyrene and fluoranthene) mineralizing bacteria belongs to *Mycobacterium* and *Rhodococcus* genera. Benzo[a]pyrene has not been utilized by bacteria as a sole carbon

source (Juhasz and Naidu, 2000), resulting in low rate of mass transfer of HMW-PAHs within the bacterial cell for sustaining the metabolic requirements. Johnsen et al. (2005) hypothesized that the low availability of PAH in soil has prevented the evolution of PAH degrading pathway in bacteria. Among all genera, *Mycobacterium* sp. has been given great attention due to its ability to mineralize 3 -, 4 - ring PAHs (Wick *et al.*, 2003).

Willumsen et al. (2001) isolated novel PAH degrading *Mycobacterium frederiksbergense* from soil which mineralizes pyrene, phenanthrene and fluoranthene as sole carbon source. Under aerobic conditions, many bacteria are reported to utilize PAHs as sole carbon source with analogous metabolic pathways. The preliminary step for PAHs mineralization follows PAH oxidation to dihydrodiol involving various enzymes. These dihydrodiol is further converted to either ortho- or a meta- cleavage pathway leading to generation of protocatechuates and catechols, which then enters the tricarboxylic acid cycle (Samanta et al, 2002). Stingley et al. (2004a) reported the presence of multiple pathways in some microorganisms for degradation of specific PAHs. Many reserachers extensively study the *Mycobacterium vanbaalenii* PYR-1 due to presence various alternative PAHs degradation pathways (Kim *et al.*, 2007). It has been proposed that Mycobacterium vanbaalenii PYR-1 have both cytochrome P450 monooxygenase and dioxygenase(s) for mineralizing PAHs (Brezna et al., 2006).

2.7.3.4. Fungal biodegradation of PAHs

Among all fungal species, ligninolytic fungi are able to degrade PAHs due to the secretion of extracellular oxidative enzymes (Bogan and Lamar, 1996; Pointing, 2001). The presence of extracellular lignolytic system in white rot fungi are able to degrade PAHs that are difficult for other fungi. Eggen and Majcherczyk (1998) studied the PAH degradation by *Pleurotus ostreatus*. They reported that benzo[a]pyrene was efficiently degraded by 28%

and 40% within a month from creosote contaminated and spiked soil, respectively, and further incubation enhanced the degradation. Though, in spiked soil complete mineralization of benzo[a]pyrene (1.0%) was not achieved due to white rot fungus, while in absence of fungus it was less than 0.1%. Zheng and Obbard (2002) investigated the LMW and HMW PAHs degradation in in soil-slurry, solid phase, and surfactant solubilised systems by *Phanerochaete chrysosporium*. In presence of fungus, phenanthrene, fluoranthene and pyrene degradation was efficiently increased by 43% in soil-slurry system as compared to control. However, in same system degradation of chrysene, benzo[a]pyrene and dibenz[ah]anthracene was very low. In contrast, benzo[a]pyrene was oxidized efficiently in surfactant solubilised systems to a 0.35% residual. Valentin et al. (2006) reported the chrysene, pyrene, fluoranthene and phenanthrene biodegradation by nine white rot fungal species from forest and salt marsh soils. Among all fungal species, *Bjerkandera adusta* (67%), *Irpex lacteus* (55%) and *Lentinus tigrinus* (53%) showed significant degradation of PAHs within 30 days. Additionally, >80% pyrene degradation was observed in PAHs mixture by these fungal species. Baborová *et al.* (2006) isolated and purified manganese peroxidase (MnP) enzyme from *Irpex lacteus*. They studied the *in vitro* degradation of PAH by MnP enzyme and found 92% and 100% degradation of pyrene and anthracene, respectively, within 168 h at an initial concentration of 15 mg L^{-1}. The degradation of PAHs by non-lignolytic fungi is carried out by cytochrome P450 (CYP450) enzyme by converting them into less reactive intermediate, which is further excreted out by conjugating with soluble moiety. Cerniglia and Gibson (1979) investigated the biodegradation of benzo[a]pyrene by *Cunninghamella elegans* and found 18% benzo[a]pyrene was converted to water soluble conjugate in 96 h.

2.8. Biodegradation of PAHs mixture

Although the degradation of PAHs individually is today, a well-established study, but their degradation in complex mixtures (in multi-contaminated system) is drawing the researcher's interest. Degradation of PAHs in mixture (both in presence of organic as well as inorganic contaminants) may result in inhibition, cometabolism, augmentation or no effect at all (Goswami et al., 2017c). McNally et al. (1999) reported in presence of phenanthrene, inhibition in pyrene degradation by *Pseudomonas putida*. Tiehm and Fritzche (1995) observed the inhibition of pyrene degradation by fluorene in a pure culture of a *Mycobacterium* sp. grown on pyruvate. Inhibition to PAHs biodegradation in a multi-contaminated system suggests that multiple PAHs are degraded utilizing the common enzymatic pathways leading to competition for the active sites of enzymes (Stringfellow and Aitken, 1995).

Some reports were there utilizing mixed consortia rather than pure cultures to biodegrade PAH in mixtures and have depicted a great potential in mitigating the observed inhibition effects. Such mixed cultures displayed a complementary degradative action, and hence, showing a greater tolerance for the recalcitrant and harmful products. Also, co-metabolism is an another mode through which the degradation of PAHs without generation of energy and carbon for the cell metabolism as a non-specific enzymatic reaction with a substrate competing with structurally similar primary substrate for the enzyme's active site. An example is the co-metabolism of benzo[a]pyrene by bacteria growing on pyrene (Boonchan *et al.*, 2000). Pure culture of *Pseudomonas* sp., unable to use fluoranthene as sole carbon source, can biodegrade the PAH in presence of phenanthrene (Bouchez *et al.*, 1995).

2.9. Biomass gasification wastewater

Amongst the various thermo-chemical energy conversion technologies, biomass gasification offers the potential, efficient and sustainable conversion of the solid biomass into synthetic gases (H_2 and CO) (Park et al., 2016; García-Labiano et al 2016). It can be defined as thermo-chemical conversion in which biomass is being converted to renewable energy, biofuels, and chemicals, utilizing gasifying agents such as air, oxygen, steam, carbon dioxide etc. for the syngas production (Goswami et al., 2017a, Kaisalo et al., 2016).

The generated synthesis gas needs to be purified before it can be utilized for the energy production in which tar is generated as the undesirable by-product (Kaisalo et al., 2016). Tar is the major component within the biomass gasification wastewater (BGWW) that is generated during the wet scrubbing of the syngas, primarily consisting phenols, heterocyclic compounds, monocyclic and polycyclic aromatic hydrocarbons (PAHs) (Goswami et al. 2018; Tian et al., 2005). Also, there is a huge deviation in the chemical oxygen demand (COD) ranging from 920-1,60,000 mg L^{-1} which is attributed mainly to the presence of diverse organic compounds present in the wastewater (Goswami et al., 2017b). Besides this, the generated wastewater is toxic, mutagenic and carcinogenic in nature and is harmful to the living organisms and the environment, therefore, sufficient treatment has to be performed prior to its discharge into the environment (Samanta et al., 2002).

Tar is distinct organic bituminous oil which occurs along with the producer gas in the vapor phase and is difficult to remove with the simple condensation or cleaning process (Prando et al., 2016). It may lead to the clogging of filters and valves, turbine fouling along with corrosion of the metallic machinery and thereby is one of the major hurdles in the commercialization of this gasification technology (Ahrenfeldt et al., 2013, Anis and Zainal, 2011). Though there are several methods/technologies like proper modifications in the

gasifier set up along with its processing by which tar reduction can be made possible. But in the midst of these modifications, there is an ample reduction in the syngas production. Henceforth, more focus can be put on the proper tar treatment (tar-cracking reactors and mechanical gas filtration) (Prando et al., 2016) or conversion of tar into some economical and efficient end-product.

Until now, no reports are there on the biological treatment of biomass gasification wastewater using any bioreactor or even at lab-scale. Though few literatures are there on the physicochemical treatment, they produce huge hazardous substituent in addition to the treatment process. Meanwhile, the bioremediation is an eco-friendly, economic and potential alternative for BGWW treatment. Microorganisms belonging to the Actinomycetes, are well capable to grow by utilizing BGWW as the sole carbon substrate for their growth and metabolic activity and are able to transform the toxic wastewater (BGWW, dairy, paper and pulp, PAHs etc.) into simple compounds (Goswami et al. 2017c). In addition, the lipid accumulated by the strain, ranging from 14-87% (w/w, cell dry weight (CDW)), is of high calorific value in assessment with the proteins and carbohydrates and is more promising than other biofuels because of its technical and economic feasibility (Kumar et al. 2015).

2.10. Different bioreactor systems for PAH contaminated wastewater

2.10.1. Stirred tank bioreactor

Recently, Paul et al., 2019, treated petroleum wastewater containing PAH in a stirred tank bioreactor. The reactor was initially operated in different operating modes including batch, fed-batch, sequential batch, continuous and continuous with cell recycle using low cost tubular ceramic membrane. Among the different strategies, the continuous cell recycle system proved efficient in terms of complete removal of chemical oxygen

demand (COD) (99%) and high lipid production (86%, w/w) at a hydraulic retention time (HRT) of 16 h (dilution rate of 0.06 h^{-1}).

2.10.2. Rotating biological contractor bioreactor

Jeswani and Mukherji (2015) reported the biological treatment of simulated biomass gasification wastewater of varying strength in a rotating biological contactor (RBC), bioaugmented with *Exiguobacterium aurantiacum*, and operated at HRT of 24 h depicted consistent high removal efficiency ranging in between 91% - 92%. Greater than 74% removal was observed for all the components although the influent concentration of phenolics and heterocyclics were much higher compared to the PAHs. Abiotic loss in absence of the biofilm was consistently low (12 - 20% COD removal). Treatment was accompanied by noteworthy reduction in acute toxicity. The biofilm consisting of *E. aurantiacum* and mixed microbial consortium thus have a good potential for removal of these toxic constituents.

2.10.3. Membrane bioreactor system

Hybrid reactor systems are very well suited for treating wastewater containing PAHs. In this system, biological treatment is followed by chemical processes or vice-versa based on the treatment requirements. Biological system comprising of either aerobic or anaerobic systems are found to be suitable for treating PAHs. Activated carbon based adsorption method is effective in removing PAHs. MBR process is efficient to treat PAH contaminated wastewater even at an elevated concentration, wherein the other treatment techniques, particularly the constructed wetland is found to be ineffective (Kasprzyk-Hordern et al., 2009). Thus, a combination of these methods called hybrid treatment systems can be applied for treating wastewater containing PAHs. For e.g., a hybrid system using

MBR followed by oxidation process is beneficial for the complete removal of PAHs from wastewater (Gruchlik et al., 2018; Babuponnusami and Muthukumar, 2014)

Over the past two decades, membrane bioreactors (MBRs) have been designed and operated for treatment of a variety of pollutants, such as particulates, carbonaceous substances, nutrients and pathogenic microorganisms (Mir-Tutusaus et al., 2018). Compared with these pollutants, which can be removed easily by conventional methods, the removal of certain other pollutants, particularly the PAHs is often very different. Therefore, examination of the fate and removal of PAHs during wastewater treatment is very much crucial for any of the treatment process to avoid their discharge into the environment (Luo et al., 2014).

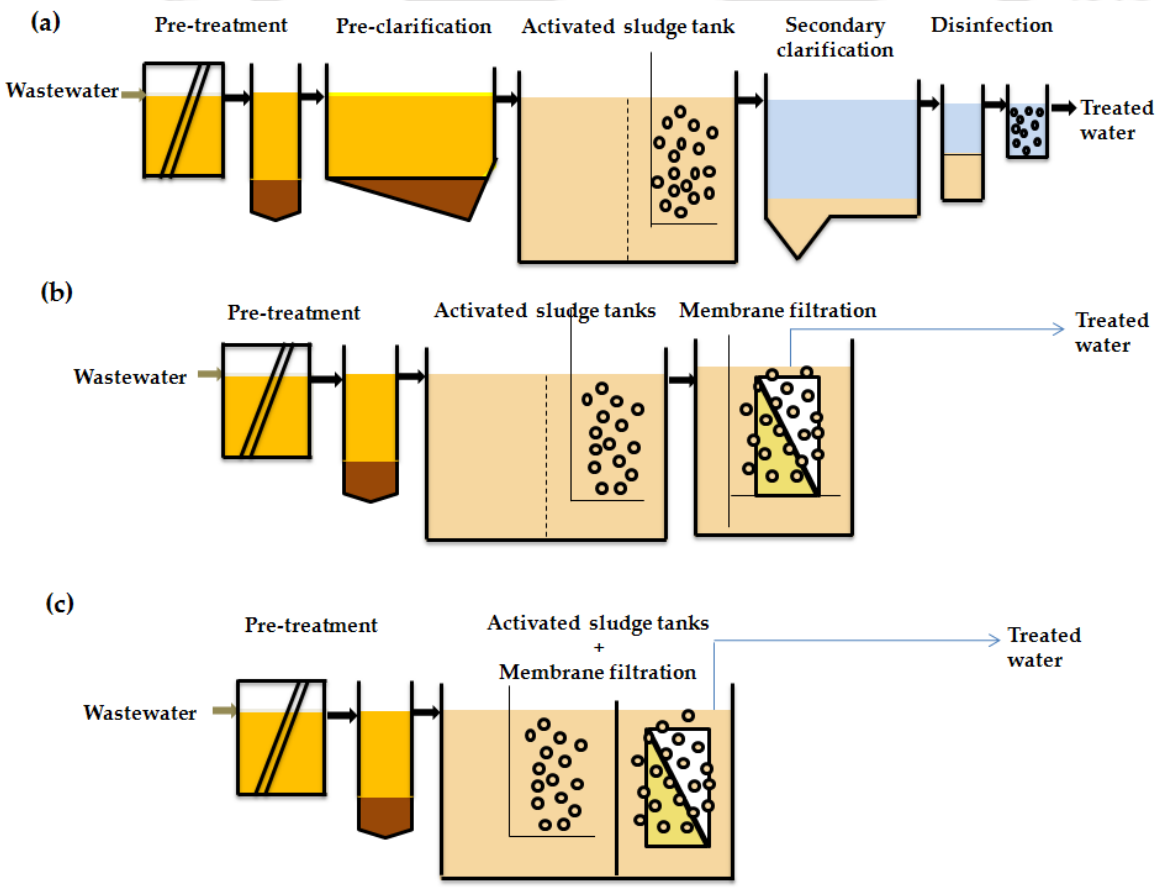

Fig. 2.2: Scheme of the (a) conventional wastewater treatment process, (b) Side stream MBR (c) submerged MBR

Membrane bioreactor (MBR) systems seem to be promising under this scenario, due to their several advantages, including high performance efficiency compared to conventional activated sludge treatment plant (CASP), less space requirement, environment friendliness (Judd, 2010). MBR is a hybrid process integrating the membrane technique with biological treatment, which enables CASP to be operated as a single step process by avoiding the need for a secondary clarifier. Fig. 2.2 compares the conventional wastewater treatment process with that employing MBR technology.

Also, Table 2.4 enlists various advantageous and limitations of MBR system for PAHs removal. In general, MBR system is categorized into two kinds in accordance with the configuration; (1) submerged membrane bioreactor (SMBR) and (2) side stream membrane bioreactor. Fig. 2.3 shows a brief schematic of MBR system. Earlier the side stream MBR was developed where the membrane module is placed outside the bioreactor for the recirculation pump. Due to its high energy consumption, in 1980s, submerged-MBR system was further developed where the membrane module was submerged within the bioreactor, thus, permitting the effluent to pass through with sludge retention. In a SMBR, aeration maintains the activated sludge in suspended mode, limiting the membrane fouling.

2.10.4. Different integrated MBR systems and hybrid processes for PAHs removal

Integrated approaches involving MBRs with some other processes such as advanced oxidation process (AOPs), membrane distillation process, bio-entrapped membrane bioreactor, granular MBRs, etc. are of recent focus as these combined processes improve permeate quality, mitigates membrane fouling problem and enhance the treatment efficiency. Fig. 2.3 represents a brief schematic of different types of integrated MBR systems for PAHs contaminated wastewater treatment.

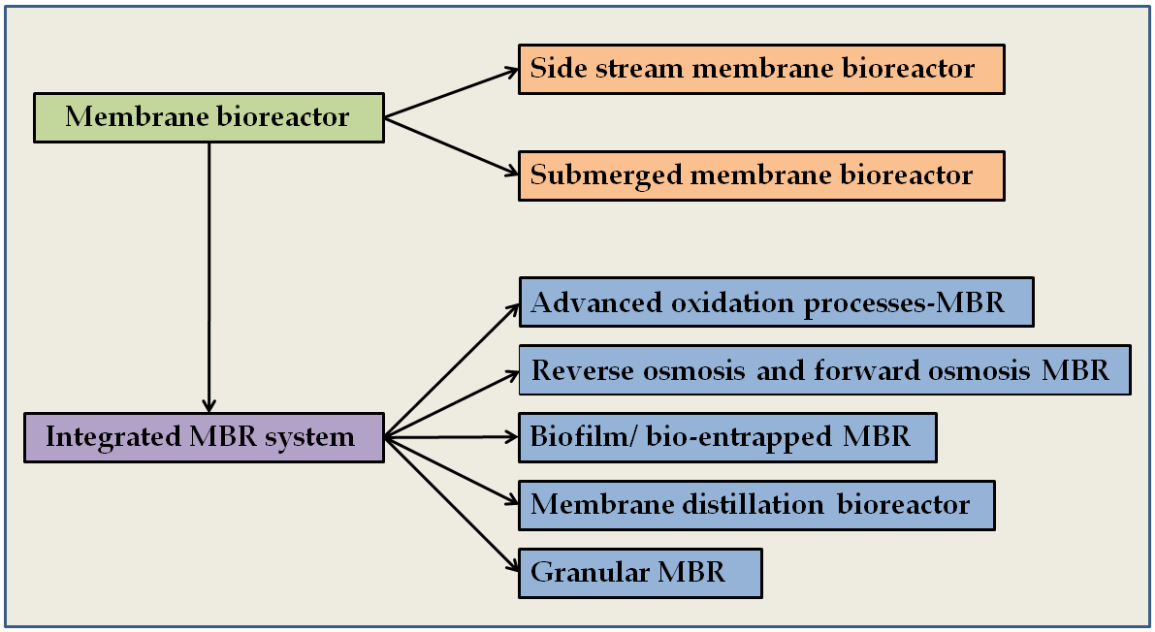

Fig. 2.3: An overview of MBR and integrated MBR systems

Table 2.4: Different advantages and limitations of MBR system for wastewater treatment

S. No.	Advantages
1.	PAHs removal can be achieved upto the discharge limits
2.	Low working space is required and lower foot print
3.	Utilized as a pre-treatment technique for RO and NF with excellent effluent quality
4.	Full retention of bacterial flocs with the membrane
5.	Membrane perform the biomass retention
6.	Perform at elevated solid retention time (SRT)
7.	Faster removal of PAHs
8.	High MLSS (10-15 g L^{-1}) and high SRT depicts low sludge yield
9.	Low feed to microorganism ratio (F/M)
	Limitations
1.	Membrane fouling
2.	No significant removal of micropollutant when activated sludge process and MBR operate at comparable SRT. Enhanced removal efficiency could be achieved integrated approach
3.	Requires high energy input to aerate MLSS and to reduce the membrane fouling

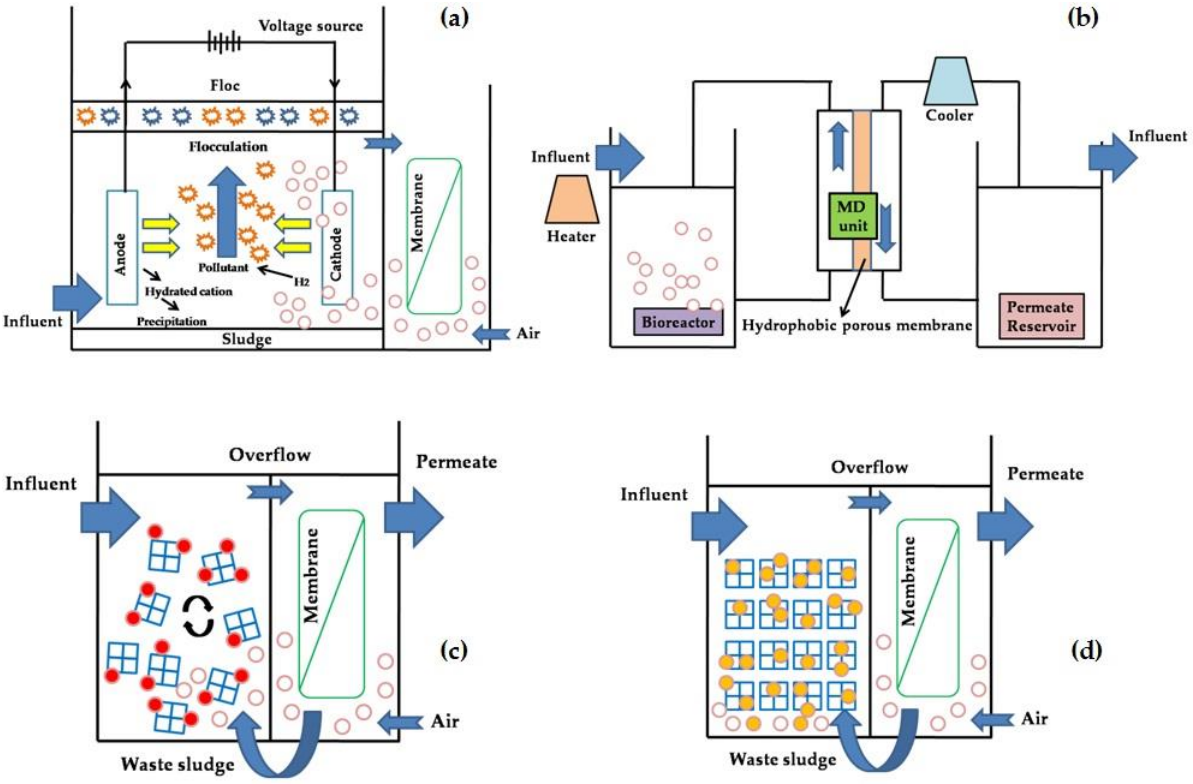

Fig. 2.4: Schematic diagram of some hybrid MBR systems (a) electrocoagulation augmented an external side stream membrane bioreactor system (b) MDBR with an external side stream membrane (c) Biofilm-Membrane Bioreactor (BF-MBR) and (d) Bio-entrapped-Membrane Bioreactor (BE-MBR)

2.11. Statistical Design of Experiments

Experiments are always considered the main tool for practically validating a theoretical hypothesis about scientific knowhow of a process or phenomenon, where the observation is Chapter 2 Literature Review expected to be correlated with some known associated process parameters. In order to identify important factors and their contribution towards an observed response, normal approach of using one-variable-at-a-time (OVAT) involves a large number of experiments to be carried out which often cannot elucidate any significant interaction among the process variables (Ryan et al., 2007). Statistical experimental designs are potent tools for improving the efficiency of experimentation and

they facilitate a better understanding of the system being investigated with a minimum number of experiments. Inclusion of replicate test conditions allows the estimation of random, experimental variation. Statistical analysis of data generated from such experiments clearly establishes the relationship between the measured parameter of interest (response) and the process parameters (input factors or factors) being studied. Details of statistical design of experiments are presented in Appendix.

2.12. Aim and Objectives

This study was aimed at biodegradation of polycyclic aromatic hydrocarbons by oleaginous *Rhodococcus opacus* and its bioenergy potential.

To accomplish this aim, the following investigations were carried out:

1. Biodegradation of polycyclic aromatic hydrocarbon contaminated wastewater by *Rhodococcus opacus* for potential biodiesel application

2. Biological treatment of wastewater containing a mixture of polycyclic aromatic hydrocarbon using *R. opacus*.

3. Simultaneous heavy metal removal and polycyclic aromatic hydrocarbon biodegradation by oleaginous bacterium *R. opacus*.

4. Biomass gasification wastewater treatment and lipid production by *R. opacus* for the biodiesel production.

5. Biochar derived from biomass gasification effluent: Preparation, characterization and application in simultaneous anthracene degradation and lipid accumulation by *R. opacus*

6. An integrated biodegradation-microfiltration system for sustainable wastewater treatment and bioenergy recovery

7. Upflow packed bed bioreactor with biochar immobilized polyurethane foam as the packing material for wastewater treatment

8. An integrated continuous system using stirred tank bioreactor and tangential microfiltration system for simultaneous biomass gasification wastewater treatment and bioenergy recovery.

2.13. Presentation and Layout of the Thesis

The present thesis covers five chapters with appropriate sections and subsections and also contains references and visible research outputs. A brief description of these chapters is mentioned as follows:

Chapter 1 details introduction of the present work. The biodegradation of polycyclic aromatic hydrocarbon contaminated wastewater using oleaginous *Rhodococcus opacus* for bioenergy production, in both simulated and real wastewater utilizing BGWW using two different types of bioreactors systems is detailed in **Chapter 2**. This chapter also deals with various technologies for bioremediation of PAHs contaminated wastewater. Also, the effect of other contaminants that affect the performance of different bioreactors and details the various bioreactors applied for treating PAHs containing wastewater and objectives and scope of the present work were presented. Materials and methods followed in the research work are described in **Chapter 3**. It details the methodology followed for analyzing and quantifying PAHs in the single and multicomponent systems and its characterization. Further, details of PAHs biodegradation using two different continuously operated laboratory scale bioreactor systems and analytical methods followed in this study

are mentioned. **Chapter 4** mainly presents and discusses the results of biodegradation of PAHs contaminated wastewater in both batch and continuous systems and the biodegradation pathway involved. This chapter thoroughly describes the PAHs biodegradation results obtained using the two continuously operated laboratory scale bioreactor systems. Summary and conclusions drawn from this study are presented in **Chapter 5**. Some useful recommendations and scope for future work are also provided in this chapter.

CHAPTER 3

MATERIALS AND METHODS

3. Materials and methods

3.1. Microorganism and culture conditions

The present chapter describes about the microorganism used, culture conditions, different techniques and methods followed in this research. The bacterium, *Rhodococcus opacus* DSM 43205 used in this study, was obtained from Microbial Type Cell Culture (MTCC, Chandigarh, India). It was maintained by sub-culturing on Luria Bertani (LB) agar plates at 4ºC and preserved in 20% (v/v) glycerol at -80ºC. For PAHs biodegradation experiments, the bacterium was cultured using Bushnell-Hass minimal salt medium (MSM) containing (g L^{-1}): $MgSO_4 \cdot 7H_2O$ (0.409), $CaCl_2 \cdot 2H_2O$ (0.0265), KH_2PO_4 (1), NH_4NO_3 (1), $Na_2HPO_4 \cdot 12H_2O$ (6) and $FeCl_3 \cdot 6H_2O$ (0.0833) and 1% (v/v) of each trace metal solution, i.e., 50 µL trace elements ($FeCl_3$ (17), $CaCl_2$ (0.6), $ZnSO_4$ (0.2), $CuSO_4 \cdot 7H_2O$ (0.2), $MnSO_4$ (0.2), $CoCl_2$ (0.8), H_3BO_3 (0.1), and $Na_2MoO_4 \cdot 2H_2O$ (0.3)) (Lee and Cho, 2009). The medium pH was adjusted to 7. The growth conditions followed were 30°C temperature and 120 rpm agitation speed.

3.2. Chemicals and reagents

Naphthalene and phenanthrene were obtained from Merck (Hohenbrunn, Germany), whereas anthracene and fluoranthene were purchased from Hi-Media Pvt. Ltd., India, with purity greater than 99% for each. All chemicals except solvents used throughout this study were of analytical grade and supplied by either Hi-Media Pvt. Ltd., India, LOBA Chemie Pvt. Ltd., India, SRL Chemicals Pvt. Ltd., India, Merck India Ltd., or CDH Pvt. Ltd., India. HPLC grade solvents such as acetone, dichloromethane and acetonitrile were obtained from Spectrochem (Mumbai, India). Membrane filtered water (reverse osmosis (RO)) was used for carrying out all experiments in the study (Sartorious, Arium 61316RO & 611UF, Germany).

3.3. Batch biodegradation of PAHs and lipid accumulation by *R. opacus*

3.3.1 Single component system

3.3.1.1. PAHs biodegradation and lipid accumulation by *R. opacus*

For PAHs biodegradation by *R. opacus*, a seed culture of the bacterium was first prepared by growing the microorganism in 250 mL Erlenmeyer flask containing 100 mL MSM with an initial PAHs concentration of 20 mg L^{-1}. The flask was incubated for 48 h at 30°C and 120 rpm in an orbital incubator shaker. For inoculation, a loop full of the microorganism from freshly cultivated agar slants containing the bacterium was used. The bacterial cells were later obtained by centrifugation (10000×g, 15 min) and washed twice with sterile Milli-Q water. The bacterium was re-grown overnight using 100 mL MSM containing 20 mg L^{-1} of the respective PAHs, present individually. Such freshly grown bacterial cultures from the mid-logarithmic grown phase were subsequently utilized as the inoculum (10% v/v) for all the batch experiments. At regular time intervals, samples were withdrawn from the flasks and were examined for biomass culture growth, residual PAHs concentration, cell dry weight (CDW) and lipid accumulation. All the experiments were performed in triplicates with 100 mL of working volume using 250 mL Erlenmeyer flasks containing MSM, inoculum and an initial PAHs concentration in the range 50-500 mg L^{-1}. The results reported are average of triplicate sample analyses with standard error. Stock solution of the selected PAHs was prepared individually utilizing 10% dichloromethane (Mahanty et al. 2008). For determining any abiotic loss of PAHs during the experiments, measurements from control flasks without the inoculum were considered and the following eq. (1) was used to determine the % PAH degradation:

$$PAH\ bio\deg radation(\%)=\left(\frac{\left(C_0-C_f\right)-C_n}{C_0}\right)\times 100 \qquad (1)$$

where C_o is the initial PAH concentration; C_f and C_n are the final PAH concentrations in the test and control flasks, respectively.

Residual concentration of PAHs in the biomass excluded samples was quantified using a high-pressure liquid chromatograph (HPLC) (Varian Prostar 210, The Netherlands) outfitted with C-18 column (Thermo hypersil) of dimensions 100 mm × 4.6 mm and a UV- detector set at 254 nm. Acetonitrile and water in the ratio 70:30 and at a flow rate of 1 mL min^{-1} was provided as the mobile phase for the analysis.

To examine the biomass growth, cell dry weight (CDW, mg L^{-1}), was determined. The CDW analysis consisted of centrifuging 5 mL of culture broth at 10,000×g for 15 min and washing the cell pellet twice with MilliQ water, followed by lyophilizing and weighing. Specific growth rate (μ) was analyzed by the following equation:

$$Specific\ growth\ rate\ (\mu)=\left(\frac{1}{X}\frac{dX}{dt}\right) \qquad (2)$$

where μ: biomass specific growth rate (h^{-1}), X: biomass concentration expressed as (w/w) CDW (mg L^{-1}) corresponding to time (h). Furthermore, the experimental data was fitted with two different kinetic models (Table 3.1) for determining the bio-kinetic constants in this study.

Table 3.1: Bio-kinetic models tested in this study

S. No	Model	Equation	References
1.	Monod model	$\mu=\frac{\mu_{max}[S]}{K_s+[S]}$	Sinharoy et al. 2015

2. Haldane model

$$\mu = \frac{\mu_{max}[S]}{K_s + [S] + \frac{[S^2]}{K_i}}$$

μ = specific growth rate (min^{-1}), μ_{max}= maximum specific growth rate (min^{-1}), [S] = concentration of PAH (mg L^{-1}), K_s= half saturation constant (mg L^{-1}), K_i= inhibition constant (mg L^{-1}), I = Inhibitory concentration of PAH (mg L^{-1}).

3.3.1.2. Total lipids analysis, characterization and transesterification

Lipid content in the biomass was determined by the standard chloroform and methanol extraction procedure with minor modifications (Axelsson and Gentili, 2014; Folch et al. 1957). Briefly, the biomass was harvested by centrifugation at 10,000×g for 10 min. The obtained pellet was then homogenized with a 20 mL mixture containing chloroform and methanol (2:1 ratio), followed by 15-20 min. of shaking in an orbital shaker set at ambient room temperature. The homogenous mixture was centrifuged to obtain the liquid stream and the solvent was rinsed with either 20% (v/v) of water or 0.9% (v/v) NaCl solution. For separating the two phases, the mixture was centrifuged at a low speed (4500×g) after vortexing; whereas the top phase was siphoned off, the lower chloroform phase containing the lipids was evaporated. Finally, the lipids extracted were quantified by gravimetric analysis.

For ^{1}H and ^{13}C Nuclear Magnetic Resonance (NMR) analyses of the extracted lipid, spectrum was recorded at 600 MHz (Bruker Biospin AG, Switzerland). Chemical shifts were given in ppm with tetramethylsilane (TMS) vapor as the internal reference with deuterated chloroform ($CDCl_3$) as the solvent.

The bacterial lipids were transesterified by heating with 1 mL methanol containing 10% (v/v) H_2SO_4 and 1 mL chloroform. The methanolysis conditions were 80°C temperature and 2 h incubation time under constant shaking. Hexane was added

after completion of the reaction, and the obtained mixture was centrifuged at 8000×g for 10 min. Following centrifugation, two layers were obtained with the top layer containing FAMEs and the bottom layer containing glycerol. The top layer was gently pipetted out and transferred into another vial. The resultant solvent and the FAMEs mixture were subjected to rotary vacuum evaporator to remove the solvent (Kumar et al. 2015).

3.3.1.3. Biodiesel characterization and its properties

For characterization of the FAMEs produced by transesterification of the lipids, a gas chromatograph (Varian 450 GC, Agilent Technologies, USA) with a flame ionization detector and CP-Sil 8CB column was used (Kumar et al. 2014). A FAME mix (Sigma–Aldrich, USA) was used as the standard for this GC-FID analysis.

Properties of the biodiesel (FAMEs) produced by transesterification of the bacterial lipids, in terms of its viscosity (η), pour point (PP), cloud point (CP), cetane number (CN), saponification value (SV), iodine value (IV) and degree of unsaturation (DU), were evaluated using the following empirical equations (Kumar et al. 2014; Su et al. 2011; Francisco et al. 2010).

$$\eta = 0.235 M_{CN} - 0.468 M_{ds} \quad (3)$$

$$CN = 3.930 M_{CN} - 15.93 M_{ds} \quad (4)$$

$$CP = 0.526\left(P_{FAME}\right) - 4.992 \quad (5)$$

$$PP = 18.80 W_C - 1.0 M_{UF} \quad (6)$$

$$SV = \frac{\sum\left(560 \times PC_F\right)}{M_r} \quad (7)$$

$$IV = \frac{\sum\left(256 \times PC_F \times N_{db}^0\right)}{M_r} \qquad (8)$$

$$DU = M_{MUFA} + \left(2 \times M_{PUFA}\right) \qquad (9)$$

where M_{CN} is the weighted average number of carbon units in the FAMEs, M_{ds} is the weighted average number of double bonds, M_{UF} represents the total unsaturated FAME content (% weight), P_{FAME} is the percentage content of palmitic acid methyl ester, PC_F is the percentage of each fatty acid, M_r is the molecular mass of the individual fatty acids, N_{db} is the number of double bonds, M_{MUFA} is the monounsaturated fatty acids (% weight), M_{PUFA} is the polyunsaturated fatty acids (% weight).

3.3.1.4. Microscopy analysis of *R. opacus* biomass and lipids

R. opacus biomass and the accumulated lipids were observed under a field emission scanning electron microscope (FESEM, Zeiss, Sigma, Germany) and a transmission electron microscope (TEM, JOEL, JEM2100, Japan), respectively. For FESEM analysis, one milliliter sample was centrifuged at 10000×g for 10 min, washed with sterile milliQ water. The pellet obtained was diluted 10 times with milliQ water and vortexed. A single drop of this bacterial sample was deposited at the top of a specimen stub and was further, coated with gold utilizing an auto fine coating instrument (JEOL JFC-1300) prior to its observation under FESEM. Similarly, for TEM examination of the lipid globules, one drop of this sample was loaded on a copper grid coated with carbon at 200 kV for TEM analysis. The sample was dried in the ambient air prior to TEM analysis.

3.3.2. Biodegradation of PAHs in a multi-component system

3.3.2.1. PAH biodegradation and lipid accumulation by *R. opacus*

Based on the results obtained from the previous study on biodegradation of PAHs in the single component system using *R. opacus*, the PAH concentration at which the strain showed the best biodegradation efficiency was chosen for studying PAHs biodegradation in a multi-component system. In this study, different combinations of high and low concentration levels of three PAHs of different aromaticity, *viz.* naphthalene (2-ring), phenanthrene (3-ring) and fluoranthene (4-ring) were chosen employing the Full-factorial design of experiments. Analysis of variance (ANOVA) and student's *t* test were then applied for statistical analysis of the results to interpret the significance and effect of these PAHs on each other biodegradation and lipid accumulation. The Full-factorial design of experiments employed in this study consisted of eleven experimental runs with different combination levels of naphthalene, phenanthrene and fluoranthene (Table 3.1). The low and high concentration levels of each of the PAHs were chosen as 50 and 200 mg L^{-1}, respectively.

Initial PAHs concentration levels mentioned in Table 3.2, as +1 or -1 indicate the high or low level of the PAHs, whereas 0 indicate center point level of the PAHs. The statistical software Minitab (Version 16, PA, USA) was used for statistical analysis of the results obtained.

Batch biodegradation of a mixture of naphthalene, phenanthrene and fluoranthene using *R. opacus* was studied similar to the previous experiments by culturing the microorganism in 250 mL Erlenmeyer flasks with 100 mL of MSM at pH 7. The flasks were incubated in an orbital shaker at 30°C temperature and 120 rpm with each PAH at

an initial PAH concentration as per Table 3.2. Samples were withdrawn every 24 h for the analysis of bacterial biomass, residual PAH concentration and lipid accumulation. Control flasks without the bacterium were maintained and examined to confirm any abiotic loss of PAH during the experiments, with identical initial concentrations of NAPH, PHEN and FLOR. Analysis of biomass, PAHs and lipids were carried out as mentioned previously (Section 3.3.1.1). All the experiments were performed in triplicate and the arithmetic mean was reported.

Table 3.2: 2^3 Full Factorial experimental design matrix showing different combination levels in the mixed PAHs biodegradation study along with the initial concentrations

Experimental Run No.	NAPH[a]	PHEN[a]	FLOR[a]
1	50 (-1)	50 (-1)	200 (+1)
2	200 (+1)	50 (-1)	200 (+1)
3	200 (+1)	200 (+1)	50 (-1)
4	200 (+1)	50 (-1)	50 (-1)
5	125 (0)	125 (0)	125 (0)
6	125 (0)	125 (0)	125 (0)
7	125 (0)	125 (0)	125 (0)
8	50 (-1)	200 (+1)	50 (-1)
9	200 (+1)	200 (+1)	200 (+1)
10	50 (-1)	50 (-1)	50 (-1)
11	50 (-1)	200 (+1)	200 (+1)

[a] NAPH: Naphthalene; PHEN: Phenanthrene; FLOR: Fluoranthene

Intermediate metabolites formed during PAH biodegradation were analyzed utilizing a liquid chromatography-mass spectrometry (LC–MS) system (WATERS, Q-Tof Premier, USA) equipped with a capillary ACQUITY UPLC® BEH shield RP 181.7 µm C–18 column (10 × 50 mm length). For LC-MS analyses, the aliquots were extracted twice with ethyl acetate under neutral conditions, and the ethyl acetate phase was

separated by centrifugation at 10,000 × g for 15 min at 4°C. Ethyl acetate extracts so obtained were combined and then acidified with 1 mL HCl (0.1 M) (Ghosh et al., 2014). The ethyl acetate containing the dissolved metabolites was filtered using a 0.2 μm nylon membrane syringe filter prior to the LC-MS analysis. For the elution of metabolites using HPLC, an isocratic flow was used (Sahoo et al. 2011). An acetonitrile-water solvent (60:40, v/v), metabolites were detected using a TOF/Q-TOF mass spectrometer under negative electrospray ionisation mode (ESI).

3.3.2.2. Toxicity test

To determine the reduction in toxicity due to PAH biodegradation by *R. opacus*, the Resazurin reduction method was followed with some inconsequential modifications (Kargi and Eker, 2004). A mixed bacterial culture isolated from sludge collected from a local wastewater treatment plant at IIT Guwahati was used. The change in colour from blue to pink indicated the reduction of resaruzin by dehyrogenase enzyme activity of the bacterium (Sahoo et al. 2011). The results of initial toxicity (%) and toxicity removed (%) were determined using the following equations (10) and (11), respectively.

$$Toxicity\,(\%) = \frac{(P-Q)}{(R-Q)} \qquad (10)$$

where P: optical density of the multi-component system, either initial or final; Q: optical density of the cell control; R: optical density of the control sample containing only reagent water and no test microorganisms.

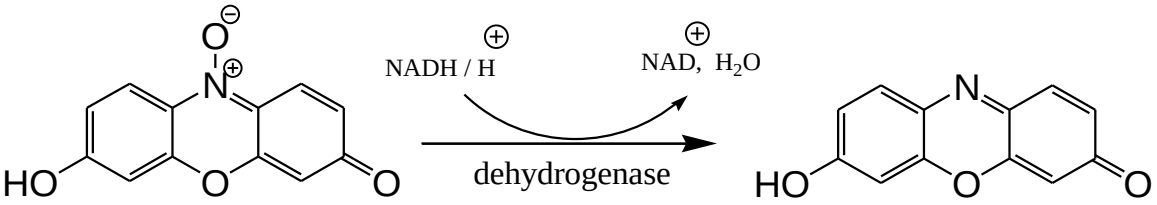

Resazurin
(Blue 610 nm)

Resorufin
(Pink 580 nm)

$$Toxicity\ removal\ (\%) = 1 - \frac{(\%Toxicity)_{Final}}{(\%Toxicity)_{Initial}} \qquad (11)$$

where (% Toxicity) $_{Final}$ and (% Toxicity) $_{Initial}$ are the percentage toxicity of the multi-component system at final and initial time, respectively.

3.3.3. Effect of heavy metals on PAH biodegradation

Individual metal stock solutions of six different heavy metals viz., iron (Fe (III)), copper (Cu (II)), zinc (Zn (II)), cadmium (Cd (II)), nickel (Ni(II)) and lead (Pb (II)) of concentration 1000 mg L^{-1} each were prepared using $FeCl_3$, $CuCl_2.H_2O$, $ZnCl_2$, $Cd(NO_3)_2$, $NiCl_2$, and $PbNO_3$, respectively. Anthracene was selected as the model PAH for determining the effect of heavy metals on PAH biodegradation. For inoculum preparation, 1 mL of the culture obtained at its mid-logarithmic growth phase was centrifuged (10000×*g*, 10 min) to obtain pellets of intact bacterial cells. Following resuspension of the intact cells in MSM, 5% (v/v) of these bacterial cells were inoculated into 250 mL Erlenmeyer flask containing MSM and anthracene at an initial concentration in the range 50-200 mg L^{-1}. The final volume was made up to 100 mL by adding the individual heavy metal stock solution so to achieve an initial concentration of 10 mg L^{-1} in the flasks. The initial concentration used in the present study was chosen based on a literature study by Pavasant et al. (2006) and Kiran et al. (2016) and for heavy

metals removal using microalgae and anaerobic sludge, respectively. 10% DCM was then added to dissolve the PAH. Flasks with no inoculum, but with the heavy metals, anthracene and MSM were used as the control in these experiments. All the flasks were placed in an orbital incubator shaker set at 120 rpm and 30°C. Sample aliquots were taken at regular time intervals for quantitative analysis of *R. opacus* biomass, lipids, residual anthracene and heavy metals.

Analysis of *R. opacus* biomass, anthracene concentration and lipid accumulation in the withdrawn samples was carried out as described earlier. Heavy metal concentration in the samples was analyzed by atomic absorption spectroscopy (AAS) (Varian, AA240, The Netherlands) as per the American Public Health Association standards (APHA 2005).

The specific anthracene uptake rate and specific lipid accumulation rate by *R. opacus* were estimated as per the following equations (2 and 3, respectively):

$$Specific\ anthracene\ uptake\ rate\ (q_A) = \left(\frac{1}{C_p} \frac{dC_p}{dt} \right) \qquad (12)$$

$$Specific\ lipid\ accumulation\ rate\ (q_L) = \left(\frac{1}{C_L} \frac{dC_L}{dt} \right) \qquad (13)$$

In the above equation, q_A is the specific anthracene uptake rate (h^{-1}), q_L is the specific lipid accumulation rate (h^{-1}), C_p and C_L are the concentrations (mg L^{-1}) of anthracene and lipid corresponding to time t (h), respectively.

3.3.3.1. Characterization of the bacterial biomass

3.3.3.1.1. FESEM and TEM analyses

Changes in *R. opacus* surface morphology observed due to simultaneous uptake of heavy metals and anthracene were examined by field emission scanning electron microscopy (FESEM) (Zeiss, Sigma, Germany). The bacterium grown in presence of both anthracene and Cu as the heavy metal was used for this analysis. 1 mL of the bacterial culture was centrifuged (10000×g, 10 min) and washed twice with sterile milliQ water. The pellet obtained was diluted 10 times with milliQ water and vortexed. Unit drop of this sample was mounted on aluminum stubs over double sided carbon tape and dried overnight at 30 °C prior to the analysis. Following drying, the sample was coated with thin gold layer by sputter coater before observation under FESEM. The spectra obtained were compared with the biomass grown in the absence of anthracene and heavy metals.

For determining the effect of heavy metals and anthracene on the size of the lipid accumulation by *R. opacus*, transmission electron microscopy (TEM) (JOEL, JEM2100, Japan) analysis of the biomass grown in presence of these pollutants was carried out. Single drop of the sample, prepared as mentioned earlier under FESEM analysis, was casted on copper grid coated with carbon (Tedpell, U.S.A.) and dried overnight at 30°C before the analysis (Section 3.3.2.4).

3.3.3.1.2. FTIR and FESEM-EDX analyses

Infrared spectroscopy of the biomass grown in presence and absence of the pollutants was carried out by Fourier transform infrared (FTIR) spectrometer with attenuated total reflectance (ATR) attachment under dry air at room temperature

(PerkinElmer, Spectrum Two, Singapore). Sample aliquots were centrifuged (10000 × g, 10 min) followed by washing with distilled water and the pellets obtained were vacuum dried prior to FTIR analysis. The samples were uniformly mixed with KBr in 100:1 ratio. The analysis was performed over the entire wavenumber range with 20 consecutive scans at a 4.0 cm^{-1} resolution. FTIR spectra were taken under the transmittance mode.

For FESEM-EDX analysis, biomass samples were vacuum dried and mounted on aluminum stubs over double sided carbon tape followed by double coating with thin gold layer by sputter coater.

3.4. Biochar aided PAH biodegradation by *R. opacus*

3.4.1. Biochar preparation from biomass gasification effluent

Biomass gasification effluent was collected from a pilot scale biomass gasifier at IIT Guwahati, Assam, India. Crude biochar was separated from the wastewater by gravity settling followed by drying and washing with the organic solvent, dichloromethane. For choosing the best solvent, four different organic solvents, viz., acetone, methylene chloride, dichloromethane (DCM) and ethyl acetate, were tested to remove tar and other impurities associated with the crude biochar. Among the four solvents, DCM proved the best. The solvent was recovered from the mixture using a rotary vacuum evaporator (R-210, Buchi, Switzerland). Biochar pH was measured after every solvent washing step by mixing the biochar with deionized water at 1:20 ratio (Cao et al., 2016). The procedure was repeated until final pH of the biochar reached 7.

Cost involved in the biochar preparation was estimated considering the cost of raw materials utilized and equipment operating cost for purifying the sample, as reported by Mahanty et al. (2010). However, other input such as manpower and instrument cost

were not taken into account in order to keep the cost analysis simple and to validate the economic viability of the process. The cost estimation was carried out in three steps: (1) cost of the raw materials used (2) purification cost of biochar and solvents used during the preparation and (3) power requirements for operating a rotary vacuum evaporator for recovering the solvent used.

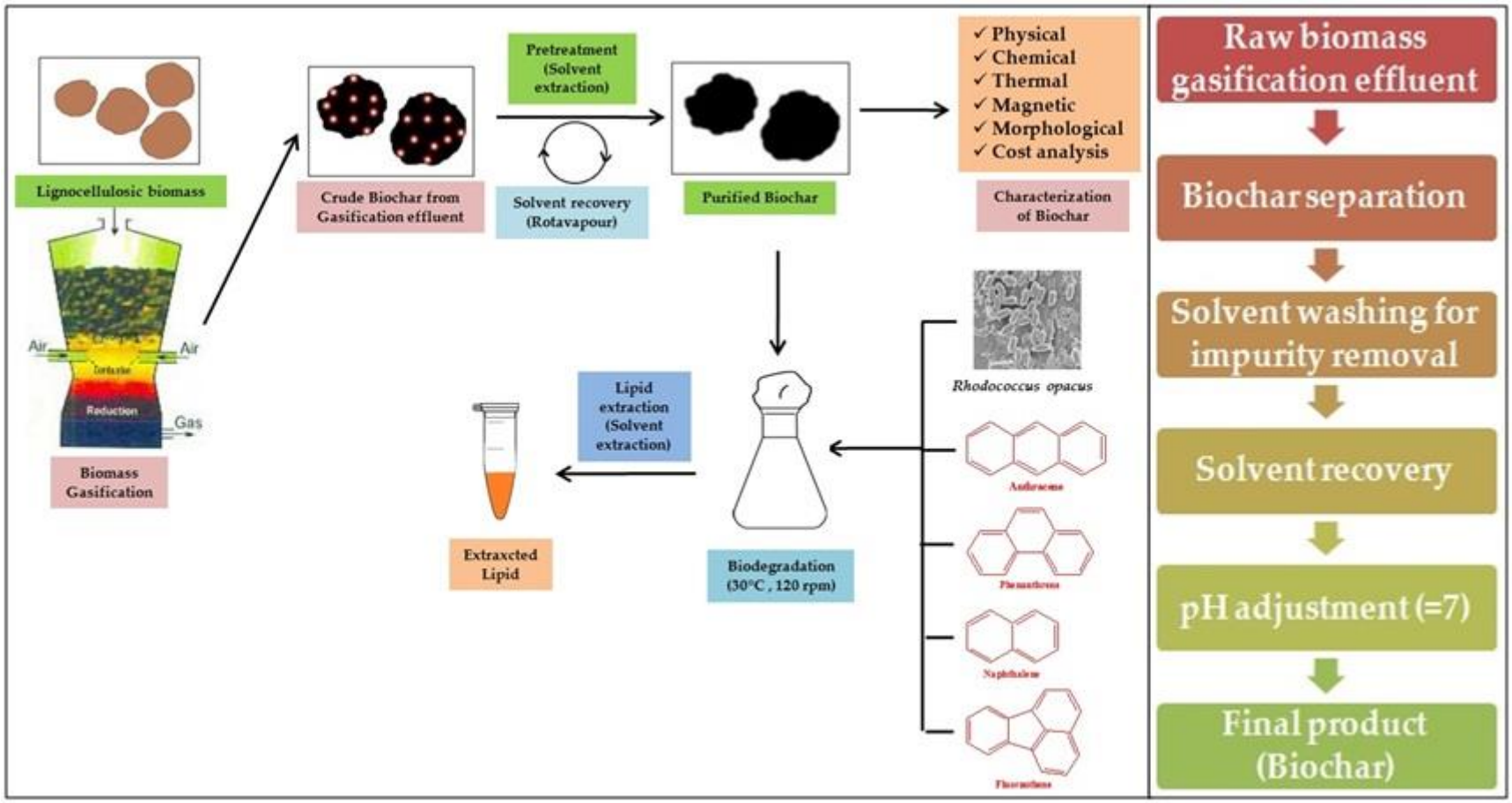

Fig. 3.1: Biochar preparation steps followed in this study

3.4.2. Biochar characterization

Biochar derived from biomass gasification effluent was characterized for its chemical, physical, surface, thermal and magnetic properties.

3.4.2.1. Physical properties

Biochar ash content was determined following the ASTM D1762-84 standard (Bind et al., 2018). Elemental composition of the biochar was examined using an elemental analyzer (Eurovector EA3000, Germany). Zeta potential (ZP) and average particle size were measured using a laser particle size analyzer (Delsa^{TM} Nano, Beckman Coulter). For contact angle (CA) measurement, the sessile drop method was followed (Bachmann et al., 2013). Surface morphology of biochar was analyzed by using a field emission scanning electron microscope (FESEM, Zeiss Sigma, Germany) at ultra-high resolution, and for which a biochar sample was mounted on copper stub using a double stick carbon tape and coated with a fine thin layer of gold for making it conductive prior to the FESEM analysis (Goswami et al. 2017b). Brunauer-Emmett-Teller (BET) analysis of the biochar was carried out to determine its surface area by N_2 multilayer adsorption at ambient temperature using Autosorb-IQ MP instrument (Quantachrome, USA).

3.4.2.2. Chemical properties

Functional groups present on the biochar surface was examined by Fourier transform infrared (FTIR) spectroscopy (IR Affinity-1 Shimadzu) whereas crystallization behavior of the biochar was determined using X-ray diffractometer (XRD) (D8Advance, Bruker AXS, Germany) utilizing CuKα as the radiation source. The XRD profile was recorded at 45 kV and 40 mA in the 2θ range of 7 - 70º at a scale rate of 0.05º per 0.5 s.

Raman Spectra of the sample were scanned in the range 100–3600 cm^{-1} with LabRam HR, Horiba, Japan, equipped with an air cooled charge coupled device detector.

3.4.2.3. Thermal and magnetic properties

Biochar thermal behavior was examined by Thermogravimetric (TG) analysis using Mettler Toledo TGA/SDTA 851® (Schwerzenbach, Switzerland). Biochar sample of weight 8 mg was placed on 150 µL platinum crucibles under N_2 atmosphere and heated in the temperature range 25 - 700 °C and at 10°C min^{-1} rate.

Magnetic property of the biochar was determined using a vibrating sample magnetometer (VSM-7410 series, Lake Shore Cryotronics, USA) and presented in the form of hysteresis loop for calculating the saturation magnetization of the material (Nguyen et al. 2011).

3.4.3. Effect of biochar on simultaneous PAH biodegradation and lipid accumulation by *R. opacus*

R. opacus seed culture was prepared by growing the strain using MSM with all the four previously mentioned PAHs (25 mg L^{-1}) as the sole source of carbon and energy. The cells were harvested at the mid-logarithmic phase by centrifugation (10000×g, 10 min), followed by washing twice with 0.01 M phosphate buffer solution (PBS) twice. The cells were then re-suspended in 250 mL Erlenmeyer flask containing MSM so as to yield a bacterial cell concentration of 10^7 colony forming units (CFU) mL^{-1} which served as the inoculum for PAH biodegradation in this study. Individual stock solutions of PAHs were prepared with dichloromethane (DCM) and the solution was filter sterilized through 0.2 µm nylon membrane filter. A suitable amount of this solution was transferred into 250 mL Erlenmeyer flask using a glass micro syringe. The flasks

were then kept for few hours in the fume hood along with cotton plug for evaporating the solvent.

MSM was finally supplemented to these flasks prior to inoculation with the bacterial seed culture. Four different flasks with a working volume of 100 mL each were set up to determine the effect of biochar on PAH biodegradation by *R. opacus*. All the flasks contained 50 mg L^{-1} of initial PAH concentration and supplemented with 0, 50, 100 or 200 mg L^{-1} of the biochar and labeled as Flask 1, 2, 3 and 4, respectively.

Following inoculation, the flasks were incubated in a rotary shaker (120 rpm) set at 30°C in the dark for avoiding any photo-degradation of the PAH. Control flasks without any added inoculum were prepared to account for any abiotic loss of PAH supplemented with the biochar. All these experiments were performed in triplicates and the error bars represent standard error in the experiments.

3.4.4. Determination of bacterial growth, PAH biodegradation and total lipid content

Bacterial growth profile using PAH along with different initial biochar concentration was studied employing the colony counting method (Ghosh et al. 2014). The culture was initially grown in MSM along with different initial biochar concentration as mentioned earlier. During the experiments and after every 24 h time period, samples taken from the flasks were suitably diluted before transferring it onto the nutrient agar plates. Colonies obtained on these plates were enumerated to determine viable cell count in the experimental flasks. Analysis of PAHs and lipids in the samples were carried out as described earlier.

3.4.5. Morphology of *R. opacus* and contact angle measurement

Morphological difference in *R. opacus* grown in presence and in absence of the biochar was examined by FESEM analysis at 1 kV with 5 mm scanning area. For this analysis, bacterial cell samples were obtained from both the experimental and control flasks. 1 mL each of the samples were centrifuged (10000×g, 10 min), followed by washing twice with sterile milliQ water, and the harvested samples were further diluted 10 times with milliQ water and vortexed (She et al., 2016). A unit drop of the obtained bacterial sample was further mounted on aluminum stubs over double sided carbon tape and dried overnight at 30 °C prior to the analysis. After drying, the prepared sample was double-coated with a thin gold layer by sputter coater prior to final observation under FESEM (Section 3.3.2.4).

For determining the mechanism of action of biochar on the biodegradation of PAHs by *R. opacus*, contact angle measurement experiments were carried out with biomass samples taken before and at the end of the biodegradation experiments by the sessile drop method (Bachmann et al. 2013).

3.5. Biomass gasification wastewater (BGWW) treatment by oleaginous *R. opacus* and biodiesel production

3.5.1. Source and characterization of BGWW

Biomass gasification wastewater was collected from a pilot scale downdraft biomass gasifier plant at the Indian Institute Technology Guwahati, Assam, India and was stored at 4°C until further use. The wastewater characterization, including color, pH, chemical oxygen demand (COD), turbidity, dissolved oxygen (DO), mixed liquor

suspended solids (MLSS) and mixed liquor volatile suspended solids (MLVSS) was carried out as per the Standard Methods (Table 3.3) (APHA, 2005).

3.5.2. Batch shake flask experiments

Biomass growth along with lipid accumulation by the bacterium using BGWW were analyzed under batch condition employing 250 mL Erlenmeyer flasks with a working volume of 100 mL each containing the wastewater with or without any added minimal salt medium (MSM). For evaluating simultaneous lipid accumulation and wastewater COD removal by *R. opacus*, five experimental flasks were set up along with 5% (v/v) of *R. opacus* seed culture as the inoculum. Flask 1 contained only BGWW, whereas flasks 2, 3, 4 and 5 contained MSM and BGWW in different proportions of 1:1, 1:2, 1:3 and 1:4, respectively. To determine the effect of inoculum size, a similar set of flasks (6-10) along with 10% (v/v) of *R. opacus* seed culture was set up. All these flasks were incubated in a rotating orbital shaker set at 30°C and 120 rpm for 6 days. The initial pH was adjusted to 7 with 1M HCl. Prior to the experiments suspended solids present in the raw wastewater were removed by centrifugation at 3500×g for 10 min. At every 24 h time interval, samples were taken and analyzed for biomass growth, lipid accumulation and COD.

Table 3.3: Composition of the raw BGWW used in this study

Parameter	**Biomass gasification**
Color	Pale yellow
pH	7.27
Conductivity (mS cm^{-1})	889
COD (mg L^{-1})	2157
Turbidity (NTU)	8.13
DO (mg L^{-1})	4.68

TDS (mg L^{-1})	41.24
TKN (mg L^{-1})	1.57
Total nitrate (mg L^{-1})	0.98
Total phosphate (mg L^{-1})	2.7
Total sulfate (mg L^{-1})	15.3
Total chloride (mg L^{-1})	12.8
MLSS (mg L^{-1})	1228
MLVSS (mg L^{-1})	941

*All the values were having a standard deviation ±5%

3.5.2.1. Analysis of *R. opacus* biomass, total lipid and COD removal

R. opacus biomass growth profile was determined by measuring optical density (OD) of the culture at 660 nm wavelength using a UV-visible spectrophotometer (Agilent Technologies, Cary 100 series, Singapore). Lipid analysis was carried out as described earlier.

COD content in the samples were analyzed by following the closed reflux method as per the Standard Methods (APHA, 2005). In this method, 2.5 mL of a suitably diluted sample taken in COD vials was added with 1.5 mL of standard potassium dichromate digestion solution (0.016 M) and 3.5 mL of sulfuric acid reagent, and the mixture was digested using a COD digester (Hach, DRB 200, USA) at 150 °C for 2 hours. Later, the solution mixture was cooled to room temperature and titrated against ferrous ammonium sulfate (FAS) solution (0.1 M) using ferroin as the indicator. A sharp color change from blue green to brick reddish was considered as the end point. Reverse osmosis water was used as the blank in the COD analysis. The FAS solution was standardized against standard 0.1 M $K_2Cr_2O_7$ digestion solution. COD in the sample was calculated using the following equation 14 and was expressed as mg O_2/L.

$$\text{Chemical oxygen demand (COD) (mg } O_2\text{/L)} = \frac{\text{(A-B)} \times 8000 \times \text{M}}{\text{V mL (Sample)}} \qquad (14)$$

where, A is the volume of FAS consumed by the sample, B is the volume of FAS consumed by blank solution and V is the sample volume, and M is the molarity of FAS solution used.

3.5.2.2. Lipid characterization and transesterification

Thermogravimetric analysis (TGA) was carried out for proximate analysis of the lipid sample in order to determine the moisture content, volatile matter, mass loss, ash and crude lipid content. For the TGA analysis using Mettler Toledo TGA/SDTA 851® (Schwerzenbach, Switzerland), samples were placed on 150µL platinum crucibles under N_2 atmosphere and heated in the temperature range 25-700°C and at 10°C/min rate.

Transesterification of the bacterial lipids to produce biodiesel was performed as described previously in Section 3.3.1.2. The FAMEs produced in this study was characterized using the empirical formulas mentioned previously in Section 3.3.1.3.

Also, the infrared spectra were analyzed by Fourier transform infrared (FTIR) spectrophotometer (IR Affinity-1 Shimadzu) from 500 to 4000 cm^{-1} for determining the functional groups present in the biodiesel product (Section 3.4.2.2).

3.6. Integrated biodegradation- microfiltration approach

For simultaneous separation of the *R. opacus* biomass and removal of residual COD following batch treatment of BGWW by *R. opacus*, a laboratory scale microfiltration system was utilized. Preparation and characterization of the low-cost ceramic membrane for microfiltration are detailed in Monash and Pugazhenthi (2011). Fig. 3.2 shows the experimental set-up of the microfiltration system used under cross-

flow mode at various applied pressure in the range of 34-172 kPa. All experiments in this study to evaluate the performance of the integrated biodegradation-microfiltration to treat BGWW were carried out under batch conditions and were carried out in triplicates. The percentage error for all the experimental data was within ±3.5% of their actual values. After every experimental procedure, the membrane was cleaned and regenerated by first wiping the membrane surface to remove any deposited slurry and recover the bacterial biomass (Monash and Pugazhenthi, 2011). For biodegradation, the experimental conditions followed were the same as mentioned earlier, i.e. 30°C temperature and 120 rpm agitation after the inoculation.

For calculating removal of residual COD present in the BGWW following the microfiltration step, equation (15) as shown below was used.

$$R\,[\text{Removal},(\%)] = 1 - \frac{C_p\,[\text{COD in permeate}]}{C_f\,[\text{COD in feed}]} \times 100 \qquad (15)$$

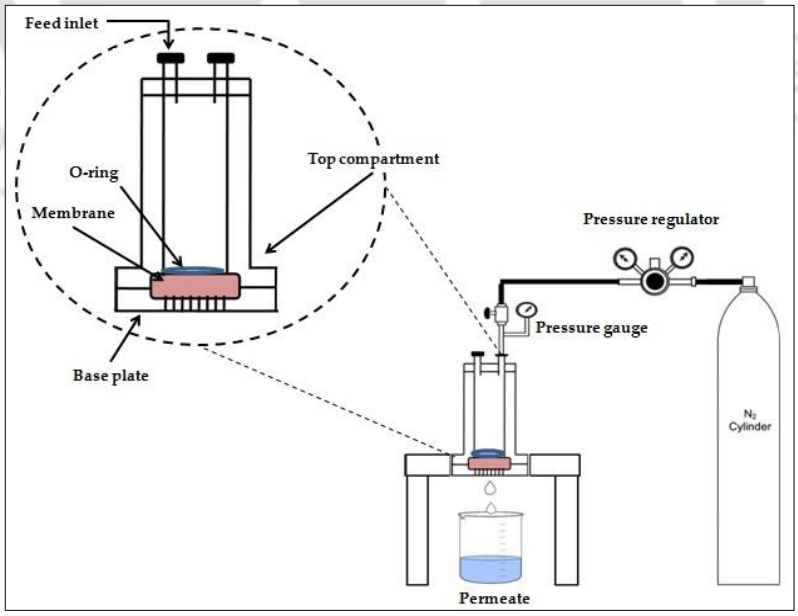

Fig. 3.2: Schematic showing the microfiltration set up in the integrated biodegradation-microfiltration approach for BGWW treatment

For determining the toxicity of the treated BGWW: Resazurin reduction method as described in Section 3.3.2.2.

Bacterial cells with intracellular accumulated lipids were observed under a field emission scanning electron microscope (FESEM, Zeiss, Sigma, Germany). Nile red staining was examined for the localization of intracellular bacterial lipids through fluorescence microscopy (Carl Zeiss AXIO SCOPE A1, Germany). A stock solution of Nile red was prepared in dimethyl sulfoxide (1 mg mL^{-1}). For staining the cells, 1:100 ratio of the dye and bacterial cells was used.

3.7. Upflow packed bed bioreactor with biochar immobilized polyurethane foam as the packing material

3.7.1. Bioreactor setup and BGWW treatment

A laboratory scale up-flow packed bed bioreactor (UFPBR) was fabricated using a perspex cylinder. The specification of UFPBR and its different components are presented in Table 3.4 for the prime bioreactor unit. Polyurethane foam (PUF) cubes of size 1 cm^3 each was utilized as the supporting material for bacterial growth owing to its high surface area and high porosity. The PUF cubes were initially rinsed with 70% (v/v) ethanol, washed thrice with double deionized water, autoclaved (120°C, 20 min), rewashed twice by soaking in 0.5 N HNO_3 and kept overnight at 85°C for drying prior to its use as a supporting material. About 760 g of the prepared oven dried PUF was kept inside the bioreactor. The temperature of bioreactor was maintained at the ambient temperature (30 ± 2 °C). Temperature, pH and dissolved oxygen (DO) concentration were continuously examined in the outflow.

For biomass immobilization onto biochar loaded PUF inside the reactor, 1000 mL of BGWW was taken in a 2000 mL conical flask and 5 gm PUF cubes were added. After autoclaving, initially 10 g of biochar was added to the flask followed by incubation for 5 days for biomass immobilization by growing onto the support material. The immobilized PUF cubes were subsequently packed inside the UFPBBR for further biomass growth and BGWW treatment. Fig. 3.3 shows the schematic of the UFPBBR.

The operational schedule of the UFPBBR is given in Table 3.4. For proper aeration and routine sampling, various ports were provided at every 25 cm throughout the height of the bioreactor. Air was supplied from an air compressor with a constant air flow rate of 4-4.5 mg L^{-1} via a 0.2 µm membrane air filter at the bottom of the bioreactor to maintain the aerobic condition. The aeration was continuously monitored with a digital flow meter (Flow-tech engineers, Mumbai, India). UFPBR was fed continuously with biomass gasification wastewater at a controlled flow rate using a peristaltic pump (Model: pp10, Miclins India). Bioreactor was operated in co-current mode of wastewater and air. DO was maintained above 4 mg L^{-1} by adjusting the air flow rate to ensure aerobic condition (Sahoo et al. 2013).

During the initial startup, the bioreactor was continuously fed with LB medium and the operation was continued for 45 days to achieve ample amount of bacterial biomass until a steady-state performance was observed. During this startup phase, the medium flow rate was maintained to obtain a hydraulic retention time (HRT) of 36 h and any washed out biomass from the outlet was recycled back into the UFPBBR.

Performance evaluation of the PUF and biochar immobilized PUF in the UFPBBR for BGWW treatment by *R. opacus* were carried out as per the operating

schedule presented in Table 3.4. Samples were withdrawn at regular time interval and were analyzed for COD, biomass, pH and DO.

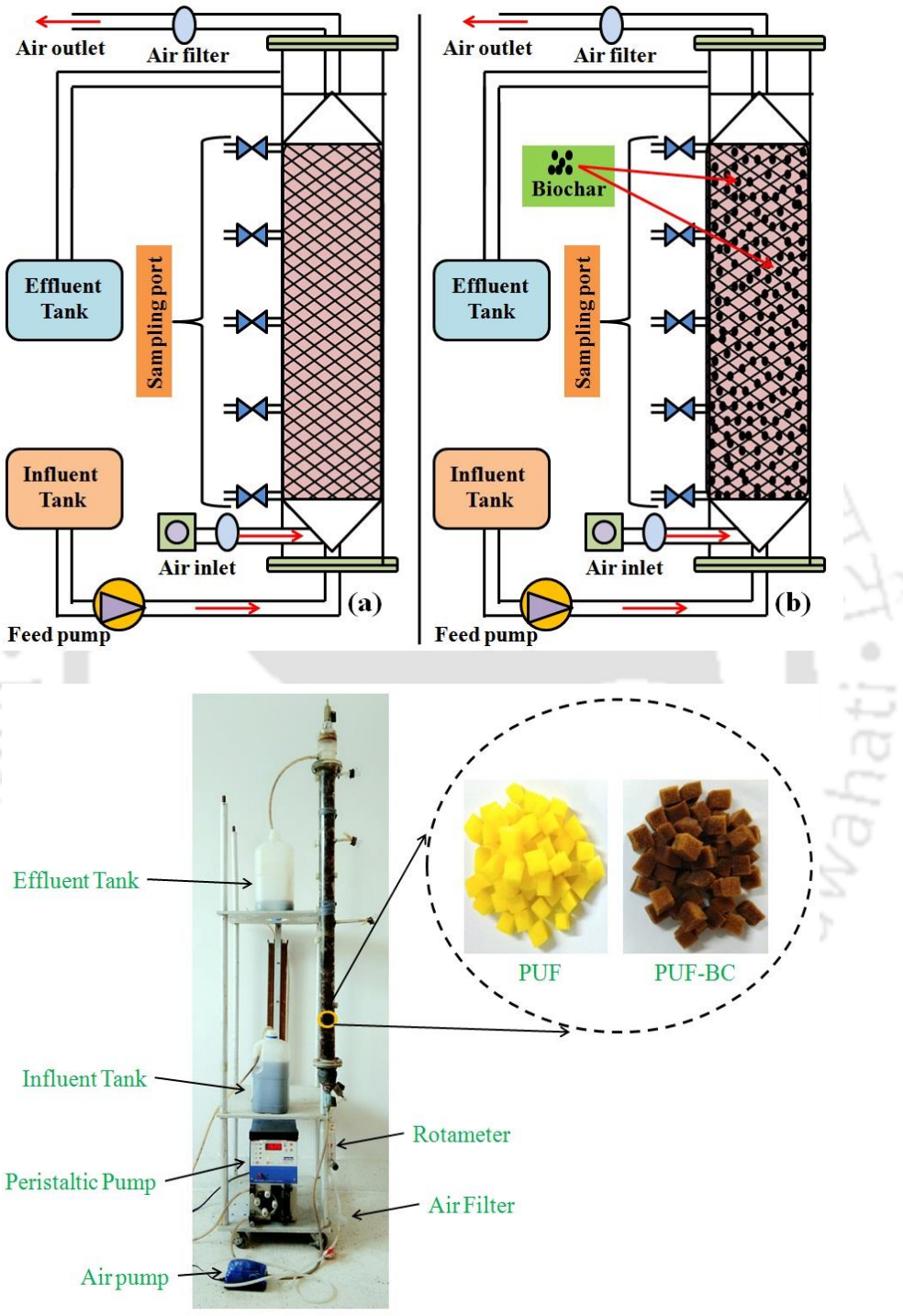

Fig. 3.3: Schematic showing experimental set up of the UFPBBR with support material (a) PUF, (b) PUF-biochar and (c) inset of PBBR used

3.7.2. Characterization of the bio-supporting materials (PUF and biochar)

Characterization of the bio-support material (polyurethane foam) and biochar loaded PUF and bacterial biomass were examined by employing field emission scanning electron microscopy (FESEM) equipped with energy dispersive spectroscopy (EDX). PUF fragments along with the biochar and the bacterial biofilm was sampled at different points and time period during the operation of the bioreactor. All the samples were initially fixed in 3.5% glutaraldehyde followed by washing twice with distilled water. The washed sample was then sequentially dehydrated using acetone (20-50%) for 10 min of exposure time. Dried sample was gold sputtered and was further observed using a FESEM (Zeiss, Sigma, Germany) (Bind et al. 2018). Further, for determining the morphological appearance of *R. opacus* in presence of biochar, transmission electron microscopy (TEM) (JEOL, JEM2100, Japan) at 200 kV was carried out.

FTIR analysis was performed over the range from 400 to 4000 cm^{-1} for PUF, PUF-BC and PUF-BC loaded biomass after 20 days.

3.7.3. Abiotic degradation of biomass gasification wastewater in UFPBBR

In order to examine the abiotic degradation of wastewater within the UFPBBR due to sorption onto the support material and volatilization (if any) with air supplied into the bioreactor. As aforementioned, PUF and PUF-biochar were utilized as the supporting material in PBR (Fava et al., 1996). For evaluating the abiotic degradation, UFPBR was operated without any aeration by passing the real wastewater. For this, HRT of the reactor was fixed of 24 h. Furthermore, the bioreactor was aerated from the ports to examine any loss due to volatilization.

Table 3.4: Operational schedule with the UFPBBR for BGWW treatment

UFPBBR operation (d)	HRT (h)	Influent concentration (mg L^{-1})
0-10*[a]	30	580
11-14*[b]	36	580
15-19	30	580
20-23	24	580
24-26	18	580
27-30	36	920
31-34	30	920
35-38	24	920
39-41	18	920
42-45	36	1340
46-49	30	1340
50-53	24	1340
54-57	18	1340
58-61	36	1820
62-65	30	1820
66-70	24	1820
71-74	18	1820
75-78	36	2270
79-82	30	2270
83-86	24	2270
87-90	18	2270
91-98*[c]	36	580
99-102	36	580
103-106	36	2270
107-110	36	2270
111-114	36	2270

115-122	18	580
123-126	18	1340
127-130	18	1340
131-134	18	1340
135-138	18	1340

UFPBBR operation schedule during

*a: DO operation
*b: bioreactor performance evaluation
*c: shock loading conditions

3.8. A hybrid continuous stirred tank bioreactor and microfiltration system

3.8.1. Bioreactor set-up and operation for BGWW treatment

An indigenously made 5 L stirred tank reactor (STR) with 3 L working volume with air diffusers and teflon coated magnetic stirrers was utilized for initial BGWW treatment by *R. opacus* in this hybrid system (Fig. 3.4). Air filters were fitted to a rotameter for determining the air flow rate in the influent and effluent. The STR was operated at a temperature of 30 ± 2°C, airflow rate of 1.5 vvm, an agitation rate of 350 rpm and 10% (v/v) inoculum size of *R. opacus* as the seed culture (Goswami et al. 2018). Initially, pH of the bioreactor was adjusted to 7 and was monitored continuously using a pH meter (Orion Star A 111, Thermo Scientific, Indonesia), whereas dissolved oxygen (DO) was measured by a DO meter (Model: HQ 40d HACH, USA) throughout the experiment. Aliquots were withdrawn at every 12 h of time intervals and the analyses were performed in triplicate and were reported within ±5% of the standard deviation. The bioreactor was operated in the continuous mode as per the operational schedule presented in Table 3.5. For making the treatment process of BGWW continuous,

following the biodegradation step, a tubular ceramic membrane was fabricated and used in this hybrid CSTR-MF system.

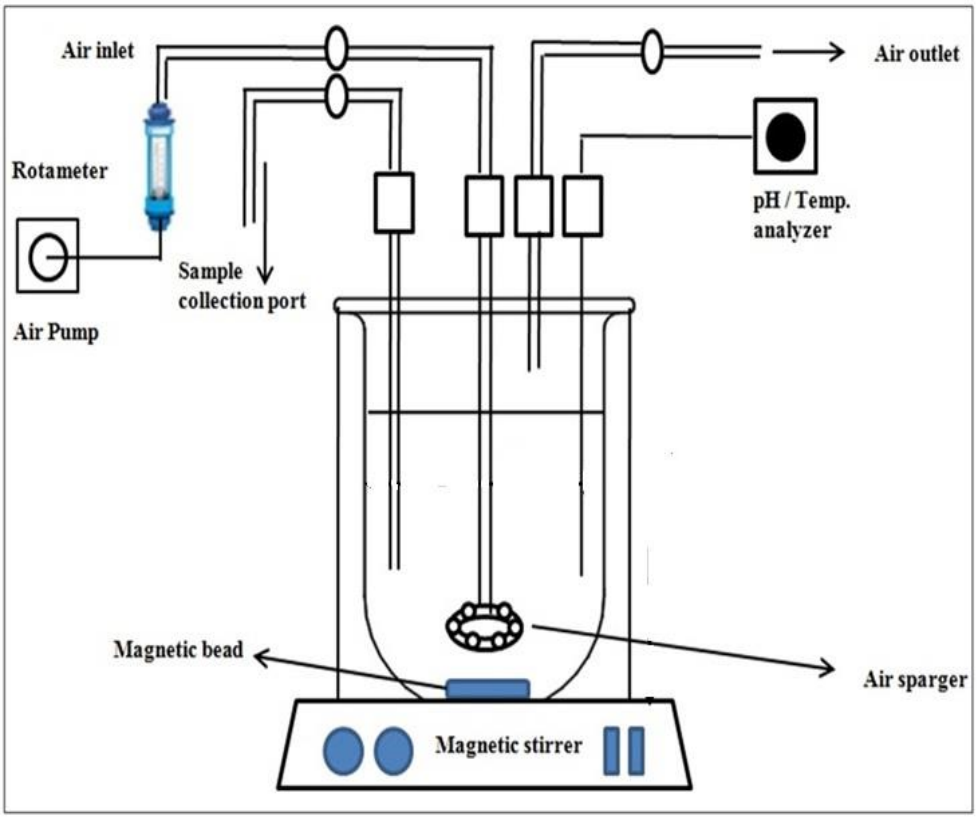

Fig. 3.4: Schematic of the stirred tank bioreactor used in the multi-component study

Fig. 3.5 (a) shows the steps followed for fabricating the low-cost tubular ceramic membrane and its characterization (Table 3.6) (Vasanth et al., 2011). In brief, locally procured low cost natural inorganic materials (clays) viz., kaolin, quartz and calcium carbonate were used for membrane preparation by extrusion technique (Kumar et al., 2016). All the raw materials were mixed well using Millipore water for extruding the membrane. Membrane of dimensions 105, 11.5 and 5.5 mm, length, external diameter and internal diameter, respectively, were extruded in the horizontal direction at room temperature and were kept for 12 h for air drying. Followed by re-drying at 100°C for 12

h and then at 200°C for 12 h in a hot air oven, the tubes were sintered at 950°C for 6 h in a box furnace with a heating rate of 0.5°C min^{-1}. These restrained thermal treatments were carried out to prevent the micro-cracking and bending of the microfitration tubes. Finally, the prepared membrane was washed with Millipore water, sonicated and dried at 100°C. Characterization of the membranes, including pore size, porosity, and water permeability was carried out as per the standard methods (Table 3.6) (Kumar et al., 2015).

Fig. 3.5 (b) is a schematic of the entire tangential microfiltration set up used in this study. In series, the system consists of a feed tank, metering pump (for feed circulation), a membrane module (possessing tubular configuration), a pressure indicator and a flow meter (to evaluate cross flow rate) with flow control valves. The prepared tubular membrane was further incorporated into the tangential module for cross-flow filtration. The inlet BGWW following its initial treatment using CSTR was pumped through the module from the feed tank and the retentate was utilized with the recirculation arrangement. Finally, the permeate flow through the elaborated membrane was analyzed utilizing an electronic weighing balance kept under open atmospheric condition. The operating pressure was adjusted manually using the flow control valves.

3.8.2. Analysis of *R. opacus* biomass, lipid content and COD removal (%)

Samples were withdrawn at regular time interval and were analyzed for COD, biomass, pH and DO.

Table 3.5: Operational schedule with the CSTR for the BGWW treatment

CSTR operation (d)	HRT (h)	Influent concentration (mg L^{-1})
0-15*[a]	30	580
16-19*[b]	30	580
20-23	24	580
24-26	18	580
27-30	15	580
31-34	30	920
35-38	24	920
39-42	18	920
43-46	15	920
47-50	30	1340
51-54	24	1340
55-58	18	1340
59-62	15	1340
63-66	30	1820
67-70	24	1820
71-74	18	1820
75-78	15	1820
79-82	30	2270
83-86	24	2270
87-90	18	2270
91-94	15	2270
95-98*[c]	30	580
99-102	30	580
103-106	30	2270
107-110	30	2270

111-115	18	580
116-120	18	1340

CSTR operation schedule during

*a: Batch operation
*b: bioreactor performance evaluation
*c: shock loading conditions

Table 3.6: Properties of tubular ceramic membrane sintered at 950°C (optimized temperature)

S. No.	Properties	Values
	Dimensions:	
1.	Outer diameter (mm)	11.5
2.	Channel diameter (mm)	5.5
3.	Thickness (mm)	3
4.	Length (mm)	105
5.	Unit surface (m^2)	1.814×10^{-3}
6.	Average pore size (µm)	0.304
7.	Porosity (%)	48.61
8.	Water permeability ($m^3\ m^{-2}\ s^{-1}$ kPa)	5.22×10^{-7}
9.	Mechanical strength (MPa)	20.87
	Chemical stability	
1.	Acid-weight loss (%)	< 2%
2.	Base-weight loss (%)	< 1%

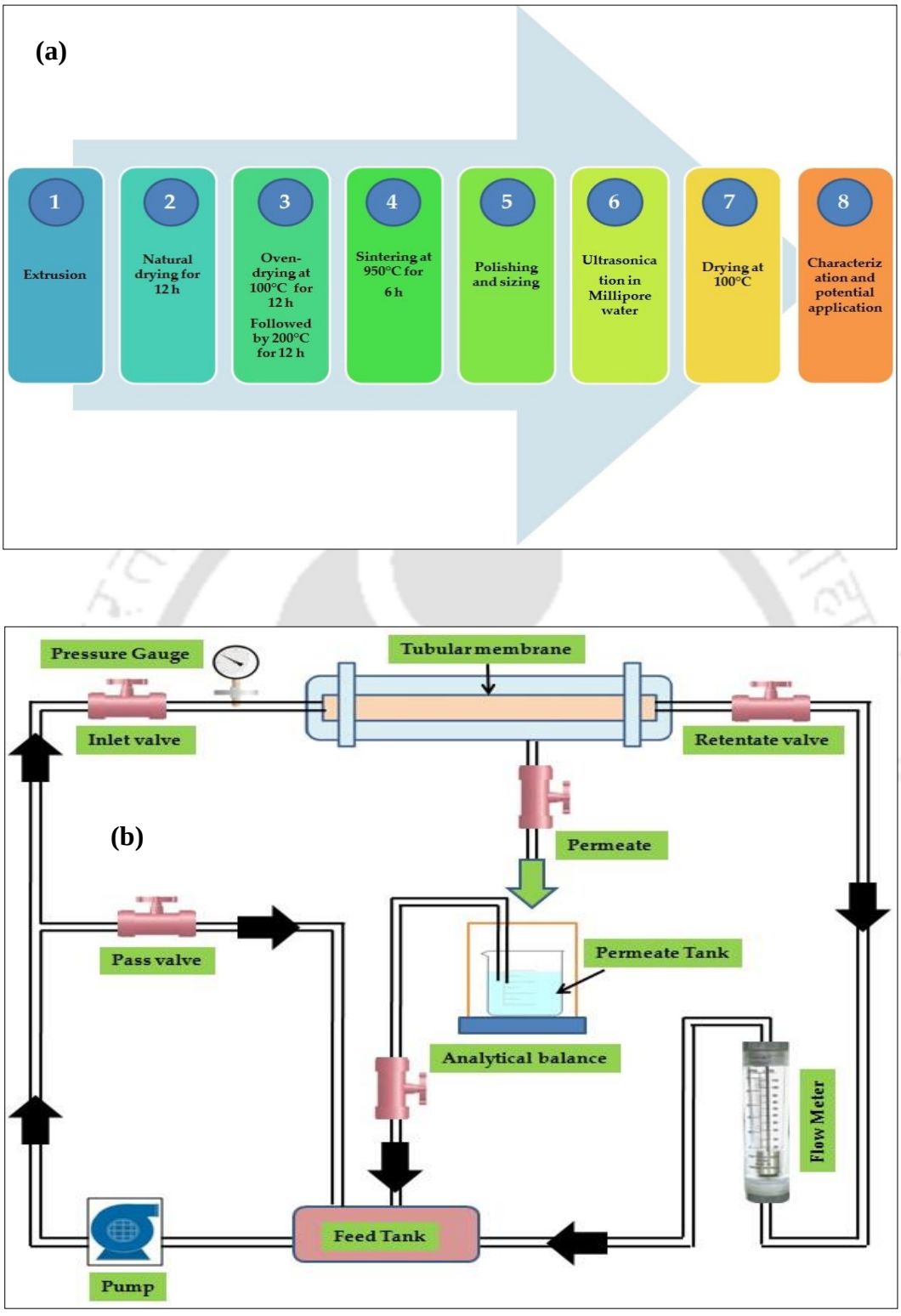

Fig. 3.5: (a) Steps followed for fabricating the tubular ceramic membrane and (b) Schematic of the MF setup

CHAPTER 4

RESULTS AND DISCUSSION

4. Results and discussion

The key highlight of the present study as outlined in the objectives is development of a sustainable system for the treatment of PAH contaminated system using oleaginous *Rhodococcus opacus* and resource recovery. In this chapter, results of batch and continuous reactor studies carried out on PAHs biodegradation in both simulated and real wastewater using *R. opacus* and biodiesel production are presented and discussed.

4.1. Batch PAHs biodegradation and lipid accumulation by *R. opacus*

4.1.1. Batch shake flask study

4.1.1.1. Biomass growth, PAH biodegradation and lipid accumulation

Batch shake flask experiments were conducted to determine the growth of *R. opacus* using naphthalene, anthracene, phenanthrene and fluoranthene as the sole carbon source at different initial concentration in the range 50-500 mg L^{-1}. Fig. 4.1 illustrates the biodegradation pattern of the four different PAHs for six different initial concentrations (50, 100, 200, 300, 400 and 500 mg L^{-1}) and 10% (v/v) inoculum size. All initial concentrations of the PAHs investigated in this study, a lag phase of 24 - 36 h in PAHs degradation is observed, but efficient degradation is achieved at a low initial concentration of the PAHs. Furthermore, PAHs biodegradability followed the order: naphthalene (2-ring) > anthracene (3-ring) > phenanthrene (3-ring) > fluoranthene (4-ring). A distinct maxima in the *R. opacus* biomass growth profile (Fig. 4.2) at seven days corroborated with a maximum accumulation of lipids (Fig. 4.3). Beyond this time period, both the culture growth and lipid accumulation were significantly reduced. The decrease in biomass growth with an increase in initial PAHs concentration was observed for all the four PAHs tested in this study.

The overall degradation efficiency range of the different 2, 3 and 4- ring PAH compounds were 69.5% - 83.8% for naphthalene, 67.8 - 81.4% anthracene, 64.7% - 76.9% for phenenthrene and 58% - 73.2% for fluoranthene for an initial concentration in the range 50 - 500 mg L^{-1} over a period of seven days. The amount of lipids accumulated by the bacteria was in the range 72.4% (w/w, CDW) for naphthalene, 70.6% (w/w, CDW) for anthracene, 68.7% (w/w, CDW) for phenanthrene and 63% (w/w, CDW) for fluoranthene (Table 4.1).

For all the PAHs tested in this study, a clear decline in their biodegradation is observed at a high initial PAHs concentration in the range 300-500 mg L^{-1} (Fig. 4.1). In all the experimental runs, abiotic loss of PAHs was found to be negligible (1.8-6.4%) only. Moreover, any loss of PAHs due to sorption on the bacterial biomass / surface was insignificant as the solvent used for extracting the PAHs was added directly to the culture broth (Graber et al., 2009).

4.1.1.2. Kinetics of *R. opacus* biomass growth on PAHs

For a clear understanding of the *R. opacus* biomass growth on PAHs as the sole carbon source, the biomass specific growth rate was estimated for the different PAHs compounds at different initial concentration (Fig. 4.4). The experimental specific growth rate was found to increase along with an increment in the initial PAHs concentration. This is due to the well-known fact that an increase in the initial PAHs concentration enhances the rate of dissolution of PAHs because of increase in the interfacial area. But at a high initial PAHs concentrations (300, 400 and 500 mg L^{-1}), a significant decline in the specific growth rate is observed. A maximum specific growth rate of 0.0071 h^{-1}, 0.0245 h^{-1}, 0.0268 h^{-1} and 0.0144 h^{-1} for naphthalene, anthracene, phenanthrene and fluoranthene, respectively, is observed for an initial PAH concentration in the range 50-500 mg L^{-1}.

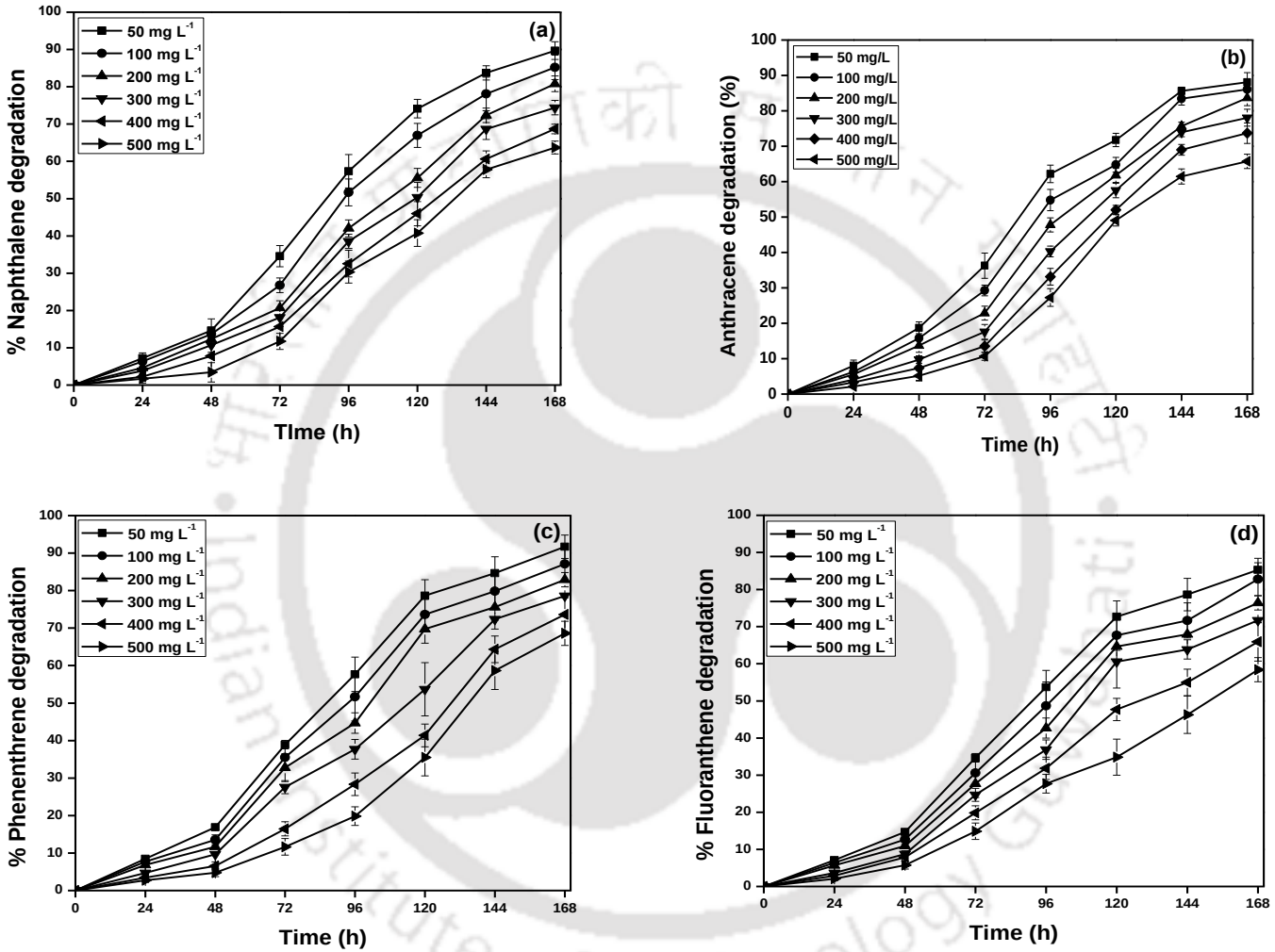

Fig. 4.1: Time profile of PAHs biodegradation at different initial concentration and 10% inoculum size: (a) naphthalene, (b) anthracene, (c) phenanthrene and (d) fluoranthene

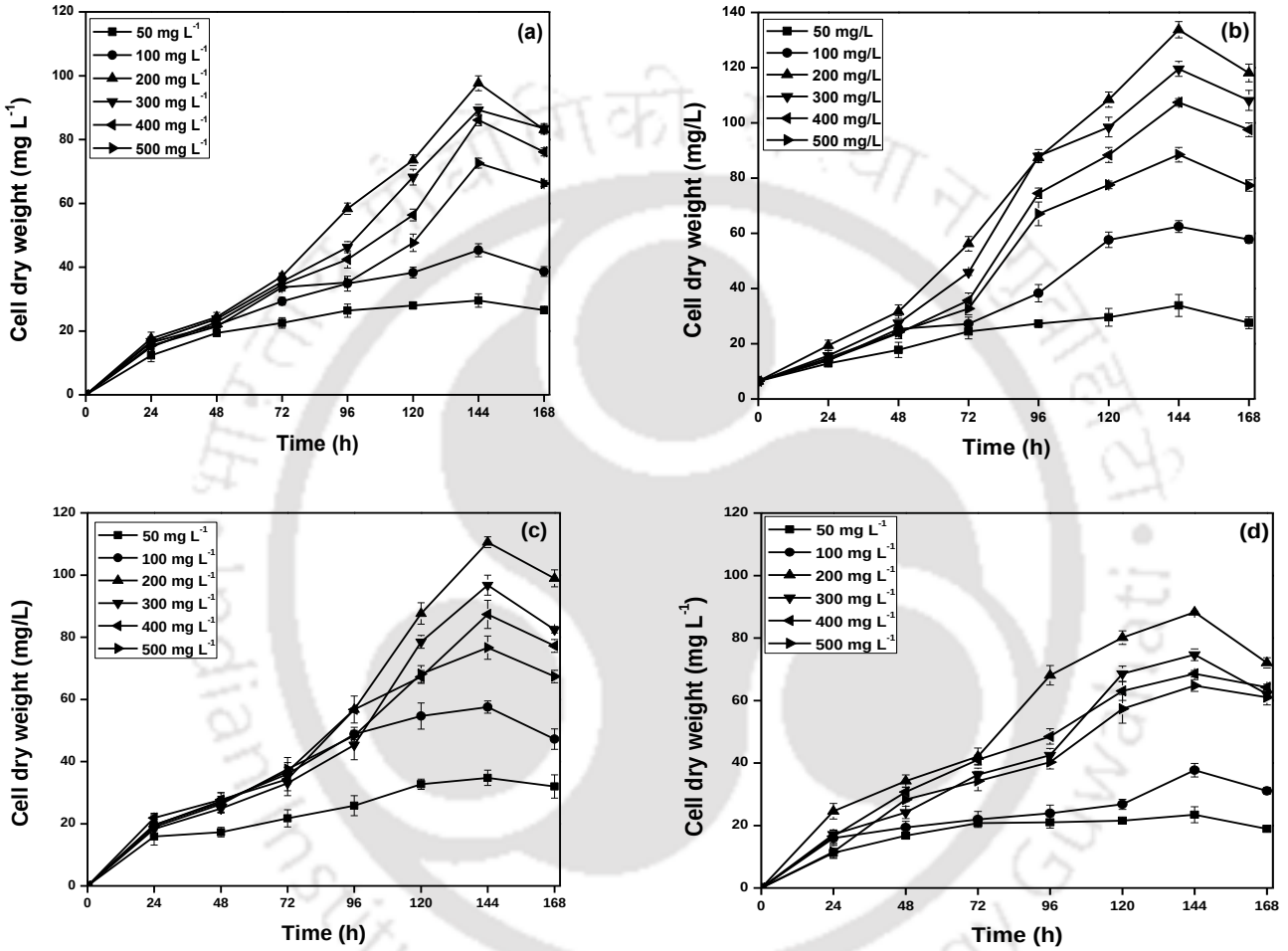

Fig. 4.2: Time profile of *R. opacus* biomass grown on (a) naphthalene, (b) anthracene, (c) phenanthrene and (d) fluoranthene at different initial concentrations

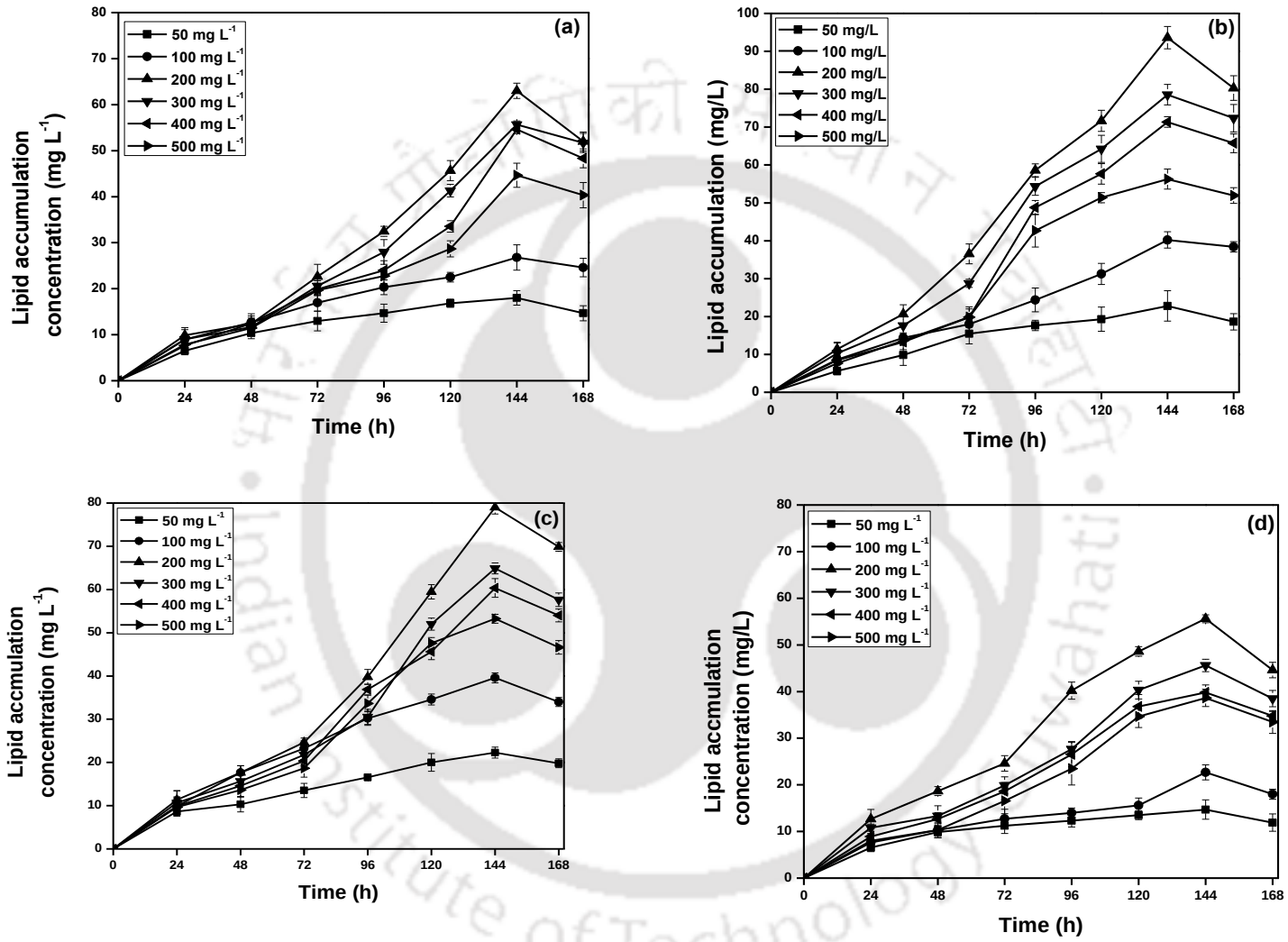

Fig. 4.3: Time profile of lipid accumulation by *R. opacus* grown using (a) naphthalene, (b) anthracene, (c) phenanthrene and (d) fluoranthene at different initial concentrations

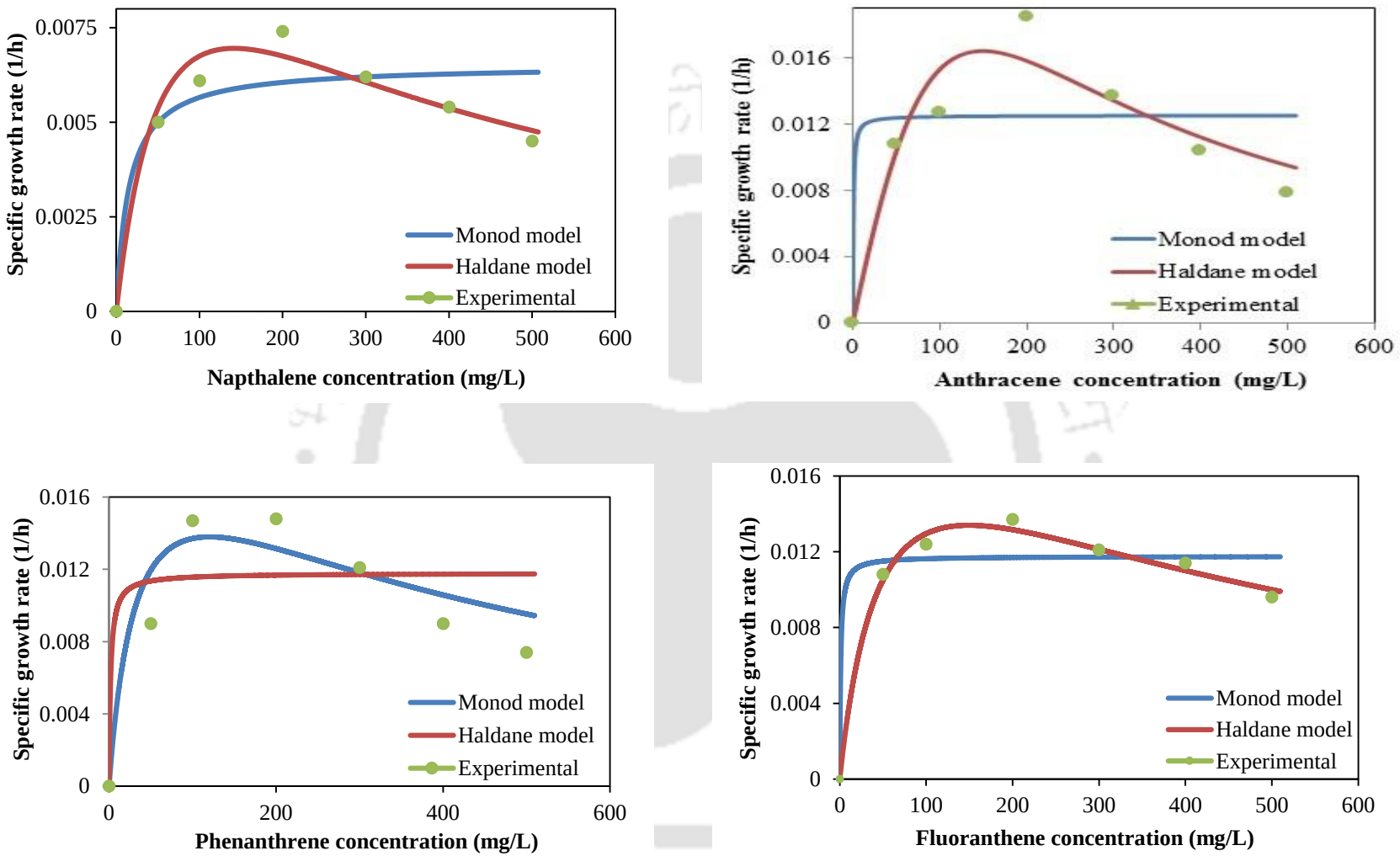

Fig. 4.4: Experimental and model predicted specific growth rate of *R. opacus* grown using different initial PAHs concentration

Very few studies have reported in the literature on the effect of initial concentration of two, three and four ring PAHs on specific growth rate of pure bacterial cultures. For instance, Walter et al., (1991) reported a specific growth rate value of 0.023 h^{-1} for *Rhodococcus* sp. UW1 for an initial pyrene concentration of 0.66 mg L^{-1}. In another study, Moscoso et al., (2012) reported an increase in the specific growth rate of *Pseudomonas stutzeri* from 0.138 to 0.243 h^{-1} as the initial phenanthrene concentration was increased from 178 mg L^{-1} to 356 mg L^{-1}.

The experimental data in this study was further fitted to Monod and Haldane models (Fig. 4.4). The estimated model kinetic parameters along with the coefficient of determination (R^2) values are presented in Table 4.2. The Monod model does not consider inhibitory effect due to substrate on microorganisms. Hence, it is found to be accurate only for a low initial PAHs concentration and did not fit well for the data obtained at a high initial PAHs concentration. On the other hand, the Haldane equation, which includes an inhibition term, offered a good fit for the biomass growth even at a high initial PAHs concentration.

In general, the Haldane model (Table 4.1, Eq. 2) is the most widely accepted model for describing biomass growth on different substrates (Su et al., 2011). The fitness due to Monod model was poor with a low R^2 value compared to that of the Haldane's model for all the three PAHs (Table 4.2), which clearly indicates that the PAH utilization by *R. opacus* biomass followed substrate inhibition kinetics. The poor fit due to Monod model may be due to the fact that it was originally proposed for soluble substrates and not for sparingly soluble substrates, such as naphthalene, anthracene, phenanthrene and fluoranthene. A similar observation on the lack of fit to Monod's model and best fit to Haldane model was reported in the literature for *Mycobacterium frederiksbergense* grown using PAHs (Mahanty et al., 2008).

Table 4.1: Estimated bio-kinetic model parameters for *R. opacus* grown using PAHs as the sole carbon source

Substrate	Model	μ_{max} (h^{-1})	Ks (h^{-1})	K_I (h^{-1})	R^2
Naphthalene	Monod	0.0065	15.13	-	0.82
	Haldane	0.0071	141	142.1	0.91
Anthracene	Monod	0.0117	1.912	-	0.77
	Haldane	0.0245	40	362.3	0.89
Phenanthrene	Monod	0.0116	1.1	-	0.82
	Haldane	0.0268	62	360.7	0.94
Fluoranthene	Monod	0.0129	0.61	39	0.67
	Haldane	0.0144	15.9	174	0.93

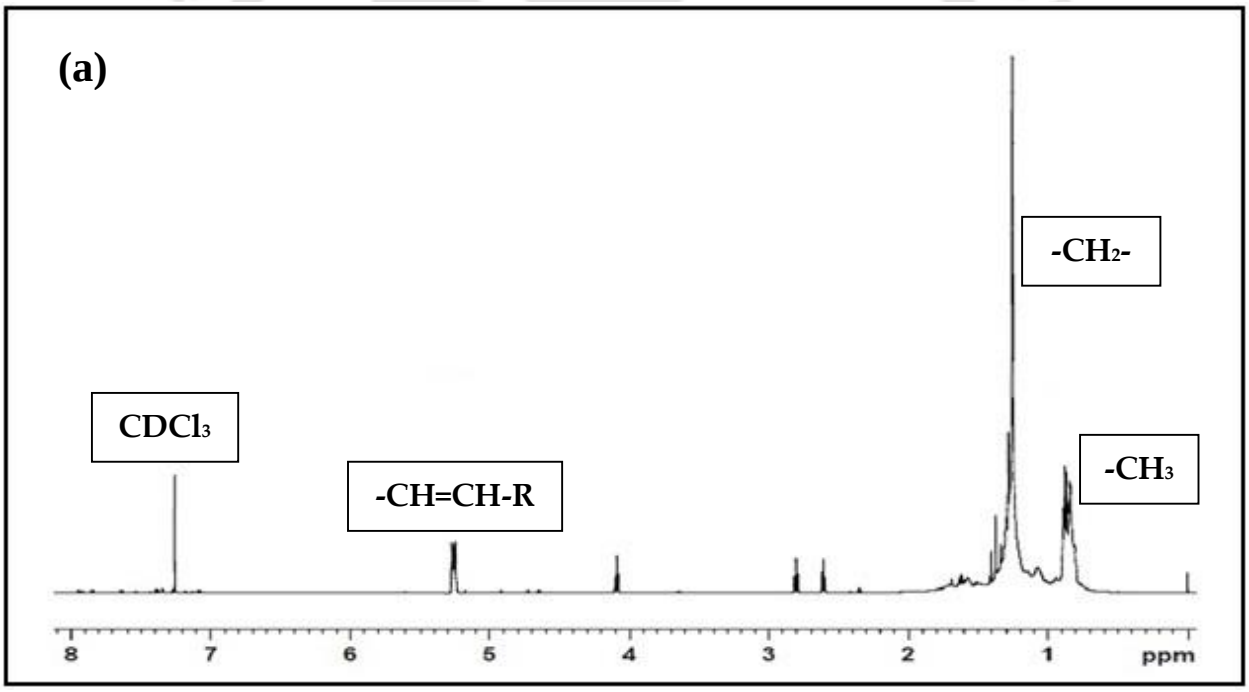

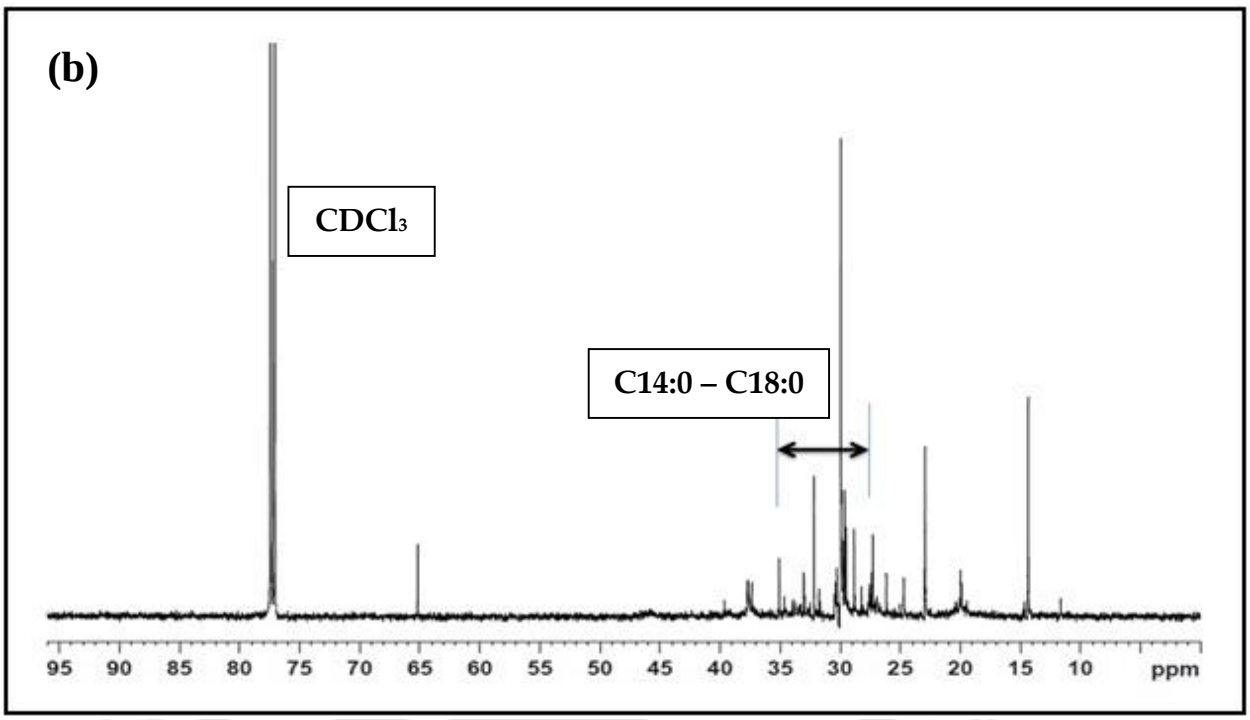

Fig. 4.5: (a) ^{1}H-NMR and (b) ^{13}C-NMR spectra of the *R. opacus* accumulated lipids

4.1.1.3. Characterization and properties of FAMEs for biodiesel application

Fig. 4.5 presents the ^{1}H and ^{13}C NMR spectra of the lipids produced in this study. From Fig. 4.5 (a), a shift in the peak from 0.8 to 2.4 ppm can be seen indicating the presence of saturated fatty acids, whereas the proton shift from 5.25 to 5.45 ppm represented the –CH=CH– group of unsaturated fatty acids in the accumulated lipids (Kumar et al., 2015). Thus, the spectra showed that the bacterial lipids were primarily composed of saturated fatty acids. Similarly, from Fig. 4.5 (b) the shift due to methyl ester carbon atoms appear from 29.6 to 34.2 indicating the presence of methyl esters (C 14:0-C 18:0). ^{1}H and ^{13}C NMR spectra of the lipids accumulated by the strain utilizing naphthalene and fluoranthene as the sole carbon and energy source were almost identical with that obtained using phenanthrene as the sole carbon source.

FAMEs produced by transesterification of the bacterial lipids were analyzed using gas chromatography (GC), and the results are presented in Table 4.2. The major products

were methyl palmitate (C16:0) and methyl stearate (C18:0); besides, methyl laurate (C12:0), methyl palmitoleate (C16:1), methyl linoleate (C18:2), methyl oleate (C18:1), methyl erucate (C21:0) and methyl myristate (C14:0) were found in moderate amount along with methyl octanoate (C8:0), methyl arachidate (C20:0) and methyl lignocerate (C24:0) in trace amounts. The presence of a high amount of saturated fatty acids than the unsaturated fatty acids as predicted from the previous NMR results was further confirmed by GC analysis of the FAMEs (Table 4.2).

The quantitative evaluation of the biodiesel produced was made by using empirical equations as a function of the experimentally determined FAMEs composition (Finnerty, 1992, Kumar et al., 2014, Francisco et al., 2010, Sarin et al., 2009, Goswami et al., 2017a). A better agreement was observed between the biodiesel properties estimated from the present study and with those of the standard values given by the American Society for Testing and Materials (ASTM) and European Standards (EN) (Table 4.3). Among the different biodiesel property values, the pour point and cloud point values differ considerably with respect to the PAH compound used. Moreover, the cloud point value of the biodiesel derived from *R. opacus* was slightly higher than the standard values, whereas the pour points value matched well with those of the standard values indicating its suitability for use in low temperature regions (Table 4.4) (Moscoso et al., 2012). Overall, these characterization results of the bacterial lipids and FAMEs produced by lipid extraction and transesterification revealed an excellent suitability of the transesterified product for biodiesel applications. Moreover, no study has been undertaken so far to demonstrate the potential of *R. opacus* for lipid accumulation using PAHs as the sole carbon source. Hence, the present study on simultaneous PAH degradation and lipid accumulation using *R. opacus* indicated very good potential of the strain for pollutant removal and bioenergy application.

Table 4.2: Composition of the FAMEs produced by transesterification of the accumulated lipids from *R. opacus* grown with different PAHs as the sole carbon source

Fatty acid composition	**Total fatty acids (%) (Transesterified product)**			
	NAPH	**ANTH**	**PHEN**	**FLOR**
C8:0 methyl octanoate	2.57	1.32	1.08	2.27
C12:0 methyl laurate	6.76	7.18	5.38	8.3
C14:1 methyl myristate	7.48	4.58	5.42	6.74
C16:1 methyl myristoleate	6.83	5.47	5.12	2.6
C16:0 methyl palmitate	38.9	32.4	39.8	36.43
C18:1 methyl oleate	2.3	5.93	3.1	2.27
C18:2 methyl linolenate	2.12	4.85	0.73	2.7
C18:0 methyl stearate	25.2	25.9	28.4	26.8
C20:0 methyl arachidate	4	8.61	5.6	9.23
C21:0 methyl erucate	0.24	2.56	0.8	0.56
C22:0 methyl behenate	Nil	3.67	0.17	Nil
C 24:0 methyl lignocerate	3.6	1.85	4.4	2.1
Total saturated content	81.27	82.17	83.63	85.69
Total fatty acid (% w/w, CDW)	100			

Table 4.3: Estimated property values of the biodiesel obtained by lipid transesterification and comparison with those of the international standards

Biodiesel property	Units	Transesterification				ASTM-D6751 Standard	EN 14214
		NAPH	ANTH	PHEN	FLOR		
Viscosity	(mm^2 s^{-1})	4.32	4.59	4.24	4.19	1.9-6.0	3.5-5.0
Cetane number		66.16	70.93	65.05	63.75	47 (min)	51 (min)
Pour point	(°C)	9.97	6.26	10.49	8.56	-3.0 to 12.0	ND
Cloud point	(°C)	15.47	12.1	15.94	14.17	-15.0 to 10.0	ND
Saponification value	mg KOH g^{-1}	212.46	211.16	212.07	216.61	ND	ND
Iodine value	gI_2 per 100 g oil	20.63	13.42	14.88	16.64	ND	120
Degree of unsaturation		20.85	14.36	17.08	17.01	ND	ND

ND: Not defined

4.1.2. Biodegradation of PAHs in a multi-component system

4.1.2.1. Biomass growth, PAH biodegradation and lipid accumulation

Under the different experimental conditions followed in this study, for degrading a mixture of PAHs, *R. opacus* showed very high degradation of all the three PAHs in mixture. Table 4.5 shows that PAH biodegradation efficiency dependent on the initial PAH (substrate) concentration; a low PAH concentration resulted in high degradation efficiency. Among the three PAHs, naphthalene was degraded the most by *R. opacus* in all the experimental runs. The minimum average percentage biodegradation of each component, i.e., NAPH, PHEN and FLOR were found to be 59.7%, 51.7% and 46.8 %,

respectively, and was attributed to a high initial concentration (200 mg L^{-1}) of each component in the mixture (run number 9). The highest biodegradation of each component was 87.6%, 78.3% and 72.8% for NAPH, PHEN and FLOR, respectively. Thus, most important factor determining the degradation percentage of each component was the overall initial concentration of PAH in mixture.

Figs. 4.6 and 4.7 depict the biomass growth profile of *R. opacus* in the experimental runs. No lag phase was observed despite the presence of PAH in the media. In single substrate degradation studies, a lag phase of 24-36 h, is observed which is followed by an exponential growth phase with a maximum optical density at 144 h (Goswami et al., 2017a). In this mixture study, as the organism was already adapted to grow using PAH as the substrate, the lag phase was eliminated.

In all the experimental runs, abiotic loss of PAHs was found to be negligible in the range of 2.7 - 4.1% only. Furthermore, the loss of PAHs due to sorption on the bacterial biomass/surface may be disregarded as the solvent utilized for extracting the PAHs was added directly to the culture broth (Goswami et al., 2017c).

Table 4.4: 2^3 Full Factorial experimental design matrix showing different combination levels of PAHs in the ternary system along with their biodegradation efficiency values

Exp. Run No.	NAPH[a]	PHEN[a]	FLOR[a]	Biodegradation[b] (%)		
				NAPH	PHEN	FLOR
1	50 (-1)	50 (-1)	200 (+1)	79.41	65.38	63.29
2	200 (+1)	50 (-1)	200 (+1)	73.82	60.23	49.73
3	200 (+1)	200 (+1)	50 (-1)	63.28	56.35	75.8
4	200 (+1)	50 (-1)	50 (-1)	75.8	72.24	69.83
5	125 (0)	125 (0)	125 (0)	70.23	66.78	61.29
6	125 (0)	125 (0)	125 (0)	72.14	69.51	64.57
7	125 (0)	125 (0)	125 (0)	74.08	68.5	63.9
8	50 (-1)	200 (+1)	50 (-1)	83.07	75.17	68.73
9	200 (+1)	200 (+1)	200 (+1)	59.72	51.73	46.78
10	50 (-1)	50 (-1)	50 (-1)	87.62	78.3	72.76
11	50 (-1)	200 (+1)	200 (+1)	76.38	53.26	52.18

[a] NAPH: Naphthalene; PHEN: Phenanthrene; FLOR: Fluoranthene : All concentration level (50 and 200 mg L^{-1})

[b] Values shown are average of triplicate sample analysis with standard deviation

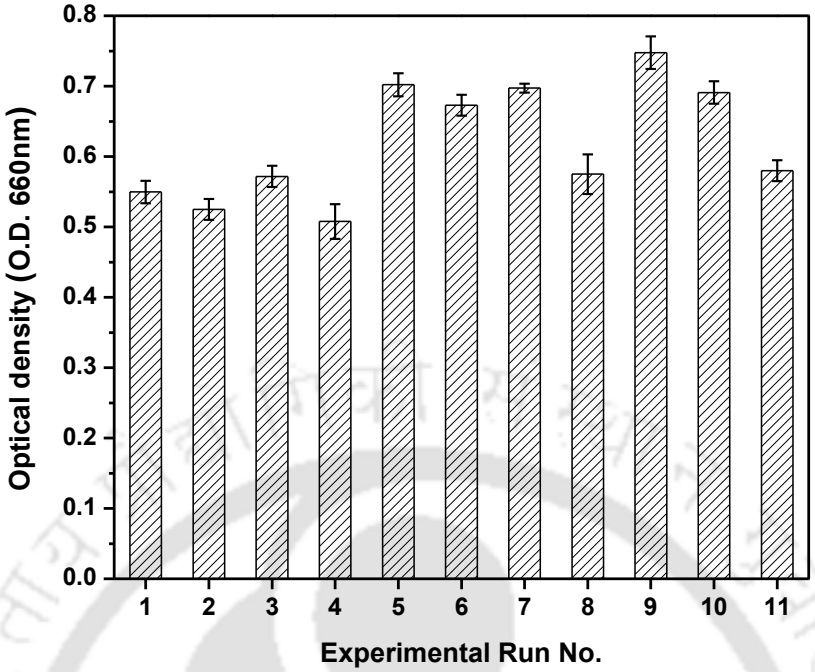

Fig. 4.6: Maximum biomass growth of *R. opacus* in multi-component PAHs system

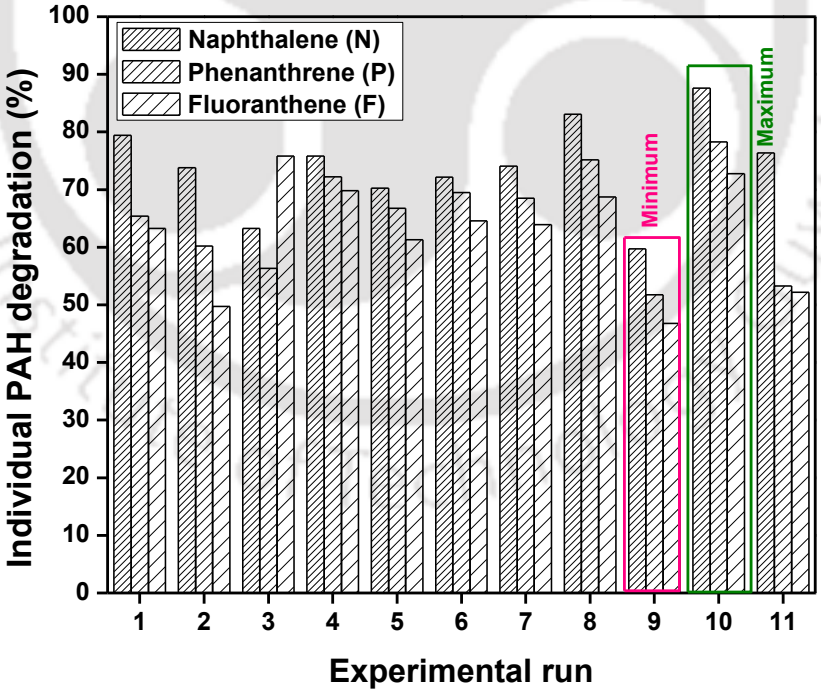

Fig. 4.7: PAH biodegradation in multi-component PAHs system

The effect of initial concentration of PAHs on specific growth rate of pure bacterial species in a single pollutant system is reported in the literature. Walter et al. (1991)

reported a specific growth rate value of 3.83×10^{-4} min^{-1} for *Rhodococcus* sp. UW1 for an initial pyrene concentration of 0.66 mg L^{-1}. In another study, Moscoso et al. (2012) reported a specific growth rate of *Pseudomonas stutzeri* in the range of 2.3×10^{-3} min^{-1} - 4.05×10^{-3} min^{-1} for phenanthrene biodegradation at an initial PAH concentration in the range 178 mg L^{-1} - 356 mg L^{-1}, respectively. In the present study, the overall biodegradation rate of PAH ranged from 0.09 to 0.19 mg L^{-1} h^{-1} in the mixed pollutant system. Despite a very high initial PAH concentration used in experimental run 10 (200 mg L^{-1} of each substrate) compared to that used in the experimental run 9 (50 mg L^{-1} of each substrate) PAH degradation was only 1.5 times the overall rate, i.e., 0.58 mg L^{-1} h^{-1} compared to 0.39 mg L^{-1} h^{-1} at 200 mg L^{-1} and 50 mg L^{-1} initial PAHs concentration, respectively. This result demonstrates that either substrate bioavailability is limited or it is inhibitory at such high concentrations. In the previous study involving PAH biodegradation by *R. opacus* in single component system, a high value of 200 mg L^{-1} for substrate inhibitory constant (K_i) was obtained, which suggested that the bacterium was tolerant to the toxic effect of these PAHs (Goswami et al. 2017a) whereas the individual PAH degradation rate in the ternary system was significantly lower than that observed in the single substrate system, the overall PAH degradation rate of NAPH, PHEN and FLOR was higher than the 0.44-0.48 mg L^{-1} h^{-1} observed in the single substrate studies (Goswami et al., 2017b). This suggests that the organism is able to rapidly degrade PAH when present individually than when present as a mixture, but the overall rate for breakdown of mixed substrates is higher than that in a single component system.

Fig. 4.8 shows the lipid accumulation by *R. opacus* in the experimental runs performed with a mixture of PAHs. The maximum lipid accumulation was observed in run no. 9 with a value of 221.3 mg L^{-1} as the initial PAH concentration used was the highest (200 mg L^{-1}) in the study. Run no. 10 yielded a very low lipid accumulation of 83.2 mg L^{-}

[1], which was preformed into the lowest initial PAH concentration of 50 mg L^{-1} of each substrate. Similarly, the lipid accumulation values represented as percentage of CDW (% w/w) were 51.3 and 56.4 % in the experimental runs 9 and 10, respectively. In single substrate degradation studies with 200 mg L^{-1} of a single PAH substrate, the lipid accumulation was 14-16 % higher than the values obtained in the present ternary substrate study (Goswami et al. 2017c). The yield of product (lipid) on substrate was marginally higher at a low PAH concentration, with a yield of 0.51 g g^{-1} for an initial concentration of 200 mg L^{-1} and 0.56 g g^{-1} for an initial concentration of 50 mg L^{-1}.

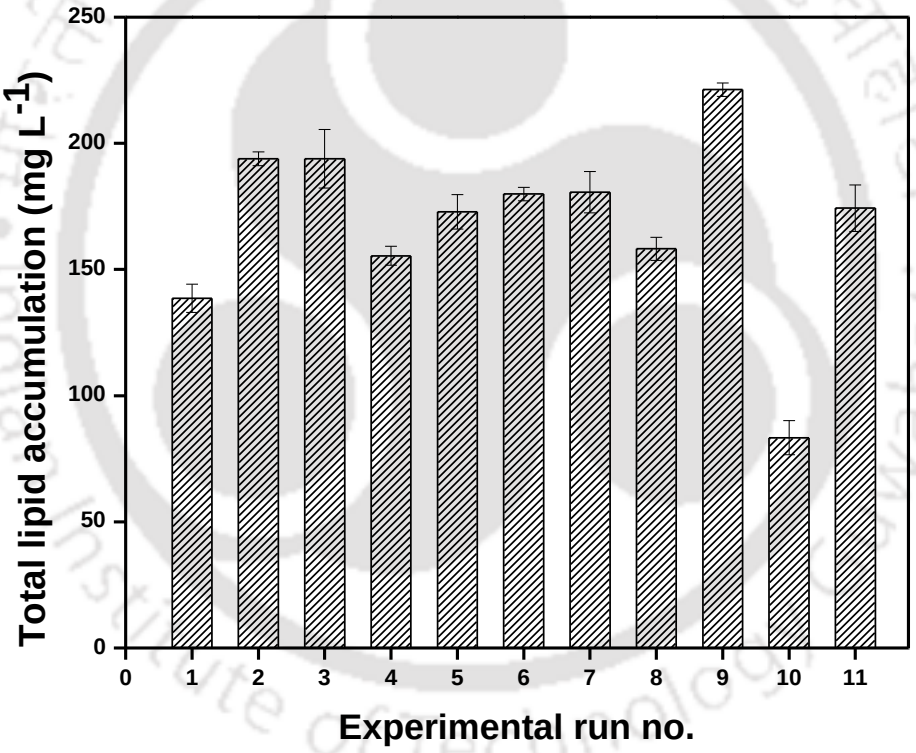

Fig. 4.8: Total lipid accumulation by *R. opacus* in the multi-component PAH system

Kumar et al. (2014) reported 51% (w/w, CDW) of lipid accumulation using *R.opacus* DSM 43205 utilizing dairy wastewater as the carbon source. In another study, 14.9 % (w/w, CDW) of lipid accumulation by *R. opacus* DSM 1069 was reported by Wei et al. (2015) using Kraft lignin. These studies, therefore, supports the results obtained in this study that the bacterium is able to accumulate lipids from recalcitrant PAHs as the sole source of carbon. If the organism could be modified to tolerate a very high PAH concentration and convert this recalcitrant substrate to lipid with a similar yield, then the production of lipids by this process could become commercially feasible.

4.1.2.2. Analysis of variance of PAH degradation

From Table 4.5, the results from analysis of variance (ANOVA) test demonstrate that the effect of individual PAH concentration was significant than the 2-way and 3-way interaction effects of the PAH concentrations on PAH biodegradation. The Student 't' test results shown in Table 4.7, show that an increase in naphthalene and phenanthrene concentrations in the mixture inhibited naphthalene biodegradation with a *P*-value < 0.0025. Increasing the naphthalene, phenanthrene and fluoranthene concentration in the mixture showed an inhibitory effect on phenanthrene removal ($P < 0.015$), due to the competitive effect for their utilization as the carbon source by the strain. Table 4.7 shows an increase in initial fluoranthene concentration in the mixture was inhibitory to its own removal with a *P* value < 0.004.

Table 4.5: ANOVA of batch biodegradation of PAHs by *R. opacus* in the ternary system (a) Naphthalene; (b) Phenanthrene and (c) Fluoranthene

(a) Naphthalene	**Df**	**SS**	**Adj MS**	**F**	**P**	**R^2**
Main effect	3	561.042	187.014	50.47	0.019	0.98
2- way interaction	3	56.267	18.756	5.06	0.169	
3- way interaction	1	1.201	1.201	0.32	0.627	
Residual error	2	7.411	3.706			
Pure error	2	7.411	3.706			
Total	10	642.271				
(b) Phenanthrene						
Main effect	3	651.937	217.312	114.06	0.009	0.99
2- way interaction	3	52.167	17.389	9.13	0.100	
3- way interaction	1	33.538	33.538	17.60	0.052	
Residual error	2	3.810	1.905			
Pure error	2	3.810	1.905			
Total	10	779.590				
(c) Fluoranthene						
Main effect	3	751.568	250.523	83.42	0.012	0.99
2- way interaction	3	139.924	46.641	15.53	0.061	
3- way interaction	1	0.423	0.423	0.14	0.743	
Residual error	2	6.006	3.003			
Pure error	2	6.006	3.003			
Total	10	899.558				

df: degrees of freedom, SS: sum of squares, MS mean sum of squares. F: Fisher's F value (calculated by dividing the MS owing to the model by that due to error), P: probability of incorrectly rejecting the null hypothesis when it is actually true

Table 4.6: Student 't' test for estimating the significance of individual and interaction effects of PAHs on each other degradation by *R. opacus* in the ternary system (N: Naphthalene; P: Phenanthrene and F: Fluoranthene)

Terms	Effect	Naphthalene Degradation		Effect	Phenanthrene degradation		Effect	Fluoranthene degradation	
		T	P		T	P		T	P
Constant		110.03	0.000		131.31	0.000		101.82	0.000
N	-13.465	-9.89	0.010	-7.890	-8.08	0.015	-3.705	-3.02	0.094
P	-8.550	-6.28	0.024	-9.910	-10.15	0.010	-3.030	-2.47	0.132
F	-5.110	-3.75	0.064	-12.865	-13.18	0.006	-18.785	-15.33	0.004
N×P	-4.760	-3.50	0.073	-2.285	-2.34	0.144	4.540	3.70	0.066
N*F	2.340	1.72	0.228	4.550	4.66	0.043	-5.775	-4.71	0.042
P*F	-0.015	-0.01	0.992	-0.400	-0.41	0.722	-4.000	-3.26	0.082
N*P*F	-0.775	-0.57	0.627	4.095	4.20	0.052	-0.460	-0.38	0.743

Fig. 4.9, a Pareto chart, demonstrates the significance of interaction among the PAH components on their biodegradation. The influence due to FLOR (4-ring) concentration on its biodegradation was the largest (negative effect) followed by that due to PHEN (3-ring) and NAPH (2-ring). Two-way interaction was statistically significant ($P < 0.05$) only in case of NAPH and FLOR on FLOR degradation, and it was minimal compared to the effect of individual component concentration. This suggests that data from single or multiple component studies could, in combination, be useful for predicting biodegradation behavior of more complex wastewater mixtures if data on the biodegradation of each component is available. Table 4.7 shows the available literature on biodegradation of PAHs in multi-component PAHs contaminated system using different microorganisms.

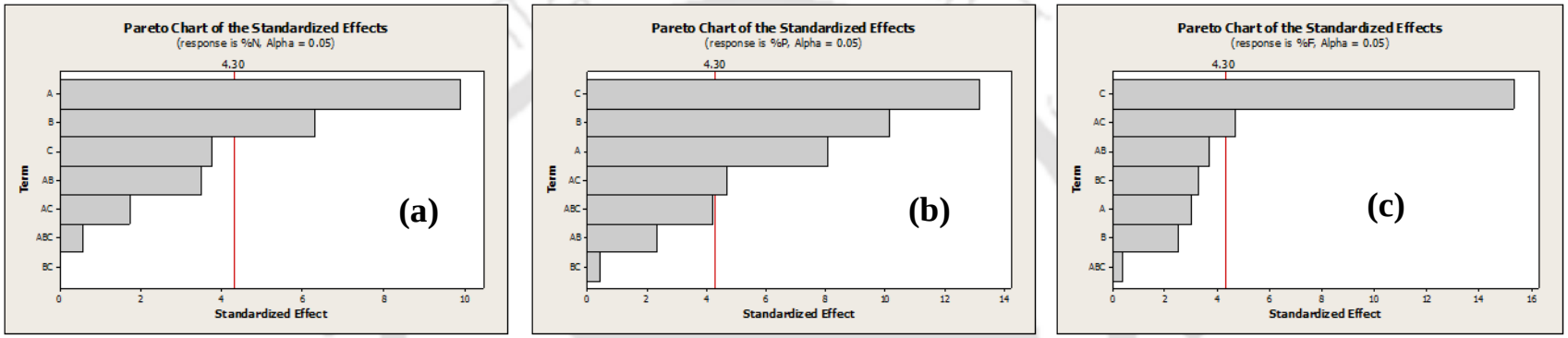

Fig. 4.9: Pareto chart showing the effect of different PAHs on each other biodegradation by *R. opacus* (a) Naphthalene, (b) Phenanthrene and (c) Fluoranthene biodegradation (vertical line showing the significance cut-off at a *P* value of 0.05)

Table 4.7: Literature on biodegradation of PAH in a multicomponent pollutant system using different microorganisms

S. No.	Microorganism	Experimental setup containing PAH	Concentration of PAHs (mg L^{-1})	Potential outcomes	Reference
1.	*Pseudomonas aeruginosa* RS1	Acenaphthene, Phenanthrene and Fluoranthene	25 (low) and 100 (high)	A high concentration of either phenanthrene or fluoranthene or both had statistically significant adverse effect on pyrene degradation while a high acenaphthene showed minimal adverse effect. Pyrene degradation exceeded 95% when all the PAHs were present at 25 mg L^{-1} Pyrene degradation in a multicomponent system containing low molecular weight (LMW) PAHs and n-alkanes was found to be hindered due to nutrient depletion and adverse effect of LMW PAHs and their metabolites	Ghosh and Mukherji 2017
2.	*Sphingomonas* sp. PheB4	Pyrene, Fluoranthene and Phenanthrene	10	Based on the kinetics and characteristics of phenanthrene metabolites, transformation of hydroxylated phenanthrene into 1-hydroxy-2-naphthoic acid was a rate-limiting step in the biodegradation Compared to a single addition of pyrene or fluoranthene, the presence of a mixture of pyrene and fluoranthene decreased the degradation rate of phenanthrene to a larger extent, as it inhibited production of 1-hydroxy-2-naphthoic acid effectively.	Zhong et al. 2010
3.	*Sphingomonas LB126*	Phenanthrene, Fluoranthene, Anthracene and Dibenzothiophene	500 (in presence of pyruvate)	Several mono- and dihydroxy and ring-cleavage products were identified Cometabolism of three compounds is a non-specific process	van Herwijnen et al. 2003
4.	*Rhodococcus opacus* DSM 43205	Naphthalene, Phenanthrene and Fluoranthene	50 (low) and 200 (high)	PAHs individual (main) effect was found to be more significant than the 2-way and 3-way interaction effects on PAH degradation The PAH exhibited an inhibitory effect according to the initial concentration of each PAH in combination with the effects of interaction between the different PAHs. Lower complexity PAH showed higher degradation than highly complex PAH.	This study

4.1.2.3. Identification of intermediate biodegradation metabolites

Co-metabolism is a common phenomenon in biodegradation for wastewater treatment because maximum microbial PAHs degradation occurs in the presence of other homologous / heterogeneous aromatic rings present in the wastewater. It has previously been shown that NAPH, PHEN and FLOR could be co-metabolized by the *R. opacus* as the sole growth substrate and the same has been confirmed in this study (Zhong et al., 2010). Various studies have earlier reported that the inhibition in co-metabolic activities is caused by competition for the common enzyme involved in PAHs biodegradation (Zhong et al., 2010). It is possible that more enzymes are involved in PAH biodegradation in a ternary component system than in an individual PAH biodegradation system.

4.1.2.3.1. Identification of naphthalene metabolites

Fig. 4.10 and Fig. 4.11 (a) show that the ortha/para pathways were followed by *R. opacus* for the degradation of NAPH, which was confirmed by the presence of intermediates in this pathway (Fig. 4.10). 1,2-dihydroxynaphthalene, 2-hydroxychromene-2-carboxylate (HCCA), trans-hydroxy benzylidenepyruvate (tHBPA), salicylaldehyde, salicylate, catechol and gentisate were formed during naphthalene biodegradation following the ortho/para pathways.

Seven different metabolites were identified in the biodegradation of naphthalene in the ternary PAH system. Fig. 4.11 (a) confirmed the presence of 1,2-dihydroxynaphthalene, 2-hydroxychromene-2-carboxylate (HCCA), trans-hydroxybenzylidenepyruvate (tHBPA), salicylaldehyde, salicylate, catechol and gentisate as revealed by comparing the mass spectra obtained with the literature. These metabolites

formed are attributed to the activity of different dioxygenase involved in the biodegradation pathway.

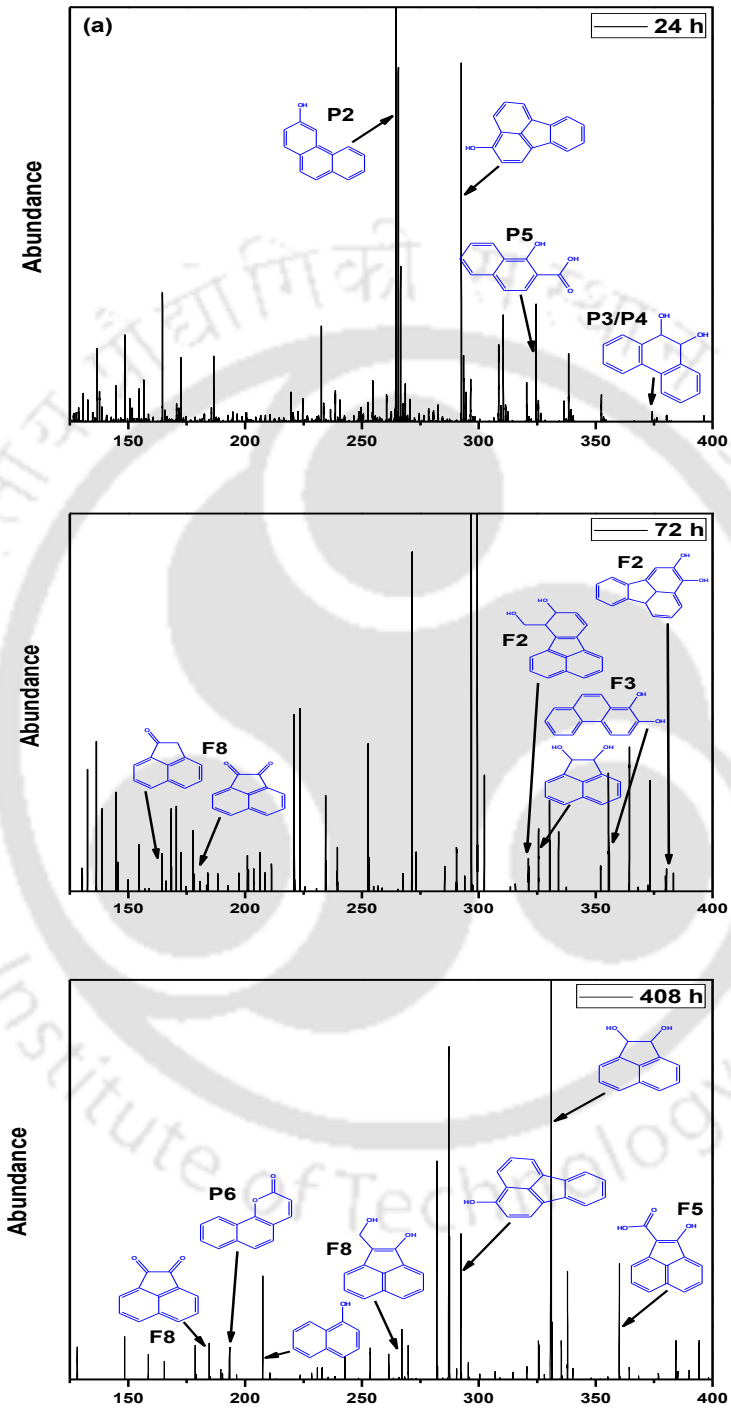

Fig. 4.10: Mass spectra of intermediate metabolites formed during biodegradation of PAHs in ternary system at (a) 24 h, (b) 72 h and (c) 408 h

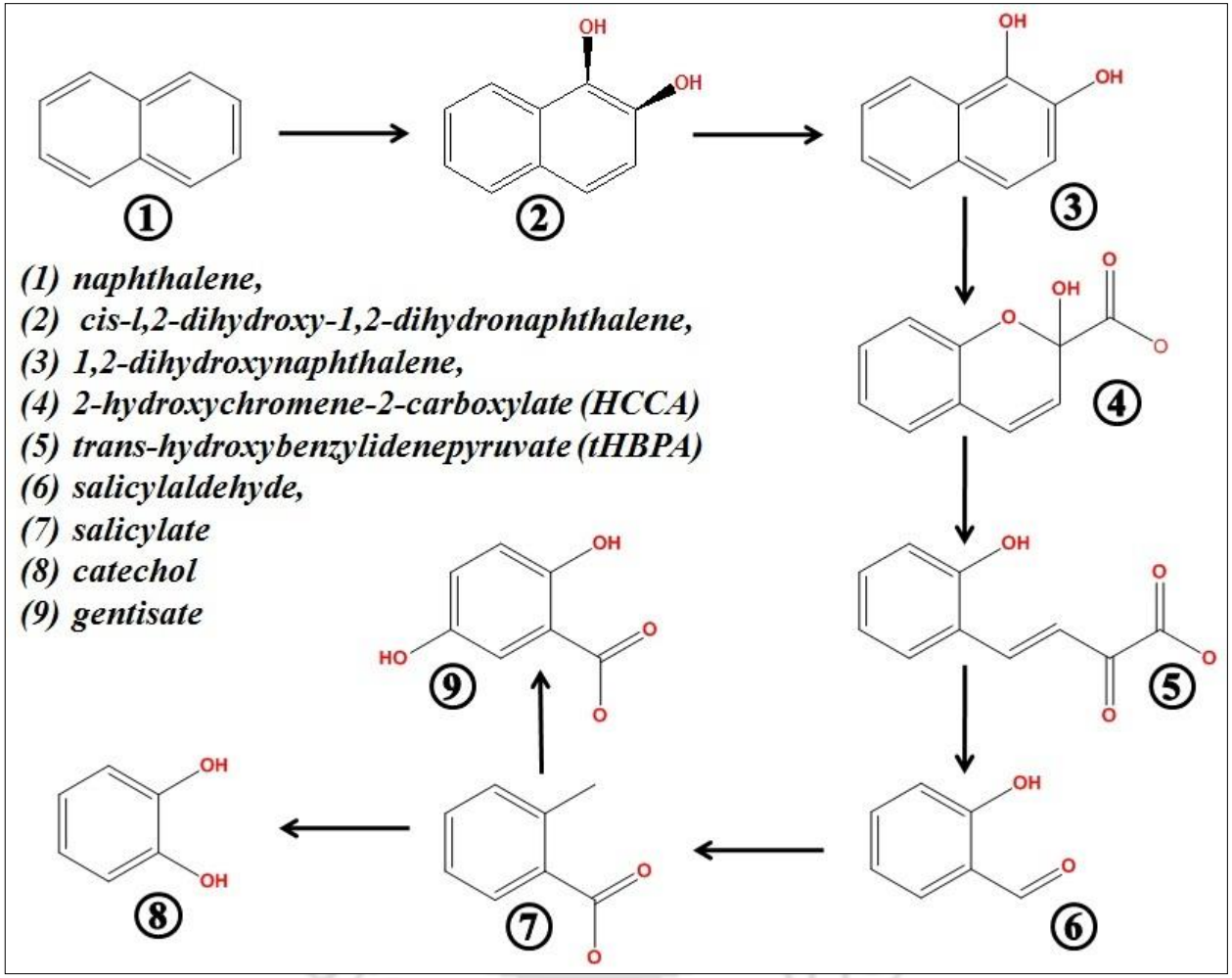

Fig. 11: (a) Proposed pathway for naphthalene biodegradation in ternary PAH system by *R. opacus*

4.1.2.3.2. Identification of phenanthrene metabolites

Fig. 4.11 (b) shows the proposed biodegradation pathway of phenanthrene by *R. opacus*. Metabolites viz., 1-phenanthrol, 1, 2-dihydroxyphenanthrene, 7,8-benzocoumarin, 1-hydroxy-2-naphthoic acid and 1-naphthol were identified. The identification of phenanthrene di-hydrodiol at 3 and 4 or 9 and 10 positions by *Sphingomonas LB126* has previously been reported which co-metabolically produces a *trans*-9, 10-dihydrodiol metabolite (Zhong et al., 2011). The identification of other cleavage product suggests that PHEN biodegradation followed at least two different pathways i.e., ortho/para and meta pathways.

1-Phenanthrol has a molecular ion (M+) at m/z 266 and major fragment ions at m/z 266 (M+, 100), 251 (72), 235 (40), 73 (27) (Table 4.8). These metabolites formed are attributed to the activity of different mono-oxygenases involved in the biodegradation pathway. Dihydroxyphenanthrene, has a molecular ion (M+) at (m/z) 354 and major fragment ions at (m/z) 354 (M+, 59), 339 (3), 266, (32), 236 (21), 73 (100). Also, dioxygenation of phenanthrene at 1,2-, 3,4-, and 9,10- positions is mainly responsible for its biodegradation by the bacterium, which results in the formation of phenanthrene 1,2-diol, phenanthrene 3,4-diol or 9,10-diol, respectively. 7,8-benzocoumarin, has a mass spectrum (M+) at m/z 196 and major fragment ions at m/z 168 (100), 139, (61), 113 (7), 89 (5), 70 (13), 63 (10) (Table 4.9 (b)) (Zhong et al., 2011). The formation of these diol metabolites is attributed to the activity of different di-oxygenase enzymes involved in the biodegradation pathway. Two other different mass spectra of the molecular ion (m/z 332, 317, 243, 185, 170, 147, 114, 73) and (m/z 216, 201, 185, 144, 115, 73) suggest the formation of 1-hydroxy-2- naphthoic acid and 1-naphthol, respectively.

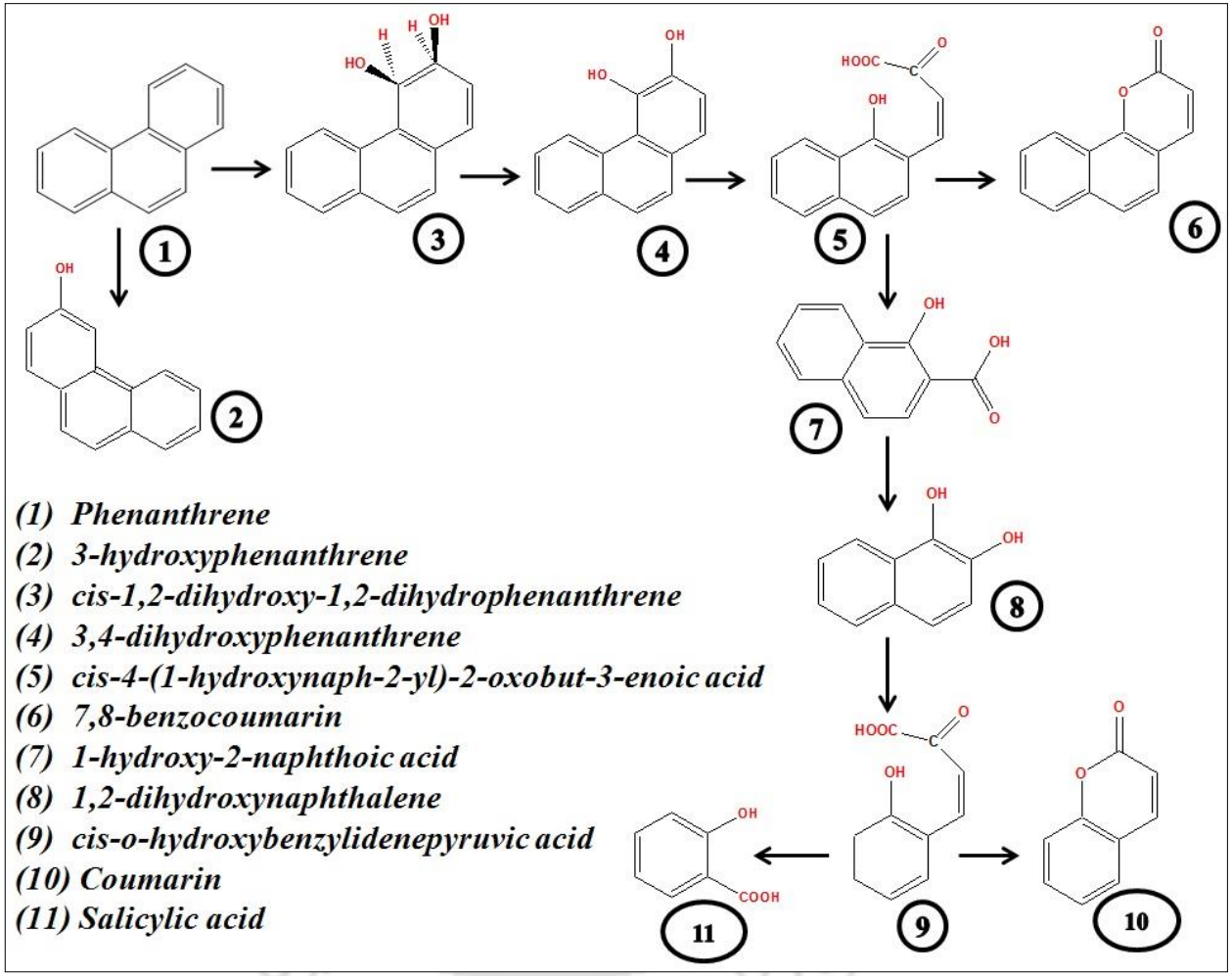

Fig. 4.11: (b) Proposed pathway for phenanthrene biodegradation in ternary PAH system by *R. opacus*

The identification of 1-hydroxy-2-naphthoic acid as an intermediate further confirmed that phenanthrene was initially attacked at C-3,4 position to form phenanthrene 3,4-diol followed by meta-cleavage to yield 1-hydroxy-2-naphthoic acid (Zhang et al. 2011). Identification of 1-hydroxy-2-naphthoic acid inferred that phenanthrene was initially degraded via 3,4-dioxygenation to form 3,4-dihydroxyphenanthrene, which could further undergo meta-cleavage and then converted to 1-hydroxy-2-naphthoic acid. Pinyakong et al. (2000) reported that 1-hydroxy-2-naphthoic acid can be further metabolized through two different pathways; (1) via salicyclic acid and catechol and (2) via o-phthalic acid. Considering the ring-cleavage reaction further, the pathway enters into tri-carboxyilic acid cycle (TCA) for further biochemical conversions.

Except 1-phenanthrol, the concentration of all the intermediate metabolites of phenanthrene degradation reached their maxima in 48-72 h and thereafter declined to undetectable limits after 96 h, suggesting that phenanthrene metabolites were transient. 1-phenanthrol was degraded completely after 120 h (data not shown), and following which both mono- and di-hydroxylated intermediate metabolites were present in the ternary system. It could be postulated that mono-hydroxyphenanthrene (i.e., 1-phenanthrol/2-phenanthrol/9-phenanthrol) was formed by dehydration of dihydrodihydroxyphenanthrene or by mono-hydroxylation of phenanthrene. In both the cases the formation of mono-hydroxyphenanthrene implies that hydroxylation of phenanthrene is not a selective process but may take place at any of its carbon atoms. Further, identification of phenanthrene dihydrodiol at 3 and 4 or 9 and 10 positions by *Sphingomonas* LB126 has previously been reported which cometabolically produces a *trans*-9,10-dihydrodiol metabolite. Thus, the results of identification of all these intermediates suggest that the biodegradation of phenanthrene followed mainly ortho/para pathways.

Table 4.8: Mass spectra of phenanthrene metabolites formed during PAHs biodegradation in the ternary system

(a) Phenanthrene	Fragments (m/z of major fragment ions)
1-Phenanthrol	**266** (M+, 100), 251 (72), 235 (40), 73 (27)
2-Phenanthrol	**266** (M+, 100), 251 (90), 235 (10), 73 (13)
3-Phenanthrol	**266** (M+, 100), 251 (76), 235 (11), 73 (13)
4-Phenanthrol	**266** (M+, 100), 251 (65), 235 (72), 73 (46)
9-Phenanthrol	**266** (M+, 100), 251 (67), 235 (25), 73 (48)
Phenanthrene dihydrodiol	**354** (M+, 59), 339 (3), 266, (32), 236(21), 73 (100)
Dihydroxyphenanthrene	**354** (M+, 100), 339 (22), 266, (3), 236(2), 73 (52)
7,8-Benzocoumarin	**196** (M+, 67), 168 (100), 139, (61), 113 (7), 89 (5), 70 (13), 63 (10)
1-Hydroxy-2-naphthoic acid	**332** (M+, 2), 317 (100), 243 (10), 185 (26), 170 (4), 147(21), 114(10), 73 (85)
1-Naphthol	**216** (M+, 100), 201 (97), 185 (49), 144 (20), 115 (40), 73 (46)

4.1.2.3.3. Identification of fluoranthene metabolites

Fig. 4.11 (c) and Table 4.9 show the various metabolites identified from the biodegradation of fluoranthene in the mixed PAHs system. The abundance of fluoranthene diols indicates that the bacterium degraded fluoranthene via dioxygenation at C-1,2, C-2,3 and C-7,8 positions to yield fluoranthene 1,2-diol, fluoranthene 2,3-diol and fluoranthene 7,8-diol, respectively (Zhong et al., 2011). These diols could further be degraded through meta-cleavage to form 1-acenaphthylenone and it was monooxygenated to form acenaphthenequinone. Formation of acenaphthenequinone is followed by spontaneous oxidation leading to the formation of 1, 8-naphthalic anhydride and 1, 8-naphthalide (Fig. 4.11 (c)). Zhong et al. (2011), Kweon et al. (2007) and López et al. (2005) reported a similar pathway for fluoranthene biodegradation in single as well in multi-component study.

LC-MS mass spectra of the molecular ion 290 (M+, 100), 275 (38), 259 (42), 73 (29) was compared with the known standards and confirmed as 3-hydroxyfluoranthene. Mono-oxygenation of the fluoranthene is attributed to the activity of mono-oxygenase enzyme present in *R. opacus*. Another molecular ion (M+) having m/z 378 along with major fragment ions at m/z 290, 260 and 73 were highly consistent with that of fluoranthene 2,3-diol (Table 4.9). The fragment ions m/z of fluoranthene diols were confirmed by the molecular ion present at 380 (381, 292, 291, 290, 275, 218, 202, 201, 189, 73). The abundance of fluoranthene diols indicates that the bacterium effectively biodegraded fluoranthene via dioxygenation at C-1,2, C-2,3 and C-7,8 positions to yield fluoranthene 1,2-diol, fluoranthene 2,3-diol and fluoranthene 7,8-diol, respectively (Zhang et al., 2011). The diol metabolites formed is attributed to the activity of dioxygenase enzyme present in the bacteria. Furthermore, a molecular ion (M+) at m/z 168 was identified and a major fragment ion at m/z 140 was identical to that of 1-acenaphthenone (López et al. 2005). Acenaphthenequinone with a molecular ion (M+) at m/z 182 along with major fragment ions at m/z 154 and 126 was also identified from the mass spectra (Poonthrigpun et al. (2006). 1, 8-naphthalic anhydride with a molecular ion (M+) at m/z 184 and major fragment ions at m/z 155, 139 and 127, was identified as 1, 8-naphthalide (Kweon et al. 2007). These LC-MS analysis results of intermediates formed verified that *R. opacus* degraded fluoranthene via initial dioxygenation at C-7,8-diol. Additionally, diol was degraded through meta-cleavage to form 1-acenaphthylenone and further monooxygenated to form acenaphthenequinone. Formation of acenaphthenequinone is followed by spontaneous oxidation leading to the formation of 1,8-naphthalic anhydride and 1,8-naphthalide (Fig. 4.11 (c)).

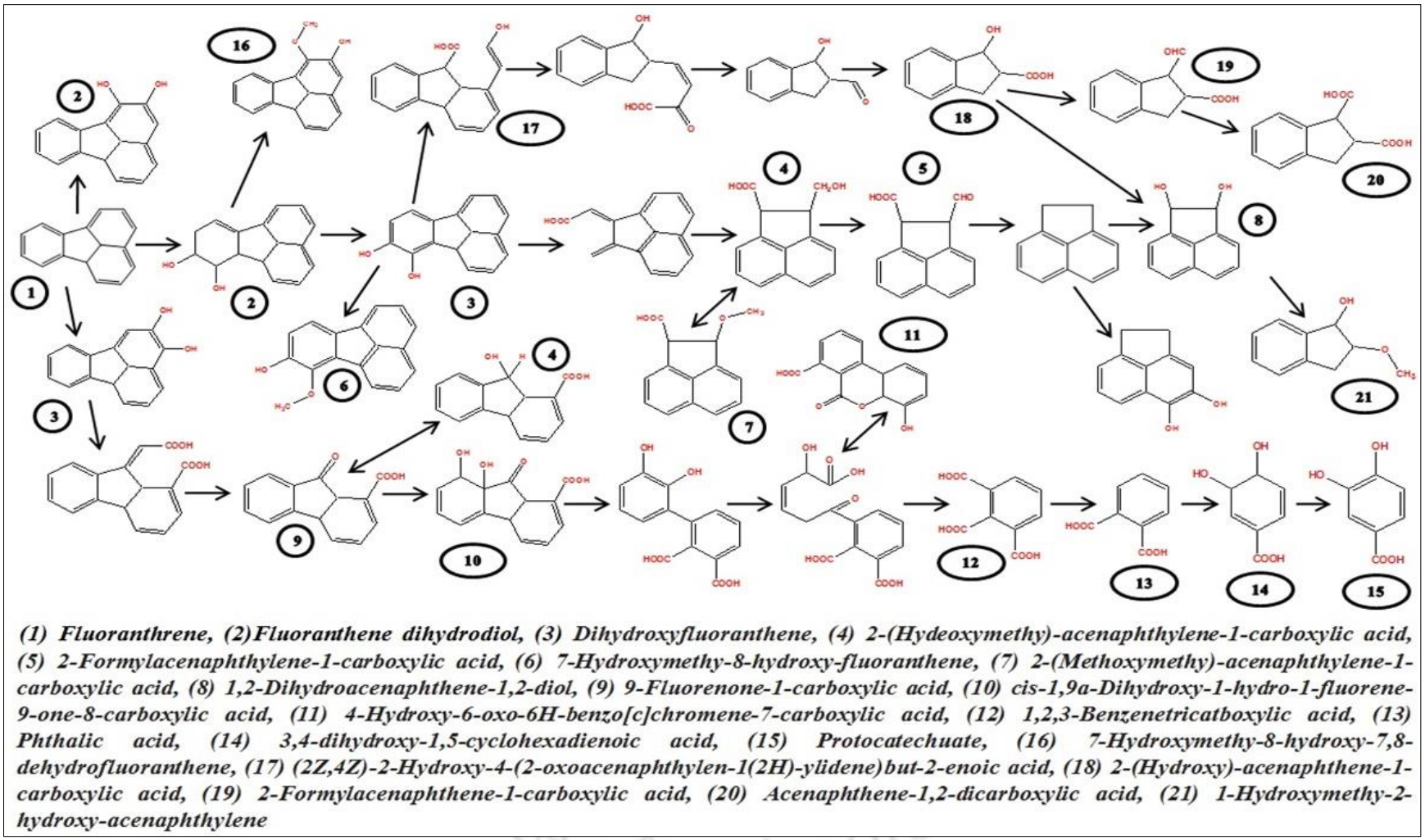

(1) Fluoranthrene, (2)Fluoranthene dihydrodiol, (3) Dihydroxyfluoranthene, (4) 2-(Hydeoxymethy)-acenaphthylene-1-carboxylic acid, (5) 2-Formylacenaphthylene-1-carboxylic acid, (6) 7-Hydroxymethy-8-hydroxy-fluoranthene, (7) 2-(Methoxymethy)-acenaphthylene-1-carboxylic acid, (8) 1,2-Dihydroacenaphthene-1,2-diol, (9) 9-Fluorenone-1-carboxylic acid, (10) cis-1,9a-Dihydroxy-1-hydro-1-fluorene-9-one-8-carboxylic acid, (11) 4-Hydroxy-6-oxo-6H-benzo[c]chromene-7-carboxylic acid, (12) 1,2,3-Benzenetricatboxylic acid, (13) Phthalic acid, (14) 3,4-dihydroxy-1,5-cyclohexadienoic acid, (15) Protocatechuate, (16) 7-Hydroxymethy-8-hydroxy-7,8-dehydrofluoranthene, (17) (2Z,4Z)-2-Hydroxy-4-(2-oxoacenaphthylen-1(2H)-ylidene)but-2-enoic acid, (18) 2-(Hydroxy)-acenaphthene-1-carboxylic acid, (19) 2-Formylacenaphthene-1-carboxylic acid, (20) Acenaphthene-1,2-dicarboxylic acid, (21) 1-Hydroxymethy-2-hydroxy-acenaphthylene

Fig. 4.11: (c) Proposed pathway for fluoranthene biodegradation in ternary PAH system by *R. opacus*

These results of fluoranthene biodegradation is consistent with those of Zhong et al., (2011); Kweon et al., (2007) and López et al., (2005).

Biodegradation of all the three PAH substrate components primarily followed the ortho/para pathway. Metabolites formed by the meta pathway leads to incomplete mineralization of the PAHs and the activity of the meta pathway may also lead to inhibition of the ortho/para pathways. The initial breakdown of the PAH by the meta-pathway proceeded at a much slower rate than by the ortho/para pathways.

Zhong et al. (2010) reported that the transformation of hydroxylated phenanthrene into 1-hydroxy-2-naphthoic acid was a rate-limiting step in the biodegradation of phenanthrene by *Sphingomonas* sp. strain PheB4. Zhong et al. (2011) reported that the use of multiple organisms, e.g., *Mycobacterium* sp. and *Sphingomonas* sp., that use different metabolic pathways, did not increase the degradation rate and efficiency of the recalcitrant PAHs. A similar biodegradation pattern was observed by Ghosh and Mukherji (2017) using a high initial concentration of phenanthrene (3-ring) or fluoranthene (4-ring) either as binary substrates or as tertiary substrates; these compounds showed statistically significant adverse effect on pyrene biodegradation by *Pseudomonas aeruginosa* RS10. According to van Herwijnen et al. (2003) the metabolic pathway of fluorene degradation and cometabolic pathways of phenanthrene, fluoranthene, anthracene and dibenzothiophene degradation by *Sphingomonas species*, is a non-specific process, which is in agreement with the present study that the inhibitory effect caused by PAHs on each other biodegradation was strongly influenced by their respective initial PAH concentrations. Complexity of a specific PAH in terms of the number of aromatic rings present imposed a strong inhibitory effect on the biodegradation of the other PAH in mixture.

Table 4.9: Mass spectra of fluoranthene metabolites formed during PAHs biodegradation in the ternary system

Fluoranthene	Fragments (m/z of major fragment ions)
Fluoranthene dihydrodiol	**380** (381,292,291,290,275,218,202,201,189,73)
	380 (381,365,291,263,218,202,189,147,73)
Dihydroxyfluoranthene	**378** (379,290,260,215,73)
2-(Hydeoxymethy)-acenaphthylene-1-carboxylic acid	**370** (355, 280,251,237,207,179,164,73)
2-Formylacenaphthylene-1-carboxylic acid	**296** (297,281,282,237,207,179,165,151,89,73)
7-Hydroxymethy-8-hydroxy-fluoranthene	**320** (321,290,291,260,187,145,130,73)
2-(Methoxymethy)-acenaphthylene-1-carboxylic acid	**312** (297,281,267,223,193,178,165,151,73)
1,2-Dihydroacenaphthene-1,2-diol	**328** (314,313,285,269,145,132,117,75,73)
	328 (314,313,285,269,171,145,132,117,75,73)
9-Fluorenone-1-carboxylic acid	**296** (297,281,282,237,207,179, 151,150,111,73)
cis-1,9a-Dihydroxy-1-hydro-1-fluorene-9-one-8-carboxylic acid	**474** (459,385,369,295,269,253,223,165,147,73)
4-Hydroxy-6-oxo-6H-benzo[c]chromene-7-carboxylic acid	**400** (401,386,385,311,240,210,75,73)
1,2,3-Benzenetricatboxylic acid	**411** (381,337,323,309,204,203,175,147,73)
Phthalic acid	**310** (295,251,221,178,103,73)
3,4-dihydroxy-1,5-cyclohexadienoic acid	**372** (357,255,239,240,173,143,73)
Protocatechuate	**369** (370,296,267,252,235,177,164,150,126,73)
7-Hydroxymethy-8-hydroxy-7,8-dehydrofluoranthene	**322** (307,292,293,294,291,260,189,146,138,73)
(2Z,4Z)-2-Hydroxy-4-(2-oxoacenaphthylen-1(2H)-ylidene)but-2-enoic acid	**410** (395,293,176,147,73)

2-(Hydroxy)-acenaphthene-1-carboxylic acid	**358** (343,269,202,179,165,147,75,73)
2-Formylacenaphthene-1-carboxylic acid	**298** (253,237,208,201,180,165,152,139,113,73)
Acenaphthene-1,2-dicarboxylic acid	**386** (387,297,269,270,255,254,240,201,165,73)
1-Hydroxymethy-2-hydroxy-acenaphthylene	**270** (227,185,171,143,87,74)
3-Hydroxyfluoranthene	**290** (M+, 100), 275 (38), 259 (42), 73 (29)
Monohydroxyfluoranthene	**290** (M+, 100), 275 (64), 259 (4), 73 (16)
Fluoranthene diol	**378** (M+, 100), 290 (37), 260 (28), 73 (82)
1-Acenaphthylenone	**168** (M+, 88), 140 (100)
Acenaphthenequinone	**182** (M+, 40), 154 (83), 126 (100), 98 (9), 63 (23)
1,8-Naphthalic anhydride	**198** (M+, 74), 154 (100), 126 (89), 63 (23)
1,8-Naphthalide	**184** (M+, 74), 155 (100), 139 (17), 127 (91)
monohydroxy-fluoranthene	**232** (*M*+, 100.0), 217 (37.8), 189 (99.1), 163 (5.3), 116 (12.3), 100 (11.4), 95 (14.9), 94 (10.9), 87 (5.7)
9-fluorenone-1- (carboxy-2-hydroxy-1-propenol)	**294** (*M*+, 19.9), 263 (10.8), 235 (100.0), 220 (48.3), 203 (4.2), 192 (4.9), 176 (13.9), 164 (25.2), 163 (23.4), 150 (5.0), 118 (6.7), 101 (2.4), 88 (22.8)
7,8-dihydroxy-fluoranthene	**262** (*M*+, 100.0), 247 (99.4), 232 (8.2), 219 (31.2), 204 (37.5), 187 (12.0), 176 (42.5), 150 (7.6), 131 (15.7), 94 (7.2), 87 (9.4), 74 (9.8)

4.1.3. Effect of heavy metals on PAH biodegradation

4.1.3.1. *R. opacus* biomass growth and anthracene biodegradation in the presence of heavy metals

The capability of *R. opacus* to simultaneously biodegrade anthracene and accumulate lipids in presence of different heavy metals was studied and is shown in Fig. 4.12 (a-c). These results reveal that in the presence of heavy metals, the bacterium showed a reduced anthracene biodegradation rate and efficiency along with a decrease in both biomass and total lipid accumulation. A separate set of flasks without the inoculum served as the control in the experiments, which indicated that the abiotic loss of the PAH was within the range 1.6 - 4.7%. Fig. 4.12 (b) reveals a clear difference in the lag phase of biomass growth in presence and absence of the heavy metals. The anthracene biodegradation efficiency decreased sharply in presence of the heavy metals when compared to that of the control (Fig. 4.12 (a)). The total time for maximum biomass growth also increased from 168 h to 216 h in presence of Fe, Cu, Zn and Pb and to 240 h in presence of Cd and Ni. The heavy metals effect on *R. opacus* biomass growth, lipid accumulation and anthracene biodegradation followed the order: Cd > Ni > Pb > Cu > Zn > Fe. A sharp decline in anthracene biodegradation efficiency in presence of the heavy metals is observed at 72-84 h, which correlates well with the decline in the cell dry weight of the bacterium. Fig. 4.13 further shows that a decrease in the specific anthracene consumption rate ($-q_A$) is observed in the presence of these heavy metals (Fig. 4.13).

A similar trend in biomass growth and total lipid content in presence of the heavy metals is observed for the other initial anthracene concentrations of 100 and 200 mg L^{-1}. These results suggest that the heavy metals are primarily responsible for the inhibition of metabolic activity, possibly due to the damage of metallothionein, an enzyme involved in

the early stage of the organism's growth (Maria et al. 2013). Hence, it could be suggested that both heavy metal removal and PAH biodegradation by *R. opacus* involves same physicochemical interactions between the pollutants and the bacterium. The effect due to heavy metals on biomass growth, anthracene biodegradation and lipid accumulation by *R. opacus* correlate well with the observation that the residual concentration of heavy metals at 24 h of the experiments is found to be nil. Heavy metal removal mechanism by the organism is primarily attributed to their quick biosorption followed by their uptake inside the cells, which is consistent with literature reports that microbial biosorption significantly influences the biodegradation of recalcitrant compounds (Roy et al. 2015; Lu and Zhu 2012; Sokhn et al. 2001). Bueno et al. (2008) investigated the sorption capacity of non-viable *R. opacus* to bind with heavy metals (Pb, Cu and Cr) from aqueous environment and observed that the sorption phenomena followed the pseudo-second order kinetics. In the literature, Chen et al. (2013) reported that Cu (II) inhibited benzo[a]pyrene biodegradation by *Stenotrophomonas maltophilia* owing to the bacterial cell wall damage.

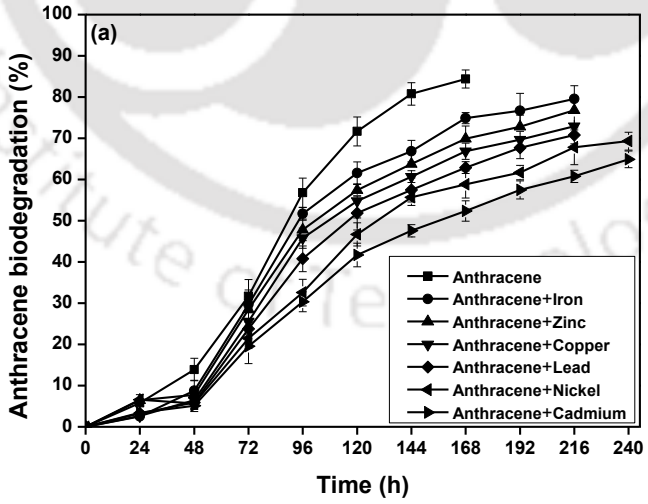

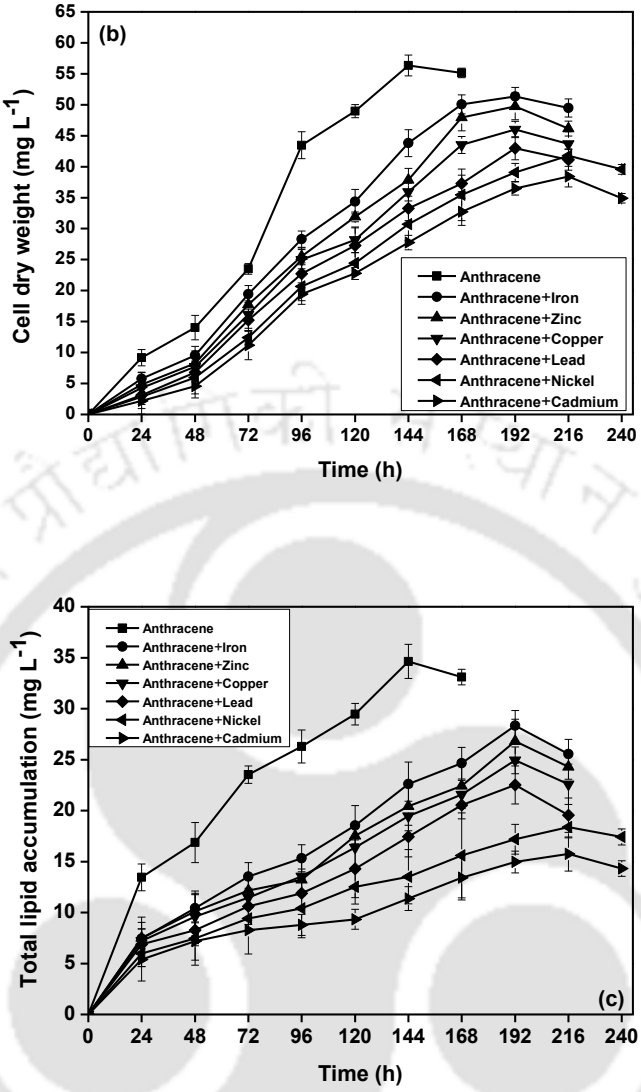

Fig. 4.12: Time profile of (a) anthracene biodegradation; (b) biomass grown and (c) total lipid accumulation by *R. opacus* in presence of different heavy metals (initial anthracene concentration=100 mg L^{-1}; initial heavy metal concentration=10 mg L^{-1})

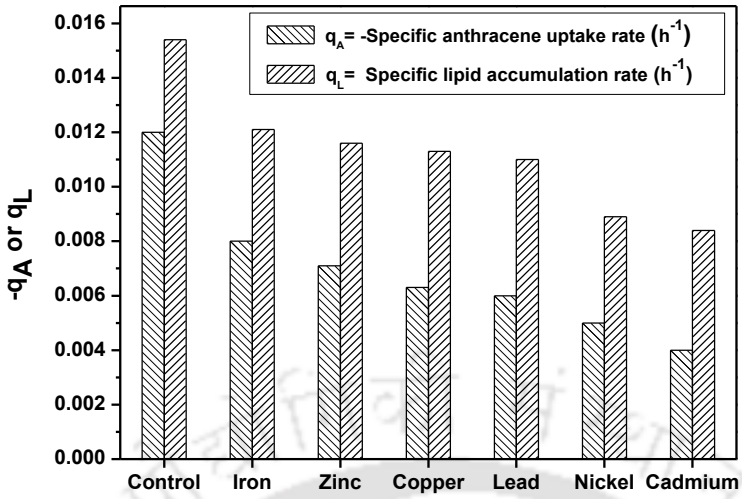

Fig. 4.13: Estimated specific anthracene uptake rate and specific lipid accumulation rate by *R. opacus* in presence of different heavy metals

4.1.3.2. Characterization of the bacterial biomass

4.1.3.2.1. FTIR spectroscopy analysis

Bacterial biomass obtained from the experiments was further characterized utilizing Fourier transform infrared (FTIR) spectrometer to study the interaction between heavy metal ions and functional groups involved on the bacterial surface (Fig. 4.14). The control biomass depicted strong peaks at 1637, 1462, 1382, 1057, 786 and 564 cm^{-1}, which are attributed to primary amine of proteins (amide III, -N-H) stretch (1650-1580 cm^{-1}), C-H alkane bend (1470–1450 cm^{-1}), -CH_2-(C=O) stretch (1400-1370 cm^{-1}), secondary amide (γ(N-H)+v(C-N), -SO_3H stretch, pyridine (I) β (C-H) and pyridine (II) β (C-H) (1300–850 cm^{-1}), C-H and O-H bending stretch (750-700cm^{-1}) and alkyl halide (-C–Cl) stretch (850–550 cm^{-1}), respectively (Ye et al., 2013). Comparison of the spectra due to control biomass with that of the heavy metal loaded biomass reveals that N-H, C–H bend, -CH_2-(C=O), C–N stretch, C-H and O-H bending and -C–Cl stretch, participated in heavy metal binding

by the bacterium. These FTIR results confirm the involvement of peptidoglycan present in the bacterial cell wall for heavy metal binding (Wei et al. 2011).

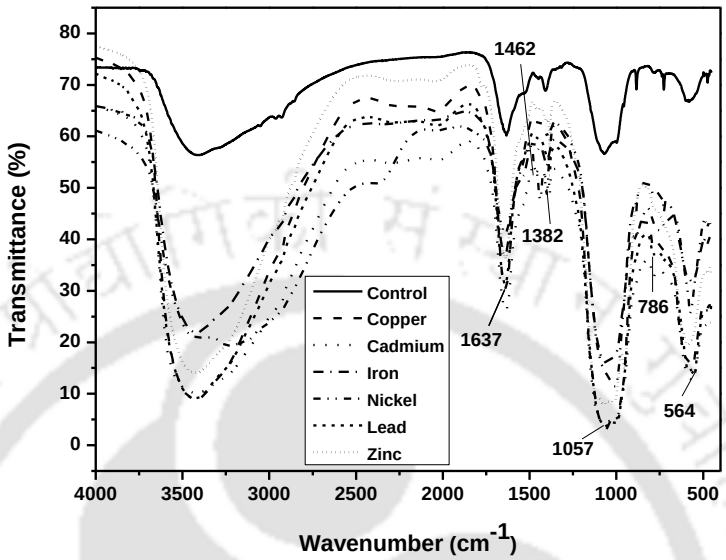

Fig. 4.14: FTIR spectra of control biomass and metal loaded biomass

4.1.3.2.2. FESEM, EDX and TEM analyses

For understanding the changes in morphology and elemental composition of the *R. opacus* biomass grown in presence of the heavy metals, FESEM-EDX analyses of control biomass and the metal loaded biomass was performed. Fig. 4.15 (a & b) clearly shows morphological difference in the bacterial cell due to the heavy metals. Inhibitory effect due to the heavy metals on lipid accumulation by the bacterium is evident from the small sized globules of the biomass observed under TEM (Fig. 4.16 (a & b)). Whereas Fig. 4.16 (a) shows TEM image of control biomass grown without any heavy metals, Fig. 4.16 (b) is TEM image of biomass grown in presence of heavy metals. Fig. 4.17 (a-f) displays EDX spectrum of the control and the heavy metal loaded biomass, which clearly reveals an extra

peak due to the respective heavy metals on the biomass. These results confirmed that heavy metal uptake by the bacteria is due to biosorption.

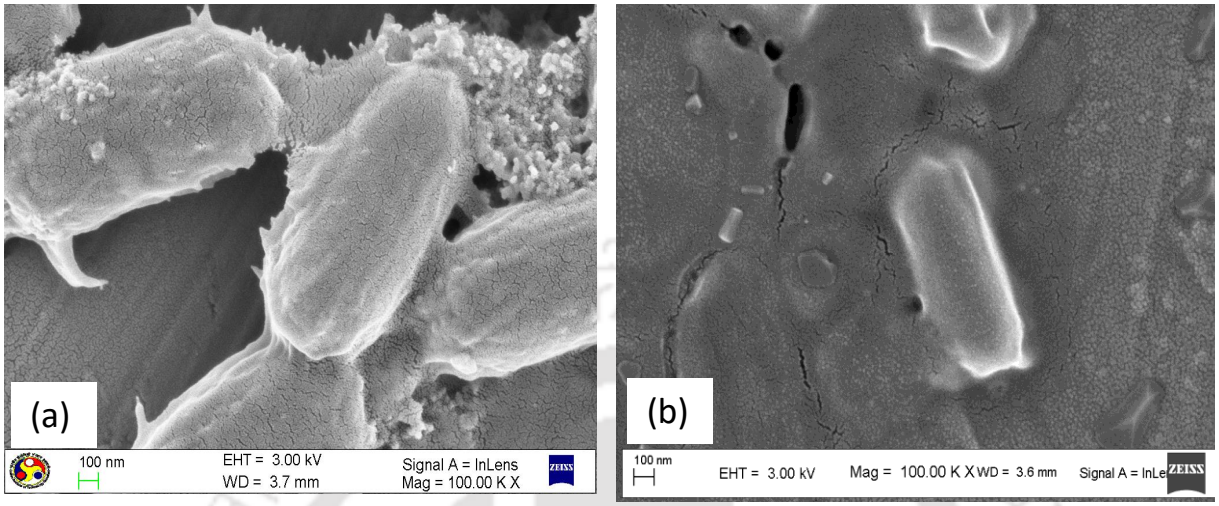

Fig. 4.15: FESEM micrographs of the bacteria (a) control biomass and (b) heavy metal loaded biomass

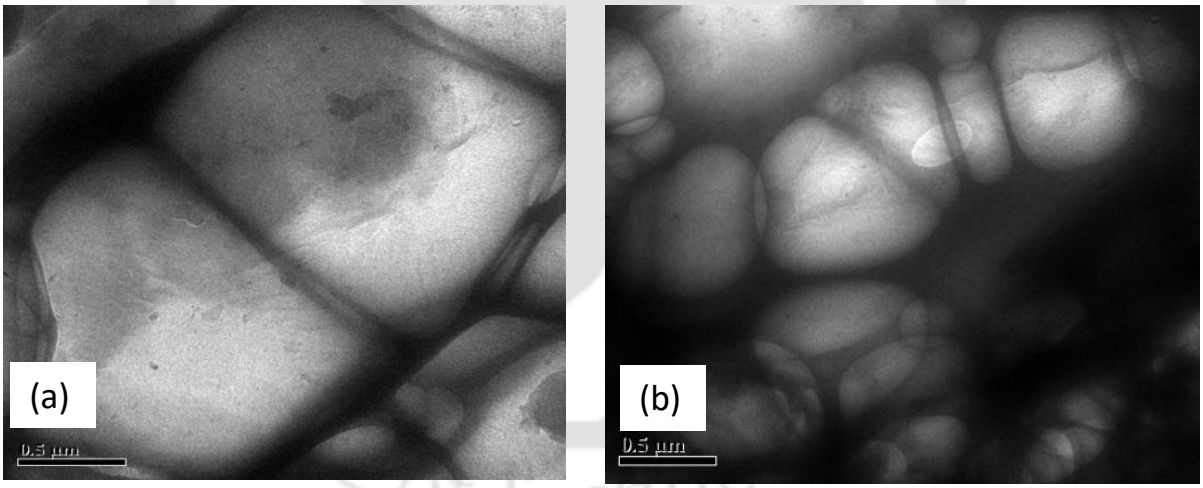

Fig. 4.16: TEM micrographs showing lipid globules accumulated inside the bacteria: (a) control biomass and (b) heavy metal loaded biomass

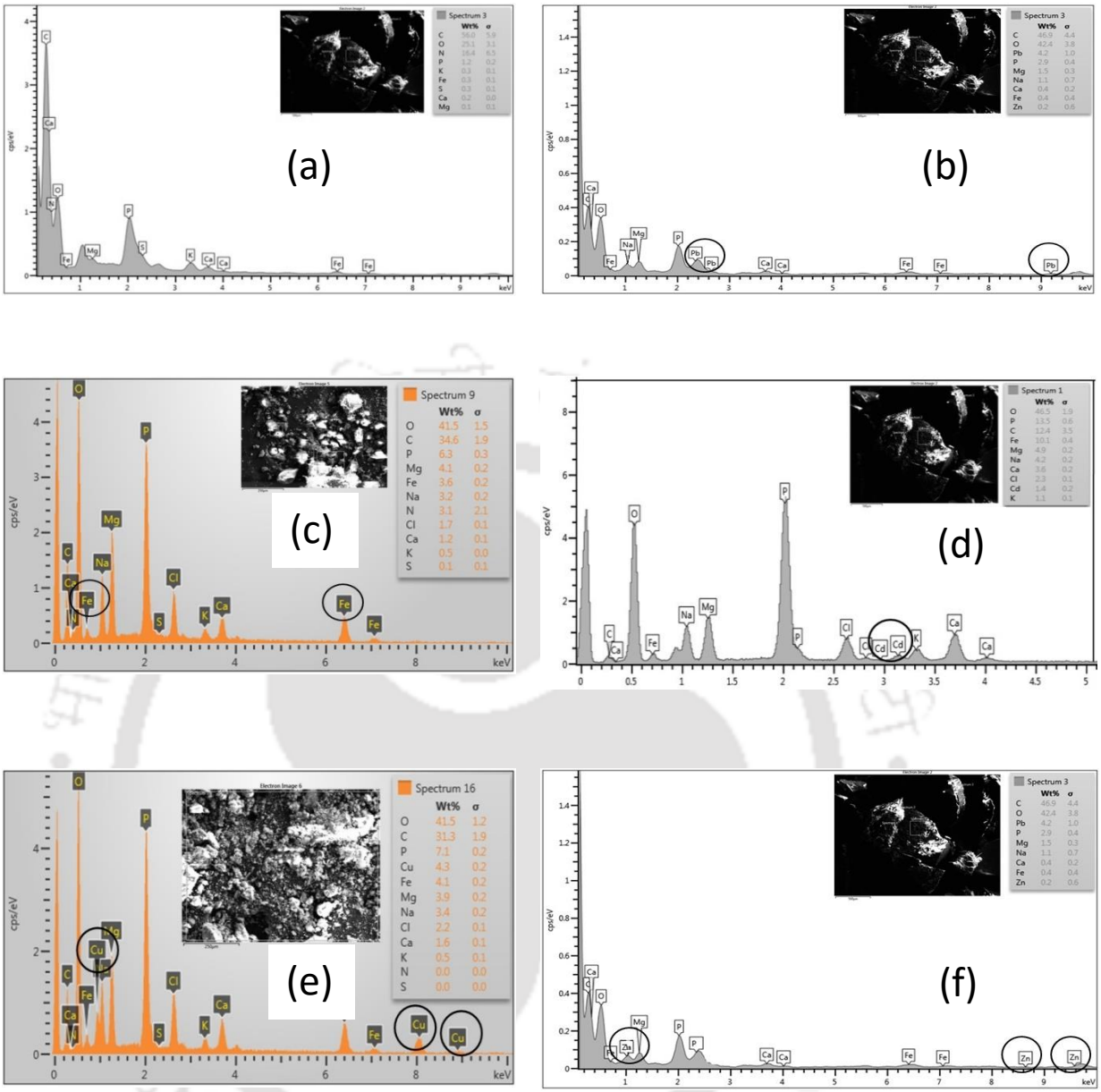

Fig. 4.17: EDX spectrum of (a) control biomass and biomass loaded with (b) Pb (II); (c) Fe (III); (d) Cd (II); (e) Cu (II); (f) Zn (II). Insert shows FESEM micrographs of the biomass loaded with the respective metals

4.2. Biochar aided PAH biodegradation by *R. opacus*

4.2.1. Biochar characterization

4.2.1.1. Physical properties

Table 4.10 and Fig. 4.18 represent the elemental composition and surface properties of the biochar prepared in this study. FESEM image of the biochar shown in Fig. 4.18 reveals a smooth and clear morphology of the material. The carbon, hydrogen and nitrogen compositions in the biochar were 58.4%, 2.65% and 2.12%, respectively (Fig. 4.18 (c)). A zeta potential value of 3.93 mV indicates that the biochar surface is covered with positively charged species. The average particle size of the biochar was found to be 844.9 nm with a total surface area of 9.19 m^2 g^{-1} and 63.1% ash content. The biochar total surface area is similar to that of biochar derived from pine wood. Das et al. (2015a) reported a total surface area of 1.6 m^2 g^{-1} for biochar prepared in this study. Similarly, Ho et al. (2015) also reported a total surface area of 0.523 m^2 g^{-1} for bamboo derived biochar.

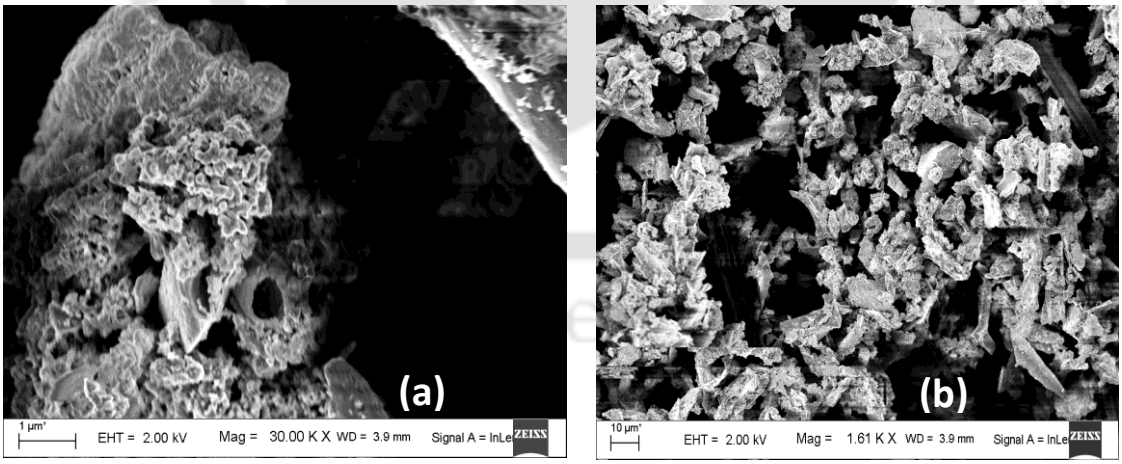

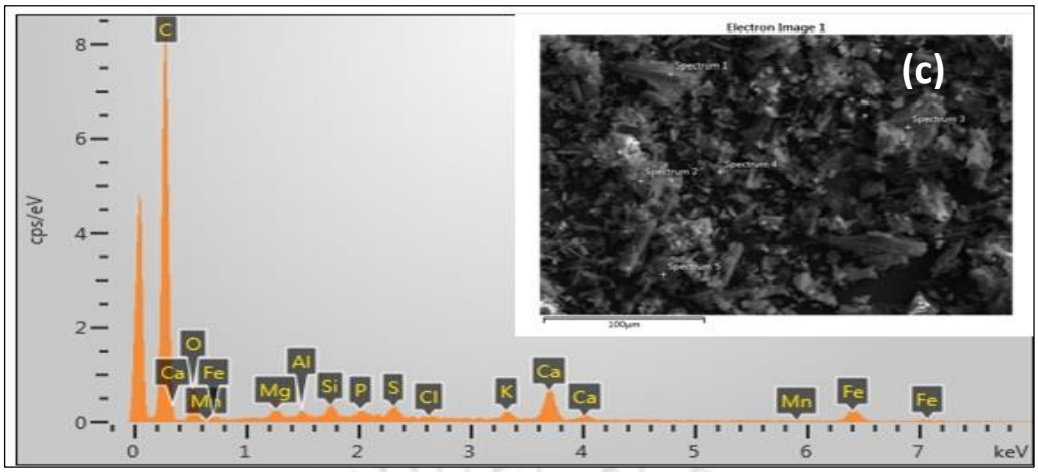

Fig. 4.18: FESEM micrographs of biochar prepared in this study (a) 1 µm and (b) 10 µm and (c) FESEM-EDX spectrum of the biochar (insert shows biochar FESEM)

In this study, contact angle of the biochar is found to be 78.4º. In general, hydrophilic surfaces have a contact angle less than 90° and impose positive capillary pressure, thus allowing water to easily enter into the pores, whereas hydrophobic surfaces have a contact angle value greater than 90° and imposes negative pressure, restricting water from entering into the pores (Gray et al., 2014).

4.2.1.2. Chemical properties

Fig. 4.19 (a-c) shows the results of chemical nature of the biochar by employing different techniques. Whereas Fig. 4.19 (a) shows the FTIR spectra of the biochar material, which depicts different vibrational frequencies due to several functional groups present in the biochar. Various types of biochar have shown to depict a wide band spectrum at around 3400 cm^{-1}, which is characteristic of the hydroxyl groups (O-H) (Bind et al. 2018). At 2918 cm^{-1}, another band of $–CH_2$ is observed (Das et al., 2015b) followed by a band spectrum at 1744 cm^{-1} corresponding to

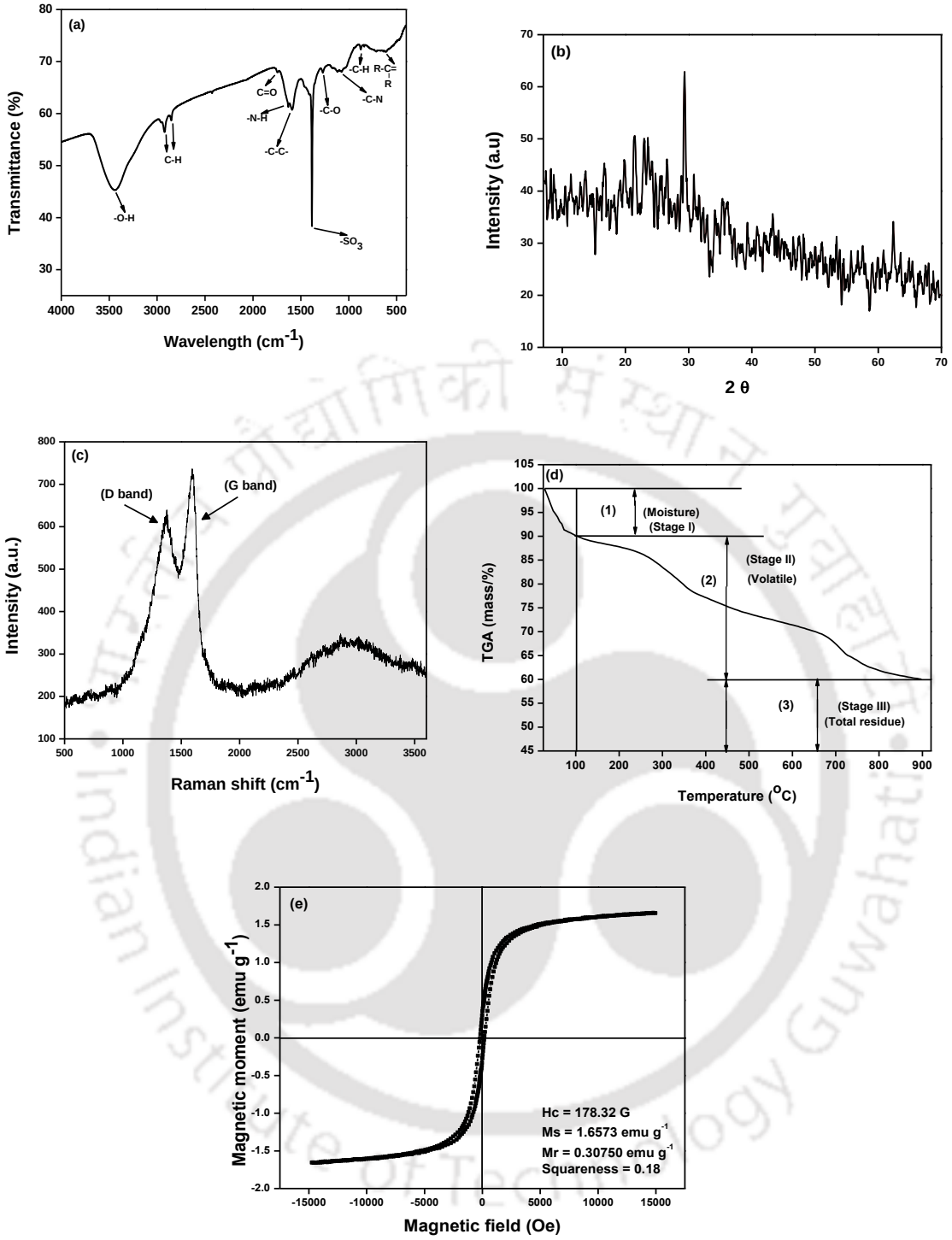

Fig. 4.19: (a) Fourier transform infrared spectroscopy; (b) X-ray diffraction; (c) Raman spectra; (d) Thermogravimetric analysis (TGA) curve; and (b) Vibrating sample magnetometer analyses of the biochar

the carbonyl of ester groups (Aran et al. 2016); a peak at 1631 cm^{-1} is assigned to the primary amine band spectra. The absorption band in the range 1615-1580 cm^{-1} signifies

the –C-C- band spectra of aromatic carbon atoms. A band spectrum between the position 1393 cm^{-1} and 1320 cm^{-1} with an intense peak at 1385 cm^{-1} signifies the presence of $-SO_3$ stretching (Sinha et al 2015). In addition, the FTIR spectra reveals–C-O, -C-N, -C-H–and R_2-C= band stretch corresponding to the functional groups alcohol/ carboxylic acid/ alkoxy, aliphatic amines, alkene and trisubstituted alkene, respectively.

Fig. 4.19 (b) shows XRD profile of the biochar in which the peak intensity in the range of 7–70° is mainly attributed to aromatic and graphite nature of the organic material. A diffraction peak at around 21.0 is clearly attributed to the cellulose crystal plane (Li et al., 2016) with a crystallinity index (I_{Cr}) of 47.4 %. In addition, the peaks at 23 and 43 clearly depict the presence of turbostratic carbons (Das et al., 2016).

Fig. 4.19 (c) shows the first order Raman spectra of the biochar. In general, a peak around 1580 cm^{-1} reveals a perfectly ordered crystalline nature, whereas distorted amorphous carbon nature of the carbon is represented by two distinct peaks: (a) graphite band (G) at about 1600 cm^{-1}, which is related to sp^2 carbon atoms and (b) distorted carbon band (D) at around 1350 cm^{-1}, signifying the sp^3 carbon atoms (Lian et al., 2016; Frost et al., 2003). In this study, both graphite band (G) and distorted carbon band appear in the spectra (Fig. 4.19 (c)). In general, the ratio of intensity of D to G bands (I_D/I_G) (i.e. R value) represents a crystallographic structure, distorted degree and average size of the sp^2 domains in graphite structure of a material (Akhavan et al., 2010). In this study, the biochar yielded two distinct peaks related to D band and G band in the Raman spectra with a I_D/I_G intensity ratio (R-value) of 0.87. These results reveal amorphous nature of the biochar with reduced domains of sp^2 in the carbon structure. All these results of functional group analysis using FTIR spectroscopy, XRD analysis and Raman spectroscopy clearly

demonstrate an excellent ability of the biochar for PAHs adsorption and in enhancing their bioavailability to degrading microorganism.

4.2.1.3. Thermal degradation analysis

TGA of the biochar is represented in Fig. 4.19 (d), which plots the residual sample mass (%) and the discrete time derivative of the residual mass (% min^{-1}) vs. temperature. This figure reveals three peaks indicating the following stages in the material weight loss: Stage I (25°C-100°C), Stage II (100°C- 870°C) and Stage III (870°C -900°C).

The second stage, i.e., devolatilization region appears over a wide temperature interval and characterizes a major mass loss of the biochar. In Fig. 4.19 (d), Stage II indicates loss due to moisture and other volatile components just before the material reaches 100°C. A slight weight loss occurred in Stage I, probably due to the release of embedded volatiles within the biochar. Further weight loss during Stage II at a high rate indicates the formation of some pyrolytic products, primarily phenols, heterocyclic compounds, mono- and polycyclic compounds. Lastly, in Stage III, gradual weight loss (i.e., solid residue devolatilization) was observed which reveals that carbonaceous material present within the solid residue degraded continuously at a very mild rate before reaching a constant value (Peng et al., 2001). Approximately 10 % initial moisture is attributed to the weight loss in Stage I. The total volatile loss can be attributed to the weight loss observed in both Stage II and Stage III. In Stage III, negligible volatile loss is observed. Overall, final residue content within the biochar at 900°C is determined to be 61.4% of the total initial biochar utilized for the TGA analysis, thereby indicating its potential for a long-term use.

4.2.1.4. Magnetic properties

Fig. 4.19 (e) is a plot of magnetization (M) Vs magnetic field (Oe) at room temperature showing the hysteresis loop obtained following the application of VSM technique on the biochar. The magnetization parameters such as saturation magnetization (M_s), remanent magnetization (M_r), coercivity (H_c) and squareness of the derived biochar are represented in Table 4.10. A low H_c value depicts that the material can be simply separated out with the help of a magnet or an externally applied magnetic field and, therefore, the material is easy to separate, recover and reuse in any process (Nguyen et al., 2011). Furthermore, following separation, the material can again be easily re-dispersed into the solution and reutilized owing to its low M_r value (Ahmed et al., 2015).

4.2.2. Cost analysis of the waste derived biochar

The cost of biochar prepared in this study was estimated considering the cost of raw materials, solvents used and power requirements for operating the instrument used for its purification and solvent recovery. Table 4.11 presents the cost involved in each step of the preparation process, which clearly demonstrates that the cost involved is much low considering the average cost of biochar ($ 2,580 per ton), in accordance with the International Biochar Initiative (IBI) report (2013). However, the estimated cost will vary if other costs due to manpower and the capital needed for equipment set up are included. Nevertheless, the biochar preparation cost estimated in this study is still very low as compared with the cost of preparation using other raw materials. Furthermore, the total biochar preparation cost estimated in this study is primarily due to the high power consumption cost of the equipment used for purification. Alternatively, low-power consuming equipment like pervaporation can be employed instead of rotavapor to keep the total preparation cost even much lower.

Table 4.10: Elemental composition, surface and magnetic properties of the biochar

Elemental composition	C (%)	58.4
	H (%)	2.65
	N (%)	2.12
	H/C	0.045
Surface area and pore diameter	BET surface area ($m^2 g^{-1}$)	9.19
	Average Pore diameter (nm)	2.12
Magnetic properties	Saturation magnetization (emu g^{-1})	14.85
	Remanent magnetization (emu g^{-1})	0.158
	Coercivity (Oe)	12.12

*C: Carbon, H: Hydrogen and N: Nitrogen

Table 4.11: Cost estimation for biochar preparation

(a) Raw material cost		
Nil		
(b) Solvent cost for biochar purification (for 50 g)		
Solvent used	Unit price (USD/ L)	Total cost of the solvent used (USD)
Dichloromethane	13.1	0.65
(c) Power requirements for operating the solvent recovery (for 50 g biochar)		
		Power (kW)
Power utilized (in units)		0.425
Cost per unit		0.17
Total cost for biochar preparation[#] (a + b + c)		5.29
Total cost for preparing 1 kg biochar (in USD)		$ 1.89
Electricity charges are based on LT-commercial tariff of AERC* (Cost per unit: 0.17 USD)		

*AERC: Assam Electricity Regulatory Commission, India

4.2.3. Effect of biochar on PAH biodegradation

Batch shake flask experiments were performed for examining the effect of biochar on PAH biodegradation by the bacterial strain. Fig. 4.20 shows PAH biodegradation (50 mg L^{-1}) by *R. opacus* in the presence of biochar with 10% (w/v) inoculums size. It could be seen that the biochar presence in the media enhanced PAH biodegradation by the bacterium. For instance, NAPH, ANTH, PHEN and FLOR removal efficiencies (50 mg L^{-1}) at the end of the experiment were observed to be 92.3%, 90.5%, 88.2% and 82.3%, respectively, in presence of 200 mg L^{-1} biochar concentration, as compared with only 79.6.3%, 76.1%, 74.1% and 71.6% without any added biochar in the medium (Goswami et al., 2017b). Hence, from these results, it is clear that biochar supplementation in the medium increased the PAH biodegradation efficiency in the range of 7.7%-14.4%.

These results confirm the synergistic role played by biochar on PAH biodegradation by *R. opacus*. In the literature, She et al. (2016) reported a very good enhancement in PHEN biodegradation by *Sphingomonas* sp. GY2B, but using expensive commercially available nano-bamboo charcoal. Zhang et al. (2015) also reported an enhancement in atrazine biodegradation up to 20% with pure carbon nanotubes. Other than these literature reports; this is the first study which demonstrates the utility of cheaply produced biochar for PAH biodegradation.

The abiotic loss of the model PAHs were in the range of 3.4 - 4.8%. Furthermore, loss of PAHs due to sorption on to the bacterial biomass or biochar surface may be ignored as the solvent used for extracting the PAHs was added directly to the culture broth (Rodrigues et al., 2013

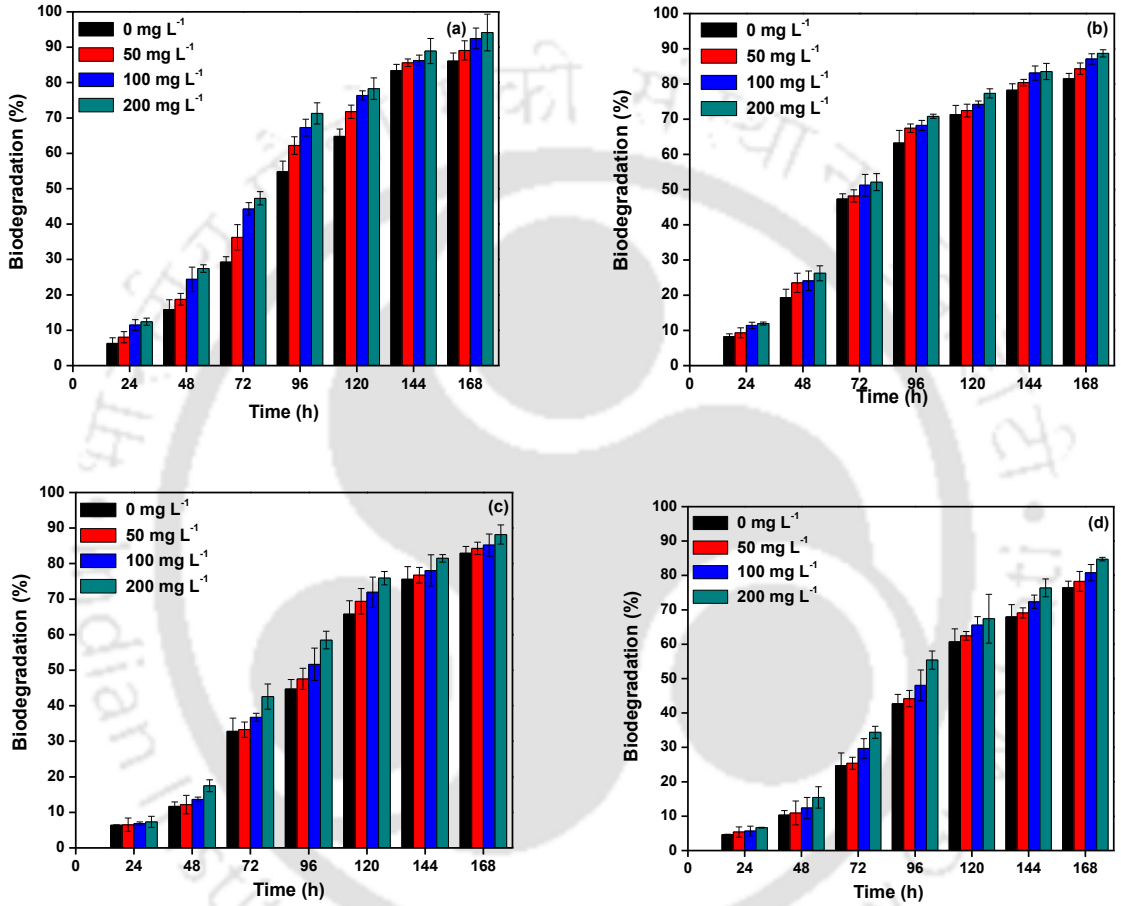

Fig. 4.20: Effect of biochar on (a) naphthalene; (b) anthracene (c) phenanthrene and (d) fluoranthene biodegradation by *R. opcaus*

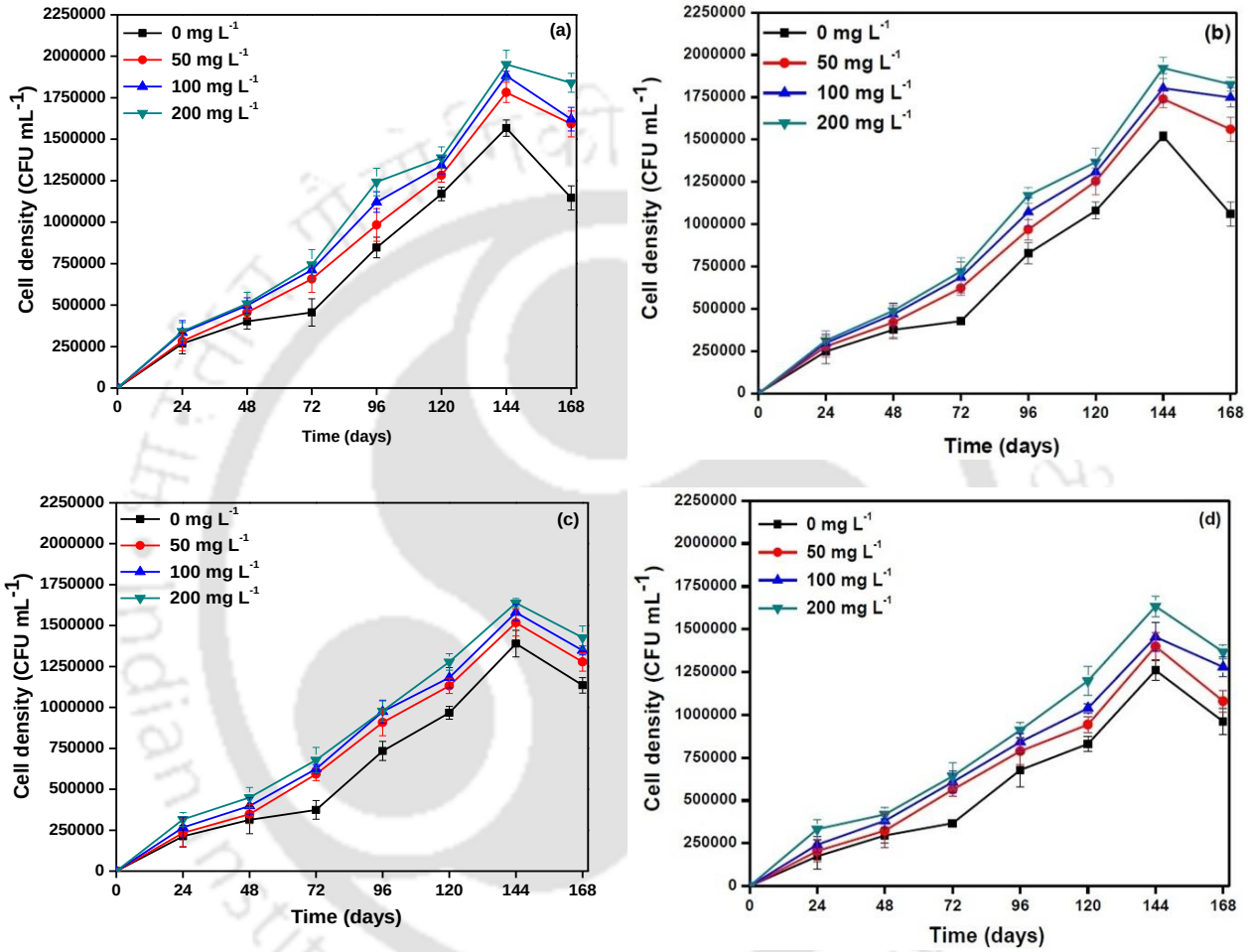

Fig. 4.21: Effect of biochar on *R. opacus* biomass growth by utilizing (a) naphthalene; (b) anthracene (c) phenanthrene and (d) fluoranthene as the substrate

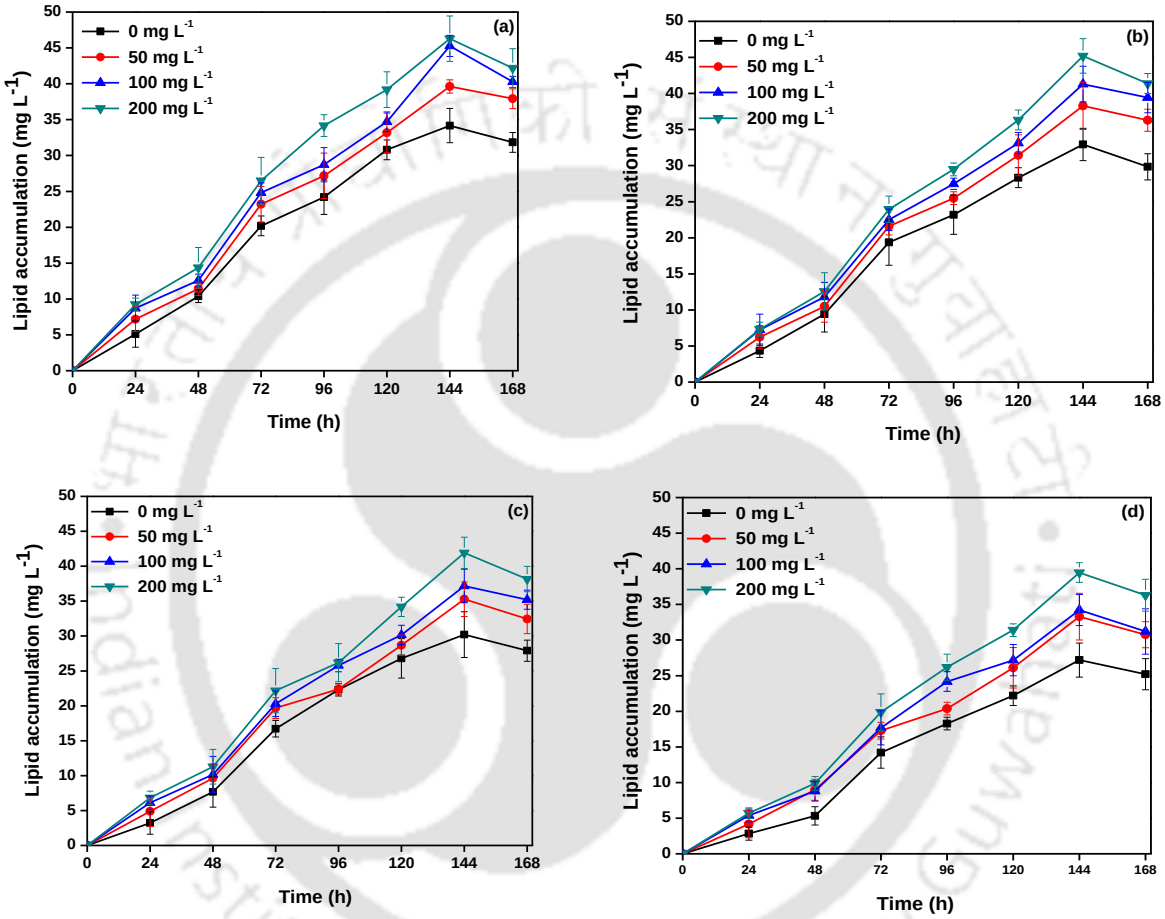

Fig. 4.22: Effect of biochar on lipid accumulation by *R. opacus* utilizing (a) naphthalene; (b) anthracene (c) phenanthrene and (d) fluoranthene as the substrate

4.2.4. Effect of biochar on *R. opacus* biomass growth and lipid accumulation

R. opacus biomass growth was examined by correlating the CFU with cell dry weight at regular time intervals during the experiment (Fig. 4.21), and it was found to be similar in presence or in absence of biochar. With a lag phase of 24-36 h, a distinct maximum is observed in the biomass growth profile at the sixth day. Also, an increase in PAH biodegradation efficiency is observed with an increase in the biochar concentration. However, the rate and efficiency of PAH biodegradation by *R. opacus* were dependent on structural complexity and aromaticity of the respective PAH. These results correlate well with the PAH biodegradation results discussed earlier (Fig. 4.20).

Moreover, an increase in the total lipids accumulated by the bacterium was observed due to an increase in the biochar concentration in the media, probably due to enhanced PAH uptake by the bacterium in the presence of biochar (Fig. 4.22). The total amount of lipids accumulated by *R. opacus* were 68.1%, 74.2%, 73.4% and 65.2% (w/w) of cell dry weight (CDW) for NAPH, ANTH, PHEN and FLOR, respectively, whereas the total lipid accumulation by the bacterium without biochar addition were 68.1%, 70.6%, 72.4% and 63% (w/w, CDW) for NAPH, ANTH, PHEN, and FLOR, respectively.

In order to understand the mechanism of action of biochar in enhancing the PAH biodegradation by the bacterial strain, contact angle of the biochar samples taken during the experiments was measured. Fig. 4.23 shows the results of contact angle measurement carried out in the study. During the initial few hours (3-4 h) of the biodegradation experiment, the biochar was found suspended throughout the medium due to inherent hydrophobicity of the constituent carbon particles (Zhang et al., 2015). This observation correlates well with a decline in the contact angle from 111.12 to 66.71 due to the biochar material. After 3-4 h of incubation, the biochar was found adsorbed onto the bacterial

surface, thereby increasing the PAH bioavailability for an enhanced PAH biodegradation, biomass growth and lipid accumulation by the strain. Fig. 4.24 shows FESEM images of *R. opacus* biomass grown in presence and in absence of biochar. These images clearly reveal biochar soption onto the bacterial surface without any change in the bacterial morphology. Fig. 4.24 (a) shows that in the absence of biochar, *R. opacus* enters the death phase at the end of 144 h due to the depletion of PAH in the medium. But, in the presence of biochar (Fig. 4.24 (b)), the death phase is delayed, suggesting that the biochar acts as a growth supplement to such bacteria in absence of other alternative substitutes (Bruun et al., 2014).

Sample	Time (s)			
	0	15	30	45
(a) Biochar + PAH				
Contact angle	111.35°	111.27°	110.63°	109.82°
(b) *R.opcaus* biomass + Biochar + PAH	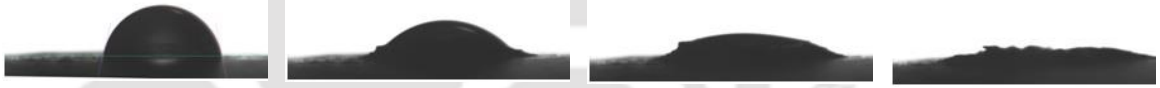			
Contact angle	66.72°	24.62°	5.68°	0°

Fig. 4.23: Contact angle of (a) biochar along with PAH and (b) *R. opcaus* biomass along with PAH and biochar

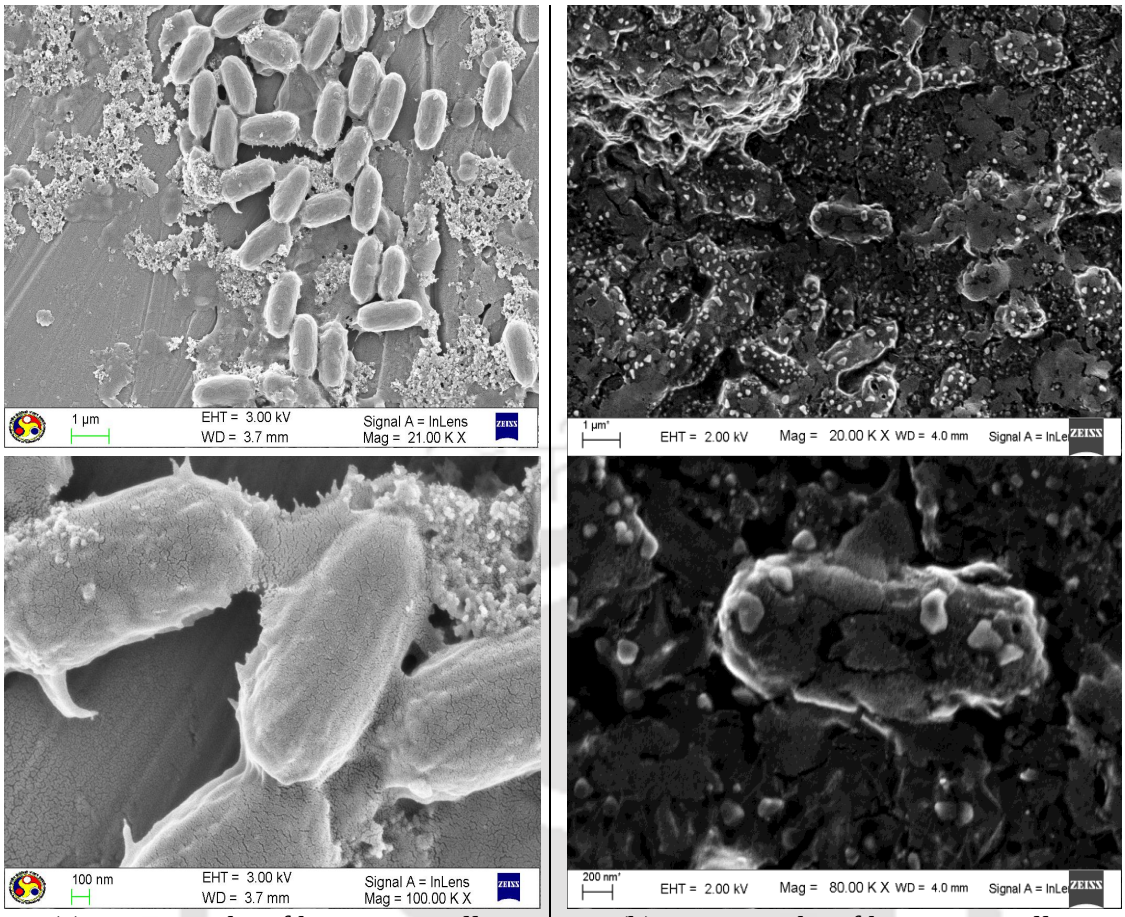

(a) Micrographs of bacterium cells (without biochar)

(b) Micrographs of bacterium cells (with biochar)

Fig. 4.24: FESEM micrographs of *R. opacus*: (a) without biochar and (b) with biochar

4.3. Batch treatment of biomass gasification wastewater (BGWW) using *R. opacus* and biodiesel production

4.3.1. Biomass growth, lipid production and COD removal by *R. opacus*

Figs. 4.25 and 4.26 depict the *R. opacus* biomass growth and lipid accumulation profiles, respectively, which indicate that the biomass growth profile followed a similar trend for both the inoculum sizes (5 and 10%). A significant increase in biomass and lipid accumulation by *R. opacus* is observed when supplementing BGWW with mineral salt media. Maximum lipid accumulation

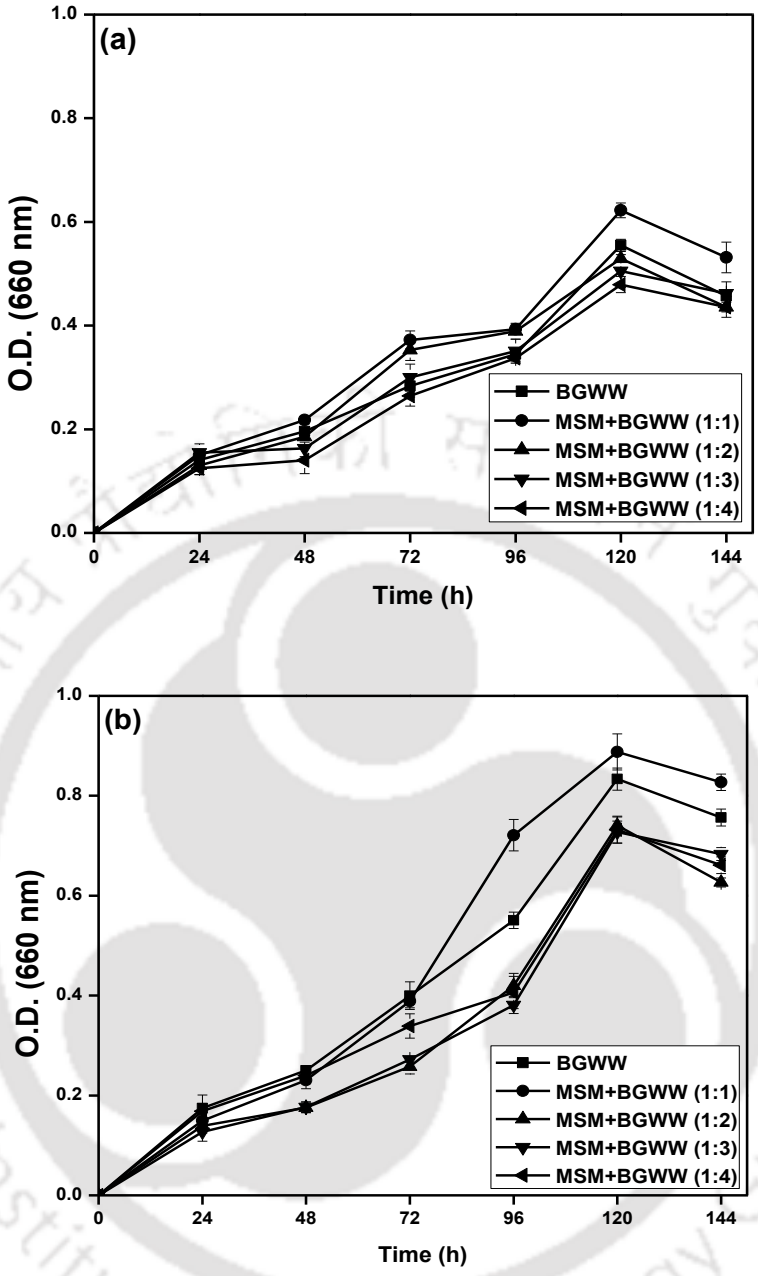

Fig. 4.25: *R. opacus* biomass growth on BGWW based media (a) 5% inoculum size and (b) 10% inoculum size

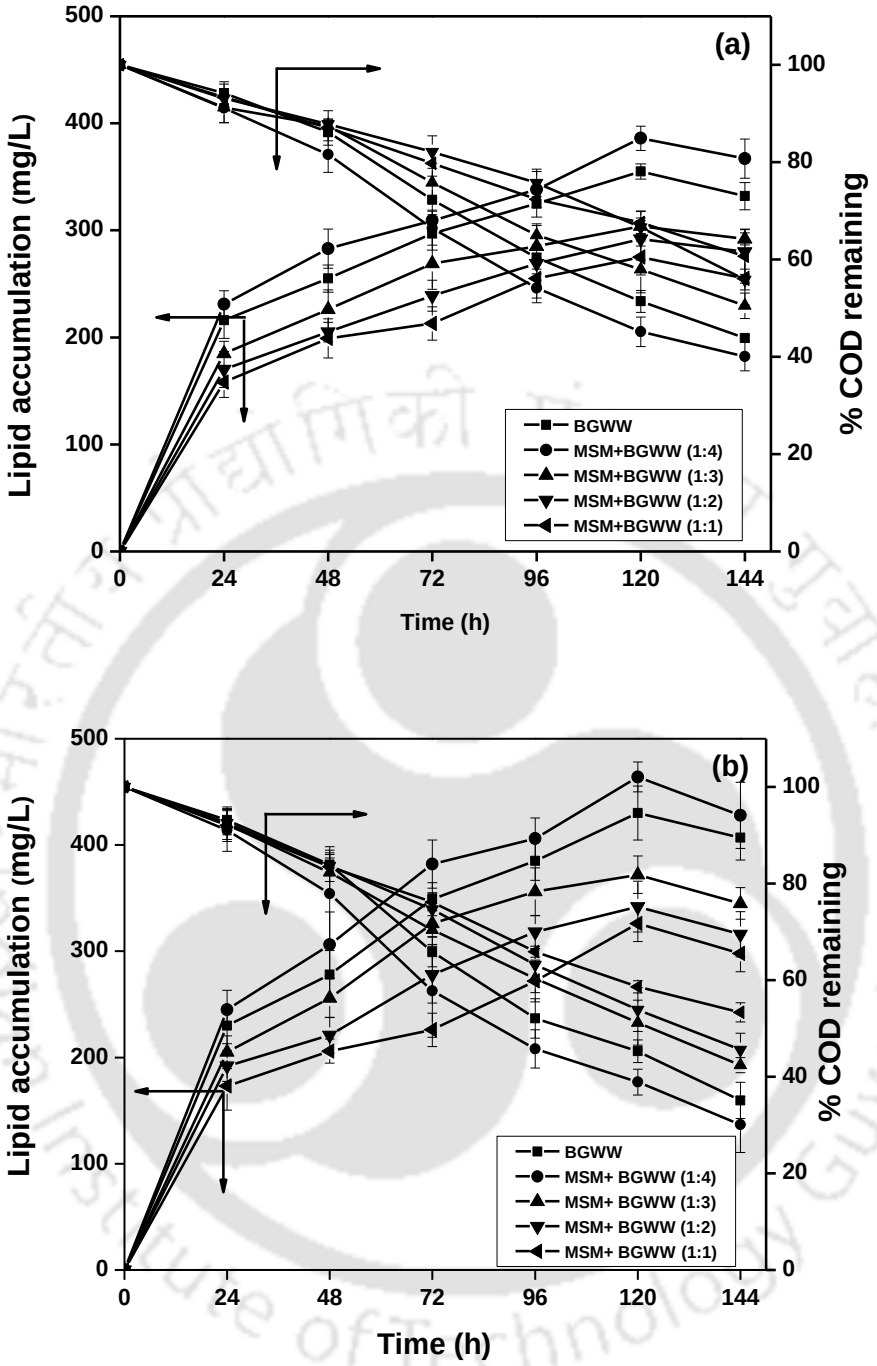

Fig. 4.26: Lipid production by *R. opacus* using biomass gasification wastewater (BGWW) based media and COD removal efficiency: (a) 5% inoculum size and (b) 10% inoculum size

and biomass growth (Figs. 4.25 and 4.26) were achieved at the fifth day i.e., during the late log phase. Later to this time period, both biomass growth and lipid accumulation reduced significantly (Figs. 4.25 and 4.26). An increase in inoculum size also had a positive effect on both the maximum COD removal and total lipids accumulated by *R. opacus*. Using the raw untreated wastewater, the bacterium accumulated 54.3% (w/w) lipid with a wastewater COD removal efficiency of 64%. However, these values were further enhanced to 62.8% (w/w) and 74%, respectively, following supplementation of the biomass gasification wastewater with mineral salt media in the ratio 4:1 for 5% and 10% inoculum sizes, respectively. These results clearly establish the potential of *R. opacus* in simultaneous BGWW wastewater treatment and lipid accumulation for potential biodiesel application. A similar observation has been made in the literature on enhanced lipid accumulation with an increase in the inoculum size by *R. opacus* using dairy wastewater as the substrate (Kumar et al., 2015).

Marjakangas et al. (2015a) studied lipid accumulation by *Galactomyces geotrichum* fungi grown using palm oil mill effluent (POME) and reported a maximum lipid accumulation of 29.1% CDW, which is very low compared with the maximum lipid content of 62.8% obtained in this study. *Chlorella vulgaris* has been reported to produce 62.5 % lipid using piggery wastewater (Marjakangas et al., 2015b). However, the algal growth significantly increased the COD of the anaerobically treated piggery wastewater, there by necessitating additional treatment step. *Chaetoceros gracilis* (Godfrey, 2012) when grown on produced water showed only 17.9% FAME composition, but with municipal wastewater the lipid accumulation slightly increased to 63.6%. The major drawback of utilizing algae for biodiesel is the requirement of large area of cultivation and prolonged incubation time. The use of bacteria, e.g., *Rhodococcus opacus* may overcome this hurdle due to their ability to produce high cell density cultures within a short time.

Several studies have reported different yeast species capable of lipid accumulation. Among the different yeasts, *Lipomyces starkeyi* is shown to yield high lipids, but it is unable to grow on raw sewage sludge (Angerbauer et al., 2008). Similarly, *Yarrowia lipolytica* has been reported to accumulate lipids efficiently, but requires media supplemented with costly simple sugars such as glucose. Wastewater such as olive mill effluent has been studied for lipase production (Bankar et al., 2009). Yet studies on characterization of the lipid produced and biodiesel production from wastewater are highly limited. Compared with the literature reports, this study, therefore, indicates the robustness of *Rhodococcus opacus* to efficiently utilize a highly toxic and PAH containing wastewater for biodiesel production.

4.3.2. TGA profiles of the accumulated lipids

The TGA and derivative thermogravimetric (DTG) curves of accumulated lipids are presented in Fig. 4.27, which revealed that the loss in weight involved mainly four phases. First between 25 and 140°C, the second in the range 140-250°C, third weight loss at 250-360°C and fourth at 360-700°C. The first region signifies the mass decrement due to dehydration of the sample; around 78± 3.7 % weight loss was due to the elimination of absorbed water in the sample. The second and third regions correspond to the loss of organic matter, whereas the fourth region depicted the loss due to degradation of lipids (Silva and de Andrade, 2008).

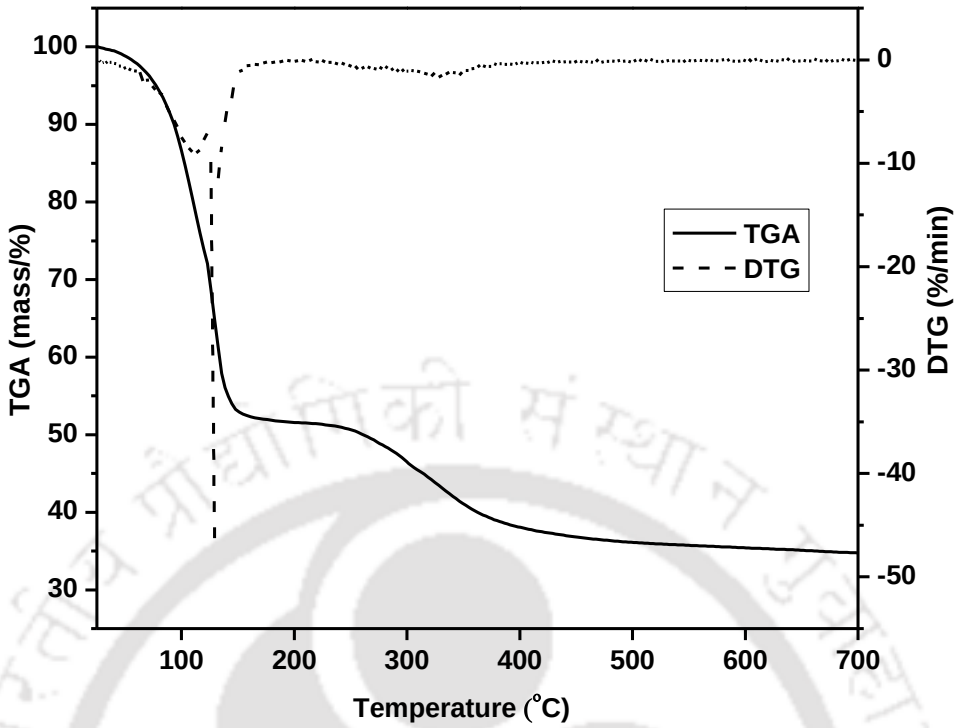

Fig. 4.27: Thermogravimetric (TGA) and differential thermogravimetric (DTG) curves of the lipids produced by *R. opacus* using BGWW as the substrate

4.3.3. Composition of FAMEs and assessment of biodiesel

Fig. 4.28 presents the composition of FAMEs obtained by transesterification of *R. opacus* lipids. Methyl palmitate (C16:0) and methyl stearate (C18:0) form the major fractions of the FAMEs, representing about 53% of the total FAME content. In addition, methyl laurate (C12:0), methyl palmitoleate (C16:1), mixture of methyl linoleate (C18:2), methyl oleate (C18:1), methyl erucate (C21:0), methyl myristate (C14:0) and methyl linoleate (C18:2) are found in moderate amounts. Trace fractions of unsaturated fatty acids, namely methyl myrist oleate (C16:1), methyl oleate (C18:1) and methyl linolenate (C18:2) are also found in the fatty acid profile. Other unsaturated fatty acids, particularly C18:3 and those with more than four (double) bonds (which should be less than 12 mol% and 1 mol%, respectively) are absent in the biodiesel product (Gouveia and Oliveira, 2009). The proportion of unsaturated fatty acids that includes mono-unsaturated fatty acids

(MUFAs) and poly-unsaturated fatty acids (PUFAs) to the saturated fatty acid fractions is very small (Fig. 4.28).

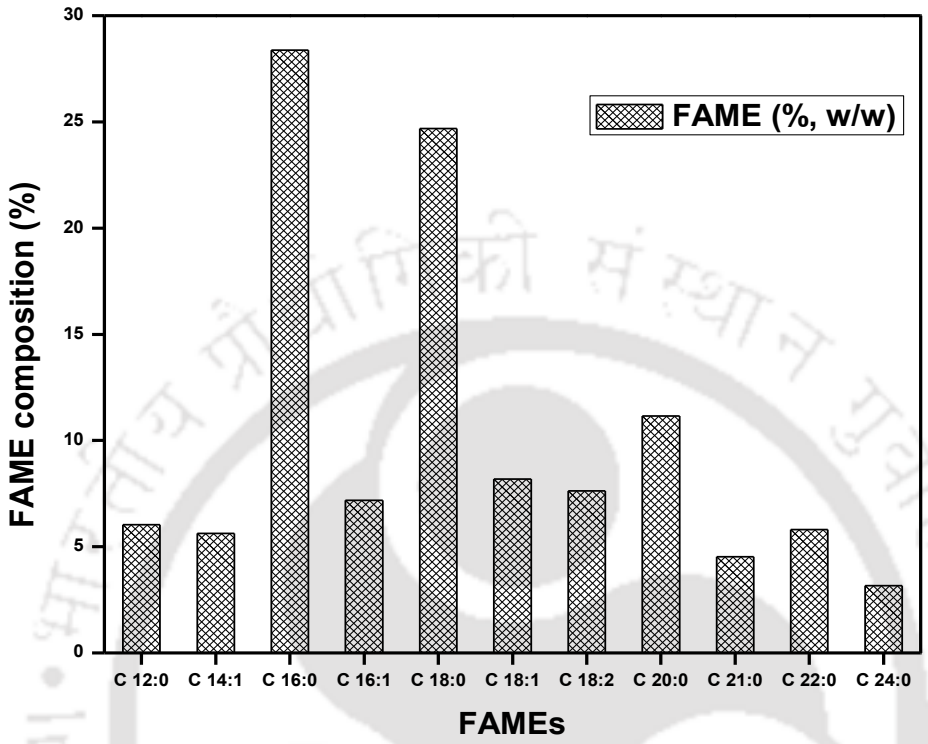

Fig. 4.28: Percentage fatty acid methyl ester (FAME) composition in the biodiesel product

FTIR spectra of the biodiesel product are presented in Fig. 4.29, which showed the presence of mono alkyl esters (peak at 1746.9 cm^{-1}), confirming the presence of ester group (Kumar et al., 2014). Table 4.12 compares the estimated property values of the biodiesel with the American Society for Testing and Materials (ASTM) as well as European (EN) Standards. In this study, majority of the parameters satisfied the limits set by the standard EN 14214.

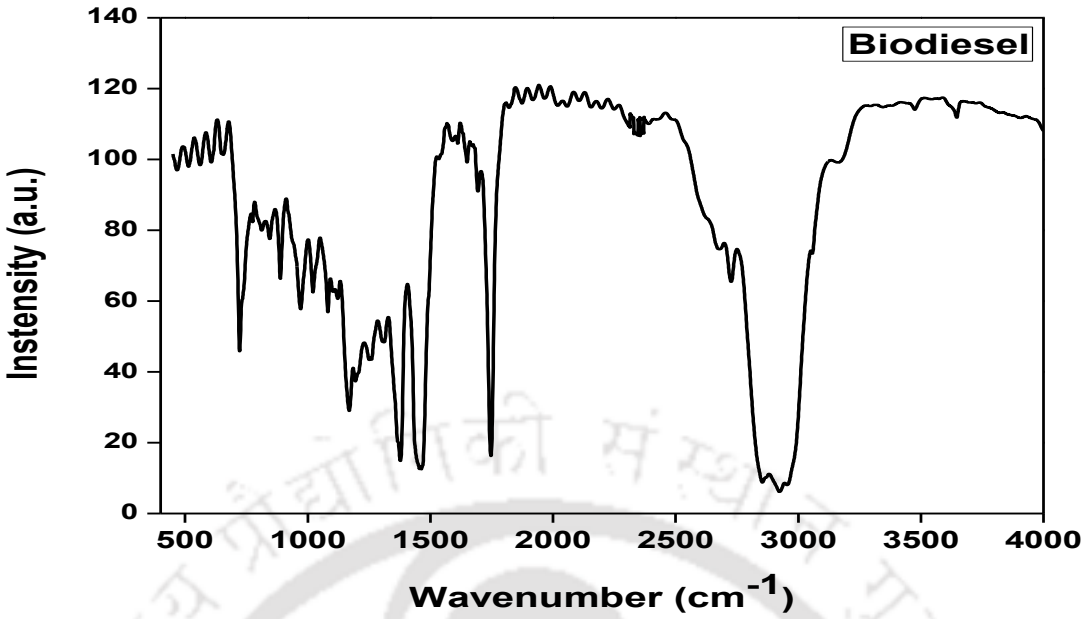

Fig. 4.29: Fourier transform infrared (FTIR) spectra of the biodiesel

Table 4.12: Estimated property values of the biodiesel obtained by lipid transesterification and comparison with those of the international standards

Biodiesel property	**Units**	**Transesterified product**	**ASTM-D6751 Standard**	**EN 14214**
Viscosity	(mm^2/s)	5.17	1.9-6.0	3.5-5.0
Cetane number	-	80.42	47 (min)	51 (min)
Pour point	(°C)	3.96	ND	ND
Cloud point	(°C)	9.93	ND	-
Saponification value	mg KOH/g	229.49	ND	ND
Iodine value	g I_2 per 100 g oil	34.07	ND	120
Degree of unsaturation	-	36.23	ND	ND

ND: Not defined

In general, high viscosity results in poor flow properties along with a low atomization quality, drop size and low penetration ability of the fuel. In this study, the

estimated viscosity (~5.17± 0.23 mm^2/s) of the biodiesel is found to be within the permissible range. Biodiesel comprising of methyl esters with carbon chain greater than 19 carbons (i.e., C20:0- C24:0) results in a low viscosity fuel, and is, therefore, highly desired. Fuels which maintain fluidity even at a very low ambient temperature are generally preferred. Cloud point (~9.93°± 1.62 C) and pour point values (Table 4.12) of the biodiesel produced in this study matched well with those of the standard values indicating its suitability for use in low temperature regions.

The cetane number is found to be higher than the proposed limits set by ASTM and EN standards. In general, biodiesel cetane number depends on the feedstock used for its production, and a high cetane number indicates the presence of esters of saturated fatty acids such as palmitic (C16:0) and stearic (C18:0) acids. On the other hand, low cetane numbers are associated with the presence of more highly unsaturated components such as esters of linoleic (C18:2) and linolenic (C18:3) acids (Knothe et al., 2006). Also, at a high temperature, unsaturated fatty acids polymerize to form glycerides, leading to the formation of deposits and deterioration of the fuel lubricating properties (Mittelbach et al., 1996). Furthermore, fuels having polyunsaturated methyl esters are unstable due to oxidation (Ramos et al., 2009).

Saponification value (SV) is an evaluation of potassium hydroxide (in milligrams) that is required to completely saponify one gram of oil, completely (Predojević, 2008). As per the ASTM-D6751 standard, SV should be in the range 185.51 to 214.09 mg KOH/g (Table 4.12). In this present study, SV of the biodiesel is ~229.49mg KOH/g, which is slightly higher than the ASTM-D6751 standard. A low degree of unsaturation in the biodiesel product is indicated by a low iodine value (Mittelbach et al., 1996). In this study, the obtained FAMEs are rich in esters of saturated fatty acids, mainly palmitic (C16:0) and

stearic (C18:0), which correlates well with the low iodine value obtained (Mittelbach et al., 1996). Overall, these estimated results of the bacterial lipids and FAMEs produced by lipid extraction and transesterification reveal an excellent suitability of the transesterified lipids for biodiesel applications. Moreover, this is the first study which reported the treatment of biomass gasification effluent using *R. opacus* for potential biodiesel application.

4.4. Integrated biodegradation-microfiltration system for BGWW treatment and energy recovery

4.4.1. Biomass growth, COD removal and lipid accumulation by *R. opacus*

Batch experiments were performed with biomass gasification wastewater to analyze biomass growth, COD removal efficiency and lipid accumulation by oleaginous *R. opacus*. The industrial wastewater samples collected from a pilot scale down-draft biomass gasifier was of pale yellow in color. Physicochemical characterization of BGWW wastewater showed a COD content of 2213 ± 14.2 mg L^{-1}, respectively, and other organic as well as inorganic salts (Table 3.1).

Figs. 4.30 and 4.31 depict the time profiles of biomass growth, lipid accumulation and COD removal efficiency by the strain. The results of biomass growth profile reveal a prolonged lag phase of 12 h in utilizing the wastewaters, and it reached a maximum value within 120 h for BGWW. These profiles matched well with the lipid accumulation profile for all the wastewaters (Fig. 4.31). BGWW contains a very high amount of persistent organics, viz., phenolics, heterocyclic, mono- and polycyclic aromatic hydrocarbons.

The lipid accumulation value was 64.8% (w/w) of the cell dry weight (CDW) for BGWW after 120 h. In addition to these results, an increase in COD removal with respect

to time was observed with all the three wastewaters. The overall COD removal efficiency for BGWW was found to be 68.9 %. Kumar et al. (2015) performed experiments using the bacterium with a batch stirred tank reactor for utilizing DWW as the sole substrate and demonstrated a COD removal efficiency of 62% and a lipid accumulation of 48% (w/w CDW) in 96 h. Similar observations on enhanced lipid accumulation by *R. opacus* using dairy and biomass gasification wastewater with an increase in inoculum size have been reported (Kumar et al., 2015). Hence, the results of COD removal and lipid accumulation by the strain with the different wastewater were higher in comparison with that reported in the literature.

Wei et al. (2015a, b, c) found 14.9%, 25.8% and 28.6% of lipid accumulation by *R. opacus* grown using Kraft lignin, pyrolysis oil and detoxified sweet gumautohydrolysate. These values are very low when compared with those obtained in the present study. In our previous study, *R. opacus* accumulated 63-72.4% of lipids by utilizing PAH simulated wastewater. All these results demonstrate excellent capability of the strain to grow on any kind of organics containing industrial wastewater for simultaneous COD removal and lipid accumulation. The accumulated bacterial lipids were further visualized by Nile red fluorescence assay (Fig. 4.32) where lipophilic fluorescent dye that selectively binds to triacylglycerol (TAG) and the lipid droplets inside the cells were clearly seen as red fluorescence (Fig. 4.32).

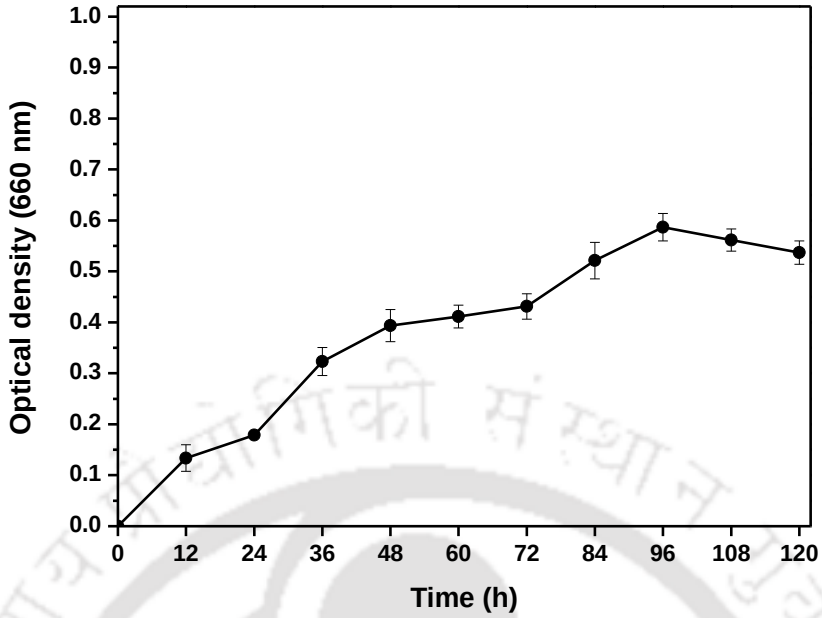

Fig. 4.30: Time profile of *R. opacus* biomass growth with different industrial wastewater

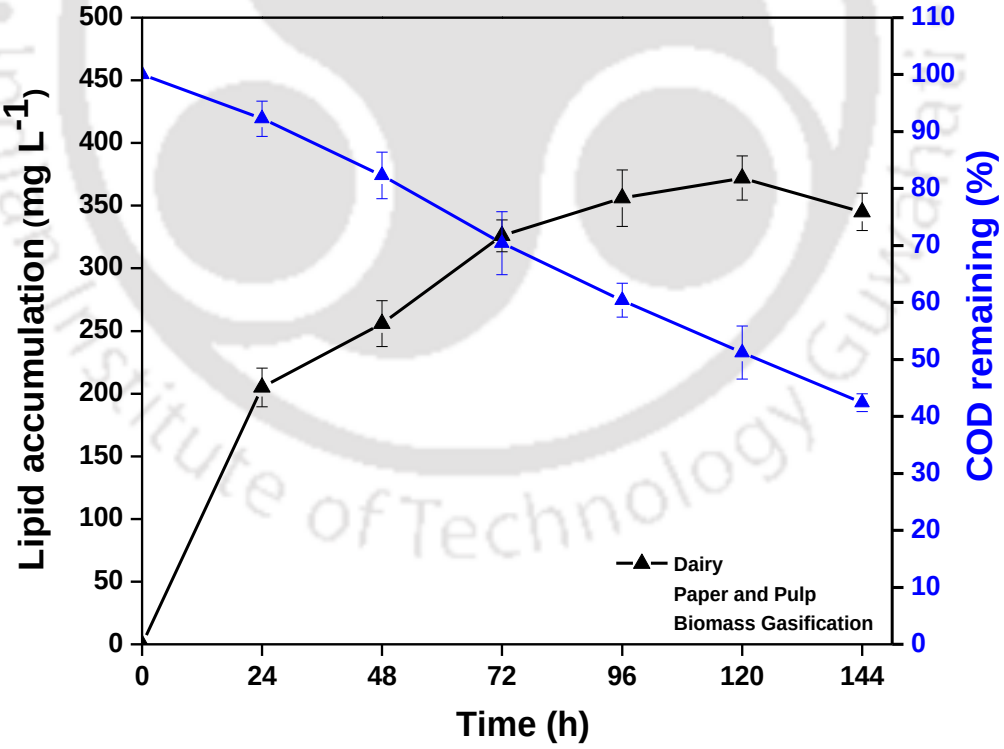

Fig. 4.31: Lipid production and COD remaining by *R. opacus* with BGWW (during biodegradation)

4.4.2. Microfiltration system

In order to recover the lipid-rich biomass from the treated wastewaters and to further reduce the level of COD in the respective wastewaters, microfiltration using a low cost ceramic membrane (pore size: 1.01 μm and porosity: 44%) was carried out. Fig. 4.33 presents the membrane flux and COD removal (%) from the different wastewaters at various operating pressures in the range of 34 - 172 kPa. With an increase in the operating pressure, the flux of the microfiltration system increased due to a high driving force acting on the membrane surface. In general, the membrane fouling is attributed to concentration polarization on the membrane surface and blocking of pores in the porous ceramic structure. The less viscous BGWW contains persistent organics (Goswami et al., 2018), and, hence it did not affect the membrane flux largely. The COD removal efficiency is directly dependent on the operating pressure up to a certain level and decreases at a high pressure, which is due to the augmented convective flux of the liquid acting on the membrane surface, thereby leading to a high undesired COD content in the permeate (Bennani et al. 2015; Chakraborty et al. 2003). Moreover, at a high pressure organic matter already retained on the membrane surface penetrated through the membrane, thus, reducing the overall percentage COD removal efficiency.

Hence, the COD removal (%) at the point of inflection enhanced from 68.9% to 88.2% for BGWW using the microfiltration system (Fig. 4.34). The retained lipids accumulated by the bacterium on the membrane surface were further extracted and characterized for biodiesel production.

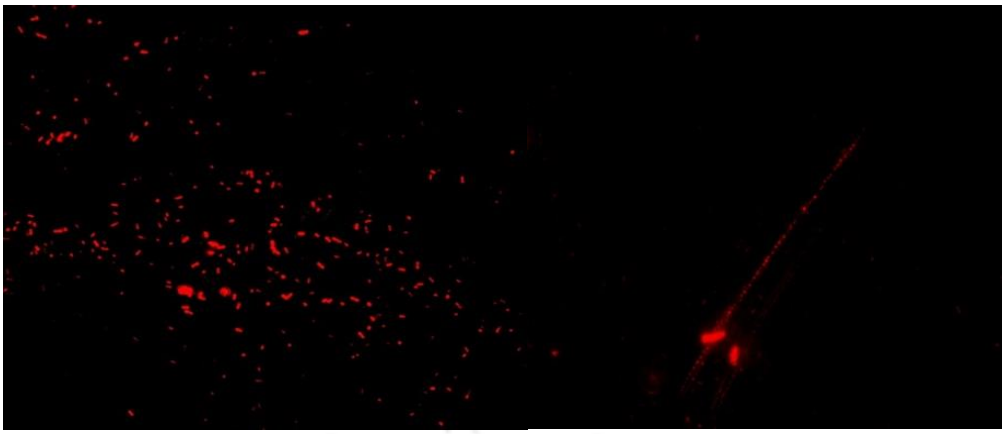

Fig. 4.32: *R. opacus* cells stained with Nile red (The cells were grown using BGWW as the substrate)

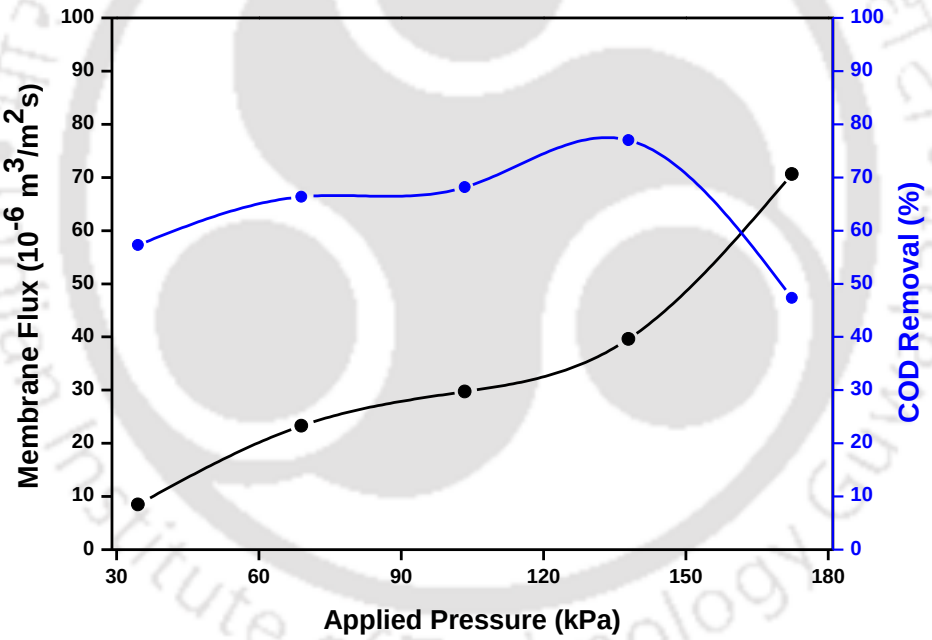

Fig. 4.33: Influence of applied pressure on permeate flux and residual COD removal (following the biodegradation process by microfiltration

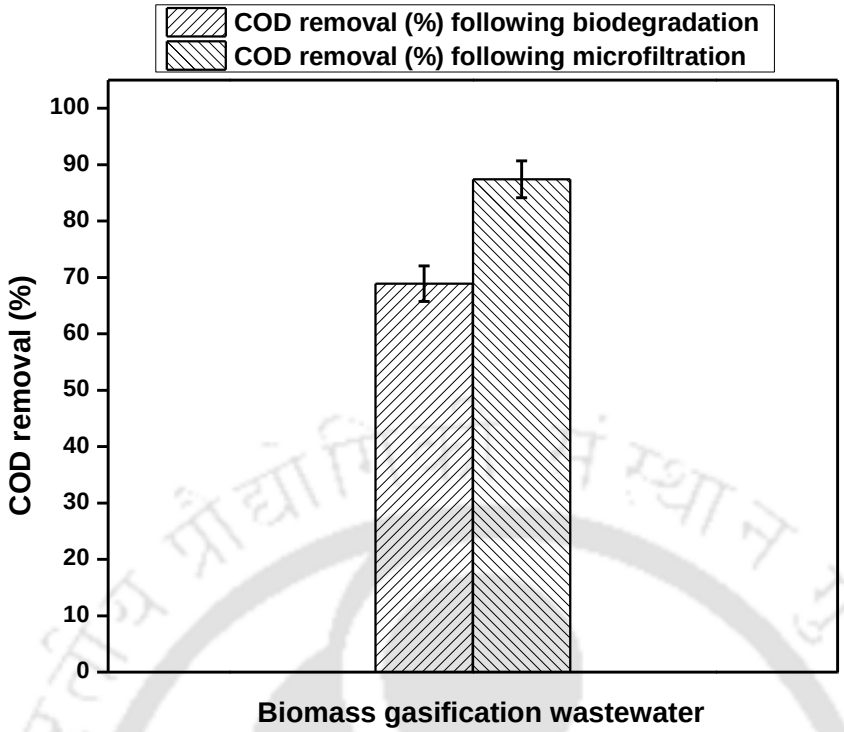

Fig. 4.34: Overall COD removal (%) using biomass gasification wastewater (Applied pressure: 138 kPa; Permeate flux: 39.6×10^{-6} m^3/m^2s)

Karhu et al. (2013) used a membrane bioreactor (MBR) for olive mill wastewater treatment and achieved 31%, 58% and 81% COD removal for an initial COD concentration of 53, 27 and 1500 mg L^{-1}, respectively, in the wastewater. Using a membrane-aerated biofilm reactor, 60.3% of COD removal was reported by Abbasi et al. (2010) for the crude oil wastewater from offshore oil platforms. KolevSlavov et al. (2017) achieved 53% total organic carbon (TOC) removal from textile mercerization wastewater using a multichannel ceramic ultrafiltration membrane. Compared with these COD removal results reported in the literature, the present study involving biodegradation-microfiltration system yielded excellent results in COD removal for BGWW along with an efficient biomass recovery for potential biodiesel production.

4.4.3. Toxicity removal from BGWW after integrated process treatment

From Table 4.13, the final toxicity (%) of the treated effluent and the total toxicity removal (%) following the integrated treatment were found to be 1.7% and 92.8%, respectively. Sahoo et al. (2014) studied 4-bromophenol biodegradation in a mixed pollutant system by *Arthrobacter chlorophenolicus* using an up-flow packed bed reactor (UPBR) and reported complete removal of pollutants along with 97% of toxicity removal from the synthetic wastewater, which matched well with the results obtained in the present study. This is mainly attributed to the complete degradation/ mineralization of the organics initially present in the wastewater to non-toxic compounds (Goswami et al., 2017a).

Thus, integrating biological process with membrane filtration proves to be beneficial in many ways (Luo et al., 2014). The combined process is highly economical and requires relatively a small area as well as reduced labour requirement for its operation. In membrane technology, ceramic membranes as compared with polymeric membranes are strongly resistant to harsh environment, microbiological degradation and high pressure conditions. Employing the membrane technique with microfiltration (MF) membrane is more favorable than ultrafiltration (UF)/nanofiltration (NF) membrane in order to attain enhanced flux and minimum irreversible fouling. Hence, integrating biodegradation with membrane filtration technique utilizing low cost MF ceramic membrane is highly promising for wastewater treatment applications (Grandclement et al., 2017). However, ceramic membranes for industrial applications need to provide good permeate flux and rejection, and the membrane cost should be low. Conversely, most of the commercially available ceramic membranes are produced from alumina, silica, zirconia and titania materials (Monash and Pugazhenthi, 2011). These ceramic membranes have limitation in

large-scale applications because of the expensive starting materials and high sintering temperature.

In this context, the low-cost ceramic membrane employed in this study has shown an immense potential to treat different kinds of industrial wastewaters (Ojajuni et al. 2015). But, the results reported in this work were obtained using a laboratory scale batch set up for short duration. In order to implement the combined biological-microfiltration industrially, a suitable geometry of the membrane would be highly desired. Also, in this study, integration of biological process and microfiltration technique with batch mode, i.e., dead-end filtration was evaluated, which needs manual cleaning of the membrane after each experiment. Furthermore, optimization of membrane regeneration process, energy consumption, and cost-benefit analysis of the process need to be carried out in detail for a better applicability of the integrated process.

4.5. Upflow packed bed bioreactor with biochar immobilized polyurethane foam as the packing material

4.5.1. Characterization of the bio-support material

4.5.1.1. TEM and XPS analyses of the biochar

Table 4.10 represents the results of physical and magnetic characterization of biochar (Goswami et al. 2018b). The TEM micrograph (Fig. 4.35) confirms that the average size of the biochar following the mechanical ball mill treatment is around 80 nm. Further, the quantitative surface functionalization of the elements was evaluated by X-ray photoelectron spectroscopy (XPS). The wide scan spectrum of the biochar is presented in Fig. 4.36. The survey scan of the biochar confirms the presence of C_{1s}, N_{1s}, O_{1s} with binding energy values of 284.5, 399.9 and 531.9 eV. The surface elemental composition was C - 80.1%, O - 17.2% and N - 2.7%. The short scan of the C_{1s}, N_{1s}, and O_{1s} after

deconvolution shows the different binding of C, N and O with each other. The short scan of C_{1s} shows three peaks with the binding energy values 284.4, 285.4 and 287.1 eV due to C-C, C-O/N and C=O, respectively. O_{1s} short scan shows two peaks at binding energy values at 531.6 and 533.1 eV of the C-O and C=O, respectively. The short scan of the N_{1s} shows only one peak after deconvolution with the binding energy of 398.9 eV of the pyridinic nitrogen. In addition, iron present in the biochar was in Fe_2O_3 form as examined by the XRF analysis along with the other compounds such as SiO_2, ZnO, Al_2O_3, PbO, MnO and P_2O_5.

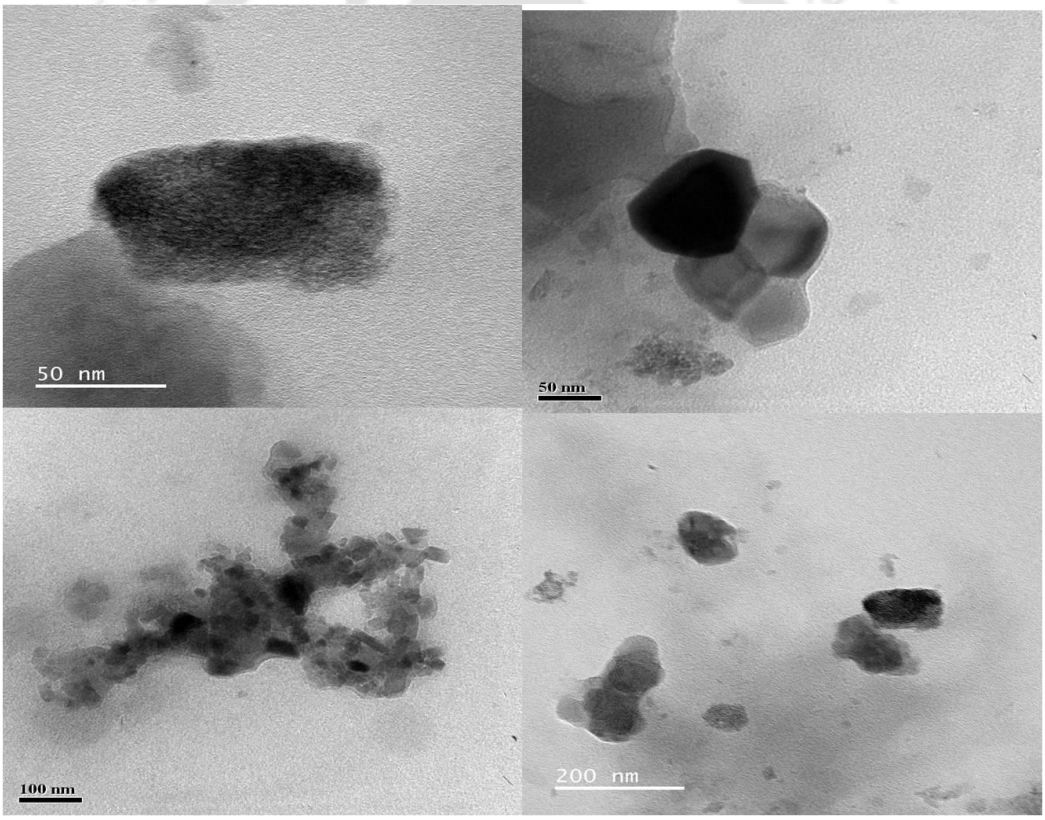

Fig. 4.35: TEM micrographs of biochar

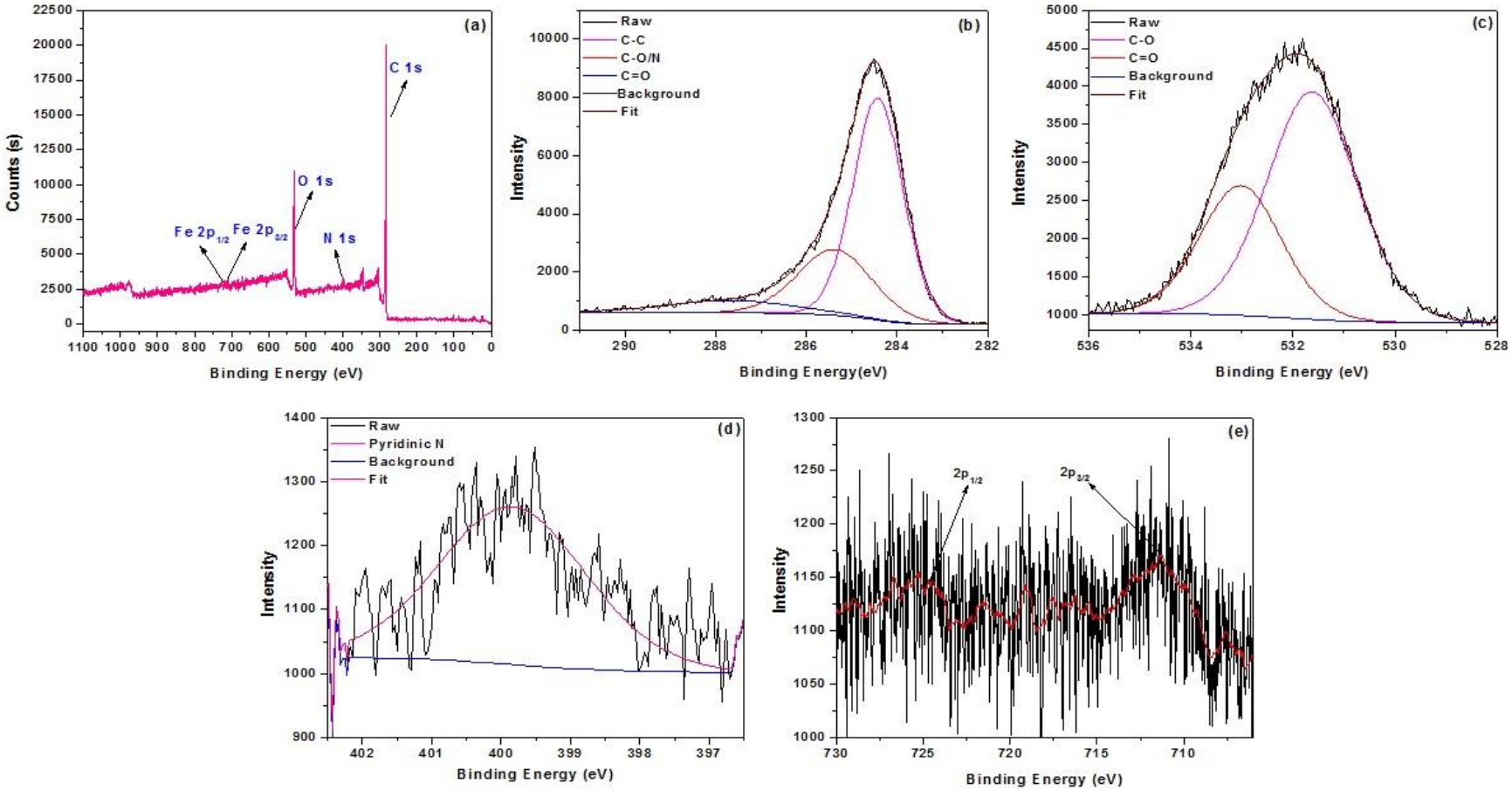

Fig. 4.36: XPS scanning of biochar (a) full scan and its short scan: (b) C_{1s} (c) O_{1s} (d) N_{1s} and (d) Fe_{2p}

4.5.1.2. FESEM, EDX and TEM analyses of the bio-support material

FESEM micrographs of PUF at initial and various stages of biofilm formation by *Rhodococcus opacus* along with the elemental composition confirmed microbial biofilm formation onto the PUF support material (Fig. 4.37 (a)). Micrographs of the support material along with the biochar as the additional support material are shown in Fig. 4.37 (b)) which reveals dense biofilm formation onto the PUF-biochar support material. FESEM–EDX analyses of PUF, PUF-biochar, and PUF-biochar-biomass were also performed. The change in elemental composition confirmed the growth and development of biofilm on to PUF and PUF embedded biochar. Mapping images of the biofilm formation for the PUF-biochar as the support material is shown in Fig. 4.37 (c).

4.5.2. Abiotic losses/degradation of BGWW

The packing bed (PUF) attains its saturation point after 84 h of bioreactor operation. The adsorption capacity of PUF was evaluated to be 22.6 mg of BGWW g^{-1} dry weight of PUF. Also, in this case, the loss of pollutants due to volatilization was evaluated to be 2.27 mg L^{-1} d^{-1} at an influent COD concentration of 2270 mg L^{-1}. Abiotic loss via volatilization has been reported to be less significant by many researchers (Sahoo et al. 2011). Furthermore, in case of biochar loaded PUF as the support material, saturation was achieved around 74 h which might be due to the biochar, as most of the surface of the support material is now exposed with the biochar, for BGWW. Therefore, the biochar easily absorbs BGWW and this resulted in an enhanced abiotic loss of COD concentration of upto 74.1 mg L^{-1}. Here, the loss via volatilization was found to be negligible 1.93 mg L^{-1} d^{-1}.

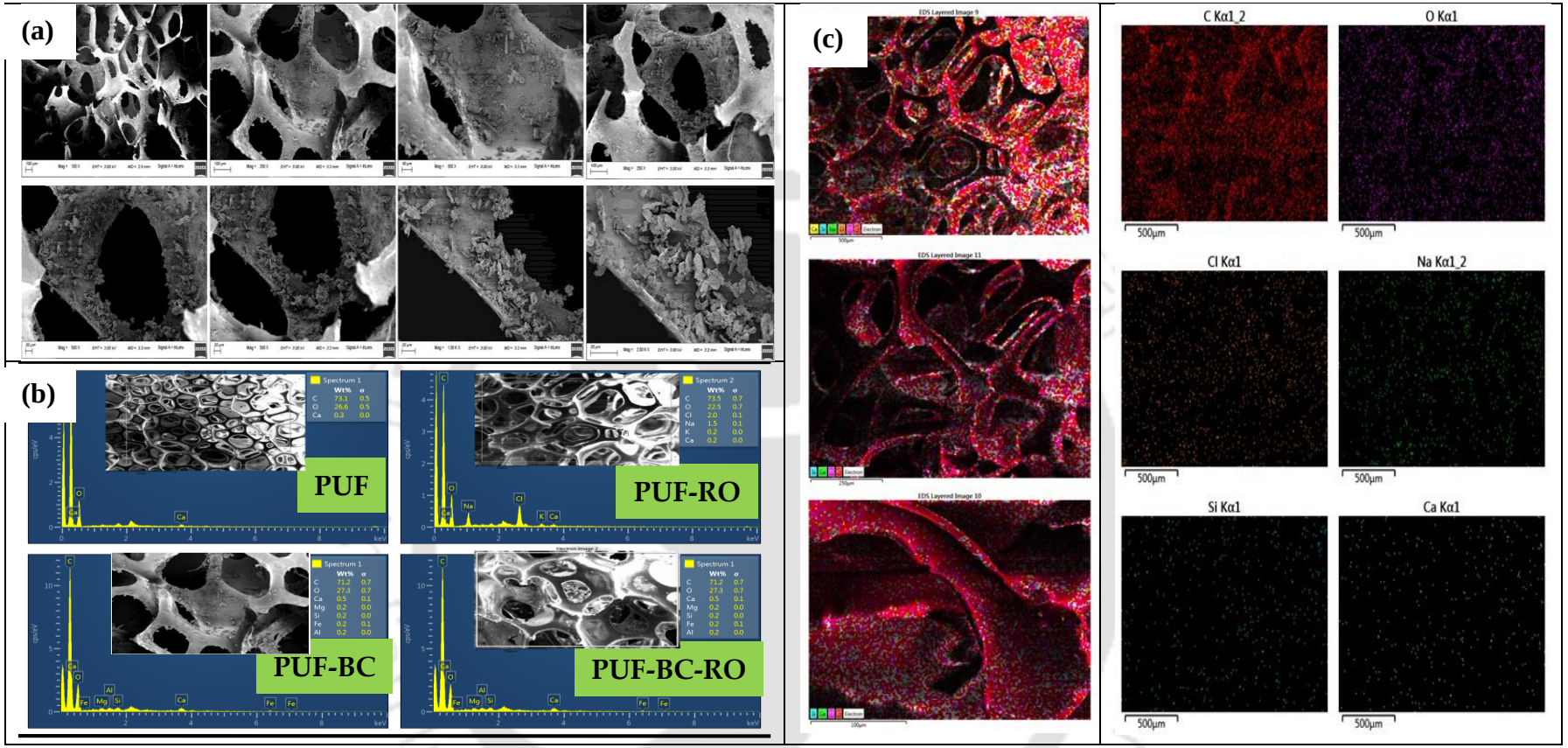

Fig. 4.37: (a) FESEM micrographs of PUF and biochar loaded PUF as the support material,

(b) FESEM-EDX of the support material (c) mapping of biofilm formation onto the support material

4.5.3. Optimization of DO concentration

The effect of dissolved oxygen (DO) on COD removal in the UFPBBR was examined with BGWW. COD removal (%) was found to be maximum when DO level was in the range 4.8-5.5 mg L^{-1} (Sahoo et al. 2011). Any further increase in DO content did not lead to enhancement in COD removal (%) efficiency by the UFPBBR. It might be because at a high DO concentration, the oxygen acts as a stronger electron withdrawing group inherent to PAHs and reduces the electron density of the aromatic ring resulting in inhibition of oxidative attack by the electrophilic oxygenases (Shelley et al. 1996; Costerton et al. 1996).

4.5.4. BGWW treatment

In the present study, BGWW was treated using the up-flow packed bed bioreactor (UFPBBR). The operational schedule of UFPBBR and its performance for BGWW treatment were presented in Table 3.3 and Fig. 4.38, respectively. The bioreactor was operated with and without biochar; loading onto the PUF material, and in both the cases, the bioreactor was operated continuously for an overall time period of 138 days. The influent COD concentration was 580 mg L^{-1}, which was increased in a stepwise manner upto an inlet COD concentration of 2270 mg L^{-1}.

4.5.4.1. Performance using PUF as the bio-support material

Initially, PUF with macropores of size 286 µm each was utilized in the bioreactor as the support material for growing *Rhodococcus* opacus. It had a wastewater adsorption capacity of 22.6 mg g^{-1}, which served to remove the COD at the initial phase of the bioreactor operation. For HRT values of 36, 30, 24, 18, and 12 h, and an inlet COD concentration of 580 mg L^{-1}, 91-94% of COD

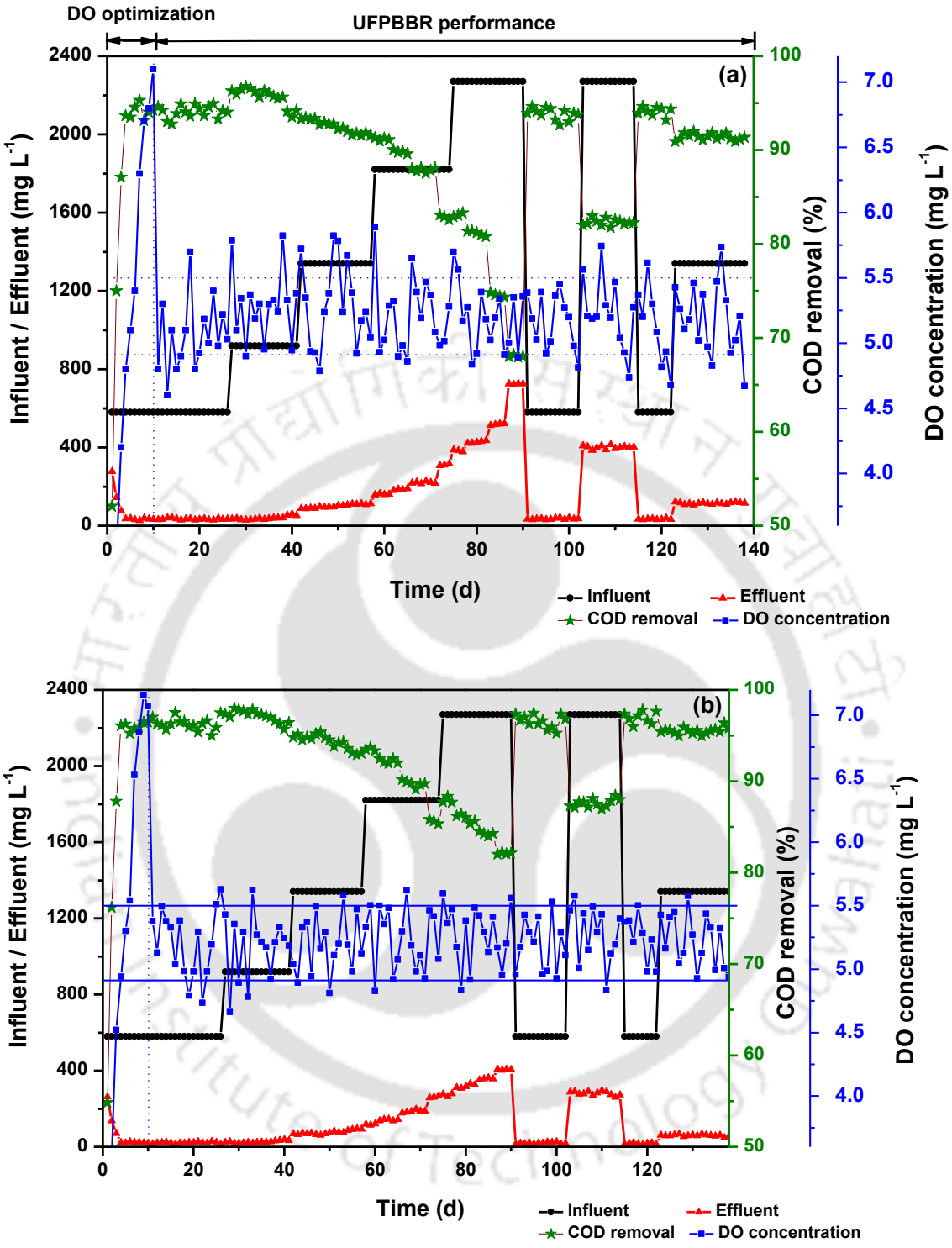

Fig. 4.38: Time profile of COD and DO in the UFPBBR treating BGWW (a) PUF as the bio-support material and (b) biochar-loaded PUF as the support material

removal was achieved in this reactor system. Following this phase of operation, a change in HRT to 36 h was applied in a stepwise manner, after ensuring steady state performance of the reactor in terms of COD removal for atleast 3-4 cycles; time for each cycle represented an equivalent time period corresponding to HRT of the wastewater. At an influent COD concentration of 1820 mg L^{-1} in UFPBBR with PUF as the support material and at 36 h, 30 h, 24 h of HRT, 88% - 91.3% of COD removal (%) was achieved. Sahoo et al. (2013) reported complete removal of 4-bromophenol in a PBBR with a HRT of 12.5 h for 2277 mg L^{-1} d^{-1} loading rate and with a concentration of 1000 mg L^{-1} using *Arthrobacter chlorophenolicus* A6. This high COD removal efficiency obtained is attributed to the fact that the bioreactor system was loaded with the single pollutant. In the present study, as the bioreactor was loaded with complex wastewater from biomass gasification industry that contains a mixture of other pollutants, a relatively low COD removal efficiency obtained is likely. Moreover, biodegradation of biomass gasification wastewater containing various mono- and polycyclic aromatic hydrocarbons by *R. opacus* may result in the formation of several intermediate metabolites that inhibit the enzymatic activity, which result in low COD removal in the system (Goswami et al. 2018a; Sahoo et al. 2013). Furthermore, the bioreactor performed poorly when it was operated at 18 h of HRT; COD removal of 74.8% and 67.9% was obtained at an influent COD concentration of 2270 mg L^{-1} and HRT of 24 h and 18 h (83^{rd} - 86^{th} days and 87^{th} - 90^{th} days), respectively.

DO profile was examined during the bioreactor operation is depicted in Fig. 4.38. In this figure, the dotted lines (parallel to x-axis) represents the optimum DO concentration, which was within the range of 4.8 and 5.5 mg L^{-1}. The optimum DO value in the UFPBBR was maintained by adjusting the air flow rate. However, a sudden increase or decrease in the DO level was observed due to variations in the organic loading rate, as a result of change in either HRT or inlet COD concentration or both. A sudden decline in

DO profile was noticed when the HRT was very low or when the inlet COD concentration was high. This result is attributed to the DO demand by the bacteria for metabolizing the COD present in the wastewater. An increase in the DO profile is also observed, which could be due to the reduced metabolic rate of the organism owing to the toxic effect of BGWW or by the intermediates formed, which is confirmed by the COD profile also. Similar kind of profiles (incline or decline) has been reported in the literature by other researchers (Salehi et al. 2011).

UPPBBR performance mainly dependent on inlet COD concentration and HRT. Fig. 4.38 shows the reactor performance in terms of COD removal (%) and COD removal rate (mg L^{-1} d^{-1}) at different HRT. It can be seen that 68% COD removal was achieved at 24 h of HRT and 2270 mg L^{-1} of influent COD concentration in BGWW. But, when the HRT was further reduced below 24 h for 2270 mg L^{-1}, the removal efficiency gradually decreased in this study. Thus, the bioreactor performance (in terms of COD removal) declined with an increase in the BGWW loading rate which resulted in a high COD concentration in the effluent stream. Hence, optimum conditions for operating the bioreactor for treating BGWW were found to be 1820 mg L^{-1} of the inlet COD concentration and 18 h HRT. Rezouga et al. (2009) reported that para-nitrophenol at an influent concentration more than 528.73 mg L^{-1} reduced the performance of a stirred tank bioreactor. In the present study, due to the aeration at 2 vvm, very less COD loss due to volatilization is observed for an influent COD concentration of 2270 mg L^{-1}, which was however, negligible in comparison to the COD removal (%) by microbial degradation.

Performance of the UFPBBR was further evaluated under the two different shock loading conditions as mentioned in Table 3.3, (1) by lowering the influent COD concentration from 2270 mg L^{-1} to 580 mg L^{-1} and (2) increasing the HRT from 18 h to 36

h after 90th day of the experimental runtime. Thus, bioreactor was operated with a decrease in the influent COD concentration to 580 mg L^{-1} and by increasing the HRT from 18 h to 36 h. During this phase of operation, the bioreactor was operated undeer this condition for 8 more days and the performance was found to be stable (Fig. 4.38). The next shock loading was applied by reducing the influent COD concentration to 2270 mg L^{-1} and keeping the HRT same at 36 h (Table 3.3). The UFPBBR performance was temporarily disturbed with a maximum COD removal of 81.6% during the 13 days of operation period. Under all these reactor operating conditions, the performance only slightly changed but it was able to recover quickly and its performance became stable with a removal efficiency of 91.4%.

4.5.4.2. Performance using PUF-biochar as the bio-support material

Using biochar loaded PUF as the bio-support material, the UFPBBR bioreactor was operated at the same HRT of 36, 30, 24, 18, and 12 h under continuous mode. The COD removal was higher than that observed using the UFPBBR with PUF as the bio-support material at all the HRTs and for the inlet concentrations of 580, 920, 1340, 1820 and 2270 mg L^{-1}. A maximum of 93.4% COD removal was attained at a COD concentration rate and 1820 mg L^{-1} having HRT of 24 h. This enhancement in the COD removal efficiency is mainly attributed to the biochar present along with the biomass. A similar kind of enhanced phenanthrene removal was reported by She et al. (2016) utilizing *Sphingomonas* sp. GY2B, supplemented with nano-bamboo charcoal, which imposed a synergistic role in the PAH biodegradation. In the previous study using biochar, an increase in PAHs biodegradation by *R. opacus* was observed (Section 4.2). Removal of other micropollutant reported an enhancement in atrazine biodegradation up to 20% using carbon nanotubes (Zhang et al., 2015).

Similar to the previous experiments with the reactor, the DO was maintained within 4.8 and 5.5 mg L^{-1} range. Though a sudden increase or decrease in DO level was observed in the reactor with biochar loaded PUF as the support material, the variation was very low in comparison to that observed in UFPBBR with PUF as the support material. Fig. 4.38 (b) shows that 95.2% COD removal was achieved at 24 h of HRT and 1340 mg L^{-1} of influent COD concentration of BGWW. When the COD loading was further increased to more than 1820 mg L^{-1}, the removal efficiency gradually decreased in this study. These results were similar to those observed previously in the case of reactor with only PUF as the support material. Thus, the optimum condition for operating the reactor with biochar loaded PUF were found to be 1820 mg L^{-1} influent COD concentration and 18 h HRT. A volatilization loss of 1.93 mg L^{-1} d^{-1} was observed for an influent COD concentration of 2270 mg L^{-1}, which is slightly less than the value observed in the case of UFPBBR with PUF as the support material.

The bioreactor with biochar loaded PUF also performed better than that with only PUF under the shock loading conditions. The first shock loading condition was characterized with a decrease in the influent COD concentration from 2270 mg L^{-1} to 580 mg L^{-1} and increasing the HRT from 18 h to 36 h (Table 3.3). With a decrease in the influent COD concentration from 2270 mg L^{-1} to 580 mg L^{-1}, no change in the reactor performance was observed during its operation; and was stable even after 12 days of continuous operation. Following this, the next shock loading was applied by increasing the influent COD concentration to 2270 mg L^{-1} by keeping the HRT same at 36 h, which resulted in 87.7% of COD removal of BGWW (Table 3.3). The influent concentration was later decreased to 580 mg L^{-1} and the HRT reduced to 18 h, and under these conditions, the reactor performance slightly changed. Finally, when the influent COD concentration was increased from 580 to 1340 mg L^{-1}, the performance of the bioreactor improved

gradually over a 3-day time period and was stable at 95.9% which is better than the UFPBBR with PUF as the bio-support material.

Fig. 4.39 represents various types of binding that are involved in sorption of organic contaminants, which include hydrogen bonding, anionic-cationic electrostatic bonding, pore filling, hydrophobic effect, etc. that play an important role in the remediation of organic contaminated wastewater (Tan et al. 2015). The interaction of iron with reactive oxygen species (ROS) such as superoxide anion and hydrogen peroxide leads to the generation of highly active hydroxyl radicals. Iron plays an important protagonist role in reducing the stress as microorganism have shown to be less sensitive towards the stress-causing agents in presence of iron (Andrews et al., 2003). Moreover, iron is utilized by strain as an essential micronutrient. Santos et al. (2008) reported that presence of iron in trace amounts stimulates *Pseudomonas* sp. for anthracene biodegradation. The presence of iron also leads to the induction, and synthesis of catalytic enzymes involved in PAHs biodegradation (Santos et al. 2008). Thus, it could be postulated that the *R. opacus* activity could be maintained by biochar that trace amount of iron for treating the complex BGWW in the UFPBBR with biochar loaded PUF as the bio-support, which resulted in a better COD removal efficiency and tolerance than that observed in the UFPBBR with only PUF as the bio-support.

It is also reported that the presence of soluble iron in trace amounts in well-aerated soils enhances the microbial activity towards biodegradation of mono- and polycyclic hydrocarbon biodegradation, thereby ensuring very good bioremediation efficiency of the strains (Dinkla and Janssen, 2003; Dinkla et al., 2001). Santos et al. (2008) reported that the supplementation of iron leads to an increase in PAHs biodegradation by enhancing the enzyme activities and enhancing the bioavailability via stimulated biosurfactant production.

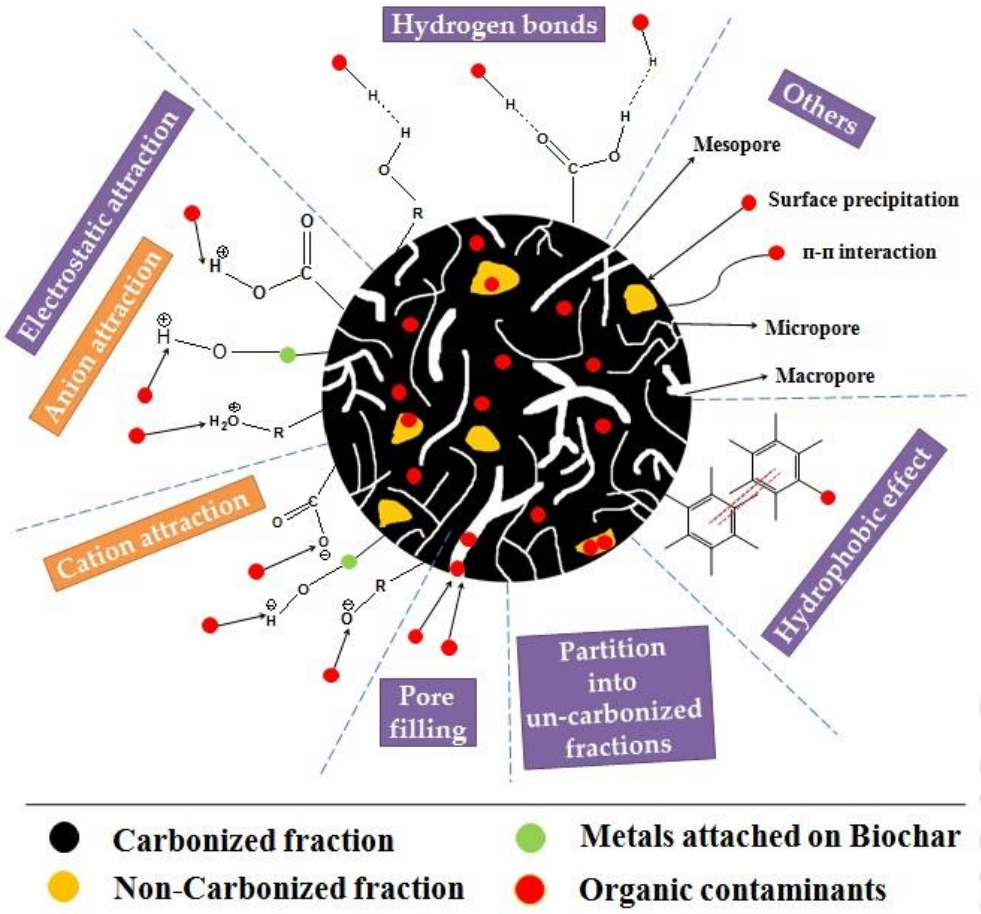

Fig. 4.39: Plausible mechanism for the removal of organic contaminants in wastewater by adsorption onto biochar

4.5.5. Toxicity removal

The toxicity (along with toxicity removal (%)) for both the support material was examined for all the different influent and effluent COD concentrations (580, 920, 1340, 1820 and 2270 mg L^{-1}) at 18 h of HRT and the values are presented in Table 4.13. For both the cases, the toxicity removal decreases with a reduction in HRT. Also, the minimum effluent toxicity was attained at the highest HRT (36 h), although the profile is in good agreement with the COD removal. The outcome from the toxicity test implies that the bioreactor can be operated without any buildup of hazardous intermediate. The removal

efficiency obtained is superior to that obtained using a stirred tank bioreactor with simulated wastewater containing a mixture of three different PAHs, in which case, 91% toxicity removal was achieved (Goswami et al. 2018a). Also, Sahoo et al., (2011) reported a toxicity removal of 93% and 97% of 4-bromophenol by utilizing mixed microbial consortium and *Arthrobacter chlorophenolius* A6, respectively.

Table 4.13: BGWW toxicity removal using the UFPBBR with two different support material and at different HRT

Influent COD (mg L^{-1})	Toxicity removal (%)	
	(a) PUF	(b) PUF-biochar
580	97.6	99.8
920	92.3	98.7
1340	89.7	98.1
1820	84.8	96.2
2270	81.3	91.1

4.6. A hybrid continuous system using stirred tank bioreactor and microfiltration for simultaneous biomass gasification wastewater treatment and bioenergy recovery

4.6.1. COD removal and lipid accumulation by *R. opacus*

For up-scaling and enhancing the BGWW treatment, the wastewater was subjected under the continuous operating mode of stirred tank bioreactor (CSTR). The operational schedule of CSTR and its performance for BGWW treatment are represented by Table 3.5 and Fig. 4.40, respectively. Initially the bioreactor was operated with an initial influent COD concentration of 580 mg L^{-1} under the batch mode for 15 days, and was further operated with the stepwise increase in the COD concentration up to 2270 mg L^{-1} with different hydraulic retention time (HRT). Fig. 4.40 represents the time profiles of COD

removal (%) and pH of the effluent over a time period of 120days. With an operation of bioreactor at HRT of 30, 24, 18, and 15 h, and an initial influent COD concentration of 580 mg L^{-1}, around 92% - 98.2% of COD removal was attained. Following this, a change in HRT of 30 h was applied in a stepwise manner, once the bioreactor acquired the steady state performance. The steady-state was continued until the bioreactor performance that is examined in terms of COD removal (%) was stable for atleast 3/4 cycles (one cycle presents the steady operation of the UFPBBR for the time period that is equal to one HRT) at the desired BGWW loading rate, it was presumed that the bioreactor had achieved the steady state condition. With an influent COD concentration of 1820 mg L^{-1} in CSTR with PUF as the support material and operated at 30, 24, 18 and 15 h of HRT, 73% - 75.6% of COD removal (%) was achieved. In addition, at many times, a sudden decline in DO profile was noticed when the HRT was very low or when the inlet COD concentration was high. This result is attributed to the DO demand by the bacteria for metabolizing the COD present in the wastewater. The maximum lipid accumulation value evaluated to be 70.8% (w/w) of the cell dry weight (CDW) for BGWW with an influent COD concentration of 2270 mg L^{-1} and at 18 h of HRT.

4.6.2. Tangential microfiltration system and COD removal

In order to recover the lipid-rich biomass from the treated wastewaters and to further reduce the level of COD in BGWW, microfiltration using a low cost ceramic membrane (pore size: 1.01 μm and porosity: 44%) was carried out at various applied pressure (i.e., 34-172 kPa) at a constant cross-flow rate of 50 L h^{-1}. With an increase in the operating pressure, the flux of the microfiltration system increased due to a high driving force acting on the membrane surface. In general, the membrane fouling is attributed to

concentration polarization on the membrane surface and blocking of pores in the porous ceramic structure.

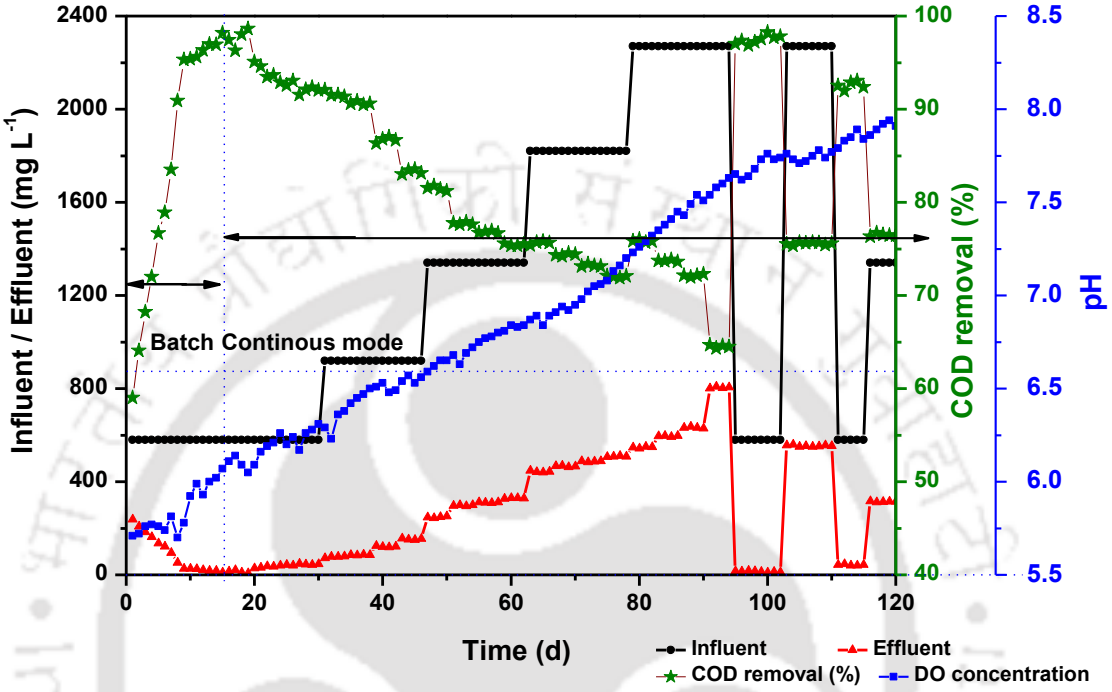

Fig. 4.40: Time profile of influent and effluent COD concentration, COD removal and pH in stirred tank bioreactor for treating BGWW

The less viscous BGWW possesses persistent organics (Goswami et al., 2018), and hence do not affect the membrane flux largely. The COD removal efficiency is directly dependent on the operating pressure up to a certain level and decreases at a high pressure, which is due to the augmented convective flux of the liquid acting on the membrane surface, thereby leading to a high undesired COD content in the permeate (Bennani et al. 2015; Chakraborty et al. 2003). Moreover, at a high pressure organic matter already retained on the membrane surface penetrated through the membrane, thus, reducing the overall percentage COD removal efficiency. Hence, the COD removal (%) at the point of

inflection enhanced from 72.3% to 96.12% for BGWW using the tangential microfiltration system. The retained lipids accumulated by the bacterium on the membrane surface were further extracted and characterized for biodiesel production.

Karhu et al. (2013) used a membrane bioreactor (MBR) for olive mill wastewater treatment and achieved 31%, 58% and 81% COD removal for an initial COD concentration of 53, 27 and 1500 mg L^{-1} in the wastewater. Using a membrane-aerated biofilm reactor, 60.3% of COD removal was reported by Abbasi et al. (2010) for the crude oil wastewater from offshore oil platforms. KolevSlavov et al. (2017) achieved 53% total organic carbon (TOC) removal from textile mercerization wastewater using a multichannel ceramic ultrafiltration membrane. Compared with these COD removal results reported in the present integrated process involving biodegradation-microfiltration system yielded excellent results (>96% COD removal efficiency) for different industrial wastewater along with an efficient biomass recovery for potential biodiesel production.

Henceforth, it can be concluded that for upscaling the integrated biodegradation-microfiltration approach for treating BGWW, the stirred tank bioreactor along with tangential microfiltration system have showed a great potential for BGWW treatment in a continuous system along with the energy recovery in the form of lipid-rich biomass.

CHAPTER 5

SUMMARY AND CONCLUSIONS

5. Summary and conclusions

The present study on biodegradation of polycyclic aromatic hydrocarbons contaminated wastewater by oleaginous bacterium *Rhodococcus opacus* was examined under batch and continuous operation conditions. The key findings of the study are presented in this section.

- Naphthalene (2-ring), anthracene (3-ring), phenanthrene (3-ring) and fluoranthene (4-ring) were initially selected as the model PAHs owing to their similar structure with most of the toxic PAHs and increasing ring complexity in their structures for biodegradation by *R. opacus*. Biodegradation of these PAHs, both individually and in multi-component systems, by *R. opacus* was evaluated in batch shake flask system. In individual PAH biodegradation system, using 2-, 3- and 4-ring PAH compounds (naphthalene, anthracene, phenanthrene and fluoranthene, respectively) biomass production and lipid accumulation by *R. opacus*, were studied. All the three PAHs yielded a high cell density lipid-rich biomass with a high biomass titer; among these compounds, the 4-ring compound yielded the least biomass growth and lipid production. Also, an increase in the inoculum size showed a positive effect on both *R. opacus* biomass growth and lipid accumulation. ^{1}H and ^{13}C-NMR analyses revealed that the accumulated bacterial lipids were primarily composed of saturated fatty acids. GC analysis and estimated properties of the biodiesel produced by transesterification of the bacterial lipids confirmed its potential application. The biodiesel properties also matched well with those of the international standards.
- In the multi-component system, the effect of three different PAHs in a ternary substrate system on each other biodegradation was evaluated using *R. opacus*. In

all the experimental runs, the individual effect of PAHs on biodegradation was more significant than the interaction between the substrates. The inhibitory effect caused by PAHs on the biodegradation was strongly influenced by their respective initial PAH concentrations, and increased complexity (increased number of rings) of a specific PAH resulted in a stronger inhibition of biodegradation of the other PAHs in mixture. *R. opacus* has potential for biodegradation of PAHs in industrial wastewater if processing time can be reduced along with the potential of producing value added lipid.

- In the study involving biodegradation of PAH (anthracene) contaminated with heavy metals, the presence of heavy metals negatively influenced *R. opacus* biomass growth, anthracene biodegradation and total lipid accumulation. The heavy metal effect followed the order: Cd >Ni > Pb > Cu > Zn > Fe. The qualitative assessment of negative effect imposed by heavy metals on the biomass surface and lipid accumulation was successfully characterized using FESEM and TEM analyses. FESEM-EDX analysis of the bacterial biomass further confirmed that the metal precipitates formed were associated with the cell surface. FTIR characterization of the biomass grown in the absence and in presence of the metals further confirmed the involvement of N-H, C–H bend, -CH_2-(C=O), C–N stretch, C-H and O-H bending and -C–Cl groups on the biomass for heavy metal binding by the bacteria. Overall, this study proved the potential/robustness of the strain to grow and survive in system contaminated with both organic and inorganic pollutants.
- Biomass gasification effluent derived biochar was successfully prepared, characterized and applied for enhancing the biodegradation of PAHs by *R. opacus*. The cheaply produced biochar exhibited excellent physical, chemical, thermal and

magnetic properties for wastewater applications. The biochar material enhanced not only PAH biodegradation by *R. opacus*, but also yielded a high lipid rich biomass for energy application. Also, an increase in PAH biodegradation efficiency is observed with an increase in the biochar concentration. However, PAH biodegradation efficiency by *R. opacus*was dependent on to the structural complexity and aromaticity of the respective PAH. Moreover, an increase in the total lipids accumulated by the bacterium was observed due to an increase in the biochar concentration in the media which facilitated a better PAH uptakeby the bacterium. The mechanism of action by biochar was attributed to an increase in pollutant bioavailability to the degrading microorganism.

- Valorization of biomass gasification wastewater (BGWW) for lipids accumulation by *Rhodococcus opacus* was evaluated in batch system. The high cell density lipid-rich biomass of the bacterium resulted in a high biomass titer along with a high wastewater COD removal efficiency. An increase in the inoculum size showed a significant effect on both these parameters. Using the raw wastewater (untreated), the bacterium accumulated 54.3% (w/w) lipid with a wastewater chemical oxygen demand (COD) removal efficiency of 64%. However, these values were further enhanced to 62.8% (w/w) and 74%, respectively, following supplementation of the wastewater with MSM in the ratio 4:1.
- An integrated system involving biodegradation and microfiltration with low-cost ceramic membrane system for the treatment of biomass gasification wastewaters was evaluated. Batch biodegradation of the BGWW was first carried out using *R. opacus*; subsequently, a microfiltration system was applied to recover the bacterial biomass as well as for the residual COD removal from the effluent. The combined process showed excellent results in terms of COD removal from BGWW with 68.9

% of COD removal by biodegradation. This value was further improved to 88.2% following the microfiltration step performed by employing a low-cost ceramic membrane. Thus, a high COD removal was achieved using the integrated system. The microfiltration step helped to separate the bacterial biomass along with complete removal of COD from the wastewater.

- The potential of *R. opcaus* to continuously treat BGWW was evaluated employing an up-flow packed bed bioreactor (UFPBBR) with nano-biochar loaded polyurethane foam as the biosupport material. The biochar immobilized polyurethane foam as the support material in UFPBBR showed excellent COD removal (%) from the wastewater. By utilizing BGWW as the sole carbon and energy source, the hydrocarbonoclastic bacterium, *R. opacus* achieved a very high COD removal along with the toxicity removal in the UFPBBR with biochar loaded PUF as the biosupport material. The reactor performance was also stable in terms of the COD removal under two different shock loading condition in the system. Overall, the results obtained using the novel UFPBBR demonstrated its potential for large scale treatment of biomass gasification wastewater.
- For upscaling the integrated biodegradation-microfiltration approach for treating BGWW, a stirred tank bioreactor was utilized in addition to the low-cost tubular ceramic membrane for biodegradation followed by tangential microfiltration treatment of the wastewater. Continuous operation with the bioreactor was first carried out which yielded a high lipid-biomass due to the growth of *R. opacus* on the wastewater as the substrate. The tangential microfiltration system with a tubular ceramic membrane in the subsequent step was useful to recover the bacterial biomass as well as for the residual COD removal from the effluent. Biodegradation by *R. opacus* yielded a COD removal of 72.3% in the continuous stirred tank

bioreactor, which was further enhanced to 96.12 %; by the tangential microfiltration system revealing that the integrated approach can be up-scaled and utilized for continuous treatment of biomass gasification wastewater and energy recovery in the form of lipid-rich biomass.

- ^{1}H and ^{13}C nuclear magnetic resonance (NMR) spectroscopy affirmed that the fatty acids accumulated by the bacterium primarily contained saturated fatty acids. Thermogravimetric analysis of the accumulated lipids showed four thermal decomposition regions each with a good stability. Gas chromatography (GC) analysis of the transesterified lipids to biodiesel further revealed the presence of methyl palmitate and methyl stearate as the major fatty acid methyl esters (FAMEs). The estimated properties of the transesterified product indicated a good agreement with those of the standard values specified by the American Society for Testing and Materials (ASTM) and European Standards (EN).

Scope for Future Work

Following are some suggestions for future work based on this thesis:

- Techno-economic feasibility study of the treatment system developed in this work.
- Blending the biodiesel product derived from *R. opacus* lipids with diesel for practical application in combustion engine.
- Development and evaluation of other suitable bioreactor based treatment systems for treating BGWW.
- Genetic engineering of *R. opacus* to overcome BGWW toxicity and biocompatibility for enhancing the COD removal and lipid accumulation.

BIBLIOGRAPHY

Bibliography

- Abbasi, M., Mirfendereski, M., Nikbakht, M., Golshenas, M. and Mohammadi, T., 2010. Performance study of mullite and mullite–alumina ceramic MF membranes for oily wastewaters treatment. *Desalination*, *259* (1-3), pp.169-178.
- Abdul-Tehrani, H., Hudson, A.J., Chang, Y.S., Timms, A.R., Hawkins, C., Williams, J.M., Harrison, P.M., Guest, J.R. and Andrews, S.C., 1999. Ferritin mutants of Escherichia coli are iron deficient and growth impaired, and fur mutants are iron deficient. *Journal of Bacteriology*, *181*(5), pp.1415-1428.
- Ahmed, M.J.K. and Ahmaruzzaman, M., 2015. A facile synthesis of Fe_3O_4–charcoal composite for the sorption of a hazardous dye from aquatic environment. J. Environ. Manage. *163*, pp.163-173.
- Akhavan, O., 2010. Graphene nanomesh by ZnO nanorod photocatalysts. *ACS nano*, *4*(7), pp.4174-4180.
- Allamandola, L.J., Tielens, A.G.G.M. and Barker, J.R., 1989. Interstellar polycyclic aromatic hydrocarbons-The infrared emission bands, the excitation/emission mechanism, and the astrophysical implications. *Astrophys. J. 71*, pp.733-775.
- American Public Health Association (APHA) (2005) Standard Methods for Examination of Water and Wastewater, American Water Works Association, Water Environment Federation, Washington D.C
- Angerbauer, C., Siebenhofer, M., Mittelbach, M. and Guebitz, G.M., 2008. Conversion of sewage sludge into lipids by *Lipomyces starkeyi* for biodiesel production. Bioresour. Technol. *99*(8), 3051-3056.

- Arán, D., Antelo, J., Fiol, S. and Macías, F., 2016. Influence of feedstock on the copper removal capacity of waste-derived biochars. *Bioresour. Technol. 212*, pp.199-206.
- Arul Manikandan, N., Alemu, A.K., Goswami, L., Pakshirajan, K. and Pugazhenthi, G., 2016. Waste litchi peels for Cr (VI) removal from synthetic wastewater in batch and continuous systems: sorbent characterization, regeneration and reuse study. *J. Environ. Eng. 142*(9), p.C4016001.
- ATSDR (Agency for Toxic Substances and Diseases Registry). (2009). Polycyclic aromatic hydrocarbons (PAHs). Atlanta, GA. http://www.atsdr.cdc.gov/ csem/csem.html
- Axelsson, M. and Gentili, F., 2014. A single-step method for rapid extraction of total lipids from green microalgae. *PloS one*, *9*(2), pp. 89643.
- Azuma, H., Toyota, M., Asakawa, Y. and Kawano, S., 1996. Naphthalene-a constituent of Magnolia flowers. *Phytochemistry*, *42*(4), pp. 999-1004.
- Bachmann, J., Goebel, M.O. and Woche, S.K., 2013. Small-scale contact angle mapping on undisturbed soil surfaces. *J Hydrol. Hydromec. 61*(1), pp.3-8.
- Baek, S.O., Field, R.A., Goldstone, M.E., Kirk, P.W., Lester, J.N. and Perry, R., 1991. A review of atmospheric polycyclic aromatic hydrocarbons: sources, fate and behavior. *Water Air Soil Pollut. 60*(3-4), pp.279-300.
- Bankar, A.V., Kumar, A.R. and Zinjarde, S.S., 2009. Environmental and industrial applications of *Yarrowia lipolytica*. Appl. Microbiol. Biotechnol., *84*(5), p.847.
- Battelle Memorial Institute. (2003). Guidance for environmental background analysis. Vol. II: Sediment. Appendix A: Chemical fingerprinting of PAHs in sediments recognizing the contribution of urban background. UG-2054-ENV.

Prepared by Battelle Memorial Institute, Columbus, OH, Earth Tech, Inc., Honolulu, HI, and New Fields, Inc., Atlanta, GA for Naval Facilities Engineering Service Center, Port Hueneme, CA.

- Bennani, C.F., Ousji, B. and Ennigrou, D.J., 2015. Reclamation of dairy wastewater using ultrafiltration process. *Desalin. Water Treat. 55*(2), pp.297-303.
- Bezza, F.A. and Chirwa, E.M.N., 2016. Biosurfactant-enhanced bioremediation of aged polycyclic aromatic hydrocarbons (PAHs) in creosote contaminated soil. *Chemosphere, 144*, pp.635-644.
- Bind, A., Goswami, L. and Prakash, V., 2018. Comparative analysis of floating and submerged macrophytes for heavy metal (copper, chromium, arsenic and lead) removal: sorbent preparation, characterization, regeneration and cost estimation. *Geol. Ecol. Landscape. 2*(2), pp.61-72.
- Biswas, B., Sarkar, B., Rusmin, R. and Naidu, R., 2015. Bioremediation of PAHs and VOCs: advances in clay mineral–microbial interaction. *Environ. Int. 85*, pp.168-181.
- Bojakowska, I. and Sokołowska, G., 2012. Polycyclic aromatic hydrocarbons in crude oils from Poland. *Geolog. Q. 45*(1), pp.81-86.
- Bruun, S., Clauson-Kaas, S., Bobuľská, L. and Thomsen, I.K., 2014. Carbon dioxide emissions from biochar in soil: role of clay, microorganisms and carbonates. *Eur. J. Soil Sci. 65*(1), pp.52-59.
- Bücker, M., Glatt, H.R., Platt, K.L., Avnir, D., Ittah, Y., Blum, J. and Oesch, F., 1979. Mutagenicity of phenanthrene and phenanthrene K-region derivatives. *Mutat. Res. Genet. Tox. 66*(4), pp.337-348.

- Bueno, B.Y.M., Torem, M.L., Molina, F.A.L.M.S. and De Mesquita, L.M.S., 2008. Biosorption of lead (II), chromium (III) and copper (II) by *R. opacus*: Equilibrium and kinetic studies. *Miner. Eng. 21*(1), 65-75.
- Cao, Y., Yang, B., Song, Z., Wang, H., He, F. and Han, X., 2016. Wheat straw biochar amendments on the removal of polycyclic aromatic hydrocarbons (PAHs) in contaminated soil. Ecotox. Environ. Safe. 130, 248-255
- Castro, A.R., Rocha, I., Alves, M.M. and Pereira, M.A., 2016. *Rhodococcus opacus* B4: a promising bacterium for production of biofuels and biobased chemicals. *Amb Express*, *6*(1), p.35.
- Cerniglia, C.E. (1992). Biodegradation of polycyclic aromatic hydrocarbons. Biodegradation. 3: 351–368.
- Cerniglia, C.E., and Heitkamp, M.A., 1989. Microbial degradation of polycyclic aromatic hydrocarbons (PAH) in the aquatic environment. In *Metabolism of polycyclic aromatic hydrocarbons in the aquatic environment*, ed. U. Varanasi. CRC Press, Boca Raton, FL, pp. 42–68.
- Chakraborty, S., Purkait, M.K., DasGupta, S., De, S. and Basu, J.K., 2003. Nanofiltration of textile plant effluent for color removal and reduction in COD. *Sep. Purif. Technol. 31*(2), pp.141-151.
- Chen, J., Henderson, G., Grimm, C.C., Lloyd, S.W. and Laine, R.A., 1998. Naphthalene in Formosan subterranean termite carton nests. *J. Agric. Food Chem.*, *46*(6), pp.2337-2339.
- Chen, S., Yin, H., Ye, J., Peng, H., Zhang, N. and He, B., 2013. Effect of copper (II) on biodegradation of benzo [a] pyrene by *Stenotrophomonas maltophilia*. *Chemosphere*, *90*(6), pp.1811-1820.

- Chen, S.J., Su, H.B., Chang, J.E., Lee, W.J., Huang, K.L., Hsieh, L.T., Huang, Y.C., Lin, W.Y. and Lin, C.C., 2007. Emissions of polycyclic aromatic hydrocarbons (PAHs) from the pyrolysis of scrap tires. *Atmos. Environ. 41*(6), pp.1209-1220.
- Cheng, M., Zeng, G., Huang, D., Lai, C., Xu, P., Zhang, C. and Liu, Y., 2016. Hydroxyl radicals based advanced oxidation processes (AOPs) for remediation of soils contaminated with organic compounds: a review. *Chem. Eng. J. 284*, pp.582-598.
- Costerton, J.W., Lewandowski, Z., Caldwell, D.E., Korber, D.R. and Lappin-Scott, H.M., 1995. Microbial biofilms. *Annu. Rev. Microbiol. 49*(1), pp.711-745.
- Daisy, B.H., Strobel, G.A., Castillo, U., Ezra, D., Sears, J., Weaver, D.K. and Runyon, J.B., 2002. Naphthalene, an insect repellent, is produced by *Muscodor vitigenus*, a novel endophytic fungus. *Microbiology*, *148*(11), pp.3737-3741.
- Das, K. and Mukherjee, A.K., 2007. Differential utilization of pyrene as the sole source of carbon by *Bacillus subtilis* and *Pseudomonas aeruginosa* strains: role of biosurfactants in enhancing bioavailability. *J. Appl. Microbiol. 102*(1), pp.195-203.
- Das, O. and Sarmah, A.K., 2015. The love–hate relationship of pyrolysis biochar and water: a perspective. *Sci. Total Environ. 512*, pp.682-685.
- Das, O., Bhattacharyya, D. and Sarmah, A.K., 2016. Sustainable eco–composites obtained from waste derived biochar: a consideration in performance properties, production costs, and environmental impact. *J. Clean. Prod. 129*, pp.159-168.
- Das, O., Sarmah, A.K. and Bhattacharyya, D., 2015. A novel approach in organic waste utilization through biochar addition in wood/polypropylene composites. *Waste. Manage. 38*, pp.132-140.

- Delistraty, D., 1997. Toxic equivalency factor approach for risk assessment of polycyclic aromatic hydrocarbons. *Toxicol. Environ. Chem. 64*(1-4), pp.81-108.
- Dinkla, I.J., Gabor, E.M. and Janssen, D.B., 2001. Effects of iron limitation on the degradation of toluene by *Pseudomonas* strains carrying the TOL (pWWO) plasmid. *Appl. Environ. Microbiol. 67*(8), pp.3406-3412.
- Dinkla, I.J.T. and Janssen, D.B., 2003. Simultaneous growth on citrate reduces the effects of iron limitation during toluene degradation in Pseudomonas. *Microb. Ecol*. *45*(1), pp.97-107.
- EEA (European Environmental Agency). (2012). *European Union emission inventory report 1990–2010 under the UNECE Convention on Long-Range Trans-Boundary Air Pollution (LRTAP)*. Technical Report 8/2012.
- Eisler, R., 1987. Polycyclic aromatic hydrocarbon hazards to fish, wildlife, and invertebrates: a synoptic review. *US fish and wildlife service biological report*, *85*(1.11), p.81.
- Fabbri, D. and Vassura, I., 2006. Evaluating emission levels of polycyclic aromatic hydrocarbons from organic materials by analytical pyrolysis. *J. Anal. Appl. Pyrol. 75*(2), pp.150-158.
- Fava, F., Di Gioia, D., Marchetti, L. and Quattroni, G., 1996. Aerobic dechlorination of low-chlorinated biphenyls by bacterial biofilms in packed-bed batch bioreactors. *Appl. Microbiol. Biotechnol. 45*(4), pp.562-568.
- Finnerty, W.R., 1992. The biology and genetics of the genus *Rhodococcus*. *Ann. Rev. Microbiol. 46*(1), pp.193-218.
- Folch, J., Lees, M. and Sloane Stanley, G.H., 1957. A simple method for the isolation and purification of total lipides from animal tissues. *J. Boil. Chem*. *226*(1), pp.497-509.

- Francisco, E.C., Neves, D.B., Jacob-Lopes, E. and Franco, T.T., 2010. Microalgae as feedstock for biodiesel production: carbon dioxide sequestration, lipid production and biofuel quality. *J. Chem. Technol. Biotechnol. 85*(3), pp.395-403.
- Frost, R.L., Weier, M.L. and Kloprogge, J.T., 2003. Raman spectroscopy of some natural hydrotalcites with sulphate and carbonate in the interlayer. *J. Raman Spectrosc. 34*(10), pp.760-768.
- Ghosh, I. and Mukherji, S., 2017. Substrate interaction effects during pyrene biodegradation by *Pseudomonas aeruginosa* RS1. *J. Environ. Chem. Eng. 5*(2), pp.1791-1800.
- Ghosh, I., Jasmine, J. and Mukherji, S., 2014. Biodegradation of pyrene by a *Pseudomonas aeruginosa* strain RS1 isolated from refinery sludge. *Bioresour. Technol. 166*, pp.548-558.
- Godfrey, V., 2012. Production of biodiesel from oleaginous organisms using underutilized wastewaters. M Sci Thesis, Utah State University, Logan, Utah.
- Goswami, L., Kumar, R.V., Arul Manikandan, N., Pakshirajan, K. and Pugazhenthi, G., 2017. Anthracene biodegradation by Oleaginous *Rhodococcus opacus* for biodiesel production and its characterization. *Polycycl. Aromat. Comp.* pp.1-13.
- Goswami, L., Kumar, R.V., Manikandan, N.A., Pakshirajan, K. and Pugazhenthi, G., 2017. Simultaneous polycyclic aromatic hydrocarbon degradation and lipid accumulation by *Rhodococcus opacus* for potential biodiesel production. *J. Water Process Eng. 17*, pp.1-10.
- Goswami, L., Manikandan, N. A., Dolman, B., Pakshirajan, K., Pugazhenthi, G. (2018). Biological treatment of wastewater containing a mixture of polycyclic

aromatic hydrocarbons using the oleaginous bacterium *Rhodococcus opacus*. *J Clean Prod.* 196(20), pp. 1282-1291.

- Goswami, L., Manikandan, N.A., Pakshirajan, K. and Pugazhenthi, G., 2017. Simultaneous heavy metal removal and anthracene biodegradation by the oleaginous bacteria *Rhodococcus opacus*. *3 Biotech*, *7*(1), p.37.
- Goswami, L., Namboodiri, M.T., Kumar, R.V., Pakshirajan, K. and Pugazhenthi, G., 2017. Biodiesel production potential of oleaginous *Rhodococcus opacus* grown on biomass gasification wastewater. *Renew. Energ. 105*, pp.400-406.
- Gouda, M.K., Omar, S.H. and Aouad, L.M., 2008. Single cell oil production by Gordonia sp. DG using agro-industrial wastes. *World J. Microbiol. Biotechnol. 24*(9), p.1703.
- Gouveia, L. and Oliveira, A.C., 2009. Microalgae as a raw material for biofuels production. *J. Ind. Microbiol. Biotechnol. 36*(2), pp.269-274.
- Graber, A., Skvarc, R. and Junge-Berberović, R., 2009. Elimination of phenols, ammonia and cyanide in wash water from biomass gasification, and nitrogen recycling using planted trickling filters. *Wat Sci Tech*, *60*(12), pp.3253-3259.
- Gray, M., Johnson, M.G., Dragila, M.I. and Kleber, M., 2014. Water uptake in biochars: the roles of porosity and hydrophobicity. *Biomass. Bioenerg. 61*, pp.196-205.
- Hadibarata, T. and Kristanti, R.A., 2012. Identification of metabolites from benzo [a] pyrene oxidation by ligninolytic enzymes of *Polyporus* sp. S133. *J. Environ. Manage. 111*, pp.115-119.
- Haritash, A.K. and Kaushik, C.P., 2009. Biodegradation aspects of polycyclic aromatic hydrocarbons (PAHs): a review. *J. Hazard. Mater. 169*(1-3), pp.1-15.

- Hawthorne, S.B., Miller, D.J. and Kreitinger, J.P., 2006. Measurement of total polycyclic aromatic hydrocarbon concentrations in sediments and toxic units used for estimating risk to benthic invertebrates at manufactured gas plant sites. *Environ. Toxicol. Chem. 25*(1), pp.287-296.
- Jürgens, A., Webber, A.C. and Gottsberger, G., 2000. Floral scent compounds of Amazonian Annonaceae species pollinated by small beetles and thrips. *Phytochemistry*, *55*(6), pp.551-558.
- Karhu, M., Kuokkanen, T., Rämö, J., Mikola, M. and Tanskanen, J., 2013. Performance of a commercial industrial-scale UF-based process for treatment of oily wastewaters. *J. Environ. Manage. 128*, pp.413-420.
- Karim, K. and Gupta, S.K., 2001. Biotransformation of nitrophenols in upflow anaerobic sludge blanket reactors. *Bioresour. Technol. 80*(3), pp.179-186.
- Kazunga, C. and Aitken, M.D., 2000. Products from the incomplete metabolism of pyrene by polycyclic aromatic hydrocarbon-degrading bacteria. *Appl. Environ. Microbiol. 66*(5), pp.1917-1922.
- Kiran, M.G., Pakshirajan, K. and Das, G., 2017. Heavy metal removal from multicomponent system by sulfate reducing bacteria: mechanism and cell surface characterization. *J. hazard. Mater. 324*, pp.62-70.
- Kleinova, A., Cvengrosova, Z., Rimarik, J., Buzetzki, E., Mikulec, J., Cvengros, J., 2012. Biofuels from Algae. Procedia Eng. 42: 231-8.
- Knothe, G., Sharp, C.A. and Ryan, T.W., 2006. Exhaust emissions of biodiesel, petrodiesel, neat methyl esters, and alkanes in a new technology engine. *Energ. Fuels. 20*(1), pp.403-408.
- Kolev Slavov, A., 2017. General characteristics and treatment possibilities of dairy wastewater–A review. *Food. Technol. Biotech. 55*(1), pp.14-28.

- Kumar, R.V., Goswami, L., Pakshirajan, K. and Pugazhenthi, G., 2016. Dairy wastewater treatment using a novel low cost tubular ceramic membrane and membrane fouling mechanism using pore blocking models. *J. Water Process Eng. 13*, pp.168-175.
- Kumar, S., Gupta, N. and Pakshirajan, K., 2015. Simultaneous lipid production and dairy wastewater treatment using *Rhodococcus opacus* in a batch bioreactor for potential biodiesel application. *J. Environ. Chem. Eng. 3*(3), pp.1630-1636.
- Kumar, V., Muthuraj, M., Palabhanvi, B., Ghoshal, A.K. and Das, D., 2014. Evaluation and optimization of two stage sequential in situ transesterification process for fatty acid methyl ester quantification from microalgae. *Renew. Energ. 68*, pp.560-569.
- Kushwaha, A., Hans, N., Kumar, S. and Rani, R., 2018. A critical review on speciation, mobilization and toxicity of lead in soil-microbe-plant system and bioremediation strategies. *Ecotox. Environ. Saf. 147*, pp.1035-1045.
- Kushwaha, A., Rani, R., Kumar, S. and Gautam, A., 2015. Heavy metal detoxification and tolerance mechanisms in plants: Implications for phytoremediation. *Environ. Rev. 24*(1), pp.39-51.
- Kushwaha, A., Rani, R., Kumar, S., Thomas, T., David, A.A. and Ahmed, M., 2017. A new insight to adsorption and accumulation of high lead concentration by exopolymer and whole cells of lead-resistant bacterium *Acinetobacter junii* L. Pb1 isolated from coal mine dump. *Environ. Sci. Poll. Res. 24*(11), pp.10652-10661.
- Kweon, O., Kim, S.J., Jones, R.C., Freeman, J.P., Adjei, M.D., Edmondson, R.D. and Cerniglia, C.E., 2007. A polyomic approach to elucidate the fluoranthene-

degradative pathway in *Mycobacterium vanbaalenii* PYR-1. *J. Bacteriol. 189*(13), pp.4635-4647.

- Lee, E.H. and Cho, K.S., 2009. Effect of substrate interaction on the degradation of methyl tert-butyl ether, benzene, toluene, ethylbenzene, and xylene by *Rhodococcus* sp. *J. Hazard. Mater. 167*(1-3), pp.669-674.
- Li, R., Wang, J.J., Zhou, B., Awasthi, M.K., Ali, A., Zhang, Z., Gaston, L.A., Lahori, A.H. and Mahar, A., 2016. Enhancing phosphate adsorption by Mg/Al layered double hydroxide functionalized biochar with different Mg/Al ratios. *Sci. Total Environ. 559*, pp.121-129.
- Liu, G., Niu, Z., Van Niekerk, D., Xue, J. and Zheng, L., 2008. Polycyclic aromatic hydrocarbons (PAHs) from coal combustion: emissions, analysis, and toxicology. In *Rev. Environ. Contam. Toxicol. 192: 1–28.* Springer, New York, NY.
- López, E.N., Medina, A.R., Moreno, P.A.G., Cerdán, L.E. and Grima, E.M., 2016. Extraction of microalgal lipids and the influence of polar lipids on biodiesel production by lipase-catalyzed transesterification. *Bioresour. Technol. 216*, pp.904-913.
- López, Z., Vila, J. and Grifoll, M., 2005. Metabolism of fluoranthene by mycobacterial strains isolated by their ability to grow in fluoranthene or pyrene. *J. Ind. Microbiol. Biotechnol. 32*(10), pp.455-464.
- Lu, H., Zhu, L. and Zhu, N., 2009. Polycyclic aromatic hydrocarbon emission from straw burning and the influence of combustion parameters. *Atmos. Environ. 43*(4), pp.978-983.
- Lu, L. and Zhu, L., 2012. Effect of soil components on the surfactant-enhanced soil sorption of PAHs. *J. Soils. Sediments. 12*(2), pp.161-168.

- Luo, Y., Guo, W., Ngo, H.H., Nghiem, L.D., Hai, F.I., Zhang, J., Liang, S. and Wang, X.C., 2014. A review on the occurrence of micropollutants in the aquatic environment and their fate and removal during wastewater treatment. *Sci. Total. Environ. 473*, pp.619-641.
- MacKay, A.A. and Gschwend, P.M., 2001. Enhanced concentrations of PAHs in groundwater at a coal tar site. *Environ. Sci. Technol. 35*(7), pp.1320-1328.
- Mahanty, B., Pakshirajan, K. and Dasu, V.V., 2008. Synchronous fluorescence as a selective method for monitoring pyrene in biodegradation studies. *Polycycl. Aromat. Comp. 28*(3), pp.213-227.
- Mahler, B.J., Metre, P.C.V., Crane, J.L., Watts, A.W., Scoggins, M. and Williams, E.S., 2012. Coal-tar-based pavement sealcoat and PAHs: implications for the environment, human health, and stormwater management. *Environ. Sci. Technol.* 46: 3039−3045.
- Mahler, B.J., Van Metre, P.C. and Foreman, W.T., 2014. Concentrations of polycyclic aromatic hydrocarbons (PAHs) and azaarenes in runoff from coal-tar- and asphalt-sealcoated pavement. *Environ. Pollut. 188*, pp.81-87.
- Maria, V.L., Gomes, T., Barreira, L. and Bebianno, M.J., 2013. Impact of benzo (a) pyrene, Cu and their mixture on the proteomic response of *Mytilus galloprovincialis*. *Aquat. Toxicol. 144*, pp.284-295.
- Marjakangas, J.M., Chen, C.Y., Lakaniemi, A.M., Puhakka, J.A., Whang, L.M. and Chang, J.S., 2015. Selecting an indigenous microalgal strain for lipid production in anaerobically treated piggery wastewater. *Bioresour. Technol. 191*, pp.369-376.

- Marjakangas, J.M., Lakaniemi, A.M., Koskinen, P.E., Chang, J.S. and Puhakka, J.A., 2015. Lipid production by eukaryotic microorganisms isolated from palm oil mill effluent. *Biochem. Eng. J. 99*, pp.48-54.
- Martinez-Guerra, E., Gude, V.G., Mondala, A., Holmes, W. and Hernandez, R., 2014. Microwave and ultrasound enhanced extractive-transesterification of algal lipids. *Appl. Energ. 129*, pp.354-363.
- McConkey, B.J., Duxbury, C.L., Dixon, D.G. and Greenberg, B.M., 1997. Toxicity of a PAH photooxidation product to the bacteria *Photobacterium phosphoreum* and the duckweed Lemna gibba: Effects of phenanthrene and its primary photoproduct, phenanthrenequinone. *Environmen. Toxicol.Chem. 16*(5), pp.892-899.
- Mittelbach, M., Roth, G. and Bergmann, A., 1996. Simultaneous gas chromatographic determination of methanol and free glycerol in biodiesel. *Chromatographia*, *42*(7-8), pp.431-434.
- Monash, P. and Pugazhenthi, G., 2011. Development of ceramic supports derived from low-cost raw materials for membrane applications and its optimization based on sintering temperature. *Int. J. Appl. Ceram. Technol. 8*(1), pp.227-238.
- Monash, P. and Pugazhenthi, G., 2011. Effect of TiO_2 addition on the fabrication of ceramic membrane supports: A study on the separation of oil droplets and bovine serum albumin (BSA) from its solution. *Desalination*, *279*(1-3), pp.104-114.
- Moscoso, F., Deive, F.J., Longo, M.A. and Sanromán, M.A., 2012. Techno economic assessment of phenanthrene degradation by *Pseudomonas stutzeri* CECT 930 in a batch bioreactor. *Bioresour. Technol. 104*, pp.81-89.

- Motelay-Massei, A., Garban, B., Tiphagne-Larcher, K., Chevreuil, M. and Ollivon, D., 2006. Mass balance for polycyclic aromatic hydrocarbons in the urban watershed of Le Havre (France): transport and fate of PAHs from the atmosphere to the outlet. *Water Res. 40*(10), pp.1995-2006.
- Nguyen, T.D., Phan, N.H., Do, M.H. and Ngo, K.T., 2011. Magnetic Fe_2MO_4 (M: Fe, Mn) activated carbons: fabrication, characterization and heterogeneous Fenton oxidation of methyl orange. *J. Hazard. Mater. 185*(2-3), pp.653-661.
- NRC (National Research Council). (1983). *Polycyclic aromatic hydrocarbons: Evaluation and effects*. Committee on Pyrene and Selected Analogues, Board on Toxicology and Environmental Health Hazards, Commission on Life Sciences, National Academy Press, Washington, DC.
- Ogala, J.E. and Iwegbue, C.M., 2011. Occurrence and profile of polycyclic aromatic hydrocarbons in coals and shales from eastern Nigeria. *Pet. Coal*. *53*(3), pp.188-93.
- Ojajuni, O., Saroj, D. and Cavalli, G., 2015. Removal of organic micropollutants using membrane-assisted processes: a review of recent progress. *Environ. Technol. Rev. 4*(1), pp.17-37.
- Parinos, C. and Gogou, A., 2016. Suspended particle-associated PAHs in the open eastern Mediterranean Sea: occurrence, sources and processes affecting their distribution patterns. *Mar. Chem. 180*, pp.42-50.
- Patel, A., Arora, N., Pruthi, V. and Pruthi, P.A., 2017. Biological treatment of pulp and paper industry effluent by oleaginous yeast integrated with production of biodiesel as sustainable transportation fuel. *J. Cleaner Prod. 142*, pp.2858-2864.

- Pavasant, P., Apiratikul, R., Sungkhum, V., Suthiparinyanont, P., Wattanachira, S. and Marhaba, T.F., 2006. Biosorption of Cu^{2+}, Cd^{2+}, Pb^{2+}, and Zn^{2+} using dried marine green macroalga *Caulerpa lentillifera*. *Bioresour. Technol. 97*(18), pp.2321-2329.
- Peng, W., Wu, Q., Tu, P. and Zhao, N., 2001. Pyrolytic characteristics of microalgae as renewable energy source determined by thermogravimetric analysis. *Bioresour. Technol. 80*(1), pp.1-7.
- Pinyakong, O., Habe, H., Supaka, N., Pinpanichkarn, P., Juntongjin, K., Yoshida, T., Furihata, K., Nojiri, H., Yamane, H. and Omori, T., 2000. Identification of novel metabolites in the degradation of phenanthrene by *Sphingomonas* sp. strain P2. *FEMS Microbiol. Lett. 191*(1), pp.115-121.
- Plows, F.L., Elsila, J.E., Zare, R.N. and Buseck, P.R., 2003. Evidence that polycyclic aromatic hydrocarbons in two carbonaceous chondrites predate parent-body formation. *Geochim. Cosmochim. Acta. 67*(7), pp.1429-1436.
- Predojević, Z.J., 2008. The production of biodiesel from waste frying oils: A comparison of different purification steps. *Fuel*, *87*(17-18), pp.3522-3528.
- Ramos, M.J., Fernández, C.M., Casas, A., Rodríguez, L. and Pérez, Á., 2009. Influence of fatty acid composition of raw materials on biodiesel properties. *Bioresour. Technol. 100*(1), pp.261-268.
- Ricca, A., Bauschlicher Jr, C.W., Boersma, C., Tielens, A.G. and Allamandola, L.J., 2012. The infrared spectroscopy of compact polycyclic aromatic hydrocarbons containing up to 384 carbons. *The Astrophys. J. 754*(1), p.75.
- RIVM., 2012. Environmental risk limits for polycyclic aromatic hydrocarbons (PAHs): For direct aquatic, benthic, and terrestrial toxicity. RIVM Report

607711007/2012. National Institute for Health and Environment (RIVM), Bilthoven, The Netherlands.

- Rodrigues, A., Nogueira, R., Melo, L.F. and Brito, A.G., 2013. Effect of low concentrations of synthetic surfactants on polycyclic aromatic hydrocarbons (PAH) biodegradation. *Int. Biodeter. Biodeg. 83*, pp.48-55.
- Roy, A.S., Hazarika, J., Manikandan, N.A., Pakshirajan, K. and Syiem, M.B., 2015. Heavy metal removal from multicomponent system by the cyanobacterium *Nostoc muscorum*: kinetics and interaction study. *Appl. Biochem. Biotechnol. 175*(8), pp.3863-3874.
- Sahoo, N.K., Ghosh, P.K. and Pakshirajan, K., 2013. Biodegradation of 4-bromophenol by *Arthrobacter chlorophenolicus* A6T in a newly designed packed bed reactor. *J. Biosci. Bioeng. 115*(2), pp.182-188.
- Sahoo, N.K., Pakshirajan, K. and Ghosh, P.K., 2011. Batch biodegradation of para-nitrophenol using *Arthrobacter chlorophenolicus* A6. *Appl. Biochem. Biotechnol. 165*(7-8), pp.1587-1596.
- Salehi, Z., Yoshikawa, H., Mineta, R. and Kawase, Y., 2011. Aerobic biodegradation of p-nitrophenol by acclimated waste activated sludge in a slurry bubble column. *Process Biochem. 46*(1), pp.284-289.
- Samanta, S.K., Singh, O.V. and Jain, R.K., 2002. Polycyclic aromatic hydrocarbons: environmental pollution and bioremediation. *TRENDS Biotechnol. 20*(6), pp.243-248.
- Santos, E.C., Jacques, R.J., Bento, F.M., Maria do Carmo, R.P., Selbach, P.A., Sá, E.L. and Camargo, F.A., 2008. Anthracene biodegradation and surface activity by an iron-stimulated *Pseudomonas* sp. *Bioresour. Technol. 99*(7), pp.2644-2649.

- Sarin, A., Arora, R., Singh, N.P., Sarin, R., Malhotra, R.K. and Kundu, K., 2009. Effect of blends of Palm-Jatropha-Pongamia biodiesels on cloud point and pour point. *Energ. 34*(11), pp.2016-2021.
- Schauer, J.J., Kleeman, M.J., Cass, G.R. and Simoneit, B.R., 2001. Measurement of emissions from air pollution sources. 3. C1− C29 organic compounds from fireplace combustion of wood. *Environ. Sci. Technol. 35*(9), pp.1716-1728.
- She, B., Tao, X., Huang, T., Lu, G., Zhou, Z., Guo, C. and Dang, Z., 2016. Effects of nano bamboo charcoal on PAHs-degrading strain *Sphingomonas* sp. GY2B. *Ecotoxicol. Environ. Saf. 125*, pp.35-42.
- Shelley, M.D., Autenrieth, R.L., Wild, J.R. and Dale, B.E., 1996. Thermodynamic analysis of trinitrotoluene biodegradation and mineralization pathways. *Biotechnol. Bioeng. 51*(2), pp.198-205.
- Shen, H., Huang, Y., Wang, R., Zhu, D., Li, W., Shen, G., Wang, B., Zhang, Y., Chen, Y., Lu, Y. and Chen, H., 2013. Global atmospheric emissions of polycyclic aromatic hydrocarbons from 1960 to 2008 and future predictions. *Environ. Sci. Technol. 47*(12), pp.6415-6424.
- Sherafatmand, M. and Ng, H.Y., 2015. Using sediment microbial fuel cells (SMFCs) for bioremediation of polycyclic aromatic hydrocarbons (PAHs). *Bioresour. Technol. 195*, pp.122-130.
- Silva, W.C., Castro, M.P.P., Perez, V.H., Machado, F.A., Mota, L. and Sthel, M.S., 2016. Thermal degradation of ethanolic biodiesel: Physicochemical and thermal properties evaluation. *Energ. 114*, pp.1093-1099.
- Sims, R.C. and Overcash, M.R., 1983. Fate of polynuclear aromatic compounds (PNAs) in soil-plant systems. *Residue Rev.* (pp. 1-68). Springer, New York, NY.

- Sinha, V., Pakshirajan, K. and Chaturvedi, R., 2015. Evaluation of Cr (VI) Exposed and Unexposed Plant Parts of *Tradescantia pallida* (Rose) DR Hunt. for Cr Removal from Wastewater by Biosorption. *Int. J. Phytorem. 17*(12), pp.1204-1211.
- Sokhn, J., De Leij, F.A.A.M., Hart, T.D. and Lynch, J.M., 2001. Effect of copper on the degradation of phenanthrene by soil micro-organisms. *Lett. Appl. Microbiol. 33*(2), pp.164-168.
- Su, Y.C., Liu, Y.A., Diaz Tovar, C.A. and Gani, R., 2011. Selection of prediction methods for thermophysical properties for process modeling and product design of biodiesel manufacturing. *Ind. Eng. Chem. Res. 50*(11), pp.6809-6836.
- Tan, X., Liu, Y., Zeng, G., Wang, X., Hu, X., Gu, Y. and Yang, Z., 2015. Application of biochar for the removal of pollutants from aqueous solutions. *Chemosphere, 125*, pp.70-85.
- Tian, S., Qian, C. and Yang, X., 2006. Biodegradation of biomass gasification wastewater by two species of *Pseudomonas* using immobilized cell reactor. *Appl. Biochem. Biotechnol. 128*(2), pp.141-147.
- Timoney, K.P. and Lee, P., 2011. Polycyclic aromatic hydrocarbons increase in Athabasca River Delta sediment: Temporal trends and environmental correlates. *Environ. Sci. Technol. 45*(10), pp.4278-4284.
- Titaley, I.A., Chlebowski, A., Truong, L., Tanguay, R.L. and Massey Simonich, S.L., 2016. Identification and toxicological evaluation of unsubstituted PAHs and novel PAH derivatives in pavement sealcoat products. *Environ. Sci. Technol. Lett. 3*(6), pp.234-242.
- van Herwijnen, R., Wattiau, P., Bastiaens, L., Daal, L., Jonker, L., Springael, D., Govers, H.A. and Parsons, J.R., 2003. Elucidation of the metabolic pathway of

fluorene and cometabolic pathways of phenanthrene, fluoranthene, anthracene and dibenzothiophene by Sphingomonas sp. LB126. *Res. Microbiol. 154*(3), pp.199-206.

- Viêgas, C.V., Hachemi, I., Freitas, S.P., Mäki-Arvela, P., Aho, A., Hemming, J., Smeds, A., Heinmaa, I., Fontes, F.B., da Silva Pereira, D.C. and Kumar, N., 2015. A route to produce renewable diesel from algae: Synthesis and characterization of biodiesel via in situ transesterification of Chlorella alga and its catalytic deoxygenation to renewable diesel. *Fuel, 155*, pp.144-154.
- Waller, R.E., 1994. 60 years of chemical carcinogens: Sir Ernest Kennaway in retirement. *J. R. Soc. Med. 87*(2), p.96.
- Walter, U., Beyer, M., Klein, J. and Rehm, H.J., 1991. Degradation of pyrene by *Rhodococcus* sp. UW1. *Appl. Microbiol. Biotechnol. 34*(5), pp.671-676.
- Wehrer, M., Rennert, T., Mansfeldt, T. and Totsche, K.U., 2011. Contaminants at former manufactured gas plants: sources, properties, and processes. *Crit. Rev. Environ. Sci. Technol. 41*(21), pp.1883-1969.
- Wei, X., Fang, L., Cai, P., Huang, Q., Chen, H., Liang, W. and Rong, X., 2011. Influence of extracellular polymeric substances (EPS) on Cd adsorption by bacteria. *Environ. Pollut. 159*(5), pp.1369-1374.
- Wei, Z., Zeng, G., Huang, F., Kosa, M., Huang, D. and Ragauskas, A.J., 2015. Bioconversion of oxygen-pretreated Kraft lignin to microbial lipid with oleaginous *Rhodococcus opacus* DSM 1069. *Green Chem. 17*(5), pp.2784-2789.
- Wei, Z., Zeng, G., Huang, F., Kosa, M., Huang, D. and Ragauskas, A.J., 2015. Bioconversion of oxygen-pretreated Kraft lignin to microbial lipid with oleaginous *Rhodococcus opacus* DSM 1069. *Green Chem. 17*(5), pp.2784-2789.

- Wei, Z., Zeng, G., Huang, F., Kosa, M., Sun, Q., Meng, X., Huang, D. and Ragauskas, A.J., 2015. Microbial lipid production by oleaginous *Rhodococci* cultured in lignocellulosic autohydrolysates. *Appl. Biochem, Biotechnol, 99*(17), pp.7369-7377.
- Wei, Z., Zeng, G., Kosa, M., Huang, D. and Ragauskas, A.J., 2015. Pyrolysis oil-based lipid production as biodiesel feedstock by *Rhodococcus opacus*. *Appl. Biochem. Biotechnol, 175*(2), pp.1234-1246.
- Wei, Z., Zeng, G., Kosa, M., Huang, D. and Ragauskas, A.J., 2015. Pyrolysis oil-based lipid production as biodiesel feedstock by *Rhodococcus opacus*. *Appl. Biochem. Biotechnol, 175*(2), pp.1234-1246.
- Wilcke, W., Krauss, M., Lilienfein, J. and Amelung, W., 2004. Polycyclic aromatic hydrocarbon storage in a typical Cerrado of the Brazilian savanna. *J. Environ. Qual. 33*(3), pp.946-955.
- Yang, H.H., Lee, W.J., Chen, S.J. and Lai, S.O., 1998. PAH emission from various industrial stacks. *J. Hazard. Mater. 60*(2), pp.159-174.
- Ye, J., Yin, H., Xie, D., Peng, H., Huang, J. and Liang, W., 2013. Copper biosorption and ions release by *Stenotrophomonas maltophilia* in the presence of benzo[a]pyrene. *Chem. Eng. J. 219*, pp.1-9.
- Zhang, Y. and Tao, S., 2008. Seasonal variation of polycyclic aromatic hydrocarbons (PAHs) emissions in China. *Environ. Pollut. 156*(3), pp.657-663.
- Zhang, Y. and Tao, S., 2009. Global atmospheric emission inventory of polycyclic aromatic hydrocarbons (PAHs) for 2004. *Atmos. Environ. 43*(4), pp.812-819.
- Zhang, Y., Han, C., Nadagouda, M.N. and Dionysiou, D.D., 2015. The fabrication of innovative single crystal N, F-codoped titanium dioxide nanowires with

enhanced photocatalytic activity for degradation of atrazine. *Appl. Catal. B: Environ. 168*, pp.550-558.

- Zhao, S.M., Wang, B., Wang, D.W., Li, X.M., Huang, B., Hu, P., Zhang, L.W. and Pan, X.J., 2014. Environmental behavior of PAHs in Dianchi Lake distributions, sources and risk assessment of polycyclic aromatic hydrocarbons in surface sediments from Dianchi Lake, China. *Int. J. Environ. Res. 8*(2), pp.317-328.
- Zhao, Z.B., Liu, K., Xie, W., Pan, W.P. and Riley, J.T., 2000. Soluble polycyclic aromatic hydrocarbons in raw coals. *J. Hazard. Mater. 73*(1), pp.77-85.
- Zhong, Y., Luan, T., Lin, L., Liu, H. and Tam, N.F., 2011. Production of metabolites in the biodegradation of phenanthrene, fluoranthene and pyrene by the mixed culture of *Mycobacterium* sp. and *Sphingomonas* sp. *Bioresour. Technol. 102*(3), pp.2965-2972.
- Zhong, Y., Zou, S., Lin, L., Luan, T., Qiu, R. and Tam, N.F., 2010. Effects of pyrene and fluoranthene on the degradation characteristics of phenanthrene in the cometabolism process by *Sphingomonas* sp. strain PheB4 isolated from mangrove sediments. *Marine Polll. Bull. 60*(11), pp.2043-2049.
- Zhou, B. and Zhao, B., 2012. Population inhalation exposure to polycyclic aromatic hydrocarbons and associated lung cancer risk in Beijing region: Contributions of indoor and outdoor sources and exposures. *Atmos. Environ. 62*, pp.472-480.

APPENDIX

Appendix

Statistical design of experiments

Experiments are always considered as major tool for practically validating a theoretical hypothesis about scientific knowhow of a process or phenomenon, where the observation is expected to be correlated with some known associated process parameter. In order to identify important factors and their contribution towards an observed response, normal approach of using one variable at a time involves a large number of experiments to be carried out which often cannot elucidate any significant interaction among the process variables (Ryan et al., 2007).

Statistical experimental designs are potent tools for improving the efficiency of experimentation and they facilitate understanding about the system being investigated with a minimum number of experiments. Inclusion of replicate test conditions allows the estimation of random, experimental variation. Statistical analysis of data generated from the experiment clearly establishes the relationship between the measured parameter of interest (response) and the process parameters (input factors or factors) being studied.

The factors may have individual, simple effects on the response (referred to as main effects) or may have effects that are interdependent (referred to as interaction effects). Since the designed experiments are generated on the basis of statistical theory, confidence in the results obtained and conclusions drawn are clearly defined (Montgomery, 1997; Altekar et al., 2006). Several statistical design types are available and their choice is determined by the aims of the experiment and information available about the experimental background. They can be categorized as (i) Plackett Burman design (ii)

Taguchi design (iii) full and factorial design (iv) response surface analysis and (v) Box-Behnken design.

Application of statistical design of experiments in process development can improve yield of a process, reduce process variability, reduce time and overall costs. One of the striking features of the statistical design of experiments is a scientific approach of planning the experiments which aids in analyzing the experimental data trough suitable statistical methods that facilitates in drawing valid, meaningful and objective conclusions. Statistical methodology plays significant role in analyzing the data where there is a chance of experimental errors (Montgomery, 1991).

Full factorial design

Many experiments involve the study of the effects of two or more factors / parameters against a response(s). Owing to the inefficient understanding and requirement of extensive experimental work with respect to use of the classical method, factorial designs are widely used in such experiments involving several factors where it is necessary to study the interaction effects of the factors on the final response(s). Since the test variables are referred as 'factors', hence the term 'factorial' has been used. The 2-level full factorial design which is most popular, includes all possible factor combinations at two levels, low and high denoted by "–" and "+", respectively, for each of the factors.

A suitable number of runs carried out to replicate the levels of variables at their center point (0) provide an estimate of the residual error associated with the experiments and also the curvature of the response. It is a powerful tool for understanding complex processes whose detailed mechanisms are unknown and for describing factor interactions in multiple factor systems. For a process involving k factors at only 2 levels, a complete

replicate of such a design requires $2 \times 2 \times \ldots \times 2 = 2k$ observations, which is called a 2k full factorial design.

The effect of a factor is described as the change in response produced by a change in the level of the factor. This is frequently called a main effect because it refers to the primary factors of interest in the experiment (Montgomery, 1991). In some experiments, it can be found that the difference in response between the levels of one factor is not the same at all levels of the other factors and this occurs when there is an interaction between the factors. In such a case, when an interaction is large, the corresponding main effects entail little practical meaning. Moreover, in the presence of significant interaction, it is necessary to usually examine the levels of one factor; say A, with levels of the other factor fixed to draw conclusion about the main effect of the factor A.

Thus, when compared to one-factor-at-a-time experiments, full factorial designs have several advantages. Furthermore, when interactions are likely to be present, a factorial design is necessary to avoid misleading conclusions. The 2 k design, in specific is particularly used in the screening experiments, when there are likely to be many factors to be investigated whose interactions may be significant. It provides the smallest number of runs with 'k' factors that can be studied in a complete design (Montgomery, 1991). Finally, full factorial design allows the effects of a factor to be estimated at several levels of the other factors, yielding conclusions that are valid over a range of experimental conditions. On the other hand, Plackett-Burman design is a very efficient screening design with minimal number of experimental runs, and is useful for detecting large main effects, assuming all interactions are negligible.

Plackett-Burman design

Different statistical methods, for instance, Plackett Burman design has been developed to avoid the application of full factorial design of experiments in industrial experimentation when the number of factors is so large that these methods are impractical. By assuming a simplified linear hypothesis, the problem of determining main effects with maximum precision is reduced which involves different combination of factors. In practical, all solutions of this have been found useful when each factor appears at two levels, whereas the solutions for more than two levels are reasonably limited. This type of design uses two levels for each factor, the extreme denoted by "+" and the nominal by "-" (Plackett and Burman, 1946). Plackett Burman designs have been used in numerous varieties of chemical and biochemical studies, analytical as well as synthetic; in practice, designs with 12 and 20 runs seem to have been well known. Plackett Burman designs are best applicable for screening purposes in systems where it is necessary to identify a few main factors affecting the response, and where interactions are not significant, but it is worth noting that if some of the factors seem to show high effect values, it signifies that interactions are indeed present (Analytical Methods Committee, AMCTB No 55). By assuming a simplified linear hypothesis, the problem of determining main effects with maximum precision is reduced which involves different combination of factors. In practical, all solutions of this have been found useful when each factor appears at two levels, whereas the solutions for more than two levels are reasonably limited. This type of design uses two levels for each factor, the extreme denoted by "+" and the nominal by "-" (Plackett and Burman, 1946).

Analysis of Variance

Analysis of variance (ANOVA) is a collection of statistical models, and their associated procedures in which the observed variance is partitioned into components due to different explanatory variables. In general terms, ANOVA explains any variation in the statistically derived model and significance of the model parameters. The model parameters, usually indicated in ANOVA, are the main effects, interaction effects and error terms, and their significance in the model is represented by Fischer „F" and associated P values. The other terms of ANOVA table are degrees of freedom (df), sum of squares (SS) and mean squares (MS). The MS value of a model term in an ANOVA table is obtained by dividing SS over df and its F value is obtained by dividing MS due to the model term by MS due to error. Normally, larger F and lower P values of a model term in ANOVA indicate good significance of the term over others.

Student 't' test

In general, a t-test is any statistical hypothesis test in which the test statistic has a Student's t distribution if the null hypothesis is true. It is generally applied when sample size is small enough and using an assumption of normality and the associated z-test leads to incorrect inference. The Student t-distribution in probability and statistics is a probability distribution that arises in the problem of estimating the mean of a normally distributed population when the sample size is small. It is the basis of the popular Student t-tests for the statistical significance of difference between two sample means and for confidence intervals for difference between two population means.

The Student t-distribution is a special case of the generalized hyperbolic distribution. A test of the null hypothesis is that the means of two normally distributed populations are equal. Given two data sets, each characterized by its mean, standard

deviation and number of data points, one can use some kind of „t" test to determine whether the means are different, provided that the underlying distributions can be assumed to be normal. All such tests are usually called Student t tests, though strictly speaking that name should only be used if the variances of the two populations are also assumed to be equal.

Statistical experimental designs (factorial design and response surface analysis) have been applied for (i) bio-precipitation of toxic metals using mixed sulfate reducing bacterial culture (White and Gadd, 1996a) (ii) to study the effect of process variables on sulfate reduction process and (iii) to study the effect of pH and different heavy metals on the growth of SRB (Kikot et al., 2010). Other than these reports, available literature on the use of these statistical experimental designs for continuous metal removal is very limited. From literature, it is clear that factorial design of experiments has been utilized and reported that the statistical approach yielded a better and meaningful interpretation of the results.

LIST OF PUBLICATIONS

List of Publications Based on This Research Work

Referred International Journals

- ✓ **Goswami, L**., Kumar, R. V., Pakshirajan, K., Pugazhenthi, G. (2019). A novel integrated biodegradation-microfiltration system for sustainable wastewater treatment and energy recovery. Journal of Hazardous Materials, 365, 707-715.
- ✓ **Goswami, L.,** Manikandan, N. A., Taube, J. C. R., Kumar M. M., Pakshirajan, K., Pugazhenthi, G. (2019). Novel waste-derived Biochar from biomass gasification effluent: Preparation, characterization, cost-estimation and application in polycyclic aromatic hydrocarbon biodegradation and lipid accumulation by *Rhodococcus opacus*. Environmental Science and Pollution Research.
- ✓ **Goswami, L**., Manikandan, N. A., Dolman, B., Pakshirajan, K., Pugazhenthi, G. (2018). Biological treatment of wastewater containing a mixture of polycyclic aromatic hydrocarbons using oleaginous bacterium *Rhodococcus opacus*. Journal of Cleaner Production, 196, 1282-1291.
- ✓ **Goswami, L**., Kumar, R. V., Borah, S. N., Manikandan, N. A., Pakshirajan, K., Pugazhenthi, G. (2018). Membrane Bioreactor and integrated membrane bioreactor systems for micropollutant removal from wastewater: A review. Journal of Water Process Engineering, 26, 314-328.
- ✓ **Goswami, L**., Namboodiri, M. T., Kumar, R. V., Pakshirajan, K., Pugazhenthi, G. (2017). Biodiesel production potential of oleaginous *Rhodococcus opacus* grown on biomass gasification wastewater. Renewable Energy, 105, 400-406.
- ✓ **Goswami, L**., Manikandan, N. A., Pakshirajan, K., Pugazhenthi, G. (2017). Simultaneous heavy metal removal and anthracene biodegradation by the oleaginous bacteria *Rhodococcus opacus*. 3 Biotech, 7 (1), 37.

- ✓ **Goswami, L.**, Kumar, R. V., Manikandan, N. A., Pakshirajan, K., Pugazhenthi, G. (2017). Anthracene biodegradation by oleaginous *Rhodococcus opacus* for biodiesel production and its characterization. Polycyclic Aromatic Compounds, 1-13.
- ✓ **Goswami, L.**, Kumar, R. V., Manikandan, N. A., Pakshirajan, K., Pugazhenthi, G. (2017). Simultaneous polycyclic aromatic hydrocarbon degradation and lipid accumulation by *Rhodococcus opacus* for potential biodiesel production. Journal of Water Process Engineering, 17, 1-10.
- ✓ **Goswami, L.**, Roy G., Kumar M. M., Pakshirajan K., Pugazhenthi, G., Industrial wastewater treatment by tangential microfiltration system using novel low-cost kaolin based tubular ceramic membrane. (Under Review)
- ✓ **Goswami, L.,** Pakshirajan, K., Pugazhenthi, G., Utilization of biochar immobilized polyurethane foam as the potential packing material in an upflow packed bed bioreactor for an enhanced biological treatment of biomass gasification wastewater by *Rhodococcus opacus*. (Under Review)
- ✓ **Goswami, L.,** Roy, G., Pakshirajan, K., Pugazhenthi, G., An integrated approach using continuous stirred tank bioreactor and tangential microfiltration for simultaneous biomass gasification wastewater treatment and biodiesel potential. (Under Review)

Book Chapter

- ✓ Kumar, R. V., Moorthy, G., **Goswami, L.,** Pugazhenthi, G., Pakshirajan, K., Silva, A. M. T., Morales-Torres, S. Analytical methods in biodiesel production to be published in the book entitled "Refining biomass residues for Sustainable Energy and Bioproducts: Technology, advances, life cycle assessment and economics" (Elsevier) (Under Review).

National and International conferences

- ✓ **Goswami, L.,** Manikandan, N. A., Pakshirajan, K., Pugazhenthi, G., Biodegradation of low molecular weight polycyclic aromatic hydrocarbons in ternary component system by *Rhodococcus opacus*: Factorial design analysis and degradation pathway elucidation, International Conference on Emerging Trends in Biotechnology for Waste Conversion, organized by CSIR-National Environmental Engineering Research Institute (NEERI), Nagpur Maharashtra, India (2017).
- ✓ **Goswami**, L., Taube, J. C. R., Pakshirajan, K., Pugazhenthi, G., Characterization and potential application of effluent derived biochar for simultaneous enhancement in fluoranthene degradation and lipid accumulation by *Rhodococcus opacus*, National symposium on Recent Advancements in Environmental Research, organized by Center for the Environment, Indian Institute of Technology Guwahati, Guwahati, Assam, India (2017).
- ✓ **Goswami, L.,** Pakshirajan, K., Pugazhenthi, G., Optimization of fatty acid methyl esters production from *Rhodococcus opacus* utilizing anthracene as the sole carbon source in a batch stirred tank reactor, National Seminar on Petroleum Biotechnology and Bioenergy, organized by Department of Molecular Biology and Biotechnology and Department of Energy, Tezpur University, Tezpur, Assam, India (2017).
- ✓ **Goswami**, L., Pakshirajan, K., Pugazhenthi, G., Biodegradation of polycyclic aromatic compounds in a binary substrate system by *Rhodococcus opacus*, Indo-EU Workshop on "Microbial electrochemical technologies for sustainability: Fuels, Chemicals and Remediation" organized by Bioengineering and Environmental Sciences Lab, EEFF Department, Indian Institute of Chemical

Technology (CSIR-IICT), Hyderabad, Telangana, India (2017). **(Best Poster Award)**

- ✓ **Goswami, L.,** Kumar, R. V., Pakshirajan, K., Pugazhenthi, G., An integrated batch biodegradation-microfiltration system for industrial wastewater treatment and biodiesel production using *Rhodococcus opacus*, International Conference on Recent Advancements in Chemical, Environmental & Energy Engineering, organized by Department of Chemical Engineering, S. S. N. College of Engineering, Chennai, India (2017).
- ✓ **Goswami, L.,** Kumar R. V., Pakshirajan, K., Pugazhenthi, G., Industrial wastewater treatment using an indigenously built lost-cost ceramic membrane: Performance evaluation and mechanism, International Conference on Membrane Technology and its Applications, organized by Department of Chemical Engineering, National Institute of Technology Tiruchirappalli (NIT-T), Tiruchirappalli, Tamilnadu, India (2017).
- ✓ **Goswami, L.,** Pakshirajan, K., Pugazhenthi, G., Biomass gasification effluent derived biochar for simultaneous lipid accumulation and anthracene biodegradation by *Rhodococcus opacus*, Solid waste management, organized by Department of Economics, T. H. B. College, at Tyagbir Hem Baruah College, Jamugurihat, Sonitpur, Assam, India (2016).
- ✓ **Goswami**, **L.,** Kumar, R. V., Manikandan N. A., Pakshirajan, K., Pugazhenthi, G., Biodegradation of Polycyclic Aromatic Hydrocarbons by oleaginous *Rhodococcus opacus* for potential biodiesel application, Research Conclave 2016, organized by Student Academic Board (SAB) at Indian Institute of Technology Guwahati, Guwahati, India (2016). **(Best Poster Award)**

- ✓ **Goswami**, **L.,** Kumar, R. V., Pakshirajan, K., Pugazhenthi, G. Simultaneous lipid production and biomass gasification effluent treatment using oleaginous *Rhodococcus opacus*. CHEMCON-2015, organized by Indian Chemical Engineering Congress at Indian Institute of Technology Guwahati, Guwahati, India (2015).
- ✓ **Goswami**, **L.,** Kumar, R. V., Pakshirajan, K., Pugazhenthi, G. Anthracene biodegradation by oleaginous *Rhodococcus opacus* for potential biodiesel production, NHBT-2015, CSIR-National Institute for Interdisciplinary Science and Technology, Thiruvananthapuram, India (2015)
- ✓ **Goswami**, **L.,** Pakshirajan, K., Pugazhenthi, G., Effect of heavy metals on biodegradation and lipid accumulation by *Rhodococcus opacus* using naphthalene as the sole carbon source, NCOCER-2015, Indian Institute of Technology Guwahati, Guwahati, India (2015).
- ✓ **Goswami**, **L.,** Koromory, T., Pakshirajan, K., Pugazhenthi, G., Biodegradation of Polycyclic Aromatic Hydrocarbons (PAHs) and biodiesel production by *Rhodococcus opacus*, NCOSDOES-2014, Indian Institute of Technology Guwahati, Guwahati, India (2014).